Publishing House ASV

begell house, inc. publishers

PAACH

Scientific coordination is carried out by the Russian Academy of Architecture and Construction Sciences (RAACS)

Volume 20 • Issue 1 • 2024

ISSN 2588-0195 (Online)
ISSN 2587-9618 (Print) Continues ISSN 1524-5845

International Journal for

Computational Civil and Structural Engineering

Международный журнал по расчету гражданских и строительных конструкций

https://ijccse.iasv.ru/

DOI: 10.22337/2587-9618
GICID: 71.0000.1500.2830

PUBLISHER

ASV Publishing House
(ООО «Издательство АСВ»)
19/1,12, Yaroslavskoe Shosse, 120338, Moscow, Russia
Tel. +7(925)084-74-24; E-mail: iasv@iasv.ru; Интернет-сайт: http://iasv.ru/

ADVISORY EDITORIAL BOARD

TECHNICAL EDITOR

EDITORIAL TEAM

INVITED REVIEWERS

AIMS AND SCOPE

The aim of the Journal is to advance the research and practice in structural engineering through the application of computational methods. The Journal will publish original papers and educational articles of general value to the field that will bridge the gap between high-performance construction materials, large-scale engineering systems and advanced methods of analysis.

The scope of the Journal includes papers on computer methods in the areas of structural engineering, civil engineering materials and problems concerned with multiple physical processes interacting at multiple spatial and temporal scales. The Journal is intended to be of interest and use to researches and practitioners in academic, governmental and industrial communities.

ОБЩАЯ ИНФОРМАЦИЯ О ЖУРНАЛЕ

International Journal for Computational Civil and Structural Engineering

(Международный журнал по расчету гражданских и строительных конструкций)

Международный научный журнал "International Journal for Computational Civil and Structural Engineering (Международный журнал по расчету гражданских и строительных конструкций)" (IJCCSE) является ведущим научным периодическим изданием по направлению «Инженерные и технические науки», издаваемым, начиная с 1999 года (ISSN 2588-0195 (Online); ISSN 2587-9618 (Print) Continues ISSN 1524-5845). В журнале на высоком научно-техническом уровне рассматриваются проблемы численного и компьютерного моделирования в строительстве, актуальные вопросы разработки, исследования, развития, верификации, апробации и приложений численных, численно-аналитических методов, программно-алгоритмического обеспечения и выполнения автоматизированного проектирования, мониторинга и комплексного наукоемкого расчетно-теоретического и экспериментального обоснования напряженно-деформированного (и иного) состояния, прочности, устойчивости, надежности и безопасности ответственных объектов гражданского и промышленного строительства, энергетики, машиностроения, транспорта, биотехнологий и других высокотехнологичных отраслей.

В редакционный совет журнала входят известные российские и зарубежные деятели науки и техники (в том числе академики, члены-корреспонденты, иностранные члены, почетные члены и советники Российской академии архитектуры и строительных наук). Основной критерий отбора статей для публикации в журнале − их высокий научный уровень, соответствие которому определяется в ходе высококвалифицированного рецензирования и объективной экспертизы, поступающих в редакцию материалов.

Журнал входит в Перечень ВАК РФ ведущих рецензируемых научных изданий, в которых должны быть опубликованы основные научные результаты диссертаций на соискание ученой степени кандидата наук, на соискание ученой степени доктора наук по научным специальностям и соответствующим им отраслям науки:

- 1.1.8 – Механика деформируемого твердого тела (технические науки),
- 1.2.2 – Математическое моделирование численные методы и комплексы программ (технические науки),
- 2.1.1 – Строительные конструкции, здания и сооружения (технические науки),
- 2.1.2 – Основания и фундаменты, подземные сооружения (технические науки),
- 2.1.5 – Строительные материалы и изделия (технические науки),
- 05.23.07 – Гидротехническое строительство (технические науки),
- 2.1.9 – Строительная механика (технические науки)

В Российской Федерации журнал индексируется Российским индексом научного цитирования (РИНЦ).

Журнал входит в базу данных Russian Science Citation Index (RSCI), полностью интегрированную с платформой Web of Science. Журнал имеет международный статус и высылается в ведущие библиотеки и научные организации мира.

Издатели журнала – *Издательство Ассоциации строительных высших учебных заведений /АСВ/* (Россия, г. Москва) и до 2017 года *Издательский дом Begell House Inc*. (США, г. Нью-Йорк). Официальными партнерами издания является *Российская академия архитектуры и строительных наук* (РААСН), осуществляющая научное курирование издания, и *Научно-исследовательский центр СтаДиО* (ЗАО НИЦ СтаДиО).

Цели журнала – демонстрировать в публикациях российскому и международному профессиональному сообществу новейшие достижения науки в области вычислительных методов

решения фундаментальных и прикладных технических задач, прежде всего в области строительства.

Задачи журнала:

• предоставление российским и зарубежным ученым и специалистам возможности публиковать результаты своих исследований;

• привлечение внимания к наиболее актуальным, перспективным, прорывным и интересным направлениям развития и приложений численных и численно-аналитических методов решения фундаментальных и прикладных технических задач, совершенствования технологий математического, компьютерного моделирования, разработки и верификации реализующего программно-алгоритмического обеспечения;

• обеспечение обмена мнениями между исследователями из разных регионов и государств.

Тематика журнала. К рассмотрению и публикации в журнале принимаются аналитические материалы, научные статьи, обзоры, рецензии и отзывы на научные публикации по фундаментальным и прикладным вопросам технических наук, прежде всего в области строительства. В журнале также публикуются информационные материалы, освещающие научные мероприятия и передовые достижения Российской академии архитектуры и строительных наук, научно-образовательных и проектно-конструкторских организаций.

Тематика статей, принимаемых к публикации в журнале, соответствует его названию и охватывает направления научных исследований в области разработки, исследования и приложений численных и численно-аналитических методов, программного обеспечения, технологий компьютерного моделирования в решении прикладных задач в области строительства, а также соответствующие профильные специальности, представленные в диссертационных советах профильных образовательных организациях высшего образования.

Редакционная политика. Политика редакционной коллегии журнала базируется на современных юридических требованиях в отношении авторского права, законности, плагиата и клеветы, изложенных в законодательстве Российской Федерации, и этических принципах, поддерживаемых сообществом ведущих издателей научной периодики.

За публикацию статей плата с авторов не взымается. Публикация статей в журнале бесплатная. На платной основе в журнале могут быть опубликованы материалы рекламного характера, имеющие прямое отношение к тематике журнала.

Журнал предоставляет непосредственный открытый доступ к своему контенту, исходя из следующего принципа: свободный открытый доступ к результатам исследований способствует увеличению глобального обмена знаниями.

Индексирование. Публикации в журнале входят в системы расчетов индексов цитирования авторов и журналов. «Индекс цитирования» – числовой показатель, характеризующий значимость данной статьи и вычисляющийся на основе последующих публикаций, ссылающихся на данную работу.

Авторам. Прежде чем направить статью в редакцию журнала, авторам следует ознакомиться со всеми материалами, размещенными в разделах сайта журнала (интернет-сайт Российской академии архитектуры и строительных наук (http://raasn.ru); подраздел «Издания РААСН» или интернет-сайт Издательства АСВ (http://iasv.ru); подраздел «Журнал IJCCSE»): с основной информацией о журнале, его целями и задачами, составом редакционной коллегии и редакционного совета, редакционной политикой, порядком рецензирования направляемых в журнал статей, сведениями о соблюдении редакционной этики, о политике авторского права и лицензирования, о представлении журнала в информационных системах (индексировании), информацией о подписке на журнал, контактными данными и пр. Журнал работает по лицензии Creative Commons типа cc by-nc-sa (Attribution Non-Commercial Share Alike) – Лицензия «С указанием авторства – Некоммерческая – Копилефт».

Рецензирование. Все научные статьи, поступившие в редакцию журнала, проходят обязательное двойное слепое рецензирование (рецензент не знает авторов рукописи, авторы рукописи не знают рецензентов).

Заимствования и плагиат. Редакционная коллегия журнала при рассмотрении статьи проводит проверку материала с помощью системы «Антиплагиат». В случае обнаружения многочисленных заимствований редакция действует в соответствии с правилами COPE.

Подписка. Журнал зарегистрирован в Федеральном агентстве по средствам массовой информации и охраны культурного наследия Российской Федерации. Индекс в общероссийском каталоге РОСПЕЧАТЬ − 18076.

По вопросам подписки на международный научный журнал “International Journal for Computational Civil and Structural Engineering (Международный журнал по расчету гражданских и строительных конструкций)” обращайтесь в Агентство «Роспечать» (Официальный сайт в сети Интернет: http://www.rosp.ru/) или в издательство Ассоциации строительных вузов (АСВ) в соответствии со следующими контактными данными:

ООО «Издательство АСВ»

Юридический адрес: 129337, Россия, г. Москва, Ярославское ш., д. 26, офис 705;

Фактический адрес: 129337, Россия, г. Москва, Ярославское ш., д. 19, корп. 1, 5 этаж, офис 12 (ТЦ Соле Молл);

Телефоны: +7 (925) 084-74-24;

Интернет-сайт: www.iasv.ru. Адрес электронной почты: iasv@iasv.ru.

Контактная информация. По всем вопросам работы редакции, рецензирования, согласования правки текстов и публикации статей следует обращаться к главному редактору журнала члену-корреспонденту РААСН *Сидорову Владимиру Николаевичу* (адреса электронной почты: sidorov.vladimir@gmail.com, sidorov@iasv.ru, iasv@iasv.ru, sidorov@raasn.ru) или к техническому редактору журнала советнику РААСН *Кайтукову Таймуразу Батразовичу* (адреса электронной почты: tkaytukov@gmail.com; kaytukov@raasn.ru). Кроме того, по указанным вопросам, а также по вопросам размещения в журнале рекламных материалов можно обращаться к генеральному директору ООО «Издательство АСВ» *Никитиной Надежде Сергеевне* (адреса электронной почты: iasv@iasv.ru, nsnikitina@mail.ru, ijccse@iasv.ru).

Журнал становится технологичнее. Издательство АСВ с сентября 2016 года является членом Международной ассоциации издателей научной литературы (Publishers International Linking Association (PILA)), осуществляющей свою деятельность на платформе CrossRef. Оригинальным статьям, публикуемым в журнале, будут присваиваться уникальные номера (индексы DOI – Digital Object Identifier), что значительно облегчит поиск метаданных и местонахождение полнотекстового произведения. DOI – это система определения научного контента в сети Интернет.

С октября 2016 года стал возможен прием статей на рассмотрение и рецензирование через онлайн систему приема статей Open Journal Systems на сайте журнала (электронная редакция): https://ijccse.iasv.ru.

Автор имеет возможность следить за продвижением статьи в редакции журнала в личном кабинете Open Journal Systems и получать соответствующие уведомления по электронной почте.

В феврале 2018 года журнал был зарегистрирован в Directory of open access journals (DOAJ) (это один из самых известных поисковых сервисов в мире, который предоставляет открытый доступ к материалам и индексирует не только заголовки журналов, но и научные статьи), в сентябре 2018 года включен в продукты EBSCO Publishing.

В ноябре 2020 года журнал начал индексироваться в международной базе Scopus.

International Journal for
Computational Civil and Structural Engineering
(Международный журнал по расчету гражданских и строительных конструкций)
Volume 20, Issue 1 ***2024***

Scientific coordination is carried out by the Russian Academy of Architecture and Construction Sciences (RAACS)

CONTENTS

International Journal for
Computational Civil and Structural Engineering
(Международный журнал по расчету гражданских и строительных конструкций)
Volume 20, Issue 1 ***2024***

Scientific coordination is carried out by the Russian Academy of Architecture and Construction Sciences (RAACS)

СОДЕРЖАНИЕ

International Journal for Computational Civil and Structural Engineering, 20(1) 14–20 (2024)

DOI:10.22337/2587-9618-2024-20-1-14-20

MIXED SCHEME OF THE FINITE ELEMENT METHOD FOR CALCULATING CABLE SYSTEMS

Aleksandr V. Baenkhaev

Far Eastern Federal University, Vladivostok, RUSSIA

Abstract: A methodology for constructing variational formulations and solving geometrically nonlinear mixed problems by the finite element method is considered using the example of equilibrium of a flexible tensile thread. The results of solving the model problem are presented.

Keywords: geometrically nonlinear problem, equilibrium of a flexible tensile thread, variational formulation, finite element method

СМЕШАННАЯ СХЕМА МЕТОДА КОНЕЧНЫХ ЭЛЕМЕНТОВ ДЛЯ РАСЧЁТА ТРОСОВЫХ СИСТЕМ

А.В. Баенхаев

Дальневосточный федеральный университет, г. Владивосток, РОССИЯ

Аннотация: Рассматривается методика построения вариационных постановок и решения геометрически нелинейных смешанных задач методом конечных элементов на примере равновесия гибкой растяжимой нити. Приведены результаты решения модельной задачи.

Ключевые слова: геометрически нелинейная задача, равновесие гибкой растяжимой нити, вариационная постановка, метод конечных элементов

INTRODUCTION

The study of the behavior of cable systems is of great importance for solving many practical problems: underwater cable systems (hydrobiotechnical structures [1], fastening systems for floating oil and gas production platforms [2]), in the design and operation of overhead power lines, etc. Moreover, with the development of technology, the range of applications of the results and methods of dynamics and statics of cable systems is steadily expanding.

Differential formulations of problems in the mechanics of flexible threads and methods for solving them are given, for example, in [3]. The stress-strain state of the thread is described by the coordinates of the thread axis, tensile strain and force in the rope. Currently, to solve various problems of calculating cable systems, numerical methods based on differential formulations of problems are used, and modern numerical methods based on variational formulations of problems are not used.

In this work, based on a formal mathematical procedure [4], we show the formation of a variational formulation of the equilibrium problem of a flexible tensile thread and a method for solving a mixed problem by eliminating part of the unknowns not at the level of the entire region (as, for example, with block elimination in a resolving system of equations), and on the subdomain (at the level of the final element). This approach to solving a mixed problem for degenerate problems of structural mechanics was considered in [5]. The same, in essence, are hybrid finite element methods, for example [6].

This division of the problem into two levels (for the subdomain and the entire domain) makes it possible to construct an iterative procedure for solving a nonlinear problem, in which a variational equation at the subdomain (finite element) level is used to clarify the values of the efforts.

DIFFERENTIAL FORMULATION OF THE PROBLEM

Let us consider the equilibrium problem of a flexible thread, the shape of which is determined by the load and connections. The position of the flexible thread axis will be described by a vector of Cartesian coordinates

$$\mathbf{x} = \begin{Bmatrix} x_1 \\ x_2 \\ x_3 \end{Bmatrix}$$

The stressed state of the thread is characterized by the force in the thread T $(T \geq 0)$. We denote the coordinate along the thread axis by s. The deformed state of the thread is characterized by relative linear deformation ε.

The thread arc differential in the stretched state ds is related to the thread arc differential in the initial state ds_0 by the relation:

$$ds = (1+\varepsilon)ds_0. \tag{1}$$

To form equations that take into account various types of boundary conditions, we will assume that one end of the thread is fixed, and we will apply a load to the other.

Then the differential formulation of the problem of a flexible tensile thread can be written as:

– static equation

$$\begin{gathered} \frac{d}{ds}\left(T\frac{d\mathbf{x}}{ds}\right) + \frac{\mathbf{p}_m}{1+\varepsilon} + \mathbf{p}_s = 0 \quad \text{or} \\ \frac{d}{ds_0}\left(\frac{T}{1+\varepsilon}\frac{d\mathbf{x}}{ds_0}\right) + \mathbf{p}_m + \mathbf{p}_s(1+\varepsilon) = 0 \end{gathered} \tag{2}$$

– geometric equation

$$\left(\frac{d\mathbf{x}}{ds}\right)^T \cdot \frac{d\mathbf{x}}{ds} = 1 \quad \text{or} \quad \left(\frac{d\mathbf{x}}{ds_0}\right)^T \cdot \frac{d\mathbf{x}}{ds_0} = (1+\varepsilon)^2 \tag{3}$$

– physical equation

$$\varepsilon = \frac{T}{EA}, \tag{4}$$

– kinematic boundary condition at $s = 0$

$$\mathbf{x}\big|_{s=0} = \mathbf{x}_0, \tag{5}$$

– static boundary condition at $s = l$

$$T\frac{d\mathbf{x}}{ds}\bigg|_{s=l} = \mathbf{F}_l \quad \text{or} \quad \frac{T}{1+\varepsilon}\frac{d\mathbf{x}}{ds_0}\bigg|_{s=l} = \mathbf{F}_l \tag{6}$$

Here

$\mathbf{p}_m = \{p_{m1} p_{m2} p_{m3}\}^T$ – vector of distributed rope mass loads;

$\mathbf{p}_s = \{p_{s1} p_{s2} p_{s3}\}^T$ – vector of distributed surface loads on the thread;

$\mathbf{x}_0 = \{x_{01} x_{02} x_{03}\}^T$ – a given coordinate vector at the starting point of the rope,

$\mathbf{F}_l = \{F_{l1} F_{l2} F_{l3}\}^T$ – load at the free end of the thread;

EA – thread stiffness.

The division of the load into mass and surface is made to take into account the reduction in mass load per unit length of the thread during tension.

BASIC INTEGRAL FORMULA

To construct variational formulations of problems that reflect the energy properties of the system under study, it is necessary that the structure of the equations admits a certain integral formula, similar to the formula for integration by parts and based on a differential operator included in the static and geometric equation of the problem.

Let's introduce arbitrary vectors

$$\mathbf{a}=\begin{Bmatrix} a_1 \\ a_2 \\ a_3 \end{Bmatrix} \quad \text{и} \quad \mathbf{b}=\begin{Bmatrix} b_1 \\ b_2 \\ b_3 \end{Bmatrix}$$

with components – functions of the coordinate s_0. Let these functions have the required degree of smoothness to ensure the ability to perform the required operations. Then the formula for integration by parts is valid for them:

$$\int_0^l \left(\frac{d\mathbf{a}}{ds_0}\right)^T \mathbf{b}\, ds = \mathbf{a}^T\,\mathbf{b}\Big|_0^l - \int_0^l \mathbf{a}^T \frac{d\mathbf{b}}{ds_0}\, ds_0. \qquad (7)$$

Integral formula (7) transfers the differentiation operation from vector $\mathbf{a}$ to vector $\mathbf{b}$. Let's write vectors $\mathbf{a}$ and $\mathbf{b}$ through an arbitrary vector $\overline{\mathbf{x}}$ and function $\overline{T}$ in the form:

$$\mathbf{a}=\overline{\mathbf{x}} \quad \text{и} \quad \mathbf{b}=\frac{\overline{T}}{1+\dfrac{\overline{T}}{EA}}\cdot\frac{d\overline{\mathbf{x}}}{ds_0}$$

and substituting into (7), we obtain the *basic integral formula* for the equilibrium problem of a tensile flexible thread:

$$\begin{aligned}&\int_0^l \frac{\overline{T}}{1+\dfrac{\overline{T}}{EA}}\left(\frac{d\overline{\mathbf{x}}}{ds_0}\right)^T \frac{d\overline{\mathbf{x}}}{ds_0}\, ds_0 = \\ &= \overline{\mathbf{x}}^T \frac{\overline{T}}{1+\dfrac{\overline{T}}{EA}}\frac{d\overline{\mathbf{x}}}{ds_0}\Big|_0^l - \\ &-\int_0^l \overline{\mathbf{x}}^T \frac{d}{ds_0}\left(\frac{\overline{T}}{1+\dfrac{\overline{T}}{EA}}\frac{d\overline{\mathbf{x}}}{ds_0}\right) ds_0.\end{aligned} \qquad (8)$$

It is obvious that formula (8) is also valid in the case when the true values of the coordinate vector $\mathbf{x}$ and force T are substituted into it:

$$\begin{aligned}&\int_0^l \frac{T}{1+\dfrac{T}{EA}}\left(\frac{d\mathbf{x}}{ds_0}\right)^T \frac{d\mathbf{x}}{ds_0}\, ds_0 = \mathbf{x}^T \frac{T}{1+\dfrac{T}{EA}}\frac{d\mathbf{x}}{ds_0}\Big|_0^l - \\ &-\int_0^l \mathbf{x}^T \frac{d}{ds_0}\left(\frac{T}{1+\dfrac{T}{EA}}\frac{d\mathbf{x}}{ds_0}\right) ds_0.\end{aligned}$$

Taking into account relations (2)-(6), we obtain:

$$\begin{aligned}&\int_0^l T\left(1+\varepsilon\right) ds_0 = \\ &= \mathbf{x}^T\mathbf{F}_l\Big|_{s_0=l} - \mathbf{x}_0^T\mathbf{R}_0 + \int_0^l \mathbf{x}^T\left[\mathbf{p}_m + \mathbf{p}_s(1+\varepsilon)\right] ds_0,\end{aligned} \qquad (9)$$

where

$\mathbf{R}_0 = T\dfrac{d\mathbf{x}}{ds}\Big|_{s=0}$ – connection reaction vector.

In this case, the formula takes on a mechanical meaning. Let's imagine two states of the system. First, the thread is folded at the origin of the coordinate system. The second state is when the thread takes on a deformed position that corresponds to the given fastenings and load. The work done by the internal force T to unwind the thread from the first state to the second (the left side of the equality) is equal to the work that external forces do during these movements (the right side of the equality).

VARIATIONAL FORMULATION OF THE PROBLEM

Taking into account that when solving the problem, kinematic boundary conditions are not difficult to take into account, we set a geometrically possible variation to the coordinate vector of the thread $\mathbf{x}$:

$$\overline{\mathbf{x}} = \mathbf{x} + \delta\mathbf{x}, \qquad \delta\mathbf{x}\big|_{s_0=0} = 0 \qquad (10)$$

and force T – arbitrary variation:

$$\overline{T} = T + \delta T \qquad (11)$$

Let us substitute them into the main integral identity (8) and after transformations we obtain a *variational equation for the equilibrium problem of an extensible flexible thread* in the form:

$$\frac{1}{2}\int_0^l \frac{\delta T}{1+\frac{T}{EA}}\cdot\left[\left(\frac{d\mathbf{x}}{ds_0}\right)^T\frac{d\mathbf{x}}{ds_0}-\left(1+\frac{T}{EA}\right)^2\right]ds_0+$$
$$+\int_0^l\left(\frac{\delta d\mathbf{x}}{ds_0}\right)^T\frac{T}{1+\frac{T}{EA}}\frac{d\mathbf{x}}{ds_0}ds_0- \qquad (12)$$
$$-\int_0^l\ \delta\mathbf{x}^T\left[\mathbf{p}_m+\mathbf{p}_s\cdot\left(1+\frac{T}{EA}\right)\right]ds_0-$$
$$-\delta\mathbf{x}^T\mathbf{F}_l\Big|_{s_0=l}=0$$

or the stationary condition of the functional:

$$B(\mathbf{x},T)=$$
$$\frac{1}{2}\int_0^l\frac{T}{1+\frac{T}{EA}}\left[\left(\frac{d\mathbf{x}}{ds_0}\right)^T\frac{d\mathbf{x}}{ds_0}-\left(1+\frac{T}{EA}\right)^2\right]ds_0- \qquad (13)$$
$$\int_0^l\mathbf{x}^T\left[\mathbf{p}_m+\mathbf{p}_s\cdot\left(1+\frac{T}{EA}\right)\right]ds_0-\mathbf{x}^T\mathbf{F}_l\Big|_{s=l}=\text{stat.},$$

defined on the class of vectors $\mathbf{x}$ satisfying kinematic boundary conditions (5).

METHOD FOR SOLVING THE MIXED VARIATIONAL PROBLEM

Functional (13) is mixed. The unknowns are the forces T and the coordinates of the thread axis $\mathbf{x}$. To solve this mixed problem, we use the technique proposed in [5], in which the computational domain is divided into subdomains, and it is assumed that part of the equations of the mixed method is satisfied in each such subdomain separately.

Let's divide the thread into n subareas - elements. We will denote l^r the length of the element with number r (r = 1,2,…,n). Let us assume that the variational equation is satisfied on each element:

$$\int_{l^r}\delta T\frac{1}{1+\frac{T}{EA}}\left[\left(\frac{d\mathbf{x}}{ds_0}\right)^T\frac{d\mathbf{x}}{ds_0}-\left(1+\frac{T}{EA}\right)^2\right]ds_0= \qquad (14)$$
$$=0,\quad r=1,2,...,n$$

Then, to solve the entire variational problem (12), it remains to consider the integral identity:

$$\int_0^l\left(\frac{\delta d\mathbf{x}}{ds_0}\right)^T\frac{T}{1+\frac{T}{EA}}\frac{d\mathbf{x}}{ds_0}ds_0-$$
$$-\int_0^l\ \delta\mathbf{x}^T\left[\mathbf{p}_m+\mathbf{p}_s\left(1+\frac{T}{EA}\right)\right]ds_0- \qquad (15)$$
$$-\delta\mathbf{x}^T\mathbf{F}_l\Big|_{s_0=l}=0,$$

defined on the class of vectors $\mathbf{x}$ satisfying kinematic boundary conditions (5).

FINITE ELEMENT DISCRETIZATION

Let us construct a finite element method scheme based on the variational formulation of problem (14)-(15). Let us define an approximation of the vector $\mathbf{x}$ and force T on the finite element in the form:

$$\mathbf{x}=\mathbf{N}^r\mathbf{X}^r,\qquad T=[1]\cdot t^r\qquad\in l^r, \qquad (16)$$

where $\mathbf{N}^r$ is the matrix of shape functions; $\mathbf{X}^r$ – vector of coordinates of nodes of element r; t^r is the value of the force in element r (force T is assumed to be a piecewise constant function).

Let us substitute (16) into the first variational equation (14)

$$\delta t^r\left(\left(\mathbf{X}^r\right)^T\frac{1}{1+\frac{t^r}{EA}}\int_{l^r}\left(\frac{d\mathbf{N}^r}{ds_0}\right)^T\frac{\mathbf{N}^r}{ds_0}ds_0\mathbf{X}^r-\right.$$
$$\left.-\int_{l^r}\left(1+\frac{t^r}{EA}\right)ds_0\right)=0,\quad r=1,2,...,n$$

and, due to the arbitrariness of the variation of efforts, we obtain

$$\left(\mathbf{X}^r\right)^T \mathbf{H}^r \mathbf{X}^r - l^r\left(1+\frac{t^r}{EA}\right)=0,\ r=1,2,...,n, \quad (17)$$

where $\mathbf{H}^r = \dfrac{1}{1+\dfrac{t^r}{EA}}\int_{l^r}\left(\dfrac{d\mathbf{N}^r}{ds_0}\right)^T\left(\dfrac{d\mathbf{N}^r}{ds_0}\right)ds_0.$

The resulting systems of equations at the finite element level (17) contain the unknown forces t^r and the squares of the nodal coordinates $\mathbf{X}^r$.

Let us present the remaining variational equation (15) as a sum over finite elements:

$$\sum_{r=1}^{n}\left[\int_{l^r}\left(\frac{\delta d\mathbf{x}}{ds_0}\right)^T\frac{T}{1+\dfrac{T}{EA}}\frac{d\mathbf{x}}{ds_0}ds_0 - \right.$$
$$-\int_{l^r}\delta\mathbf{x}^T\left(\mathbf{p}_m+\mathbf{p}_s\left(1+\frac{T}{EA}\right)\right)ds_0 -$$
$$\left.-\delta\mathbf{x}^T\mathbf{F}_l\Big|_{s_0=l}\right]=0.$$

Using the approximation of the unknowns in the form (16), we obtain

$$\sum_{r=1}^{n}\left\{\delta\left(\mathbf{X}^r\right)^T\left[\frac{t^r}{1+\dfrac{t^r}{EA}}\int_{l^r}\left(\frac{d\mathbf{N}^r}{ds_0}\right)^T\frac{d\mathbf{N}^r}{ds_0}ds_0\mathbf{X}^r - \right.\right.$$
$$-\int_{l^r}\left(\mathbf{N}^r\right)^T\left(\mathbf{p}_m+\mathbf{p}_s\left(1+\frac{t^r}{EA}\right)\right)ds_0 -$$
$$\left.\left.-\left(\mathbf{N}^r\right)^T\mathbf{F}_l\Big|_{s_0=l}\right]\right\}=0$$

or

$$\sum_{r=1}^{n}\left(\left(\delta\mathbf{X}^r\right)^T\left(\mathbf{H}_t^r\mathbf{X}^r-\mathbf{P}^r\right)\right)=0 \quad (18)$$

where

$\mathbf{H}_t^r = t^r\mathbf{H}^r,$

$$\mathbf{P}^r=\int_{l^r}\left(\mathbf{N}^r\right)^T\left(\mathbf{p}_m+\mathbf{p}_s\left(1+\frac{t^r}{EA}\right)\right)ds_0+\left(\mathbf{N}^r\right)^T\mathbf{F}_l\Big|_{s_0=l}$$

Performing the usual procedure of the finite element method to form the global matrix $\mathbf{H}_t$ and the load vector $\mathbf{P}$, taking into account the connections between the finite elements and kinematic boundary conditions, we come to the solution of a system of algebraic equations for the unknowns – the vector of nodal coordinates $\mathbf{X}$:

$$\mathbf{H}_t\mathbf{X}=\mathbf{P} \quad (19)$$

The system of equations contains unknown coordinates in the nodes of the system $\mathbf{X}$ and unknown forces in the elements t^r (implicitly in the matrix $\mathbf{H}_t$).

The final system of algebraic equations has the form

$$\begin{cases}\left(\mathbf{X}^r\right)^T\mathbf{H}^r\mathbf{X}^r - l^r\left(1+\dfrac{t^r}{EA}\right)=0,\ r=1,...,n\\ \mathbf{H}_t\mathbf{X}=\mathbf{P}\end{cases} \quad (20)$$

ITERATION PROCEDURE

Let us reduce equation (17) to the form:

$$\frac{\left(\mathbf{X}^r\right)^T\mathbf{H}^r\mathbf{X}^r}{l^r\left(1+\dfrac{t^r}{EA}\right)}=1,\quad r=1,2,...,n, \quad (21)$$

The iterative procedure for solving the problem is as follows. The initial values of the forces in the $t^r_{(0)}$ elements are set. The system of algebraic equations (19) is solved, linear with respect to the unknown coordinates $\mathbf{X}$. To clarify the values of t^r, relation (21) is used in the form:

$$t^r_{(k)} = t^r_{(k-1)} \cdot \sqrt{\frac{\left(\mathbf{X}^r\right)^T \mathbf{H}^r \mathbf{X}^r}{l^r\left(1+\frac{t^r_{(k-1)}}{EA}\right)}}, \quad r = 1,2,...,n, \qquad (22)$$

where k is the iteration number.

With updated values of t^r, the system of algebraic equations (19) is solved again. Iterations continue until the required accuracy of force calculation is achieved.

SOLUTION OF THE MODEL PROBLEM OF EQUILIBRIUM OF FLEXIBLE TENSILE THREAD

Examples of solving model problems for a flexible *inextensible* thread are given in [7]. Calculations have shown that the proposed finite element method for an inextensible thread allows already in the first iterations to achieve the correct position of the ropes in accordance with the specified loads and connections, and about 10-15 iterations are enough to calculate the forces in the thread with acceptable accuracy.

In this paper, the problem of the equilibrium of a flexible *tensile* thread for different values of the stiffness of the *EA* thread is solved. The results are shown in Figure 1.

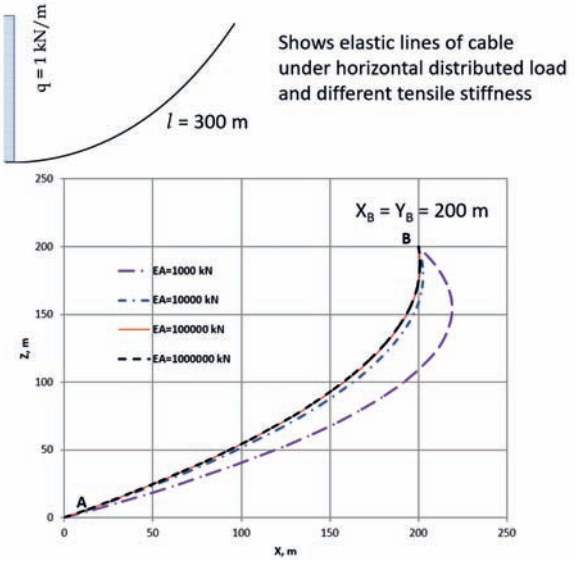

Figure 1. Elastic lines of cable

CONCLUSION

The proposed finite element method allows solving problems of statics of any cable systems and gives good results even with a small number of iterations.

The considered technique for constructing a finite element method for solving the equilibrium problem of a flexible tensile thread can also be applied to solve other nonlinear problems.

REFERENCES

1. **Stotsenko A.A**. Hydrobiotechnical constructions. Vladivostok: Far Eastern State University Press, 1984. 136 p.
2. **Sukhorukov A.L**. The Theory of Underwater Cable Systems and its Engineering Applications. Moscow: FIZMATLIT, 2017. 272 p.
3. **Merkin D.V.** Introduction into the mechanics of flexible string. Moscow: Nauka, 1980. 240 p.
4. **Rozin L.A.** Variation Formulations of the Problems for the Elastic Systems. Leningrad: Leningrad State University Press, 1978. 224 p.
5. **Rozin L.A., Baenkhaev A.V**. Mixed schemes of the finite element method and their application to the solution of the problems of the theory of elasticity // News of the All-Union Scientific Research Institute of Hydraulic Engineering named after B.E. Vedeneeva. 1986. Vol. 194. pp. 79-84.
6. **Pian T.H.H.** State-of-the-art development of hybrid/mixed finite element method // Finite Elements in Analysis and Design. 1995, Vol. 21, Issues 1-2, pp. 5–20. https://doi.org/10.1016/0168-874X(95)00024-2
7. **Baenkhaev A.V.** Finite element simulation of flexible ropes. // APCSCE 2018. IOP Conf. Series: Materials Science and Engineering, 2018. Vol. 456, 012101. https://doi.org/ 10.1088 /1757-899X/456/1/012101

СПИСОК ЛИТЕРАТУРЫ

1. **Стоценко А.А.** Гидробиотехнические сооружения. Владивосток: Изд-во Дальневосточного ун-та. 1984. 136 с.
2. **Сухоруков А.Л**. Теория подводных тросовых систем и её инженерные приложения. М.: ФИЗМАТЛИТ. 2017. 272 с.
3. **Меркин Д.В.** Введение в механику гибкой нити. М.: Наука. 1980. 240 с.
4. **Розин Л.А.** Вариационные постановки задач для упругих систем. Л.: Изд-во Ленингр. ун-та. 1978. 224 с.
5. **Розин Л.А., Баенхаев А.В.** Смешанные схемы МКЭ и их применение к решению задач теории упругости // Известия ВНИИГ. Л.: Энергоатомиздат. 1986. Т. 194. С. 79-84.
6. **Pian T.H.H.** State-of-the-art development of hybrid/mixed finite element method // Finite Elements in Analysis and Design. 1995. Vol. 21, Issues 1-2, pp. 5–20. https://doi.org/10.1016/0168-874X(95)00024-2
7. **Baenkhaev A.V**. Finite element simulation of flexible ropes. // APCSCE 2018. IOP Conf. Series: Materials Science and Engineering. 2018, Vol. 456, 012101. https://doi.org/10.1088/1757-899X/456/1/012101

Aleksandr V. Baenkhaev — Ph. D., Associate Professor, Department of Geoinformation Technologies, Far Eastern Federal University (FEFU), 10, Ajax, Russky Island, Vladivostok, 690922, Russia, baenkhaev.av@dvfu.ru, +74232652424

Баенхаев Александр Викторович — кандидат технических наук, доцент департамента геоинформационных технологий, Дальневосточный федеральный университет (ДВФУ), 10, п. Аякс, остров Русский, г. Владивосток, 690922, Россия, baenkhaev.av@dvfu.ru, +74232652424

DOI:10.22337/2587-9618-2024-20-1-21-34

POLYMER COMPOSITES FOR EXTERNAL REINFORCEMENT OF BUILDING STRUCTURES

Evgeniy E. Shmoilov [1], Mikhail Yu. Fedotov [2], Igor A. Sharutin [1], Roman V. Ilyukhin [1], Stanislav A. Stepanov [1], Natalya N. Panina [1], Lidiya I. Gurenchuk [3], Pavel D. Kapyrin [4], Oleg V. Kabantsev [4], Oleg A. Kornev [4]

[1] Prepreg-MCM Joint Stock Company, Moscow, RUSSIA
[2] Russian Engineering Academy, Moscow, RUSSIA
[3] Prepreg-Dubna Limited Liability Company, Dubna, RUSSIA
[4] Moscow State University of Civil Engineering (National Research University), Moscow, RUSSIA

Abstract: Key aspects of developing effective systems for the external reinforcement of building structures, made of composite polymer materials containing carbon fibers and no-bake polymer binders, ensuring shape formation in the temperature range of 15 - 40 °C no more than 24 hours, characterized by operability in the temperature range from minus 45 ° C to plus 60 ° C. PCM-based SVA has a number of advantages compared to clips and metal profiles traditionally used for repairing building structures: the load-bearing capacity of the rods increases, the cost of the strengthening of load-bearing structures is reduced, and the seismic resistance of engineering structures is increased. In relation to composite SVA building structures, the following types of construction chemicals are used: primer, putty, adhesive, protective coating. The production of unidirectional tapes was carried out on a Dornier double rapier loom, modernized for processing carbon fibers. The results of experimental studies of the developed polymer binders and carbon reinforcing fillers are presented. It is shown that the developed materials can be successfully used to strengthen and repair engineering structures. The technological features of strengthening and repairing building structures with composite external reinforcement systems using the contact molding method and ready-made lamellas are described. Installation of composite clamps on vertical surfaces is carried out by fixing the canvas in the extreme position, followed by laying, smoothing and rolling along its length. Rolling is done from the middle to the edges. Before gluing the blanks, the lamellas are laid out on a work table (workbench) and thoroughly wiped with a rag moistened with acetone. Results of the large-scale implementation of these new materials and technologies in the construction industry are presented.

Keywords: thermosetting matrix, reinforcing carbon filler, building structure, composite external reinforcement system, reinforcement, repair

ПОЛИМЕРНЫЕ КОМПОЗИТЫ ДЛЯ ВНЕШНЕГО АРМИРОВАНИЯ СТРОИТЕЛЬНЫХ КОНСТРУКЦИЙ

Шмойлов Е.Е. [1], Федотов М.Ю. [2], Шарутин И.А. [1], Илюхин Р.В. [1], Степанов С.А.[1], Панина Н.Н. [1], Гуренчук Л.И. [3], Капырин П.Д. [4], Кабанцев О.В. [4], Корнев О.А.[4]

[1] АО «Препрег – СКМ», г. Москва, РОССИЯ
[2] Российская инженерная академия, г. Москва, РОССИЯ
[3] ООО «Препрег-Дубна», г. Дубна, РОССИЯ
[4] НИУ МГСУ, г. Москва, РОССИЯ

Аннотация: Рассмотрены ключевые аспекты создания эффективных систем внешнего армирования строительных конструкций полимерными композитными материалами на основе углеродных волокон и полимерных связующих холодного отверждения, обеспечивающих формообразование в интервале температур (15 – 40) °С не более 24 часов, характеризующихся работоспособностью в интервале температур от минус 45 °С до плюс 60 °С. СВА на основе ПКМ обладает рядом преимуществ по сравнению с традиционно используемыми для ремонта строительных конструкций обоймами и металлическими профилями: несущая

способность стержней увеличивается, затраты на усиление несущих конструкций снижаются, повышается сейсмостойкость инженерных сооружений. Применительно к композитным СВА строительных конструкций применяются следующие типы строительной химии: праймер, шпатлевка, адгезив, защитное покрытие. Выработка однонаправленных лент осуществлялась на двурапирном ткацком станке фирмы Dornier, модернизированном для переработки углеродных волокон. Приведены результаты экспериментальных исследований разработанных полимерных связующих и углеродных армирующих наполнителей. Показано, что разработанные материалы могут успешно применяться для усиления и ремонта инженерных сооружений. Описаны технологические особенности усиления и ремонта строительных конструкций композитными системами внешнего армирования с использованием метода контактного формования и готовых ламелей. Установка композитных хомутов на вертикальные поверхности осуществляется фиксацией холста в крайнем положении с последующей укладкой, разглаживанием и прокаткой по длине. Прокатка производится от середины к краям. Перед наклейкой заготовки ламели раскладываются на рабочем столе (верстаке) и тщательно протираются смоченной ацетоном ветошью. Представлены результаты широкого внедрения созданных материалов и технологий в строительной отрасли.

Ключевые слова: термореактивная матрица, углеродный армирующий наполнитель, строительная конструкция, композитная система внешнего армирования, усиление, ремонт

1. INTRODUCTION

Development of advanced polymer composite materials (PCM) is impossible without advanced techniques in the field of construction materials and technologies [1-3]. Thus, in the process of curing, novel binders should not only form a high-strength polymer matrix, ensuring maximum strength of reinforcing fibers in materials, they should have high-tech characteristics, comply with the principles of "green chemistry", and ensure their recycling using inexpensive technologies.

However the curing process typical for traditional technologies applied to manufacture PCM products, containing thermosetting matrices, are characterized by high energy consumption, namely, those PCM products that contain hot-setting polymer binders. This process is time consuming (6 - 9 hours): a temperature rise is followed by a long-term exposure of the molded element to high temperature. Special autoclave equipment is frequently used for this purpose.

Cold-curing polymer binders, applicable in the temperature range between 15 and 40 °C, do not require any expensive and energy-consuming autoclave equipment. Their application facilitates the development of simplified energy-efficient and resource-saving PCM production technologies for the construction industry. Such technologies can be applied at the site of construction or renovation of a construction facility by using the so-called composite external reinforcement systems (ERS) [4 - 6]. Therefore, the task is to make PCM containing various reinforcing fillers (carbon, glass, mixtures) and polymer binders for ERS of building structures, using the contact molding method that ensures the forming process in the temperature range between 15 and 40 °C within 24 hours. These building structures can be operated in the temperature range from minus 45 °C to plus 60 °C.

In the Russian Federation, the annual building reinforcement market capacity is about 5 billion rubles; it depends on the rate of (1) repair of worn-out infrastructure and (2) construction. The market capacity of external PCM reinforcement is about 850 mln. rubles, and its rate of growth is 15 – 20% per year. In the future, replacement of existing repair materials with PCM can boost the demand for PCM to 200 million rubles per year.

It is necessary to emphasize the expanding application of PCM containing carbon and hybrid fabrics, laminates and meshes by the construction industry [7 - 9]. In Switzerland, these materials are already used in more than 80% of cases of reinforcement of reinforced concrete, masonry and metal building structures. According to the experts, the global market of such PCMs is expected to double in the coming 5 - 7 years.

Composite ERS, entering the construction industry market, should contribute to the solution of the following problems [10 - 13]:

- ensuring the repair of load-bearing elements of reinforced concrete, masonry, and metal structures featuring substantial wear and tear;
- ensuring the reconstruction of load-bearing elements of structures in a short period of time, if the main items of equipment are replaced;
- increasing the "survivability" of buildings and structures subjected to natural and man-made factors, including terrorist attacks.

PCMs entered the construction market quite recently, although they are known to be in use abroad since the late 70s of the 20th century. In the Russian Federation they are used since the late 90s, and are widely used in foreign and domestic construction industries.

ERSs containing PCMs have a number of advantages compared to cases and metal shapes traditionally used to repair building structures [14, 15]:
- the load-bearing capacity of structures increases by 70% (including complex geometric shapes and cases of confined spaces) without any substantial increase in their weight, while there is an additional opportunity to correct inaccuracies that may arise at the design stage;
- the cost of reinforcement of load-bearing structures reduces by 20 - 60% due to the fact that there is no need to use heavy-duty equipment and to suspend the operation of a structure, which is extremely important, for example, for railroad bridges;
- the seismic resistance of engineering structures operated under such conditions increases by 2 - 3 grades.

2. EXPERIMENTAL STUDIES AND THEIR DISCUSSION

2.1. Construction chemicals for composite systems of external reinforcement of building structures

The following types of construction chemicals are used to make composite ERS building structures:

1. The primer used to ensure adhesion. The average primer consumption is 100 - 300 g/m^2.
2. The putty used to correct minor defects. Its composition differs slightly depending on the manufacturer; its consumption rate depends on the extent of structural damage.
3. The adhesive substance (the glue) used to bond tapes (if their length is up to 250 m; width up to 15 cm), canvases (if their width is 600 mm or up to 1500 mm, which is less frequent) (Figure 1a), and lamellas (pre-impregnated and cured tapes with aligned edges (length up to 100 m, thickness 1,2 – 1,4 mm) (Figure 1b) to the surface of the structure. The adhesive substance, applied to different types of materials, differs mainly in viscosity.

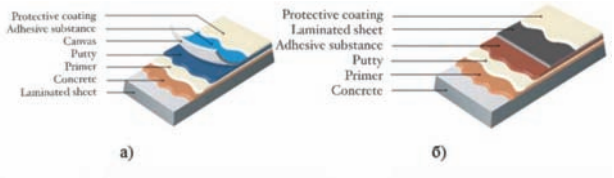

Figure 1. Lay-up sequence of ERS components for: a) tapes and canvases; b) lamellas

There are "dry" and "wet" methods of applying adhesive substance to canvas. The "dry" method involves applying the adhesive substance to the structure, then attaching the canvas and bonding it to another layer of adhesive over it. The "wet" method involves applying the adhesive substance to the tape/canvas, whose side that has glue on it is attached to the concrete of the structure and then bonded to another layer of the adhesive substance. The adhesive substance used for the "wet" method is more viscous. The main difference in the choice of application methods is the simplicity of application of the binder needed to bond the ERS reinforcement components. The adhesive substance is characterized by thixotropy and is generally the same if used to bond glass and aramid fibers. The consumption of the adhesive substance varies from 0,7 to 4 kg/m^2, depending on the brand and type of tape/canvas.

As part of the experimental research, compositions of primers, putties and adhesive substances were developed for composite ERS building structures and their properties were investigated. Table 1 shows physical and mechanical properties of the novel primer Fibarm resin 530+, putty FibArm Repair EP 301, and adhesive Fibarm resin 530+.

Table 1. Physical and mechanical properties of Fibarm resin 530+ primer, FibArm Repair EP 301 putty, and Fibarm resin 530+ adhesive substance

	Measurement unit	Value		
		primer	putty	adhesive
Modulus of elasticity in tension	GPa	≥ 0,5	≥ 3	≥ 3
Modulus of elasticity in bending	GPa	≥ 0,5	≥ 3	≥ 3
Tensile strength	MPa	≥ 20	≥ 40	≥ 40
Bending strength	MPa	≥ 20	≥ 40	≥ 40
Ultimate relative strain in tension	%	1 – 3	1 – 3	1 – 3
Mortar life time (at + 20 °C)	min	30 – 45	30 – 45	30 – 45
Application temperature	°C	+5 – +30	+5 – +30	+5 – +30
Operating temperature	°C	-40 – +60	-40 – +60	-40 – +60
Density of ready-mixed mortar	kg/l	1,0 – 1,1	1,5 – 1,7	1,0 – 1,3
Adhesion to concrete (steel)	MPa	≥ 3	≥ 3	≥ 3
Strength development time (at + 20 °C)	days	7	7	7

The critical strength development time is 30 - 40 min for each of the primer, putty, and adhesive substance.

4. As a rule, protective coating is not a mandatory component of the system of structural reinforcement, rather, it is a supplementary one; its functional purpose is fire resistance, aesthetics or anti-vandal properties.

Based on the development results and experimental studies, cold-curing polymer binders FibAm Resin 230+, FibAm Resin 530+, FibAm Resin HT+, FibAm Resin Laminate+ were developed and introduced into ERSs of building structures [16 - 19].

2.2. Experimental studies of the unidirectional carbon filler designed for external reinforcement systems of building structures

In the course of the research undertaking, JSC "Prepreg – MCM" conducted activities aimed at developing domestic reinforcing carbon fillers. Let's analyze the development process and use the unidirectional carbon fabric as an example.

In foreign and domestic literature, materials with a width of up to 400 mm are usually called tapes; the material whose width exceeds 400 mm is called fabric. Thus, the carbon fiber filler, having unidirectional structure, will be called a unidirectional tape. Therefore, the technology was tested, the pilot batch was produced, and the stability of characteristics of prototypes of a carbon fiber filler featuring unidirectional structure was studied. The filler fastened with a thermoplastic mesh was also analyzed.

Unidirectional tapes were produced using a Dornier double rapier loom, modernized for the processing of carbon fibers. Up to five canvases can be produced simultaneously depending on the width of carbon tapes. Since the material being manufactured must have particular physical and mechanical properties, Umatex UMT49-12K-EP carbon filament with a linear density of 760 tex was chosen as the raw material for the warp filament. Its basic physical and mechanical characteristics are provided in Table 2.

Table 2. Physico-mechanical characteristics of carbon filler Umatex UMT49-12K-EP

Raw material	Characteristics	Values
Filament Umatex UMT49-12K-EP 760 tex	Linear density, tex	760
	Fiber density, g/cm^3	1,78
	Mass fraction of finishing agent	0,8 ± 1,5
	Modulus of elasticity, GPa	260
	Breaking tensile stress of filament (elementary), MPa	4900

Glass filament with polymer coating was used as filling yarn; its technical characteristics are provided in Table 3.

Table 3. Technical characteristics of glass filament with thermoplastic coating

Raw material	Characteristic	Value
Glass filament with thermoplastic coating 70 tex	Linear density, tex	87,5
	Mass fraction of polymer in filament, %	50
	Breaking tensile stress of filament, N/decitex	3,5

In the process of manufacturing specimens of unidirectional carbon tapes from UMT49-12K-EP carbon filaments, a double rapier loom with a weaving width of 1700 mm, equipped with a bobbin holder for 1200 bobbins, was used. To produce a 300 mm-wide tape with a warp filament density of 1,5 filaments/cm, 45 carbon fiber bobbins are required. The existing bobbin holder was modified to produce the required unidirectional carbon fiber tape. Filament guides and collectors with ceramic eyes were removed from the bobbin holder, and new ones were installed. Thus, the filament, leaving the bobbin and reaching the feed shaft of the DORNIER weaving machine, had no contact with neighboring filaments and was clearly oriented in space (without torsion). The bobbin holder threading scheme and photograph are shown in Figure 2.

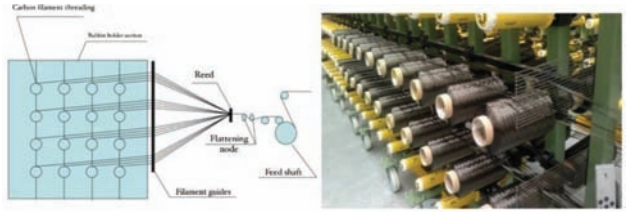

Figure 2. Scheme and photograph of bobbin holder threading

One of the requirements for the properties of a unidirectional tape was the minimum distance between warp filaments. However, this could not be achieved when standard heddles were used (Figure 3a). The main weakness of this type of heddle is the oval shape of the eye. At the moment of full opening of the gap, maximum tension arises in warp filaments, since they come into contact with part of the filament-conducting eye of the heddle. As a result, the carbon yarn changes its shape, and gaps emerge on the tape surface. To eliminate this defect, special heddles were selected that made it possible to maintain the flat structure of the carbon bundle at the moment of peak stresses during gap formation. Special heddles were made with an accuracy of 0,01 mm; they are shown in Figure 3b. The heddle, developed by the authors, has two parallel plates connected by a metal cylinder. Top and bottom cylinders serve to strengthen the structure, since the heddle walls are made of metal 0,3 mm thick. A pair of central cylinders act as a filament guide element. The distance between the heddle walls corresponds to the width of the carbon warp filament.

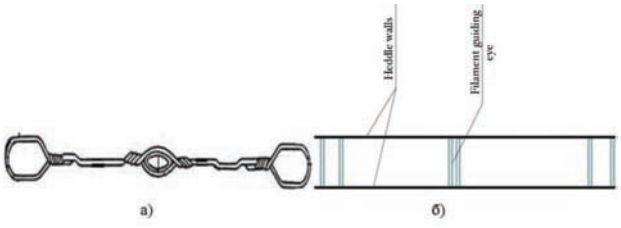

Figure 3. Types of heddles: a) twisted wire heddle; b) special heddle

Heddles are located on heddle frames, strictly parallel to the teeth of the reed. As part of the research, a special reed with a tooth wall thickness of 0,3 mm was designed and manufactured. When standard reeds were used, the fabric had large distances between warp filaments, since the standard version of a reed with a pre-set tooth density per centimeter has a wall thickness of 1,2 mm. The threading of filaments into the heddle of heddle frames and the rear reed is shown in Figure 4.

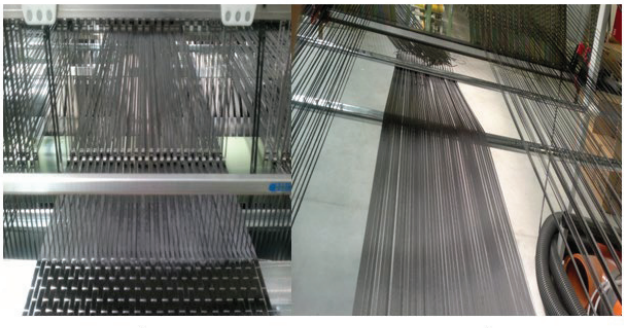

Figure 4. The threading of filaments into the heddle of a heddle frame (a) and the rear reed (b)

These unidirectional carbon tapes are similar to the UOL-300-R type tape. According to the specifications, the yarn filament density of the prototype is 1,2 ± 0,3 filaments/cm. Therefore, when this type of tape was produced, the yarn filament density varied from 1,2 to 0,9 filaments/cm. The yarn filament density of 0,9 reduces the surface density of the tape. The optimal operating parameters are as follows: the machine speed is 120 rpm of the main shaft of the machine; the infrared lamp temperature is 120 °C. The photograph of the carbon tapes, developed by the authors, is shown in Figure 5.

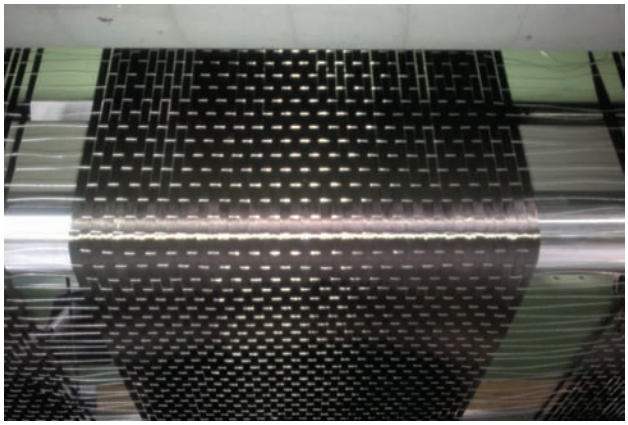

Figure 5. Unidirectional carbon tape St-1105

Based on the research results and experimental studies, reinforcing fillers titled Fibarm Tape 230, Fibarm Tape 530, containing carbon fibers, were developed and implemented for ERS of building structures.

2.3. Technological characteristics of reinforcement and repair of building structures using composite external reinforcement systems

The requirements, applied to the installation of composite ERS, depend on the type of material and raw materials used for its manufacture. Thus, lamellas are PCM, while canvases, tapes and fabrics are raw materials for PCM production. Composite lamellas should be bonded to smooth surfaces. Contact molding using fabrics, canvases and tapes, impregnated directly on the facility being repaired, is possible on variable-geometry (curvilinear) concrete surfaces.

The process of reinforcing the structure with Fibarm Tape canvases, developed by JSC "Prepreg - MCM" is shown in Figure 6. The installation of composite clamps on vertical surfaces is carried out by fixing the canvas in the extreme position, followed by laying, smoothing and rolling along the length. Rolling is done from the middle to the edges. Before gluing, lamellas are arranged on the workbench and thoroughly wiped with a rag moistened with acetone. The 1 – 2 mm layer of the adhesive substance is applied to the prepared concrete surface.

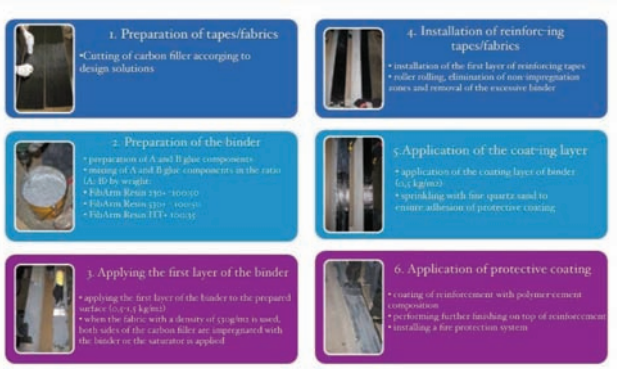

Figure 6. The process of surface reinforcement using Fibarm Tape canvases

This done, an Δ-profile is formed from the adhesive substance on the completely dry lamella surface using a specially manufactured dispensing device (conductor) or trowel; the thickness of the adhesive layer in the middle should be 2 mm, reaching 1 mm towards the edges. The process of surface reinforcement with Fibarm Laminate lamellas is shown in Figures 7 and 8.

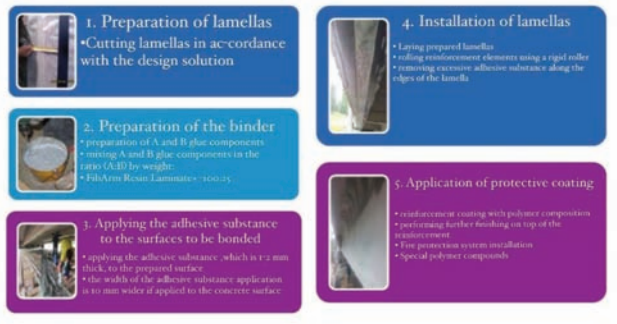

Figure 7. Process of surface reinforcement using Fibarm Laminate lamellas

Figure 8. Installation of Fibarm Laminate lamellas

After applying the adhesive substance, the lamella is laid over the base and rolled with a rigid roller to remove air from the adhesive layer. Excessive adhesive substance is removed with a spatula. In the case of gluing several layers of lamellas, they are preliminarily glued on the workbench, cured during the polymerization period of the adhesive substance, and then the laminated sheet is glued to the base.

3. USING NOVEL COMPOSITE MATERIALS AND EXTERNAL REINFORCEMENT TECHNOLOGIES TO REINFORCE AND REPAIR BUILDING STRUCTURES

These novel materials and technologies are widely used at more than 300 facilities in the Russian Federation and CIS countries [20-25].
During the operation of the building of the History Museum (Moscow), technological and design parameters of the building changed due to new access holes needed for utility pipelines. The strength values of some floor slabs was unacceptably low due to the lack of reinforcement. The deficit of strength was identified as a result of calculations and the survey data. A decision was made to strengthen sections of structures using carbon fiber Fibarm canvases and the cold-curing binder.
The appearance of the structures before the reinforcement is shown in Figure 9.

Figure 9. The appearance of structures of the History Museum building before the reinforcement

The appearance of the structures after the reinfrocement is shown in Figure 10.

Figure 10. The appearance of the reinforced structures of the History Museum building

The load-bearing capacity of the floor slabs was restored as a result of the repair activities aimed at the reinforcement of load-bearing structures with carbon-composite polymer materials.
Another interesting project that involved the use of composite ERS was the reinforcement of hollow-core slabs in the building of the Government House of the Russian Federation. The appearance before the reinforcement activities is shown in Figure 11a; the post-reinforcement appearance is shown in Figure 11 b.
The reinforcement was carried out in accordance with the customized engineering solution. Composite ERS installed on site ensure the design level of loading as well as the safe operation of the building.

а) б)

Figure 11. Structural elements of the building of the Government House of the Russian Federation: a) before reinforcement; b) after reinforcement with composite ERS

4. CONCLUSIONS

Given the results of integrated projects implemented in 2013 – 2023 and focused on the development of new generation PCM production technologies and design solutions for the construction industry, also implemented within the framework of Subprogram 14 “Development of production of composite materials (composites) and products” of the State Program of the Russian Federation titled “Development of the industry and increasing its competitiveness” and others programs, the authors obtained and implemented the following specific results:

- the production of woven (unidirectional and bidirectional) and non-woven materials for ERS with a tensile strength of, at least, 3 GPa and the elastic modulus of 200 GPa, the surface density of 230 - 530 g/m^2, width of 150 - 600 mm, suitable for reinforcing any types of structures (concrete, masonry, metal) was arranged;
- the production of carbon fiber lamellas using the pultrusion method with lamellas having a tensile strength of, at least, 2,9 GPa and the elastic modulus of, at least, 150 GPa was arranged;
- the pilot production of carbon anchor cable with a diameter of 10 - 20 mm and a tensile strength of, at least, 3,7 GPa, and the elastic modulus of, at least, 230 GPa was arranged to ensure the seismic reinforcement;
- the pilot production of two types of carbon meshes (dry and pre-impregnated with polymer compositions) for ERS with a tensile strength of, at least, 2,6 GPa, and the elastic modulus of 180 GPa was arranged;
- the pilot production of cold-curing epoxy binders for impregnation of carbon and hybrid ERS materials with adhesion to concrete, equaling, at least, 3,5 MPa, and glass transition temperature of, at least, 60 °C, was arranged;
- the pilot production of heat-resistant polymer cold-curing binders (glass transition temperature not less than 100 °C) was arranged;
- sets of engineering and design documentation, albums of standard solutions and software for the design and reinforcement of building structures, including those used in seismic zones, by composite ERS, were compiled;
- albums of standard solutions and software for ERS were compiled;
- novel engineering solutions were implemented at more than 300 facilities in Russia and abroad.

REFERENCES

1. **Kalgin A., Fakhratov M., Chulkov V., Chulkova V.** (ed.) (2006) *Proizvodstvo i ispol'zovanie stroitel'nyh materialov: organizac.-antropotehn. nadezhnost'* [Production and use of construction materials: organizational-anthropotechnical reliability]. Moscow: SvR-ARGUS. (in Russian)
2. **Boudenne, A.; Ibos, L.; Candau, Y.; Thomas, S.** *Handbook of Multiphase Polymer Systems*[Wiley: Hoboken] NJ, USA, 2011; Volume 1.
3. **Kalgin A., Fakhratov M., Chulkov V., Chulkova V.** (ed.) (2011) *Proizvodstvo i ispol'zovanie stroitel'nyh materialov, izdelij i sistem* [Production and use of construction materials: organizational-anthropotechnical reliability] Moscow: SvR-ARGUS. (in Russian)
4. Simakov O. (2019) Primenenie v kachestve vneshnego armirovanija zhelezobetonnyh jele-mentov tkanyh setok iz uglerodnyh vo-

lokon [Using woven mesh made of carbon fibers as external reinforcement for reinforced concrete elements]. *Izvestija vysshih uchebnyh zavedenij. Tehnologija tekstil'noj promyshlennosti*, no 3(381), pp. 57-61.

5. **Suleymanov A., Shakirov A.** (2023) Jeksperimental'noe issledovanie naprjazhenno-deformirovannogo sostojanija zhelezobetonnyh balok, usilennyh ugleplastikom [Experimental study of the stress-strain state of reinforced concrete beams reinforced with carbon fiber plastic]. *Stroitel'nye materialy*, no 4, pp. 10-17.doi: 10.31659/0585-430X-2023-812-4-10-17
6. **Mailyan D., Georgiev S.** (2023) K opredeleniju progibov gibkih vnecentrenno szhatyh zhelezobeton-nyh stoek, usilennyh v poperechnom napravlenii kompozitnymi materialami [Deflections of flexible eccentrically compressed reinforced concrete pillars, reinforced with composite materials in the transverse direction]. *Zhelezobetonnye konstrukcii*, vol. 2, no 2, pp. 32-41.doi: 10.22227/2949-1622.2023.2.32-41
7. **Merkulov S., Esipov S., Esipova D**. (2022) Kompozitnye sistemy vneshnego armirovanija zhelezobetonnyh konstrukcij [Composite systems of external reinforcement of reinforced concrete structures]. *Vestnik Belgorodskogo gosudarstvennogo tehnologicheskogo universiteta im. V.G. Shuhova*, no 4, pp. 39-48.doi: 10.34031/2071-7318-2021-7-4-39-48
8. **Simakov O.** (2023) Pereraspredelenie izgibajushhih momentov v perekrytijah s vneshnim armirovaniem [Redistribution of bending moments in floor slabs with external reinforcement]. *Promyshlennoe i grazhdanskoe stroitel'stvo*, no 2, pp. 53-56.doi: 10.33622/0869-7019.2023.02.53-56
9. **Denisova A., Kuzhman E., Shekhovtsov A**. (2023) Vlijanie temperatury na rabotu kompozicionnogo materiala, primenjaemogo pri usilenii zhelezobetonnyh konstrukcij, pri rastjazhenii [The effect of temperature on performance of a composite material used to strengthen reinforced concrete structures under tension]. *Zhilishhnoe stroitel'stvo*, no 5, pp. 46-53.doi: 10.31659/0044-4472-2023-5-46-53
10. **Fedotov M., Budadin O., Kozelskaya S., Ovchinnikov I., Shelemba I.** (2022) Vneshnee armirovanie kompozitnymi materialami i opticheskij monitoring nadezhnosti jekspluatacii stroitel'nyh sooruzhenij [External reinforcement with composite materials and optical monitoring of the reliability of operation of building structures]. *Konstrukcii iz kompozicionnyh materialov*, no 1(165), pp. 57-67.doi: 10.52190/2073-2562_2022_1_57
11. **Fedotov M., Koshman N., Gusev B., Speransky A., Loskutov M., Ovchinnikov I., Bokarev S., Shelemba I., Budadin O., Kozelskaya S.** (2019) Opyt primenenija kompozitnyh sistem vneshnego armirovanija i opticheskogo monitoringa stroitel'nyh sooruzhenij [Experience in the use of composite systems of external reinforcement and optical monitoring of building structures]. *Transportnye sooruzhenija*, vol. 6, no 4, p. 8.doi: 10. 10.15862/09SATS419
12. **Rubin O., Antonov A., Karablin N., Baklykov I.** (2023) Podhod k ocenke sostojanija metallokonstrukcij glavnogo korpusa teplovoj jelektrostancii i predlozhenija po usileniju dlja obespechenija sejsmostojkosti [Approach to assessing the state of metal structures of the main building of a thermal power plant and reinforcement options to ensure seismic resistance]. *Vestnik evrazijskoj nauki*, vol. 15, no 3.
13. **Smerdov D.** (2022) Jeksperimental'nye issledovanija vlijanija temperaturnoj relaksacii i naprjazhenija polimernyh kompozicionnyh materialov, rabotajushhih v sostave izgibaemyh zhelezobetonnyh jelementov, pri dlitel'nom vozdejstvii nagruzok [Experimental studies of the effect of temperature relaxation and stress of polymer composite materials as part of reinforced concrete elements in bending under prolonged exposure to loading]. *Vestnik Tomskogo gosudarstvennogo arhitekturno-*

stroitel'nogo universiteta, vol. 24, no 1, pp. 150-163.doi: 10.31675/1607-1859-2022-24-1-150-163

14. **Gusev B., Budadin O., Fedotov M., Kozelskaya S., Shelemba I.** (2020) Opyt monitoringa tehnicheskogo sostojanija i usilenija povrezhdennyh stroitel'nyh konstrukcij polimernymi kompozicionnymi materialami [Experience in monitoring the technical condition and reinforcement of damaged building structures with polymer composite materials]. *Voprosy oboronnoj tehniki. Nauchno-tehnicheskij sbornik. Serija 15. Kompozicionnye nemetallicheskie materialy v mashinostroenii*, no 3-4, pp. 85-94.
15. **Fedotov M., Budadin O., Kozelskaya S., Ovchinnikov I., Shelemba I.** (2020) Monitoring volokonno-opticheskimi datchikami nadezhnosti jekspluatacii stroitel'nyh konstrukcij s vneshnim kompozitnym armirovaniem [Using fiber-optic sensors to monitor the reliability of operation of building structures with external composite reinforcement], *Kontrol'. Diagnostika,* no 7, pp. 54-64.doi: 10.14489/td.2020.07.pp.054-064
16. **Shmoilov E., Chursova L., Panina N., Grebeneva T.** (2021) Patent № 2772286 C1 Russian Federation, IPC C08L 63/02, C08G 59/56. Cold-curing epoxy composition: № 2021115519.
17. **Shmoilov E., Panina N., Chursova L., Golikov E.** (2019) Patent № 2706661 C1 Russian Federation, IPC C08L 63/00, B32B 27/38. The epoxy binder, the prepreg that it contains, and a product made from it: № 2019114163.
18. **Shmoilov E., Chursova L., Kogan D.** (2019) Patent № 2688608 C1 Russian Federation, IPC C08L 63/00, C08L 79/02, C08K 5/17. Cold-curing epoxy binder for external reinforcement systems: № 2018123955.
19. **Shmoilov E., Chursova L., Panina N**. (2023) Patent № 2791395 C1 Russian Federation, IPC C08L 63/00, C08L 79/02, C08K 5/17. Cold-curing adhesive composition: № 2022129044.
20. **Fedotov M., Shmoilov E., Kozelskaya S.** (2023) *Development of a complex system for reinforcing building structures with carbon composite polymer materials, diagnostics of their quality and evaluation of their service life*. Proceedings of the *Advanced engineering science: Collection of articles of the 14th International Science Forum*, Moscow, May 17, 2023, pp. 292-298.
21. **Spiridon I., Darie R.N., Kangas H.** *Influence of fiber modifications on PLA/fiber composites*. *Behavior to accelerated weathering.* [Compos] Part B Eng. 2016, 92, 19–27.
22. **Liao G., Li Z., Cheng Y., Xu D., Zhu D., Jiang S., Guo J., Chen X., Xu G., Zhu Y.** *Properties of oriented carbon fiber/polyamide 12 composite parts fabricated by fused deposition modeling.* [Mater] Des. 2018, 139, 283–292.
23. **Ma Y., Ueda M., Yokozeki T., Sugahara T., Yang Y., Hamada H.** *A comparative study of the mechanical properties and failure behavior of carbon fiber/epoxy and carbon fiber/polyamide 6 unidirectional composites.* [Compos. Struct] 2017, 160, 89–99.
24. **Sharma M., Rao I.M., Bijwe J.** *Influence of orientation of long fibers in carbon fiber-polyetherimide composites on mechanical and tribological properties.* Wear 2009, 267, 839.
25. **Scaffaro R., Di Bartolo A., Dintcheva N.T.** *Matrix and Filler Recycling of Carbon and Glass Fiber-Reinforced Polymer Composites: A Review.* [Polymers] 2021; 13(21):3817.

СПИСОК ЛИТЕРАТУРЫ

1. **Кальгин, А.А.** Производство и использование строительных материалов : организац.-антропотехн. надежность : учеб. пособие / А.А. Кальгин ; А.А. Кальгин, М.А. Фахратов, В.О. Чулков ; под ред. В.О. Чулкова. – Москва : СвР-

АРГУС, 2006. – 247 с. – (Инфографические основы функциональных систем : ИОФС). – ISBN 5-86949-058-8.
2. **Boudenne, A.; Ibos, L.; Candau, Y.; Thomas, S.** Handbook of Multiphase Polymer Systems // Wiley: Hoboken, NJ, USA, 2011; Volume 1. ISBN 9780470714201.
3. **Кальгин, А.А.** Производство и использование строительных материалов, изделий и систем : учебное пособие/ А.А. Кальгин; А.А. Кальгин, М.А. Фахратов, В.О. Чулков ; под ред. В.О. Чулкова. – Изд. 2-е, перераб. и доп. – Москва : СвР-АГРУС, 2011. – 288 с. – ISBN 978-5-86949-064-3.
4. **Симаков, О.А.** Применение в качестве внешнего армирования железобетонных элементов тканых сеток из углеродных волокон / О.А. Симаков // Известия высших учебных заведений. Технология текстильной промышленности. – 2019. – № 3(381). – С. 57-61.
5. **Сулейманов, А.М.** Экспериментальное исследование напряженно-деформированного состояния железобетонных балок, усиленных углепластиком / А.М. Сулейманов, А.Р. Шакиров // Строительные материалы. – 2023. – № 4. – С. 10-17. – DOI 10.31659/0585-430X-2023-812-4-10-17.
6. **Маилян, Д.Р.** К определению прогибов гибких внецентренно сжатых железобетонных стоек, усиленных в поперечном направлении композитными материалами / Д.Р. Маилян, С.В. Георгиев // Железобетонные конструкции. – 2023. – Т. 2, № 2. – С. 32-41. – DOI 10.22227/2949-1622.2023.2.32-41.
7. **Меркулов, С.И.** Композитные системы внешнего армирования железобетонных конструкций / С.И. Меркулов, С.М. Есипов, Д.В. Есипова // Вестник Белгородского государственного технологического университета им. В.Г. Шухова. – 2022. – № 4. – С. 39-48. – DOI 10.34031/2071-7318-2021-7-4-39-48.
8. **Симаков, О.А.** Перераспределение изгибающих моментов в перекрытиях с внешним армированием / О. А. Симаков // Промышленное и гражданское строительство. – 2023. – № 2. – С. 53-56. – DOI 10.33622/0869-7019.2023.02.53-56.
9. **Денисова, А.Д.** Влияние температуры на работу композиционного материала, применяемого при усилении железобетонных конструкций, при растяжении / А.Д. Денисова, Е.Д. Кужман, А.С. Шеховцов // Жилищное строительство. – 2023. – № 5. – С. 46-53. – DOI 10.31659/0044-4472-2023-5-46-53.
10. Внешнее армирование композитными материалами и оптический мониторинг надежности эксплуатации строительных сооружений (Обзор) / М.Ю. Федотов, О.Н. Будадин, С.О. Козельская, И.Г. Овчинников, И.С. Шелемба // Конструкции из композиционных материалов. – 2022. – № 1(165). – С. 57-67. – DOI 10.52190/2073-2562_2022_1_57.
11. Опыт применения композитных систем внешнего армирования и оптического мониторинга строительных сооружений / М.Ю. Федотов, Н.П. Кошман, Б.В. Гусев, А.А. Сперанский, М.Л. Лоскутов, И.Г. Овчинников, С.А. Бокарев, И.С. Шелемба, О.Н. Будадин, С.О. Козельская // Транспортные сооружения. – 2019. – Т. 6, № 4. – С. 8. – DOI 10. 10.15862/09SATS419.
12. Подход к оценке состояния металлоконструкций главного корпуса тепловой электростанции и предложения по усилению для обеспечения сейсмостойкости / О. Д. Рубин, А. С. Антонов, Н. П. Караблин, И. В. Баклыков // Вестник евразийской науки. – 2023. – Т. 15, № 3.
13. **Смердов, Д.Н.** Экспериментальные исследования влияния температурной релаксации и напряжения полимерных композиционных материалов, работающих в составе изгибаемых железобетонных элементов, при длительном воздействии нагрузок / Д. Н. Смердов // Вестник Томского государственного архитектурно-строительного университета. –

2022. – Т. 24, № 1. – С. 150-163. – DOI 10.31675/1607-1859-2022-24-1-150-163.

14. Опыт мониторинга технического состояния и усиления поврежденных строительных конструкций полимерными композиционными материалами / Б. В. Гусев, О.Н. Будадин, М. Ю. Федотов, С. О. Козельская, И. С. Шелемба // Вопросы оборонной техники. Научно технический сборник. Серия 15. Композиционные неметаллические материалы в машиностроении. – 2020. – Вып. (3-4). – С. 85-94.
15. Мониторинг волоконно-оптическими датчиками надежности эксплуатации строительных конструкций с внешним композитным армированием / М. Ю. Федотов, О. Н. Будадин, С. О. Козельская, И. Г. Овчинников, И. С. Шелемба // Контроль. Диагностика. – 2020. – № 7. – С. 54-64. – DOI 10.14489/td.2020.07.pp.054-064.
16. Патент № 2772286 C1 Российская Федерация, МПК C08L 63/02, C08G 59/56. Эпоксидная композиция холодного отверждения: № 2021115519: заявл. 31.05.2021: опубл. 18.05.2022 / Е. Е. Шмойлов, Л. В. Чурсова, Н. Н. Панина, Т. А. Гребенева; заявитель Акционерное общество «Препрег – Современные Композиционные материалы» (АО «Препрег – СКМ»).
17. Патент № 2706661 C1 Российская Федерация, МПК C08L 63/00, B32B 27/38. Эпоксидное связующее, препрег на его основе и изделие, выполненное из него: № 2019114163: заявл. 13.05.2019: опубл. 19.11.2019 / Е. Е. Шмойлов, Н. Н. Панина, Л. В. Чурсова, Е. И. Голиков; заявитель Акционерное общество «Препрег – Современные Композиционные материалы» (АО «Препрег – СКМ»).
18. Патент № 2688608 C1 Российская Федерация, МПК C08L 63/00, C08L 79/02, C08K 5/17. Эпоксидное связующее холодного отверждения для систем внешнего армирования: № 2018123955: заявл. 02.07.2018: опубл. 21.05.2019 / Е. Е. Шмойлов, Л. В. Чурсова, Д. И. Коган; заявитель Акционерное общество «Препрег – Современные Композиционные материалы» (АО «Препрег – СКМ»).
19. Патент № 2791395 C1 Российская Федерация, МПК C08L 63/00, C08L 79/02, C08K 5/17. Клеевая композиция холодного отверждения: № 2022129044: заявл. 09.11.2022 г.: опубл. 07.03.2023 / Е. Е. Шмойлов, Л. В. Чурсова, Н. Н. Панина; заявитель Акционерное общество «Препрег – Современные Композиционные материалы» (АО «Препрег – СКМ»).
20. **Федотов, М.Ю.** Создание комплексной системы армирования строительных конструкций углекомпозитными полимерными материалами с диагностикой их качества и оценкой ресурса / М. Ю. Федотов, Е. Е. Шмойлов, С. О. Козельская // Перспективные задачи инженерной науки: Сборник статей XIV Международного научного форума, Москва, 17 мая 2023 года. – Москва: ООО «Инженерный центр «Импульс», Федеральное государственное бюджетное образовательное учреждение высшего образования «Российский государственный университет имени А.Н. Косыгина (Технологии. Дизайн. Искусство)», 2023. – С. 292-298.
21. **Spiridon I., Darie R.N., Kangas H.** Influence of fiber modifications on PLA/fiber composites. Be-havior to accelerated weathering // Compos. Part B Eng. 2016, 92, C. 19–27.
22. **Liao G., Li Z., Cheng Y., Xu D., Zhu D., Jiang S., Guo J., Chen X., Xu G., Zhu Y.** Properties of oriented carbon fiber/polyamide 12 composite parts fabricated by fused deposition modeling // Mater. Des. 2018, 139, C. 283–292.
23. **Ma Y., Ueda M., Yokozeki T., Sugahara T., Yang Y., Hamada H.** A comparative study of the mechanical properties and failure behavior of carbon fiber/epoxy and carbon fiber/polyamide 6 unidirectional com-

posites // Compos. Struct. 2017, 160, C. 89–99.
24. **Sharma M., Rao I.M., Bijwe J.** Influence of orientation of long fibers in carbon fiber-polyetherimide composites on mechanical and tribological properties. Wear 2009, 267, c. 839.
25. **Scaffaro R., Di Bartolo A., Dintcheva N.T.** Matrix and Filler Recycling of Carbon and Glass Fiber-Reinforced Polymer Composites: A Review // Polymers. 2021; 13(21):3817, C. 17-20.

Evgeniy Evgenievich Shmoilov, Chief expert, Research and development department, JSC "Prepreg-Modern Composite Materials" (JSC "Prepreg-MCM"), Building 5, 42 Volgogradsky avenue, Moscow, 109316, Russia, e.shmoylov@umatex.ru, +7 916-082-51-38.

Mikhail Yurievich Fedotov, Candidate of Engineering Sciences, Deputy President, All-Russian public organization "Russian Engineering Academy" (RAE), Building 4, 9 Gazetny lane, Moscow, 125009, Russia, fedotovmyu@gmail.com, +7 909-691-12-88.

Igor Aleksandrovich Sharutin, Head of sales in the construction industry, JSC "Prepreg-Modern Composite Materials" (JSC "Prepreg - MCM"), Building 5, 42 Volgogradsky avenue, Moscow, 109316, Russia, i.sharutin@umatex.ru, + 7 495-198-01-23.

Roman Vladimirovich Ilyukhin, Leading design engineer, JSC "Prepreg-Modern Composite Materials" (JSC "Prepreg - MCM"), Building 5, 42 Volgogradsky avenue, Moscow, 109316, Russia, r.ilyukhin@umatex.ru, + 7 495-198-01-23.

Stanislav Aleksandrovich Stepanov, Head of technical support, JSC "Prepreg-Modern Composite Materials" (JSC "Prepreg - MCM"), Building 5, 42 Volgogradsky avenue, Moscow, 109316, Russia, s.stepanov@umatex.ru, + 7 495-198-01-23.

Natalia Nikolaevna Panina, Leading engineer, Research and development department, JSC "Prepreg-Modern Composite Materials" (JSC "Prepreg - MCM"), Building 5, 42 Volgogradsky avenue, Moscow, 109316, Russia, n.panina@umatex.ru, + 7 495-198-01-23.

Lidiya Ivanovna Gurenchuk, Head of textile section, Prepreg-Dubna Limited Liability Company (Prepreg-Dubna LLC), 8 Technologicheskaya Street, Dubna, 141981, Russia, l.gurenchuk@umatex.ru, + 7 495-198-01-23.

Pavel Dmitrievich Kapyrin, Candidate of Engineering Sciences, Associate Professor, Director, Department of Science and Technology, Federal State Budget Educational Institution of Higher Education "Moscow State University of Civil Engineering (National Research University)" (MGSU), 26 Yaroslavskoye Shosse, Moscow, 129337, Russia, Kapyrin@mgsu.ru, +7 495-287-49-14.

Oleg Vasilievich Kabantsev, Doctor of Engineering Sciences, Professor, Director, Department of Research and Technology Projects, Federal State Budget Educational Institution of Higher Education "Moscow State University of Civil Engineering (National Research University)" (MGSU), 26 Yaroslavskoye Shosse, Moscow, 129337, Russia, KabantsevOV@mgsu.ru, +7(495)739-03-14.

Oleg Aleksandrovich Kornev, Managing Director, Science and Research Institute of Experimental Mechanics, Federal State Budget Educational Institution of Higher Education "Moscow State University of Civil Engineering (National Research University)" (MGSU), 26 Yaroslavskoye Shosse, Moscow, 129337, Russia, KornevOA@mgsu.ru, +7 495-287-49-14.

Евгений Евгеньевич Шмойлов, главный эксперт департамента исследований и разработок АО «Препрег-Современные композиционные материалы» (АО «Препрег-СКМ»), корпус 5, дом 42, Волгоградский проспект, Москва, 109316, Россия, e.shmoylov@umatex.ru, +7 916-082-51-38.

Михаил Юрьевич Федотов, к.т.н., заместитель президента, Общероссийская общественная организация «Российская инженерная академия» (РИА), строение 4, дом 9, Газетный пер., Москва, 125009, Россия, fedotovmyu@gmail.com, +7 909-691-12-88.

Игорь Александрович Шарутин, руководитель направления продаж в строительство, АО «Препрег-Современные композиционные материалы» (АО «Препрег-СКМ»), корпус 5, дом 42, Волгоградский проспект, Москва, 109316, Россия, i.sharutin@umatex.ru, + 7(495) 198 01 23.

Роман Владимирович Илюхин, ведущий инженер-конструктор, АО «Препрег-Современные композиционные материалы» (АО «Препрег-СКМ»), корпус 5, дом 42, Волгоградский проспект, Москва, 109316, Россия, r.ilyukhin@umatex.ru, + 7(495) 198 01 23.

Станислав Александрович Степанов, руководитель службы технической поддержки, АО «Препрег-Современные композиционные материалы» (АО «Препрег-СКМ»), корпус 5, дом 42, Волгоградский проспект, Москва, 109316, Россия, s.stepanov@umatex.ru, + 7(495) 198 01 23.

Наталия Николаевна Панина, ведущий инженер департамента исследований и разработок, АО «Препрег-Современные композиционные материалы» (АО «Препрег-СКМ»), корпус 5, дом 42, Волгоградский проспект, Москва, 109316, Россия, n.panina@umatex.ru, + 7(495) 198 01 23.

Лидия Ивановна Гуренчук, начальник текстильного участка, Общество с ограниченной ответственностью «Препрег-Дубна» (ООО «Препрег-Дубна»), д. 8, улица Технологическая, Дубна, 141981, Россия, l.gurenchuk@umatex.ru, + 7(495) 198 01 23.

Павел Дмитриевич Капырин, к.т.н., доцент, начальник Научно-технического управления, Федеральное государственное бюджетное образовательное учреждение высшего образования «Национальный исследовательский Московский государственный строительный университет» (НИУ МГСУ), д. 26, Ярославское шоссе, Москва, 129337, Россия, Kapyrin@mgsu.ru, +7 495-287-49-14.

Олег Васильевич Кабанцев, д.т.н., профессор, директор Дирекции научно-технических проектов, Федеральное государственное бюджетное образовательное учреждение высшего образования «Национальный исследовательский Московский государственный строительный университет» (НИУ МГСУ), д. 26, Ярославское шоссе, Москва, 129337, Россия, KabantsevOV@mgsu.ru, +7 495-739-03-14.

Олег Александрович Корнев, заместитель директора, Научно-исследовательский институт экспериментальной механики, Федеральное государственное бюджетное образовательное учреждение высшего образования «Национальный исследовательский Московский государственный строительный университет» (НИУ МГСУ), д. 26, Ярославское шоссе, Москва, 129337, Россия, KornevOA@mgsu.ru, +7 495-287-49-14.

International Journal for Computational Civil and Structural Engineering, 20(1) 35–45 (2024)

DOI:10.22337/2587-9618-2024-20-1-35-45

ENERGY PROPERTIES OF SYMMETRIC DEFORMABLE SYSTEMS

Leonid Yu. Stupishin, Vladimir L. Mondrus

National Research Moscow State University of Civil Engineering, Moscow, RUSSIA

Abstract: Energy methods for calculating structures, which have become popular for a century, are based on the Lagrange principle and have the meaning of equality of work of external forces and internal forces. Having proved their effectiveness in the overwhelming majority of problems of structural mechanics, they became the dominant approach in formulating the problems of studying solid deformable systems and gave rise to the main methodology for solving problems. As a result, a situation has arisen that the internal potential energy of a deformed body remains insufficiently studied.

The paper develops an approach to the study of the symmetric structure at critical levels of strain energy. The criterion of critical levels of strain energy, based on the concepts of "self-stress" ("self-balance") of a deformable body. Limiting values of the structure strain energy may get by varying the reactions and deflections in the nodal points. The extreme values of forces and displacements of the rods are calculated in matrix form from the values of nodal reactions (displacements).

Methodology for studying the energy properties of a system is shown on the examples of the study of symmetric rod systems without involving the concept of external forces. The technique is based on matrix methods of structural mechanics and the mathematical apparatus of eigenvalue problems. The comparison of structural design and structural analysis solution of structural mechanics tasks by traditional methods and with the proposed methodology is carried out.

Keywords: structural analysis, structural design, matrix methods, strain energy, critical strain energy levels, self-stress, reaction of structures, limit state design

ЭНЕРГЕТИЧЕСКИЕ СВОЙСТВА СИММЕТРИЧНЫХ ДЕФОРМИРУЕМЫХ СИСТЕМ

Л.Ю. Ступишин, В.Л. Мондрус

Национальный исследовательский Московский государственный строительный университет, г. Москва, РОССИЯ

Аннотация. Энергетические методы расчета конструкций, получившие распространение в течение столетия, основаны на принципе Лагранжа и имеют смысл равенства работ внешних и внутренних сил. Доказав свою эффективность в подавляющем большинстве задач строительной механики, они стали доминирующим подходом при постановке задач исследования твердых деформируемых систем и положили начало основной методологии решения задач. В результате возникла ситуация, когда внутренняя потенциальная энергия деформируемого тела остается недостаточно изученной.

В статье развивается подход к исследованию симметричной структуры при критических уровнях энергии деформации. Критерий критических уровней энергии деформации, основанный на понятиях "самонапряжения" ("саморавновесия") деформируемого тела. Предельные значения энергии деформации конструкции можно получить, изменяя реакции и прогибы в узловых точках. Экстремальные значения усилий и перемещений стержней вычисляются в матричной форме из значений узловых реакций (перемещений).

Методика изучения энергетических свойств системы показана на примерах исследования симметричных стержневых систем без привлечения понятия внешних сил. Методика основана на матричных методах строительной механики и математическом аппарате задач на собственные значения. Проведено сравнение решений проектных и поверочных задач строительной механики традиционными методами и по предлагаемой методике.

Ключевые слова: проектные и поверочные задачи строительной механики, матричные методы механики деформируемого тела, критические уровни энергии, самонапряжение, реакция упругой системы, предельное состояние

1. INTRODUCTION

The energetic methods of structural mechanics have proven their effectiveness in the minimum total strain energy form (problem in Lagrange form).Closely connected with the mathematical apparatus of the calculus of variations, they became the basis for obtaining approximate solutions in complex problems of stability and dynamics of structures, as well as solving nonlinear problems of deformation of spatial systems [1-5]. It is difficult to find such an area of structural mechanics where it would be possible to do without variational approaches and variational principles [6-10]. A special place is occupied by numerical methods for studying complex systems operating in the nonlinear stage of deformation [11-16], based on variational formulations of structural mechanics problems [17-24], which served as the basis for the creation of software systems using FEM, MGE and others methods of structural mechanics.

It should be noted that the overwhelming majority of the formulations of the problems mentioned above are based on the Lапrange approach, when the minimum of the total energy of the system leads to the equations of state of the system, which depend on the acting external loads. In this case, one might get the impression that the behavior of the system is completely determined by the magnitude, type and law of changes in the external load.

In a number of works [25,26] it is noted that such an approach does not always make it possible to calculate systems subject to the guiding loads, temperature and similar impacts. The necessity of formulating problems in the form of homogeneous systems of equations is noted, on the basis of which one can then restore the form of a possible external load.

Thus, there is an insufficient study of the properties of the internal potential energy of deformable systems. The hypothesis that any deformable body has levels of critical energy values at which the system can change the form of the law of equilibrium states or a model of the structure, made it possible to obtain a criterion for critical levels of potential energy, which was tested on a number of well-known simple problems of stability and bending of rod systems [27].

This work is devoted to the study of the strain energy of symmetric rod systems.

2. EQUATIONS OF CRITICAL ENERGY OF SYMMETRIC STATICALLY INDETERMINATE SYSTEMS

In [28], the equations of state of a system with lumped parameters at critical energy levels were obtained, written in the matrix form

$$[\mathrm{L}]\left\{\delta\Phi_{\mathrm{k}}^{\mathrm{in}}\right\}=\left[\lambda_{0}^{\mathrm{L}}\right]\left\{\delta\Phi_{\mathrm{k}}^{\mathrm{in}}\right\}, \qquad (1)$$

Here we have introduced the notation for the flexibility matrix $[\mathrm{L}]$ systems and eigenvalue matrices $\left[\lambda_{0}^{\mathrm{L}}\right]$ variations of effort. The eigenvalues $\lambda_{0\mathrm{i}}^{\mathrm{L}}$ are the main values of the flexibility of the system, and the eigenvectors $\left\{\delta\Phi_{\mathrm{k}}^{\mathrm{in}}\right\}$ are the amplitude values of the distribution of self-stress forces. For variations of nodal displacements (system reactions), the relation for the eigenvalues of the flexibility and stiffness matrices is valid

$$[\lambda_{0\mathrm{i}}^{\mathrm{K}}]=[(\lambda_{0\mathrm{i}}^{\mathrm{L}})]^{-1}. \qquad (2)$$

Here $\lambda_{0\mathrm{i}}^{\mathrm{K}}$ are the eigenvalues of the stiffness matrix of the system.

The physical meaning of the derived equations (1), (2) is the state of self-stress in a statically indeterminate system at critical energy levels. The solution of the eigenvalue problem gives the main nodal displacements system and the corresponding vectors of the amplitude values of the nodal reaction forces. To understand the processes of changing the internal potential energy of an elastic rod structure, consider the three-rod system shown in Figure 1.

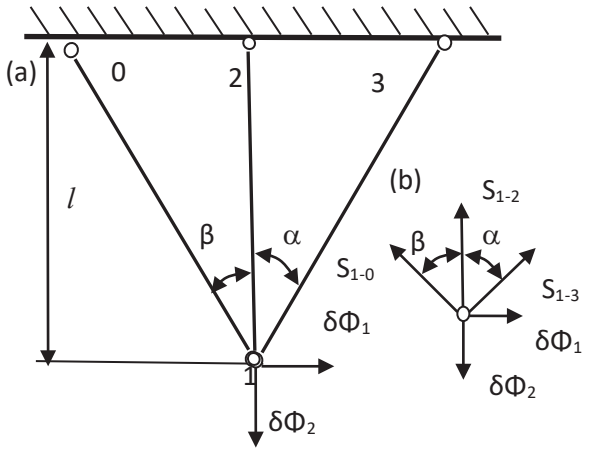

Figure 1. Three-rod system: (a) design model, (b) node 1

The internal potential energy of deformation of the system in matrix form can be represented as

$$2\{U\} = \{\xi\}^{T}[K]\{\xi\} = \{\Phi\}_{in}^{T}[L]\{\Phi\}_{in}. \qquad (3)$$

It is easy to see that the levels of the internal potential energy of deformation are determined by the values of the stiffness (flexibility) matrices of the system. Strain energy at any level we may get multiplying the initial self-stress energy state at constant value. Let structure has elastic initial self-stress energy.

A symmetric redundant system has the same angles $\alpha = \beta = \pi/4$ of inclined rods and stiffness values $\eta_i = EA/E_iA_i$ $\eta_l = \eta_2 = \eta_3 = 1$.

Due to the symmetry of the structure, the flexibility matrix is diagonal, which indicates that the eigenvalues of the flexibility matrix are located on the main diagonal.

$$[L] = \frac{l}{EA}\begin{vmatrix} 1.414 & 0 \\ 0 & 0.5858 \end{vmatrix}. \qquad (4)$$

It is easy to write out the eigenvectors of the external compliance matrix

$$[\vartheta^{L}] = \begin{vmatrix} 1 & 0 \\ 0 & 1 \end{vmatrix}, \qquad (5)$$

that is, the initially selected axes are the principal axes of the system's ultimate energy. The stiffness matrix of the system is also diagonal and containing the eigenvalues

$$[K] = \frac{EA}{l}\begin{vmatrix} 0.7072 & 0 \\ 0 & 1.707 \end{vmatrix}, \qquad (6)$$

with their corresponding eigenvectors

$$[\vartheta^{K}] = \begin{vmatrix} 1 & 0 \\ 0 & 1 \end{vmatrix}. \qquad (7)$$

The ellipsoid of limiting displacements has a maximum radius equal to the first eigenvalue of the flexibility matrix $\delta_{11} = \lambda^{L}_{max} = 1.414l/EA$, (see Figure 2).

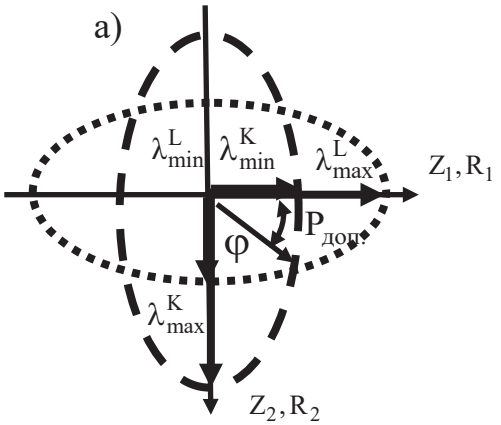

Figure 2. Ellipses of external flexibility (points), and external rigidity (dotted line) of the system for the first state of self-stress

The minimum radius of flexibility is located along the second vector of variations of external forces $\delta_{22} = \lambda^{L}_{min} = 0.5858l/EA$. Only two states of self-tension of the system correspond to these values.

For the stiffness matrix, we have an ellipse of the limiting stiffness of the structure with the maximum radius $k_{22} = \lambda^{K}_{max} = 1.707EA/l$ located along the second direction of the reactive forces of the system, and the minimum radius

$k_{11} = \lambda^{K}_{min} = 0.7072EA/l$ located along the first direction (see Figure 2). As we can see, the axes of ellipses are mutually perpendicular.

To demonstrate the physical meaning of the results obtained, we represent the system in the form of an absolutely rigid disk, and we refer the elastic properties of the system to the support rods (see Fig. 3).

The flexibility and stiffness vectors shown in node 1 represent the maximum and minimum values of flexibility (stiffness) of the structure.

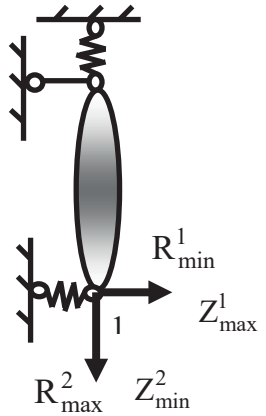

Figure 3. The physical meaning of the eigenvalues of the stiffness and flexibility matrices

In the matrix expressions of the force method and the displacement method, which are consequences of the expressions for the stationarity of the total energy of system (1), we have

$$[K]\{\xi\} = \{\Phi\}_{ex}; [L]\{\Phi\}_{in} = \{\xi\}. \tag{8}$$

For the symmetric structures that we are considering, the principal vectors coincide with the originally selected axes and we can write that

$$\begin{aligned} [\lambda^{K}_{min,\,max}]\{\vartheta^{K}\} &= \{R_{min,\,max}\} = -\{\Phi_{ex}\}; \\ [\lambda^{L}_{max,\,min}]\{\vartheta^{L}\} &= \{Z_{max,\,min}\} = -\{\xi\}. \end{aligned} \tag{9}$$

In this case, the vectors $\{R_{min}\}$ and $\{Z_{max}\}$ are mutually perpendicular, which makes it possible to assess the values of the limiting stiffness and flexibility of the system, as well as to compare with the acting load. If we assume that the loss of the bearing capacity by the system occurs from the loss of strength according to the first hypothesis, then in the direction of minimum stiffness (1 axis) the reaction of the system according to (9)

$$[\lambda^{K}_{min}]\{\vartheta^{K}\} = \{R_{min}\} = \sigma_1 A. \tag{10}$$

Then the displacement of the system in the direction of axis 2 will have the maximum possible value

$$\{Z_{max}\} = \{\vartheta^{K}\} = \frac{\sigma_1 l}{0.7071E}. \tag{11}$$

Substituting the resulting value in the expression for maximum flexibility

$$[\lambda^{L}_{max}]\{\vartheta^{L}\} = \{Z_{max}\} = \frac{\sigma_1 l}{0.7071E}, \tag{12}$$

we get an expression for the minimum force in a rod located along the first axis

$$\{R_{min}\} = \{\vartheta^{L}\} = \frac{\sigma_1 A}{0.7071 \times 1.414} = \sigma_1 A. \tag{13}$$

This confirms the correctness of our assumption about the reciprocity of the values of the reactions and displacements of the system in the main directions, as well as the results known from the theory of eigenvalue problems. Let us show what types of stress states of the system are realized for the obtained flexibility (stiffness) matrix of the system. By varying the values of the reaction of the system in the direction of the first axis indicated in Figure 3, we obtain the internal forces in the rods of the structure for the first state of self-stress. So, for the first direction of the unit vector of the internal reaction $\delta\Phi^{1}_{in} = 1$ according to

$$[S] = [B]^{-1}[A]^{T}[L]\{\delta\Phi_{in}\}, \tag{14}$$

we get forces

$$S_{1-2} = 0,\ S_{1-0} = -S_{1-3} = 0.7071. \qquad (15)$$

That is, the first state of self-stress corresponds to the case of compression of the right inclined bar and the tension left one. There is no force in the vertical middle bar. The values obtained from single impacts have the dimension [unit strength]. For the second state of self-stress, in the case of variation of system nodal reaction in the direction of the second eigenvector $\delta\Phi_{in}^{2} = 1$, we have the following distribution of efforts

$$S_{1-2} = -0.5858,\ S_{1-0} = S_{1-3} = 0.2929, \qquad (16)$$

when two inclined rods are tensioned with the same force, and the vertical one is compressed. Note that the obtained results (15), (16) completely coincide with the values of the efforts given in [29] for solving a similar problem. Here it should be noted that the sign of the efforts is important only for choosing the type of limiting state: loss of strength during tension (compression) or stability of the rod.

The limiting value of internal efforts $S_{1-0}^{cr} = 0,7071P^{cr}$ obtained at the first stage (until the moment the link is turned off from work) is selected in accordance with the formulation of the limiting state. If this is the limiting state in the elastic stage of the work of a brittle material, then $P_e^{cr} = A\sigma_I$, where the limiting value of the load is the product of the cross-sectional area of the bar A and the equivalent stress according to the first hypothesis of strength σ_I. Then the condition for the onset of the limiting state will have the form

$$\sigma_{1-0}^{cr} = \frac{S_{1-0}^{cr}}{A} = 0.7071\sigma_1. \qquad (17)$$

If elastic - plastic work of the material is allowed, then the limiting stress σ_t, and the value of the limiting load $P_t^{cr} = A\sigma_t$. Similarly, we do for the cases of bar stability, crack theory and other types of stress state. If we now compare the value of a single external load applied in the main direction of the maximum flexibility of the system (minimum stiffness), then the condition for the equality of its minimum reactive stiffness of the structure gives

$$\{\bar{F}^{cr}\} = -[A]\{S_{max}\}. \qquad (18)$$

Then, taking into account (9), we obtain

$$\{\bar{F}^{cr}\} = -\{\delta\Phi_{in}^{max}\} = -[\lambda_{max}^{K}]\{\vartheta^{K}\}. \qquad (19)$$

Since the vector $\{\vartheta^{K}\}$ coincides in direction with the vector of the unit load $\{\bar{F}^{cr}\}$, the difference between the maximum response of the system and the external load that can be applied in the node in the direction of maximum flexibility of the structure, is equal to the first eigenvalue (6) of the flexibility matrix.

Since the forces in the rods from a unit external load, and the forces corresponding to the vector of maximum flexibility of the system, are applied towards each other, then the internal forces in the rods of the system will differ by the value of their eigenvalues for the specified loading options. Obviously, the result obtained will be valid when symmetric systems are loaded with a load of any size. Therefore, the ellipses of the critical values of flexibility and stiffness can serve as limit curves that limit the permissible values of external loads in the nodes of the structure. The condition of the permissible external load follows from the geometric relationships of the ellipse (see Fig. 2)

$$P_{доп.} \le \frac{R_{max}R_{min}}{\sqrt{R_{max}^{2}(\sin\varphi)^{2} + R_{min}^{2}(\cos\varphi)^{2}}}. \qquad (20)$$

Similarly, you can determine the value of the limiting displacement of node 2. In the considered example, the value of the largest force in

the structure bar from the external limiting nodal unit load is determined by (19). The maximum value of the reaction in direction 1 reaches $k_{11} = \lambda^{K}_{min} = 0.7072EA/l$. It is easy to check that for, $\{\delta\Phi in\} = 1$

$$[S] = [C]\ [A]^{T}[L][\lambda^{K}]\left\{\begin{matrix}\vartheta^{K}_{max,}\\ min\end{matrix}\right\} \qquad (21)$$

we get the same values of efforts presented in (15), (16). That is, with the magnitude of the external load, which coincides with the magnitude of the reaction of the system, the structure does not have a ultimate factor of safety. Note that A.R. Rzhanitsyn gave an example of a system that did not have a safety factor, and it was symmetric [29].

3. EXAMPLES OF SOLUTION OF CONSTRUCTION MECHANICS PROBLEMS FOR SYMMETRIC SYSTEMS

Example 3.1. Structural analysis problem.
For the system shown in Figure 1, with geometric parameters $\alpha = \beta = \pi/4$, $l = 2\text{m}$, identical areas of the circular cross-section of rods ($A = 0.785*10^{-4}\text{m}^2$), diameter $d = 10\text{mm}$, modulus of elasticity $E = 2{,}1*10^{5}\text{MPa}$, and yield strength $\sigma_t = 240$ MPa, check the load-carrying capacity of the system, loaded by $P_1 = 10\text{кN},\ P_2 = 20\text{кN}$.

Solution 3.1.1 Comparison of external load and system response to variations in external influences.

We find the resultant external forces and the angle of its inclination to the horizontal axis, as well as the normalized value of the load.

$$P = \sqrt{20^2 + 10^2} = 22.36\text{кN},$$
$$\text{tg}\varphi = 20/10 = 2, \varphi = 63.43^{0},\ \overline{P} = P/22.36 = 1.0.$$

We calculate the maximum and minimum radii of gyration of the ellipse of the system's reaction according to the method described above.

We get, $R_{max} = 1.707EA\vartheta^{K}/l$, $R_{min} = 0.7072EA\vartheta^{\kappa}/l$. Recall that due to the symmetry of the problem, we have $\vartheta^{K} = \sigma_t l/0.7071E$. Then the values of the reactive components of the system $R_{max} = 2.414\sigma_t A, R_{min} = \sigma_t A$.

We find the dimensionless value of the permissible load according to (14), per unit of movement of the system node, and having the same direction as the given load

$$\overline{P}_{доп.} = 2.205\,.\,\overline{P}_{доп.} = \frac{P_{доп.}}{\sigma_t A}$$

Then the greatest value of the reactive nodal force created by the system in the direction of the acting external load will be $P_{доп.} = \sigma_t A_1 = 38.622\text{кN}$. The value of the resulting specified external load $P = 22.36\text{кN}$, which is less than the permissible value obtained by (20). The system will not lose its bearing capacity from a given load. According to the set task, this means that no yield stress will arise in any of the rods of the system. The structure has a margin of safety for the load (or residual resource of the bearing capacity), and can be subjected to the optimization procedure according to the criteria: equal strength of the rods, minimum weight at a given load, etc.

Solution 3.1.2. Comparison of the forces in the rods from a given normalized load and the forces derived from self-tension of the system.

We normalize the external load by the resulting value and obtain the vector of external influences in the form

$$\left\{\overline{P}\right\} = \{P\}/22.36 = \{0.4472, 0.8945\}^{T}.$$

We determine the internal forces in the rods of the system from the normalized vector of the external load by the formula

$$\left[S_P\right] = -\left[B\right]^{-1}\left[A\right]^T\left[L\right]\overline{\{P\}}. \quad (22)$$

We obtain the distribution of efforts from the dimensionless components of the external load vector in the form

$$\left[\overline{S}^P\right] = \begin{vmatrix} 0.5782 \\ 0.524 \\ -0.05423 \end{vmatrix}. \quad (23)$$

Find the vector of internal efforts from the nodal reaction vector of the system

$$\left[\overline{S}_{\delta\Phi_{in}}\right] = \begin{vmatrix} 1.0 \\ 0.5858 \\ -0.4141 \end{vmatrix}. \quad (24)$$

From the results obtained, it follows that the force in the 0-1 rod from the external load is less than the force from self-stress in the same rod $\overline{S}^P_{0-1} \succ \overline{S}^{\delta\Phi_{in}}_{0-1}$. Therefore, the specified bar should not lose strength from a given load. Compared efforts can be presented in dimensional units. Internal force from external load in the rod 0-1

$$S^P_{0-1} = 0.5782 \times P = 12.93\text{кN}.$$

The magnitude of the force in the same rod from the nodal reaction of the system

$$S^{\delta\Phi_{in}}_{0-1} = \sigma_t A = 18.84\text{кN}.$$

The permissible maximum value of the force in the rod from the value of the reaction of the system is greater than the force from the given load by 5.91кN.

Solution 3.1.3. Comparison of stresses in rods from a given load and allowable stresses (design resistances) according to the traditional method.

According to the algorithm of matrix structural mechanics, according to the formula

$$\left[S\right] = -\left[C\right]\left[A\right]^T\left[L\right]\{P\}. \quad (25)$$

Here is $\left[C\right]$ - the matrix of internal flexibility; $\left[A\right]$ - static matrix; $\left[L\right]$ - is the flexibility matrix of the system, $\{P\} = \{10;20\}(\text{kN})$ - is the load vector.

Determine internal forces in rods, structures (in kN)

$$\left[S\right] = \begin{vmatrix} 12.93 \\ 11.72 \\ -1.213 \end{vmatrix}. \quad (26)$$

$$\sigma^{cr}_{1-0} = \frac{S^{cr}_{1-0}}{A} = 164.7\text{MPa}, \quad (27)$$

which is less than the yield stress of the rod material. That is, the rod, and therefore the system, will not lose the non-existing ability.

Example 3.2. Structural design problem

For the system shown in Figure 1, with geometrical parameters, $\alpha = \beta = \pi/4$, $l = 2\text{m}$, modulus of elasticity $E=2.1*10^5\text{MPa}$, and yield point $\sigma_t = 240\text{ MPa}$, select the area of a rod of circular cross-section from a given load $P_1 = 10\text{кN}$, $P_2 = 20\text{кN}$.

Solution 3.2.1. Traditional method of strength of materials.

Based on the results obtained in Section Solution 3.3, we obtain from expression (23)

$$A = \frac{S^{cr}_{1-0}}{\sigma_t} = 0.5388*10^{-4}\text{m}^2. \quad (38)$$

We get the diameter of the rod $d = 8.3\text{mm}$.

Solution 3.2.2. The use of forces in the rods from the normalized values of the load.

For the obtained value of the forces in the rods (23), we find the cross-sectional area

$$A = \frac{S^{cr}_{1-0}}{\sigma_t} = 0.5388*10^{-4}\text{m}^2 \quad (39)$$

4. THE CONCLUSIONS

The study of the strain energy of deformable systems shows the possibilities of new formula-

tions of problems in structural mechanics, based on the concept of "self-stress" or "self-balance" of a structure. Bringing the stiffness properties of the system to characteristic nodes and then varying the nodal reactions of the structure or nodal displacements makes it possible to construct ellipses of restrictions on possible displacements (nodal reactions) acting on the structure. The study of the limiting values of the strain energy of deformation leads to problems on the eigenvalues for the stiffness (flexibility) matrices of the structure, which makes it possible to assess the limiting possibilities of perceiving external influences before determining the stresses in the elements of the system. The solved examples of structural design and structural analysis tasks of structural mechanics show coincidence of the results with the tasks solved by the classical method.

REFERENCES

1. **Abovsky N.P., Andreev N.P., Deruga A.P**. (1978) Variatsionnye prinsipy teorii uprugosti i teorii obolochek [Variational principles of elasticity theory and shell theory]. Moscow: Nauka. (in Russian)
2. **Berdichevsky V.L.** (2009) Variational principles of continuum mechanics. Springer-Verlag Berlin Heidelberg. doi: 10.1007/978-3-540-88467-5
3. **Pelliciari M., Sirotti S., Tarantino A.M.** (2023) A strain energy function for large deformations of compressible elastomers. Journal of the Mechanics and Physics of Solids. 175.doi:10.1016/j.jmps.2023.105308
4. **Vashizu K.** Variational methods in elasticity and plasticity. Pergamon press, 1982.
5. **Aggarwala A., Jensenb B.S., Pantd S., Chung-Hao Lee** (2023) Strain energy density as a Gaussian process and its utilization in stochastic finite element analysis: Application to planar soft tissues. Computer Methods in Applied Mechanics and Engineering. 404, 115812 doi:10.1016/j.cma.2022.115812
6. **Lantsosh K.** (1965) Variatsionnye prinsipy mechaniki [Variational principles of mechanics]. Moscow: Mir. (in Russian)
7. **Michlin S.G.** (1966) Chislennaya realizatsiya variatsionnych metodov [Numerical implementation of variational methods]. Moscow: Nauka. (in Russian)
8. **Mosolov P.P., Myasnikov V.P**. (1971) Variatsionnye metody v teorii techenii zestko-vyazko-plasticheskih sred [Variational methods in the theory of flow of rigid-viscous-plastic media]. Moscow: MGU. (in Russian)
9. **Prager V.** (1969) Variatsionnye prinsipy lineynoy staticheskoy teorii uprugosti pri razryvnyh deformatsiyah i napryazeniyah [Variational principles of linear static theory of elasticity under breaking deformations and stresses]. №5 ,117. (in Russian)
10. **Reyssner A.** (1961) O nekotoryh variatsionnyh teoremah uprugosti [Some variational theorems of the theory of elasticity]. - Moscow: AN SSSR. (in Russian)
11. **Reddy J.N.** Energy Principles and Variational Methods in Applied Mechanics. John Wiley & Sons, 2002.
12. **Rozin L.A.** (1978) Variatsionnye postanovki zadach dlya uprugich system [Variational problem statements for elastic systems]. - Leningrad: LGU. (in Russian)
13. **Zolotov A.B., Akimov P.A., Sidorov B.N., Mozgaleva M.L.** (2008) Matematicheskie metody v stroitelnoy mehanike (s osnovami teorii obobshennyh funktsiy) [Mathematical methods of structural mechanics (with the basics of the theory of generalized functions)]. Moscow: ASV. (in Russian)
14. **Zolotov A.B., Akimov P.A., Sidorov B.N., Mozgaleva M.L.** (2010) Diskretnokontinualnye metody rascheta soorusheniy [Discrete-Continuous Methods for Structural Analysis]. Moscow: Arhitektura-S. (in Russian)
15. **Renaud A., Heuzéb T., Stainier L.** (2020) The discontinuous Galerkin material point method for variational hyperelastic–plastic solids. Computer Methods in Applied Me-

chanics and Engineering, Vol.365. doi: 10.1016/j.cma.2020.112987
16. **Nairn J.A., Hammerquist C.C., Smith G.D.** (2020) New material point method contact algorithms for improved accuracy, large-deformation problems, and proper null-space filtering. Computer Methods in Applied Mechanics and Engineering, Vol.362. doi: 10.1016/j.cma.2020.112859
17. **Coombs W.M., Augarde C.E., Brennan A.G., Brown M.J., Charlton T.J., Knappett J.A., Motlagh Y.G., Wang L**. (2020) On Lagrangian mechanics and the implicit material point method for large deformation elasto-plasticity. ComputerMethods in Applied Mechanics and Engineering. Vol.358. doi:10.1016/j.cma.2019.112622
18. **Portillo D., Oesterle B., Thierer R., Bischoff M., Romero I.** (2020) Structural models based on 3D constitutive laws: Variational structure and numerical solution. Computer Methods in Applied Mechanics and Engineering. ComputerMethods in Applied Mechanics and Engineering. Vol. 362. doi: 10.1016/j.cma.2020.112872
19. **Wang X., Xu Q., Atluri S.N.** (2019) Combination of the variational iteration method and numerical algorithms for nonlinear problems. Applied Mathematical Modelling, Vol.79. doi: 10.1016/j.apm.2019.10.034
20. **Samaniego E., Anitescu C., Nguyen-Thanh V.M., Guo H., Hamdia R., Zhuang X., Rabczuk K.** (2020) An energy approach to the solution of partial differential equations in computational mechanics via machine learning: Concepts, implementation and applications. Computer Methods in Applied Mechanics and Engineering, Vol.362. doi: 10.1016/j.cma.2019.112790
21. **Ba K., Gakwaya A.** (2018) Thermomechanical total Lagrangian SPH formulation for solid mechanics in large deformation problems. Computer Methods in Applied Mechanics and Engineering, Vol. 342. doi: 10.1016/j.cma.2018.07.038
22. **Bai L., Wadee M.A., Köllner A., Yang J.** (2021) Variational modelling of local–global mode interaction in long rectangular hollow section struts with Ramberg–Osgood type material nonlinearity. International Journal of Mechanical Sciences. doi: 10.1016/j.ijmecsci.2021.106691
23. **J.N. Reddy** (2017) Energy Principles and Variational Methods in Applied Mechanics. Wiley.
24. **Yang S., Shi W., Chen Z., Qian C., Yang C., Hang L.** (2019) Composite mechanics and energy method based stiffness prediction model for composite leaf springs. Mechanics Based Design of Structures and Machines, Vol. 47, Issue 3. doi: 10.1080/15397734.2018.1559738
25. **Alfutov N.A.** (1991) Osnovy rascheta na ustoichivost uprugih system [Basics of calculating the stability of elastic systems]. Moscow: Mashinostroenie. (in Russian)
26. **Bryan G.H.** (1891) On the Stability of a Plane Plate Under Thrusts in Its Own Plane, with Applications to the 'Buckling' of the Sides of a Ship//Proc. London Math. Soc. Vol. 22
27. **Stupishin L.U.** (2014) Variational criteria for critical levels of internal energy of a deformable solid. applied mechanics and materials. Vol. 578-579. pp 1584-1587. doi: 10.4028/www.scientific.net/AMM.578-579.1584
28. **Stupishin L.Yu.** (2018) Predelnoe sostoyanie ctroitelnykh konstruktsiy i kriticheskie urovni energii [Structural Limit State and Critical Energy Levels]. Promyshlennoe i grazhdanskoe stroitelstvo [Industrial and civil construction]. No 10. Pp. 102-106. (in Russian)
29. **Rzhanitsin A.R.** (1954) Raschet sooruzheniy s uchetom plasticheskikh svoistv materialov [Calculation of structures taking into account the plastic properties of materials]. Moscow: Gos. izd. lit. po stroit. i arkhit. (in Russian)
30. **Stupishin L.Yu., Moshkevich M.L.** (2021) Zadacha ob opredelenii «slabogo zvena» v konstruksii na osnove kriteriya kriticheskih urovney energii [The problem of determining the «weak link» based on the internal energy critical levels of the construction] /

Izvestiya vuzov. Stroitelstvo [«News of Higher Educational Institutions. Construction»]. №2. 11-23 p. doi: 10.32683/0536-1052-2021-746-2-11-23

СПИСОК ЛИТЕРАТУРЫ

1. **Абовский Н.П., Андреев Н.П., Деруга А.П.** Вариационные принципы теории упругости и теории оболочек. М.: Наука, 1978. - 287 с.
2. **Бердичевский В.Л**. Вариационные принципы механики сплошной среды. - М: Наука, 1983,- 448 с.
3. **Pelliciari M., Sirotti S., Tarantino A.M.** A strain energy function for large deformations of compressible elastomers// Journal of the Mechanics and Physics of Solids. Vol.175, 2023. doi: 10.1016/j.jmps.2023.105308
4. **Васидзу К.** Вариационные методы в теории упругости и пластичности. - М.: Мир, 1987.- 546 с.
5. **Aggarwala A., Jensenb B.S., Pantd S., Chung-Hao Lee**. Strain energy density as a Gaussian process and its utilization in stochastic finite element analysis: Application to planar soft tissues// Computer Methods in Applied Mechanics and Engineering. 2023, Vol. 404, 115812 doi: 10.1016/j.cma.2022.115812
6. **Ланцош К.** Вариационные принципы механики. - М.: Мир, 1965. - 408 с.
7. **Михлин С.Г.** Численная реализация вариационных методов. - М.: Наука, 1966. - 432 с.
8. **Мосолов П.П., Мясников В.П.** Вариационные методы в теории течений жёстко-вязко-пластических сред. - М.: МГУ, 1971. - 114 с.
9. **Прагер В.** Вариационные принципы линейной статической теории упругости при разрывных смещениях, деформациях и напряжениях. В сб. пер. “Механика”, 1969, №5 (117). с.139-144
10. **Рейсснер Э**. О некоторых вариационных теоремах упругости. - В кн.: Проблемы механики сплошной среды.-М.: Изд-во АН СССР, 1961. - с. 326 - 377.
11. **Розин Л.А.** Вариационные постановки задач для упругих систем. - Л.: Изд-во ЛГУ, 1978. - 232 с.
12. **Тонти Е.** Вариационные принципы в теории упругости.: В сб. перев. “Механика”, 1969, № 6 (117). - с. 124-138.
13. **Золотов А.Б., Акимов П.А., Сидоров В.Н., Мозгалева М.Л.** Математические методы в строительной механике (с основами теории обобщенных функций). М.: Издательство АСВ, 2008. - 336 с.
14. **Золотов А.Б., Акимов П.А., Сидоров В.Н., Мозгалева М.Л.** Дискретноконтинуальные методы расчета сооружений. М.: Издательство «Архитектура - С», 2010. - 336 с.
15. **Renaud A., Heuzéb T., Stainier L.** The discontinuous Galerkin material point method for variational hyperelastic–plastic solids// Computer Methods in Applied Mechanics and Engineering, Vol. 365, 2020. doi: 10.1016/j.cma.2020.112987
16. **Nairn J.A., Hammerquist C.C., Smith G.D.** New material point method contact algorithms for improved accuracy, large-deformation problems, and proper null-space filtering// Computer Methods in Applied Mechanics and Engineering Vol. 362, 2020. doi: 10.1016/j.cma.2020.112859
17. **Coombs W.M., Augarde C.E., Brennan A.G., Brown M.J., Charlton T.J., Knappett J.A., Motlagh Y.G., Wang L.** On Lagrangian mechanics and the implicit material point method for large deformation elasto-plasticity. ComputerMethods in Applied Mechanics and Engineering. Vol. 358, 2020. doi: 10.1016/j.cma.2019.112622
18. **Portillo D., Oesterle B., Thierer R., Bischoff M., Romero I.** Structural models based on 3D constitutive laws: Variational structure and numerical solution. Computer Methods in Applied Mechanics and Engineering// ComputerMethods in Applied Mechanics and Engineering. Vol. 362, 2020. doi: 10.1016/j.cma.2020.112872
19. **Wang X., Xu Q., Atluri S.N**. Combination of the variational iteration method and numeri-

cal algorithms for nonlinear problems// Applied Mathematical Modelling, Vol. 79, 2019. Pp. 243-259. doi: 10.1016/j.apm.2019.10.034
20. **Samaniego E., Anitescu C., Nguyen-Thanh V.M., Guo H., Hamdia R., Zhuang X., Rabczuk K.** An energy approach to the solution of partial differential equations in computational mechanics via machine learning: Concepts, implementation and applications// Computer Methods in Applied Mechanics and Engineering, Vol.362, 2020. doi: 10.1016/j.cma.2019.112790
21. **Ba K., Gakwaya A**. Thermomechanical total Lagrangian SPH formulation for solid mechanics in large deformation problems// Computer Methods in Applied Mechanics and Engineering, Vol. 342, 2018. doi: 10.1016/j.cma.2018.07.038
22. **Bai L., Wadee M.A., Köllner A., Yang J.** Variational modelling of local–global mode interaction in long rectangular hollow section struts with Ramberg–Osgood type material nonlinearity// International Journal of Mechanical Sciences, 2021. doi: 10.1016/j.ijmecsci.2021.106691
23. **J.N. Reddy** Energy Principles and Variational Methods in Applied Mechanics. Wiley, 2017. P. 760
24. **Yang S., ShiW., Chen Z., Qian C., Yang C., Hang L**. Composite mechanics and energy method based stiffness prediction model for composite leaf springs// Mechanics Based Design of Structures and Machines, Vol. 47, Issue 3, 2019. doi: 10.1080/15397734.2018.1559738
25. **Алфутов Н.А.** Основы расчёта на устойчивость упругих систем. - М.: Машиностроение, 1991.- 336 с.
26. **Bryan G.H.,** On the Stability of a Plane Plate Under Thrusts in Its Own Plane, with Applications to the ‘Buckling’ of the Sides of a Ship//Proc. London Math. Soc., 1891. Vol. 22
27. **Ступишин Л.Ю**. Вариационный критерий критических уровней внутренней энергии деформируемого тела // Промышленное и гражданское строительство. 2011, №8, С. 21-23.
28. **Ступишин Л.Ю.** Предельные состояния конструкций и критические уровни энергии// Промышленное и гражданское строительство. 2018. №10. С. 102-107
29. **Ржаницын А.Р.** Расчет сооружений с учетом пластических свойств материалов. - М.: Госстройиздат, 1954. - 288 с.
30. **Ступишин Л.Ю., Мошкевич М.Л.** Задача об определении «слабого звена» в конструкции на основе критерия критических уровней энергии// Известия вузов. Строительство. №2, 2021. С. 11-23. doi: 10.32683/0536-1052-2021-746-2-11-23

Leonid Yulianovich Stupishin - Doctor of Technical Sciences, Professor, Professor of the Department of Construction and Theoretical Mechanics, Institute of Industrial and Civil Engineering, National Research Moscow State Construction University (NIU MSCU). 405, 26, Yaroslavskoe Shosse, Moscow, 129337, Russia. stupishinlyu@mgsu.ru, +7 (495) 287-49-14 ext. 3074

Ступишин Леонид Юлианович – д.т.н., профессор, профессор кафедры строительной и теоретической механики, института Промышленного и гражданского строительства, Национальный Исследовательский Московский Государственный Строительный Университет (НИУ МГСУ). 405, 26, Ярославское шоссе, Москва, 129337, Россия. stupishinlyu@mgsu.ru, +7 (495) 287-49-14 доб. 3074

Mondrus Vladimir Lvovich - Doctor of Technical Sciences, Professor, Corresponding Member of RAASN, Head of the Department of Structural and Theoretical Mechanics, Institute of Industrial and Civil Engineering, National Research Moscow State Construction University (NIU MSCU). 405, 26, Yaroslavskoe Shosse, Moscow, 129337, Россия.mondrusvl@mgsu.ru, +7 (495) 287-49-14 ext. 3074

Мондрус Владимир Львович – д.т.н., профессор, член корр. РААСН, зав. каф. строительной и теоретической механики, институт Промышленного и гражданского строительства, Национальный Исследовательский Московский Государственный Строительный Университет (НИУ МГСУ). 405, 26, Ярославское шоссе, Москва, 129337, Россия. E-mail: mondrusvl@mgsu.ru, +7 (495) 287-49-14 доб. 3074

DOI:10.22337/2587-9618-2024-20-1-46-56

ANALYTICAL APPROACH TO DETERMINE LONGITUDINAL DEFORMATION OF THE EXISTING PRECAST TUNNEL DURING CONSTRUCTION OF A FULL-LENGTH EXCAVATION PIT

Nguyen Trong Tam [1]***, Nguyen Van Hung*** [2]

[1] Ho Chi Minh City University of Transport, Ho Chi Minh City, VIETNAM
[2] University of Engineering and Technology (VNU-UET), Hanoi, VIETNAM

Abstract: In the realm of urban construction employing excavation techniques, safeguarding existing underground structures from detrimental consequences arising from surface construction operations poses a formidable challenge. The reduction of loads due to excavation activities can induce unintended responses, potentially jeopardizing subterranean infrastructure, particularly high-safety-demanding structures like Tunnel Boring Machine (TBM) tunnels. This article introduces an uncomplicated method for ascertaining the axial displacement of TBM tunnels amidst concurrent surface excavation activities. Primarily, the approach entails the identification of stress variations encountered during soil excavation at the tunnel face. Subsequently, employing the solutions derived for the determination of tunnel deformation subjected to concentrated loads, the deformation incurred by the tunnel due to alterations in excavation-induced stress is quantified. The analytical outcomes are meticulously juxtaposed against results generated from a three-dimensional computational model. The comparative analysis demonstrates that the displacement values and axial deviations calculated using the proposed analytical method exhibit only marginal disparities of 4,3% and 1%, respectively, when compared to those obtained through finite element analysis. This study underscores the efficient predictive capabilities of the analytical method in assessing tunnel deformations, enabling a preliminary estimation of critical parameters associated with the excavation pit. These findings have significant implications for mitigating adverse impacts on existing subterranean infrastructure in densely populated urban areas.

Keywords: existing tunnel, TBM tunnel longitudinal deformation, analytical approach, excavation pit settlement, full-length

АНАЛИТИЧЕСКИЙ ПОДХОД К ОПРЕДЕЛЕНИЮ ПРОДОЛЬНОГО СМЕЩЕНИЯ СУЩЕСТВУЮЩЕГО СБОРНОГО ТОННЕЛЯ ПРИ ВЫЕМКЕ КОТЛОВАНА ПО ВСЕЙ ДЛИНЕ

Там Н.Ч. [1]***, Хунг Н.В.*** [2]

[1] Хошиминский университет транспорта, г. Хошимин, ВЬЕТНАМ
[2] Инженерно-технологический университет (VNU-UET), г. Ханой, ВЬЕТНАМ

Анотация: При проведении земляных работ в условиях городской застройки защита существующих подземных сооружений от пагубных последствий, возникающих в результате наземных строительных работ, представляет собой сложную задачу. Снижение нагрузок в результате земляных работ может вызвать непредвиденные реакции, потенциально ставя под угрозу подземную инфраструктуру, особенно конструкции с высокими требованиями к безопасности, такие как сборные тоннели (TBM). В данной статье представлен простой метод определения осевого смещения тоннелей TBM при создании котлована над тоннелем. Прежде всего, этот подход предполагает выявление изменения напряжений, возникающего во время выемки котлована над тоннелем. Впоследствии, используя решения, полученные для определения деформации тоннеля, подвергающегося сосредоточенным нагрузкам, количественно определяется деформация тоннеля вследствие изменения напряжений, вызванного выемкой грунта. Аналитические результаты тщательно сопоставляются с результатами, полученными на основе трехмерной вычислительной модели. Сравнительные результаты показывает, что значения смещения и осевые отклонения, рассчитанные с использованием предложенного аналитического метода,

демонстрируют лишь незначительные расхождения в 4,3% и 1% соответственно по сравнению со значениями, полученными с помощью конечно-элементного анализа. Это исследование подчеркивает эффективные прогностические возможности аналитического метода при оценке деформаций тоннеля, что позволяет предварительно оценить критические параметры работ по выемке котлована. Эти результаты имеют важное значение для смягчения негативного воздействия на существующую подземную инфраструктуру в густонаселенных городских районах.

Ключевые слова: существующий сборный тоннель, продольное смещение тоннеля TBM, аналитическое решение, осадка котлована, по всей длине

1. INTRODUCTION

In recent times, there has been a rapid surge in construction demand in Vietnam, particularly in urban areas. Major cities have initiated the deployment of their first underground railway systems to cater to the increasing mobility needs of the populace. With a growing population and escalating transportation requirements, the expansion and development of underground railway networks within urban centers have become a top priority. Moreover, due to space constraints within cities and the trend towards developing compact urban clusters around subway stations, there has been a significant increase in the construction of commercial buildings and transportation infrastructure near subway lines. The continuous development of urban transportation infrastructure has also contributed to this phenomenon. This has led to situations where construction activities must take place in close proximity and at different elevations to intersect with the subway tunnel system.

During the construction of excavation pits above tunnels, changes in load due to excavation activities can have significant and even damaging effects on underground tunnels. A notable example is documented in the Pachio project in Taiwan [1], where the construction of a nearby building caused damage to the TBM (Tunnel Boring Machine) tunnel lining. Therefore, assessing tunnel deformation and predicting tunnel behavior when subjected to changes in surface loads is crucial, particularly in the context of today's large cities.

The behavior of existing tunnels below has attracted the attention of many researchers and has been approached through various methods. Among these methods are monitoring methods [2], physical modeling methods [3,4], numerical methods [5,6,7,8,9], and analytical methods [10,11,12].

Among these methods, conducting field experiments or using centrifuge machines has the drawback of long cycles and high costs. The utilization of finite element software methods can model complex intersection structures and depict tunnel-terrain interactions. However, it demands expenses for commercial software and expertise in handling intricate models. With such models, it consumes a significant amount of time and requires high-performance computers.

An analytical approach is a fast and cost-effective method to predict the deformation of tunnels subjected to surface excavation. This can be considered as a suitable approach in the early stages of project design and construction. In the published studies, the tunnel within the terrain is simplified into a problem of a beam on an elastic foundation, employing either the Euler-Bernoulli or Timoshenko beam models on a Winkler or Pasternak foundation model. In this paper, the authors present an analytical approach, with the tunnel modeled using the Euler-Bernoulli beam, and the surrounding soil modeled using a Winkler foundation model. For comparison, the analytical results will be compared with a 3D finite element model based on data from the urban railway line No.1 in Ho Chi Minh City.

2. DEFORMATION PROCESS OF TUNNELS DUE TO FOUNDATION EXCAVATION

Before excavation, the interaction between the tunnel and the subsurface is stable, and the tunnel is in a state of force equilibrium, as shown in Fig. 1a. When excavating the soil above the tunnel, the stress state of the subsurface changes, affecting the structure of the tunnel below. Vertical excavation-induced loading results in the uplift of the soil beneath the excavation pit and an upward displacement of the tunnel below due to a reduction in the overlying soil pressure. The lateral stress on both sides of the tunnel is increased due to the confining effect of the soil. The influence of the excavation-induced loading on the overlying soil pressure of the tunnel is reduced, and the cross-sectional shape of the tunnel appears as a vertically elongated ellipsoid, as shown in Fig. 1b.

3. ANALYTICAL APPROACH

In the analytical approach, several assumptions are made to simplify the problem:1. The soil environment is considered as a linearly elastic, isotropic, and homogeneous medium; 2. The tunnel is treated as a beam on an elastic foundation (1D problem), without considering deformations within the cross-section, and it is assumed to have infinite length.

3.1. Load acting on the Tunnel lining

After excavation, an uplift pressure, p(x), directed upward, is generated at the bottom of the excavation pit. p(x) represents the change in soil load removed per unit area. In the case of a full-length excavation pit, the 3D environmental problem becomes a 2D deformation problem (Figure 2) with a uniform distributed load, p0, within the segment 2a, corresponding to the boundary conditions:

$$p(x)=\begin{cases} -p_0, & |x|<a \\ 0, & |x|>0 \end{cases} \tag{1}$$

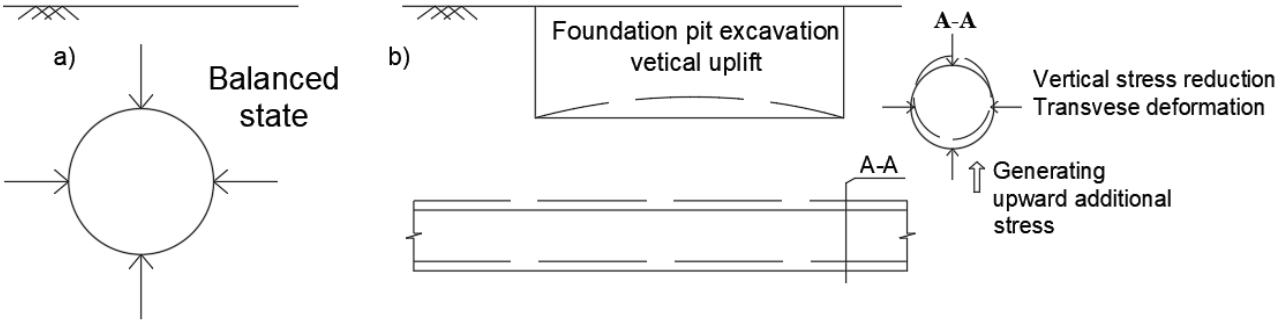

Figure 1. a) Pre-Excavation balanced State; (b) Changes in Stress-Strain State during Excavation

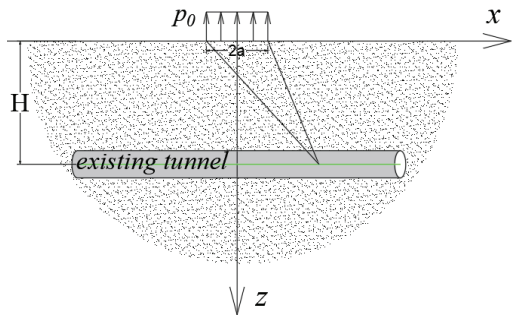

Figure 2. Force Distribution in a homogeneous elastic half-space

The problem of a uniformly distributed pressure on an infinite half-space surface was solved by Sneddon using Fourier transforms in 1951 [13], with the stress distribution determined as:

$$\sigma_{xx} = -\frac{p_0}{\pi}\left(\begin{array}{l}\arctan\left(\frac{x+a}{z}\right)-\arctan\left(\frac{x-a}{z}\right)\\ -\frac{(x+a)z}{(x+a)^2+z^2}+\frac{(x-a)z}{(x-a)^2+z^2}\end{array}\right)$$

$$\sigma_{zz} = -\frac{p_0}{\pi}\left(\begin{array}{l}\arctan\left(\frac{x+a}{z}\right)-\arctan\left(\frac{x-a}{z}\right)\\ +\frac{(x+a)z}{(x+a)^2+z^2}-\frac{(x-a)z}{(x-a)^2+z^2}\end{array}\right) \quad (2)$$

$$\sigma_{xz} = -\frac{p_0}{\pi}\left(\frac{z^2}{(x+a)^2+z^2}-\frac{z^2}{(x-a)^2+z^2}\right)$$

In this problem, the influence of the tunnel on stress generation, as well as the longitudinal and shear stresses within the tunnel, are neglected. In this case, the vertical stress at a depth H, induced by the distributed load placed at the bottom of the excavation pit in an upward direction, is determined by the following formula:

$$\left[\sigma_{zz}(x)\right]_{z=H} = -\frac{\gamma_0 H_0}{\pi}\left(\begin{array}{l}\arctan\left(\frac{x+a}{H-H_0}\right)-\arctan\left(\frac{x-a}{H-H_0}\right)\\ +\frac{(x+a)(H-H_0)}{(x+a)^2+(H-H_0)^2}-\frac{(x-a)(H-H_0)}{(x-a)^2+(H-H_0)^2}\end{array}\right) \quad (3)$$

where: γ_0- the unit weight of the soil layer within the excavation pit; H_0- the distance from the bottom of the excavation pit to the ground surface; H- the distance from the existing tunnel axis to the ground surface.

3.2. Tunnel deformation equation

The existing tunnel is considered as an Euler-Bernoulli beam resting on a Winkler foundation model. The Winkler foundation model is regarded as a one-dimensional spring, with individual springs acting independently of each other. The differential equation for the beam on the elastic foundation [11] is expressed as:

$$EI_{eq}\frac{d^4w(x)}{dx^4}+KDw(x)=D\sigma_{zz}(x) \quad (5)$$

where: D- the outer diameter of the existing tunnel; E- the elastic modulus of the tunnel material; I_{eq}- the equivalent inertial moment of the existing tunnel accounting for the influence of longitudinal connections in the tunnel; K- the subgrade coefficient of the surrounding soil environment; w(x)- the displacement of the tunnel axis, $\sigma_{zz}(x)$- the vertical stress acting on the tunnel. The equation (5) is solved through the solution of the homogeneous equation:

$$EI_{eq}\frac{d^4w(x)}{dx^4}+KDw(x)=0 \quad (6)$$

Due to the symmetric distribution of the load applied to the tunnel through the excavation pit, the calculation can be simplified by considering only a portion of $x\geq 0$. With the condition as x approaches $+\infty$, w=0, the homogeneous solution of Eq. (6) takes the following form:

$$w(x)=e^{-\beta x}\left(C_1\cos\beta x+C_2\sin\beta x\right) \quad for \quad x\geq 0 \quad (7)$$

where: $\beta=\sqrt[4]{\frac{KD}{4EI_{eq}}}$

To analyze the impact of excavation above the tunnel below, the tunnel with its concentrated load on its Winkler foundation is considered initially. The total vertical stress, P, is simplified to act on the neutral axis of the tunnel, and it can then be directly applied to the foundation as a concentrated load, as illustrated in Fig. 3.

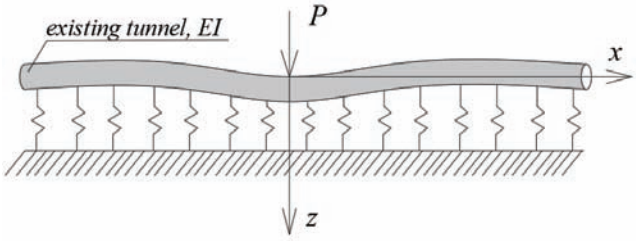

Figure 3. The tunnel on an elastic foundation is subjected to the action of a concentrated load

By applying boundary conditions for the case of a concentrated load: shear force Q = -PD/2 and angular deflection w' = 0 at x=0, we can derive the deflection equation of the tunnel:

$$w(x)=\frac{PD}{8EI\beta^3}e^{-\beta|x|}\left(\cos\beta|x|+\sin\beta|x|\right) \quad (8)$$

Once we obtain the deflection of the tunnel under the influence of the concentrated load, we can use this result to deduce the deformation of the existing tunnel under a uniformly distributed load. As depicted in Fig. 4, the load q(ξ)dξ placed at the position ξ, based on Eq. (8), the derivative of the deflection dw(x) at any position x within the tunnel can be determined through a coordinate shift as follows:

$$dw(x)=\frac{q(\xi)D}{8EI_{eq}\beta^3}e^{-\beta|x-\xi|}\left(\cos\beta|x-\xi|+\sin\beta|x-\xi|\right)d\xi \quad (9)$$

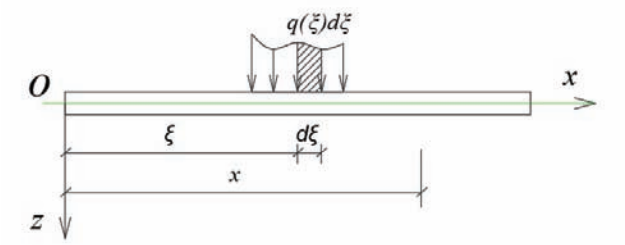

Figure 4. A uniformly distributed load acts on the beam

Based on Eq. (9), the deformation of the tunnel caused by excavation within the range (x1, x2) is determined:

$$w(x)=\int_{x_1}^{x_2}\frac{\sigma_{zz}(\xi)D}{8EI_{eq}\beta^3}e^{-\beta|x-\xi|}\left(\cos\beta|x-\xi|+\sin\beta|x-\xi|\right)d\xi \quad (10)$$

According to Eq. (10), the deflection of the existing tunnel due to excavation above is determined as follows:

$$\varphi(x)=\frac{dw(x)}{dx}=-\int_{x_1}^{x_2}\mathrm{sgn}(x-\xi)\frac{\sigma_{zz}(\xi)D}{4EI_{eq}\beta^2}e^{-\beta|x-\xi|}\sin\beta|x-\xi|d\xi \quad (11)$$

where: $\mathrm{sgn}(x-\xi)=\begin{cases}1 & for\ x-\xi\geq 0\\ -1 & for\ x-\xi<0\end{cases}$

Considering the problem of full-length excavation pit, the displacement and axial deflection of the tunnel are determined as follows:

$$w(x)=\int_{-\infty}^{\infty}\frac{\sigma_{zz}(\xi)D}{8EI_{eq}\beta^3}e^{-\beta|x-\xi|}\left(\cos\beta|x-\xi|+\sin\beta|x-\xi|\right)d\xi \quad (12)$$

$$\varphi(x)=\frac{dw(x)}{dx}=-\int_{-\infty}^{\infty}\mathrm{sgn}(x-\xi)\frac{\sigma_{zz}(\xi)D}{4EI_{eq}\beta^2}e^{-\beta|x-\xi|}\sin\beta|x-\xi|d\xi \quad (13)$$

The convolution integrals Eq. (12) and Eq. (13) for determining displacement and angular deflection will be implemented in MATLAB with a sufficiently large integration range. Typically, the region of significant influence when excavating a pit is about 5 times the width of the excavation pit, so the integration limits for the displacement Eq. (12) and angular deflection Eq. (13) of the tunnel axis will be taken from -10a to 10a.

3.5. Determine the parameters

The deformation behavior of the tunnel below is influenced by the interaction between geological layers and the structural capacity of the existing tunnel to resist deformation. Therefore, determining the relevant parameters needs special attention, such as the flexural stiffness EI, reflecting the deformation resistance of the assembled tunnel, and the subgrade coefficient K, determining the level of foundation settlement.

3.5.1. Equivalent Flexural Stiffness of the Assembled Metro Tunnel Lining

Due to the segmented tunnel connections spaced 1,2 or 1,5 meters apart in the longitudinal direction, the overall flexural stiffness of the shield tunnel is significantly lower compared to a continuous concrete pipe structure. Therefore, some authors have proposed the concept of equivalent flexural stiffness in the longitudinal direction of the shield tunnel. Liao [14] concluded that the approximate equivalent flexural stiffness in

the longitudinal direction of a shield tunnel is about 1/5 to 1/7 compared to the flexural stiffness of a continuous tunnel, which has been verified and is consistent with on-site tests. Therefore, the equivalent flexural stiffness in the longitudinal direction EI_{eq} in this paper can be calculated as follows:

$$EI_{eq} = \frac{E_c}{5 \sim 7}\frac{\pi\left(D^4 - d^4\right)}{64} \tag{16}$$

where *Ec* is the Young's modulus of shield tunnel segments; *D* is the outer diameter of the shield tunnel; and *d* is the inner diameter of the shield tunnel.

3.5.2. Subgrade Modulus coefficient

Determining the parameter of the subgrade modulus coefficient is complex and affected by the size and distribution of the foundation pressure, soil compressibility, buried depth, field test conditions and other factors. For deep shield tunnels, this paper estimates the subgrade modulus coefficient k from an empirical formula in the reference literature [15].

$$K = \frac{1,3E_s}{B\left(1-\mu^2\right)}\sqrt[12]{\frac{E_s B^4}{EI}} \tag{17}$$

where E_s is the elastic modulus of the soil, μ is Poisson's ratio, *B* is the width of the beam section (*B*=*D* in this paper), and *EI* is equal to EI_{eq}.

Then, the influence of the embedment depth was quantified by Yu et al. [16], where the following coefficient η was proposed:

$$\eta = \begin{cases} 2,18 & H/D \le 0,5 \\ 1 + \dfrac{1}{1,7H/D} & H/D > 0,5 \end{cases} \tag{18}$$

where H is the buried depth of the existing tunnel in this paper.

Thus, the calculation formula of *K* is updated as follows:

$$K = \frac{1,3E_s}{\eta D\left(1-\mu^2\right)}\sqrt[12]{\frac{E_s D^4}{EI}} \tag{19}$$

4. RESULTS AND DISCUSSION

In order to provide visual insights from the analytical results obtained, the author's team considered an example from a real project in Ho Chi Minh City and compared it with the results from a 3D finite element model.

4.1 Case study

The Ho Chi Minh City Urban Railway Line 1, with a total length of 19,7 km, consists of 2,6 km underground and 17,1 km elevated tracks. The underground section includes two bored shield tunnels: The Eastbound (EB) and the Westbound (WB) tunnels, constructed using a pressure-balanced Tunnel Boring Machine (TBM).

According to the geological survey results from the Urban Railway Line 1 Ben Thanh - Suoi Tien project, hydrogeological data used in the model were obtained from experiments conducted at borehole U-175 (km 1+553), located approximately 2 meters along the tunnel alignment of the TBM tunnel. Through analysis, the soil layers were categorized into three basic types: Fill, Alluvial Soil, and Flood Deposit Soil. More specifically, the layers at the intersection area consist of five main soil layers: Fill, AC2, AS1, AS2, DC. The distribution of these layers is shown in Fig. 5, with the TBM tunnel situated within layer 3-AS1.

Geological and hydrogeological data were derived from the geological reports of the Metro railway line, as summarized in Table 1. The intersection point of the underground drainage system project and the TBM tunnel Line 1 is located at km 1+555 (according to the urban railway system's alignment). The relevant parameters related to the tunnel lining are presented in Table 2.

Table 1. Properties of soils

Parameter	Layer				
	Fill	AC2	AS1	AS2	DC
E (kPa)	10000	3000	12500	37500	136000
ν	0,3	0,3	0,3	0,3	0,3
γ (kN/m^3)	19	16,5	20,5	20,5	21
K_0	0,577	0,8	0,5	0,455	0,5
γ_{sat} (kN/m^3)	19	16,5	20,5	20,5	21
k (m/s)	1x10^{-6}	1x10^{-9}	2x10^{-5}	2x10^{-5}	1x10^{-8}
c (kPa)	10	0	0	0	170
φ (°)	25	24	30	33	35

Table 2. Parameters for tunnel lining

Parameter	Tunnel lining
Tunnel Inner Diameter, D_{int} (m)	6,05
Tunnel lining thickness (m)	0,3
Tunnel center line position, H (m)	11
Equivalent Elastic Modulus, E* (kPa)	7,2x10^6
Poisson's Ratio, ν	0,2
Bulk Density, γ (kN/m^3)	24

The values **E*** in the table are equivalent values, indicating the reduction in the flexural stiffness of the shield tunnel in the model.

The excavation pit has corresponding dimensions: width 2a = 4,68m; depth of the pit: H_0 = 1,6m; the pit is located in the Fill surface soil layer, γ_0 = 19 kN/m3.

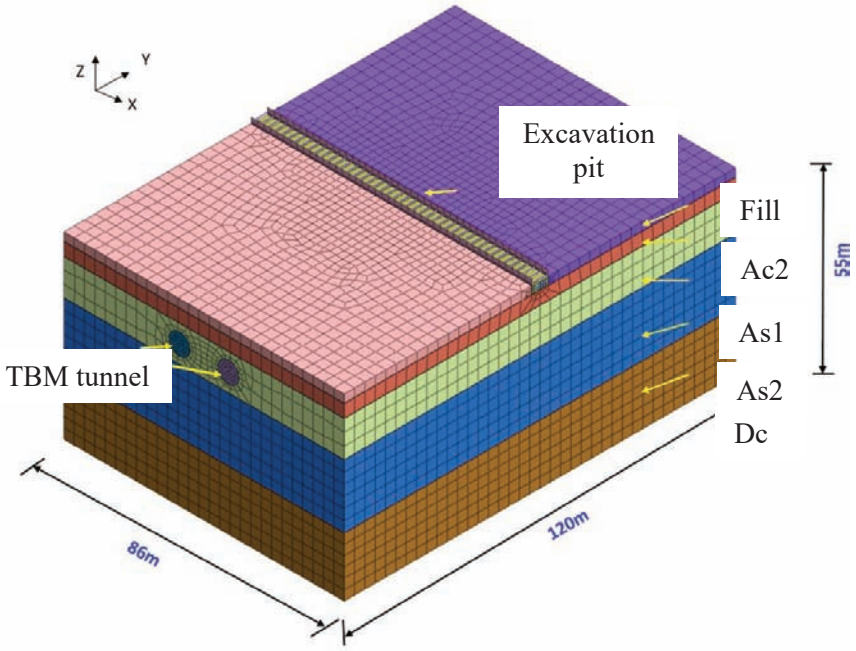

Figure 5. Dimensions of the 3D Model

The value of uniformly distributed load due to the process of unloading the soil mass in the pit is: p0= γ_0 *H_0 = 30,4 (kPa).

4.2 Finite element model

Using the finite element method based on the MIDAS GTS software platform, with soil layers modeled using the Mohr-Coulomb model with Hexadetrol elements, the tunnel lining is simulated as a thick plate. Interface elements are used to model the interaction between the soil and the tunnel lining, with a reduction factor Rinter=0,67. The model dimensions are shown in Figure 5 [7]. The displacement of the tunnel axis is determined by the average of the displacements at the top and bottom of the tunnel.

4.3 Results of analysis and discussion

After performing calculations using the MATLAB software with the input data considered in section 4.1, the vertical stress distribution values are shown in Fig. 6. The load applied at the corresponding floor is p = -30,4 kPa, and the maximum stress value at the tunnel axis position is $(\sigma_{zz})max$ = -9,68 kPa.

The displacement of the tunnel axis is shown in Fig. 7, with the maximum displacement value of the tunnel axis by analytical method being 4,6 mm, while according to the finite element method, it is 4,4 mm. The displacement value of the tunnel axis from model is determined by the average value of the displacement at the tunnel crown and the displacement at the tunnel invert.

The vertical deflection angle of the tunnel axis is shown in Fig. 8, with the maximum deflection angle by the analytical method being 0,165 ‰, and by the finite element method, it is 0,178‰. The corresponding bending point for the analytical method is located about 16 meters away from the excavation center, while according to the finite element method, it is approximately 10 meters away.

4.4 Discussion

The displacement value of the tunnel axis is greater by approximately 4,3% according to the analytical method compared to the finite element method (FEM), and the deformation zone according to the analytical method is larger. The area of influence affecting the displacement of the tunnel axis extends about 40 meters (approximately 10 times the width of the excavation) on either side. Beyond this 40-meter range, the displacement value becomes negligible.

The deflection angle along the tunnel axis is nearly the same for both methods, differing by only 1%. However, the location of the bending point differs by approximately 40% between the two methods, with the analytical method indicating a point farther from the excavation site than the FEM.

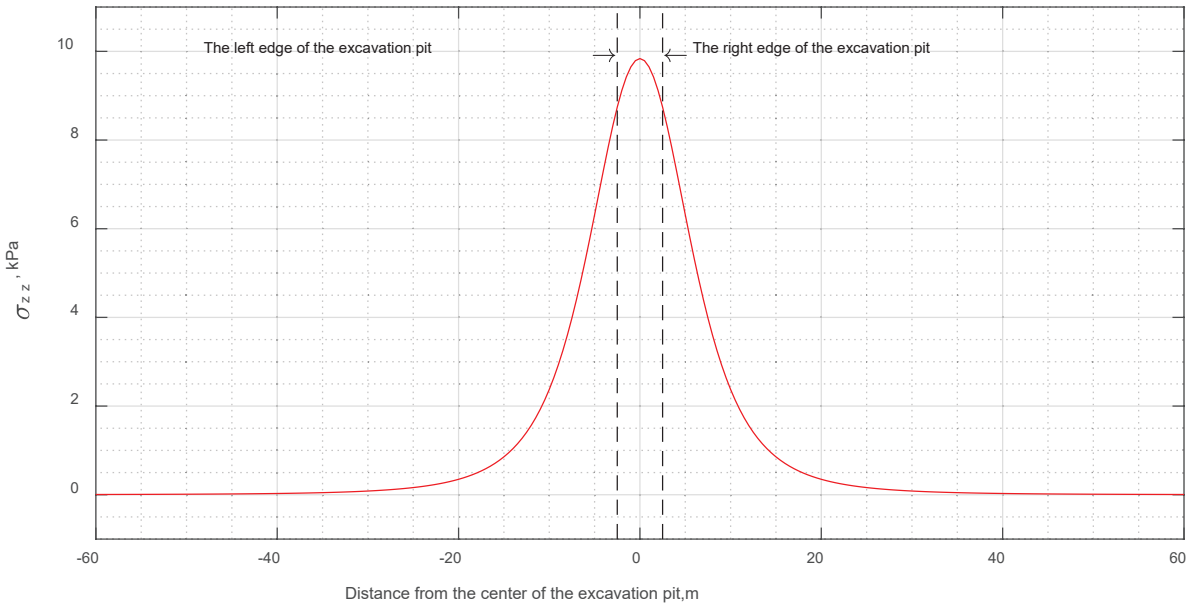

Figure 6. Vertical Stress Distribution

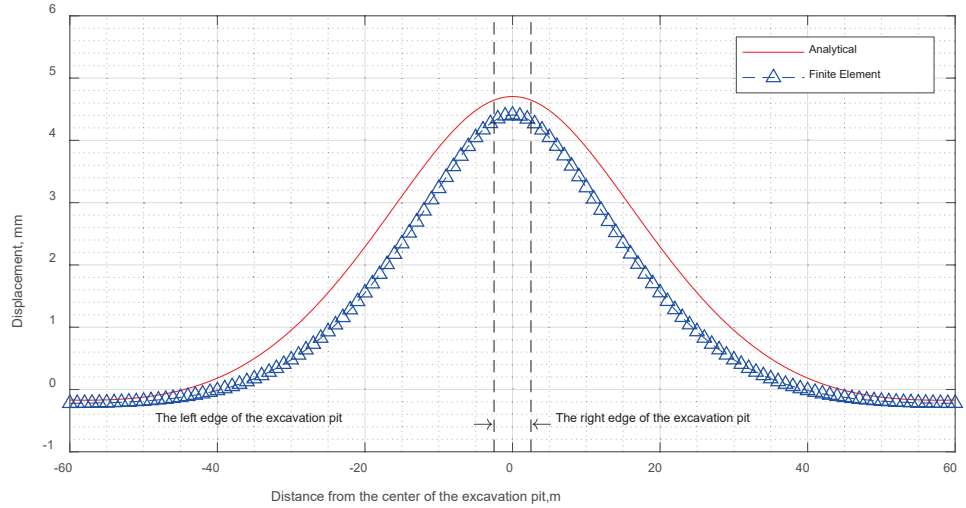

Figure 7. Displacement of the Tunnel Axis

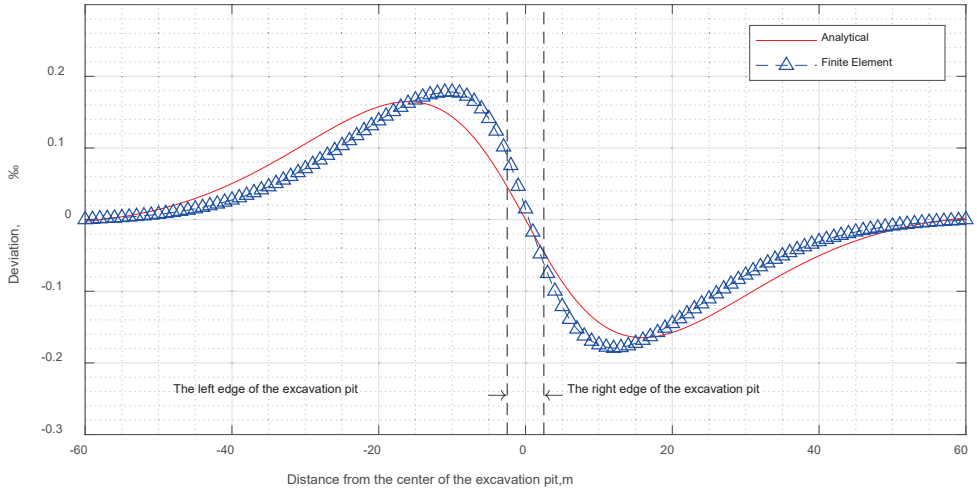

Figure 8. Vertical Deflection Angle of the Tunnel Axis

From the analysis of these results, it is observed that the analytical method provides a higher safety margin in terms of displacement. This can be explained by the following reasons: (1) The soil model does not consider the sliding interaction between layers (two-coefficient soil model), (2) The influence of different soil layers is not accounted for in the model, affecting the foundation coefficient determination.

5. CONCLUSIONS

The analytical approach to determine the displacement of the tunnel axis during the construction of full-length underground culverts is a practical problem with initial evaluation significance and serves monitoring purposes during the culvert construction process.

The analytical approach simplifies the process of determining the displacement and deflection of the tunnel axis, making it straightforward and efficient, without the need for complex tools such as the finite element method. However, the results obtained through the analytical method tend to be more conservative compared to the finite element method because they do not consider all influencing factors, such as the foundation stiffness and the two-coefficient soil model.

Therefore, further research is needed to address the problem while taking into account factors

that influence the soil stiffness, such as the two-coefficient soil model and various soil layers.

REFERENCES

1. **Chang C.T., Sun C.W., Duann S.W., Hwang R.N.** (2001). Response of a Taipei rapid transit system (TRTS) tunnel to adjacent excavation. *Tunnelling and underground space technology*, pp. 151-158.
2. **Yang Z., Wang X.** (2020). Influence of metro tunnel excavation on deformation of existing pedestrian underpass in changzhou railway station platform. *IEEE Access,* 2981343.
3. **Charles W.W.Ng., Jiangwei S., Hong Y.** (2013). Three-dimensional centrifuge modelling of basement excavation effects on an existing tunnel in dry sand. *Can. Geotech. J. 50,* pp. 874-888.
4. **Huang H., Huang X., Zhang, D.** (2014). Centrifuge modelling of deep excavation over existing tunnels. *Proc. ICE- Geotech Eng,* 167.
5. **Hung N.V., Tam N.T.** (2022). Impact of the underground culvert construction process with different construction segments on the existing tunnel. *Transportation magazine*, 63, pp. 30-34.
6. **Lou P., Li Y., Lu S., Xiao H., Zhang Z.** (2022). Deformation and mechanical characteristics of existing foundation pit and tunnel itself caused by shield tunnel undercrossing. *Symmetry*, 14020263.
7. **Tam N.T., Hung N.V., Bac N.V., Tuan, N.A.** (2023). Deformation analysis of existing tunnel using finite element method during construction of a full-length excavation pit. *Journal of Transportation Science and Technology*, 12, pp. 1-9.
8. **Tao X., Luan P., Ma J., Song W.** (2022). Influence of sublevel unloading excavation with deep consideration of the Superposition effect on deformation of an existing tunnel under an intelligent geotechnical concept. *Wireless communications and mobile computing*, 1400114.
9. **Zhao X., Li Z., Dai G., Wang H., Yin, Z., Cao, S.** (2022). Numerical study on the effect of large deep foundation excavation on underlying complex intersecting tunnels. *Appl. Sci*., 12, 4530.
10. **Liu J., Shi C., Lei M., Cao C., Lin Y.** (2020). Improved analysis method for evaluating the responses of shield tunnel to adjacent excavations and its application. *Tunnelling and underground space technology*, 98, 103339.
11. **Zhang Z., Huang M., Wang W.** (2013). Evaluation of deformation response for adjacent tunnels due to soil unloading in excavation engineering. *Tunnelling and Underground space technology*, pp. 244-253.
12. **Zhuang, X., Ou X., Fu, J.** (2017). Deformation response of an existing tunnel to upper excavation of foundation pit and associated dewatering. *International journal of Geomechanics*, 04016112.
13. **Verruijt A.** (2009). *An introduction to soil dynamics.* Delft university of technology.
14. **Liao S.M., Peng F.L., Shen S. L.** (2008). Analysis of shearing effect on tunnel induced by load transfer along longitudinal derection. *Tunnelling and underground space technology,* 23, pp. 421-430.
15. **Attewell P.B., Yeates J., Selby A.R.** (1987). Soil movements induced by tunnelling and their effects on pipelines and structures. *Tunnelling and underground space technology,* 2, 102.
16. **Yu J., Zhang C.R., Huang M.S.** (2005). Soil – pile interaction due to tunnelling: comparision between Winkler and elastic continuum solutions. *Geotechnique*, 55, pp. 461-466.

СПИСОК ЛИТЕРАТУРЫ

1. **Chang C.T., Sun C.W., Duann S.W., Hwang R.N.** (2001). Response of a Taipei rapid transit system (TRTS) tunnel to adjacent excavation. *Tunnelling and underground space technology*, pp. 151-158.
2. **Yang Z., Wang X.** (2020). Influence of metro tunnel excavation on deformation of existing

pedestrian underpass in changzhou railway station platform. *IEEE Access,* 2981343.
3. **Charles W.W.Ng., Jiangwei S., Hong Y.** (2013). Three-dimensional centrifuge modelling of basement excavation effects on an existing tunnel in dry sand. *Can. Geotech. J. 50,* pp. 874-888.
4. **Huang H., Huang X., Zhang, D.** (2014). Centrifuge modelling of deep excavation over existing tunnels. *Proc. ICE- Geotech Eng,* 167.
5. **Hung N.V., Tam N.T.** (2022). Impact of the underground culvert construction process with different construction segments on the existing tunnel. *Transportation magazine*, 63, pp. 30-34.
6. **Lou P., Li Y., Lu S., Xiao H., Zhang Z.** (2022). Deformation and mechanical characteristics of existing foundation pit and tunnel itself caused by shield tunnel undercrossing. *Symmetry*, 14020263.
7. **Tam N.T., Hung N.V., Bac N.V., Tuan, N.A.** (2023). Deformation analysis of existing tunnel using finite element method during construction of a full-length excavation pit. *Journal of Transportation Science and Technology*, 12, pp. 1-9.
8. **Tao X., Luan P., Ma J., Song W.** (2022). Influence of sublevel unloading excavation with deep consideration of the Superposition effect on deformation of an existing tunnel under an intelligent geotechnical concept. *Wireless communications and mobile computing*, 1400114.
9. **Zhao X., Li Z., Dai G., Wang H., Yin, Z., Cao, S.** (2022). Numerical study on the effect of large deep foundation excavation on underlying complex intersecting tunnels. *Appl. Sci*., 12, 4530.
10. **Liu J., Shi C., Lei M., Cao C., Lin Y.** (2020). Improved analysis method for evaluating the responses of shield tunnel to adjacent excavations and its application. *Tunnelling and underground space technology*, 98, 103339.
11. **Zhang Z., Huang M., Wang W.** (2013). Evaluation of deformation response for adjacent tunnels due to soil unloading in excavation engineering. *Tunnelling and Underground space technology*, pp. 244-253.
12. **Zhuang, X., Ou X., Fu, J.** (2017). Deformation response of an existing tunnel to upper excavation of foundation pit and associated *dewatering*. *International journal of Geomechanics*, 04016112.
13. **Verruijt A.** (2009). *An introduction to soil dynamics.* Delft university of technology.
14. **Liao S.M., Peng F.L., Shen S. L.** (2008). Analysis of shearing effect on tunnel induced by load transfer along longitudinal derection. *Tunnelling and underground space technology,* 23, pp. 421-430.
15. **Attewell P.B., Yeates J., Selby A.R.** (1987). Soil movements induced by tunnelling and their effects on pipelines and structures. *Tunnelling and underground space technology,* 2, 102.
16. **Yu J., Zhang C.R., Huang M.S.** (2005). Soil – pile interaction due to tunnelling: comparision between Winkler and elastic continuum solutions. *Geotechnique*, 55, pp. 461-466.

Nguyen Trong Tam, Doctor of phylosophy, Head of the Department of Railways and Metro, Ho Chi Minh City University of Transport; 717066 Vietnam, Ho Chi Minh City, Vo Oanh, 2, tel. +842838991373, email: trongtam.nguyen@ut.edu.vn

Nguyen Van Hung, Doctor of phylosophy, lecturer, Faculty civil engineering, university of engineering and tecnology, 123105 Vietnam, Hanoi, Xuan Thuy, 144, email: vanhung.nguyen@vnu.edu.vn

Нгуен Чонг Там, кандидат технических наук, заведующий департаментом «Железные дороги и метрополитены», Хошиминский университет транспорта; 717066 Вьетнам, г. Хошимин, Во Оань, стр. 2, тел. +842838991373, e-mail: trongtam.nguyen@ut.edu.vn

Нгуен Ван Хунг, кандидат технических наук, предподователь кафедры «Строительные - транспортные технологии», университет технологий (VNU-UET); 123105 Вьетнам, Ханой, Суан Тхуй, стр. 144, email: vanhung.nguyen@vnu.edu.vn

DOI:10.22337/2587-9618-2024-20-1-57-67

METHOD OF EQUAL RATE SURFACES IN STRUCTURAL AERODYNAMICS

Vadim K. Akhmetov [1], Viktor Y. Shkadov [2]

[1] Moscow State University of Civil Engineering, Moscow, RUSSIA

[2] Lomonosov Moscow State University, RUSSIA

Abstract. The problem of combustion of natural fuels is now an extremely important environmental issue. Flue gas emitted into the atmosphere has a negative impact on the environment. The consequences can range from precipitation containing acidic compounds to increased levels of lung disease in the population. A solution to this problem of fuel combustion in thermal power plants can be a design called a combined high-rise structure. It combines two components: the cooling tower and the chimney itself. The study of the flow gases nature in such a structure is an extremely important task, since the process of mixing the smoke with the additionally supplied air in the pipe determines the concentration of the emission of harmful substances into the atmosphere. This article is devoted to the numerical study of gas dynamics in the structures under consideration. A generalization of equal rate surfaces method to describe the internal aerodynamics of the structure is presented. The problem statement is based on the viscous compressible gas model. The flow is described by the Navier-Stokes system of equations, which is written in a parabolic form and supplemented by an algebraic turbulence model. The numerical solution is carried out by the finite difference method. Various variants of the structure geometry and initial conditions are considered. The favorable effect of the initial swirling of the flow on the intensive mixing of flue gases and the decrease in the concentration of harmful substances at the outlet of the chimney was noted. Based on this research, recommendations for the design and profiling of structures under construction have been developed.

Keywords: high-rise structures, numerical calculation methods, swirling flows, gas mixing

МЕТОД ПОВЕРХНОСТЕЙ РАВНЫХ РАСХОДОВ В СТРОИТЕЛЬНОЙ АЭРОДИНАМИКЕ

В.К. Ахметов [1], В.Я. Шкадов [2]

[1] Национальный исследовательский Московский государственный строительный университет, г. Москва, РОССИЯ

[2] Московский государственный университет им. М.В. Ломоносова, г. Москва, РОССИЯ

Аннотация. Проблема сжигания природного топлива в настоящее время является крайне важной экологической задачей. Дымовой газ, выбрасываемый в атмосферу, негативно влияет на окружающую среду. Последствия этого могут быть самыми разнообразными, от выпадения осадков, содержащих кислотные соединения, до повышения уровня легочных заболеваемостей населения. Решением проблемы сжигания топлива при выработке энергии в тепловых электростанциях может служить конструкция, называемая комбинированным высотным сооружением. Она объединяет в себе две составляющие: градирню и, непосредственно, дымовую трубу. Исследование характера течения газов в таком сооружении является чрезвычайно важной задачей, так как от процесса смешения дыма с дополнительно подаваемым воздухом в трубу зависит концентрация выброса вредных веществ в атмосферу. Данная статья посвящена численному изучению газодинамики в рассматриваемых сооружениях. Представлено обобщение метода поверхностей равных расходов для описания внутренней аэродинамики сооружения. В основе математической модели используется вязкий сжимаемый газ. Течение описывается системой уравнений Навье-Стокса, записанной в параболизованной форме, дополненной алгебраической моделью турбулентности. Численное решение проводится методом конечных разностей. Рассмотрены различные варианты геометрии конструкции и начальных условий. Отмечено благоприятное воздействие начальной закрутки потока на интенсивность смешения дымовых газов и уменьшение концентрации вредных веществ на выходе из трубы. На основе проведенных исследований разработаны рекомендации для проектирования и профилирования возводимых сооружений.

Ключевые слова: высотные сооружения, численные методы расчета, закрученные течения, смешение газов

1. INTRODUCTION

The use of natural fuel in the combustion process has a significant negative impact on the environment. The standards established for the maximum permissible content of harmful substances in the flue gases discharged. In particular, for sulfur compounds the limit is not more than 200-400 mg/m^3 SO_2. Devices for flue gas discharge should be designed to ensure the fulfillment of these requirements.

In the mid-seventies, the first studies were carried out to improve the technology for reducing harmful flue gas emissions by designing combined high-rise structures. This design combines a chimney and a wet cooling tower. The flue gas is pre-cleaned in a special desulfurization device. Then it enters the lower part of the extraction tower, where the heat exchanger is located. The jet of warm air forms the flue gas plume, mixes with it and is removed into the atmosphere due to natural draught. The ratio of flue gas volume to warm air amounts from 1:5 to 1:25. This provides the following advantages compared to a conventional chimney: the system of reheating the smoke and related energy costs are eliminated, the concentration of harmful substances and the temperature of the exhaust gases are significantly reduced.

The efficiency of combined high-rise structures is largely determined by gas dynamic processes of turbulent mixing of flue gases and humid air. To intensify the mixing process, it is preferable to supply flue gas to the exhaust tower with some initial swirling of the flow.

A large number of studies have been devoted to the investigation of swirling flows. Practical applications for various technical devices are considered in [1, 2]. Numerical studies of swirling flows in pipes are presented in [3-7], and experimental results are reflected in [8-10]. The issues of mixing and gas dynamics of flows in swirling combustion chambers are discussed in [11,12], and for flows in gas turbines in [13-15]. One of the most important features of swirling flow is the effect of swirl decay, which occurs when a certain flow swirl is reached. This phenomenon is associated with the loss of flow stability. Studies of hydrodynamic stability of swirling flows [16-21] support this conclusion.

The objective of this study is to investigate the processes of turbulent mixing of heated flue gases with warm air flow in the field of gravity. For this purpose, it uses a mathematical model based on parabolized Navier-Stokes equations. It presents an efficient numerical method of solution, which allows to pass from a general system of partial differential equations to a system of ordinary differential equations written on current lines.

2. PROBLEM STATEMENT AND RESEARCH METHOD

We consider the gas-dynamic process of mixing of heated flue gases entering the pipe by jet flow. The principle flow diagram is shown in Fig. 1. The flue gas is fed into the central part of the chimney $0 \le r \le R_1$ at the base of the $z = 0$.

It may have an initial swirl to improve mixing. Warm air is introduced coaxially into the lower part of the pipe $R_1 \le r \le R_0 = R(0)$. This flow is usually supplied without a swirl. The design of the structure has the following typical dimensions: bottom diameter of about 90 m, total height of the structure of about 100 m, flue gas to warm air flow ratio of 300:5000 m3/s, flue gas and moist air temperatures of about 120 ºC and 70 ºC respectively.

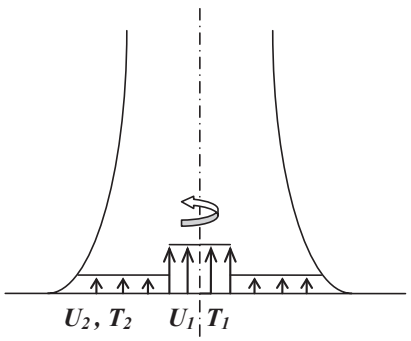

Figure 1. Flow diagram

The system of parabolized Navier-Stokes equations (as an analogue of the Prandtl boundary layer equations) is a set of laws of conservation of mass, momentum and energy. This mathematical model includes the following equations:

$$\frac{\partial(r\rho U)}{\partial z}+\frac{\partial(r\rho V)}{\partial r}=0,$$
$$\frac{\partial[(p+\rho U^2)r]}{\partial z}+\frac{\partial(\rho rUV)}{\partial r}=\frac{\partial}{\partial r}(r\tau)-\rho gr,$$
$$\frac{\partial(r\rho UH)}{\partial z}+\frac{\partial(r\rho VH)}{\partial r}=$$
$$=\frac{\partial(rq)}{\partial r}+\rho VW^2+\mu r\left(\frac{\partial W}{\partial r}-\frac{W}{r}\right)^2, \quad (1)$$
$$\frac{\partial(r\rho UE)}{\partial z}+\frac{\partial(r\rho VE)}{\partial r}=\frac{\partial(\mu r\gamma_\alpha)}{\partial r},$$
$$\frac{\partial(r\rho UW)}{\partial z}+\frac{\partial(r\rho VW)}{\partial r}=$$
$$=\frac{\partial}{\partial r}\left(\mu r\frac{\partial W}{\partial r}\right)-\frac{\rho VW}{r}-\mu\frac{W}{r^2},$$
$$h=c_pT,\ \ H=h+\frac{U^2}{2}+gz,$$
$$q=\frac{1}{\sigma}\mu\frac{\partial}{\partial r}\left(h+0{,}5\sigma U^2\right),$$
$$\gamma_\alpha=\frac{1}{\sigma_\alpha}\frac{\partial E}{\partial r},\ \ \sigma=\frac{1}{\lambda}\mu c_p,\ \ \tau=\mu\frac{\partial U}{\partial r}.$$

In this system of equations U, V, W are thevelocity components (axial, radial and azimuthal) in the cylindrical coordinate system r,φ,z; T is the temperature, μ is the dynamic viscosity; h is the enthalpy; g is the gravity acceleration; E is the impurity concentration; τ is the friction force; c_p is the specific heat capacity; q is the heat flux; γ_α is the impurity mass flux; σ, σ_α are the Prandtl numbers.

Let us consider the method of surfaces of equal flow rates. For the first time this method for the description of jet flows was developed in [22]. Later it was widely developed for solving various problems of hydrodynamics and heat and mass transfer with an interface [23]. For the solution of (1) in the coordinate system r,φ,z, let us introduce smooth lines $r=\delta_n(z)$, $n=0,1,2,...,N$, which will be current lines and satisfy Eq:

$$U\frac{\partial\delta_n}{\partial z}=V \quad \text{for} \quad r=\delta_n(z).$$

These lines should be found. It follows from the problem statement that $\delta_0=0$ since this is the axis of symmetry, and $\delta_N=R(z)$ defines the pipe wall. We will search for the solution of the system (1) on intermediate lines

$$r=\delta_{n+1/2}(z)=\frac{1}{2}(\delta_n+\delta_{n+1}),$$
$$n=0,1,2,...,N-1.$$

The system of equations (1) can be represented in compact form:

$$\frac{\partial(r\rho UA)}{\partial z}+\frac{\partial(r\rho VA)}{\partial r}=\frac{\partial Q}{\partial r}-\varepsilon_A\omega r, \quad (2)$$
$$A=\{1,U,H,E,W\},$$
$$Q=\{0,r\tau,rq,r\mu\gamma_\alpha,\mu r\partial W/\partial r\},$$
$$\varepsilon_A=1,\ \omega=\frac{\partial p}{\partial z}+\rho gz \ \text{ for } A=U,$$
$$\varepsilon_A=1,\ \omega=-\frac{\rho VW^2}{r}-\mu\left(\frac{\partial W}{\partial r}-\frac{W}{r}\right)^2 \text{ for}$$
$$A=H,$$
$$\varepsilon_A=1,\ \omega=\frac{\rho VW}{r}+\mu\frac{W}{r} \ \text{ for } A=W,$$
$$\varepsilon_A=0 \ \text{ for } A=1,E.$$

Let us introduce the functions

$$f_{n+1/2}=0.5(\delta_{n+1}^2-\delta_n^2),\ n=0,1,2,...,N-1.$$

Then the following relationships can be obtained for $\delta_n(z)$:

$$\delta_1^2 = 2f_{1/2}, \quad \delta_2^2 = 2(f_{1/2} + f_{3/2}), \quad ...,$$
$$\delta_N^2 = 2\sum_{n=1}^{N} f_{n-1/2}.$$

Having integrated (2) from r to $r = \delta_n$ taking into account Leibniz's rule, the original system can be represented by a set of ordinary differential equations to be solved on lines $r = \delta_{n+1/2}(z)$:

$$U\dot{U} = \frac{1}{\rho f} R_u - (1 - \frac{1}{\gamma})\pi_T \frac{1}{\rho}\dot{p} - \pi_g,$$
$$U\dot{T} = \frac{1}{\rho f} R_T - (1 - \frac{1}{\gamma}) U \frac{1}{\rho}\dot{p} + \frac{1}{\rho}\frac{\pi_w^2}{\pi_T} G_T,$$
$$U\dot{E} = \frac{1}{\rho f} R_E, \qquad (3)$$
$$U\dot{W} = \frac{1}{\rho f} R_w + \frac{1}{\rho} G_w,$$
$$\frac{\dot{f}}{f} = -\frac{\dot{p}}{p} + \frac{\dot{T}}{T} - \frac{\dot{U}}{U}.$$

In system (3), the point denotes the derivative on the coordinate z. Dimensionless variables of velocity, temperature, density, concentration and pressure are referred to the maximum values of U_1, T_1, ρ_1, E_1, p_1, W_1 of the internal flue gas flow at $z = 0$, and f – to R_0^2. Dimensionless parameters of the system (3) are Froude number $\pi_g = R_0 g / U_1^2$, swirl parameter $\pi_w = W_1 / U_1$ and $\pi_T = c_p T_1 / U_1^2$ as an analog of Mach number: $\pi_T = 1/(M^2(\gamma - 1))$.

For the case of flow without pre-twisting of the flue gas flow, the pressure distribution is determined from the equation $\partial p / \partial r = 0$, and for flow with twisting from the equation of the form:

$$\frac{\partial p}{\partial r} = \frac{\gamma}{\gamma - 1}\frac{\pi_w^2}{\pi_T}\rho\frac{W^2}{r}.$$

It can be integrated as follows:

$$p(z,r) = p^w(z,r) + p_0(z),$$
$$p^w(z,r) = \frac{\gamma}{\gamma - 1}\frac{\pi_w^2}{\pi_T}\int_0^r \rho\frac{W^2}{r} dr.$$

The integral for a function $p^w(z,r)$ is calculated using the trapezoidal formula and then calculated $\dot{p}^w(z,r)$ using recurrence formulas:

$$\dot{p}_1^w = \alpha_{1/2} f_{1/2}, \quad \dot{p}_{n+1}^w = \dot{p}_n^w + \alpha_{n+1/2} f_{n+1/2},$$
$$n = 1,2,\ldots,N-1,$$
$$\dot{p}_{n+1/2}^w = 0{,}5(\dot{p}_n^w + \dot{p}_{n+1}^w), \quad n = 0,1,2,\ldots,N-1,$$
$$\alpha_{n+1/2} = \frac{\gamma}{\gamma - 1}\frac{\pi_w^2}{\pi_T}\frac{\rho f}{r^2}\left(2W\dot{W} - W^2\frac{\dot{U}}{U}\right)\Bigg|_{\delta_{n+1/2}}.$$

The function $p_0(z)$ is obtained by integrating the equation

$$\dot{p}_0\sum_{n=0}^{N-1} g_{n+1/2} + \sum_{n=0}^{N-1}\dot{p}^w g_{n+1/2} =$$
$$= R\dot{R} - \sum_{n=0}^{N-1}(\pi_g\frac{f_{n+1/2}}{U^2} + \frac{R_T}{\rho UT} + \qquad (4)$$
$$+ \frac{f_{n+1/2}}{\rho UT}\pi_w^2\frac{G_T}{\pi_T} - \frac{R_u}{\rho U^2})$$

where

$$g_{n+1/2} = -\frac{f_{n+1/2}}{\gamma(p^w + p_0)} + \left(1 - \frac{1}{\gamma}\right)\pi_T f_{n+1/2}\frac{1}{\rho U^2}.$$

The following expressions are used to calculate the density ρ at each line:

$$\rho(z, \delta_{n+1/2}) = \frac{p(z, \delta_{n+1/2})}{T(z, \delta_{n+1/2})}. \qquad (5)$$

The dissipation terms of equations (3), (4) are calculated by the formulas:

$$R_u = [r\mu \frac{\partial U}{\partial r}],\ R_w = [r\mu \frac{\partial W}{\partial r}],$$

$$R_E = \frac{1}{\sigma_\alpha}[r\mu \frac{\partial E}{\partial r}],\qquad (6)$$

$$R_T = \frac{1}{\sigma}[r\mu \frac{\partial T}{\partial r}] + \frac{1}{\pi_T}\left([r\mu U \frac{\partial U}{\partial r}] - U[r\mu \frac{\partial U}{\partial r}]\right),$$

$$G_T = \mu\left(\frac{\partial W}{\partial r} - \frac{W}{r}\right)^2 + \frac{\rho V W^2}{r},$$

$$G_w = -\frac{\rho V W}{r} - \mu \frac{W}{r^2}.$$

The square brackets in (6) imply the difference between two consecutive values: $[Q] = Q_{n+1} - Q_n$.

To solve the system (3) it is necessary to set boundary conditions on the boundary of the solution region. For the variables of velocity, temperature, concentration it is obvious from the requirement of flow symmetry at $r = 0$. On the pipe wall, the boundary layer is assumed to be thin enough. Therefore, the following conditions were used:

$$\frac{\partial A}{\partial r} = 0 \text{ for } \delta = 0 \text{ and } \delta = R(z),$$

$$A = \{U, W, T, E\}. \qquad (7)$$

An algebraic turbulence model was used to complete the system of equations (3)-(6):

$$l_i^2 = \nu_{ti}\left\{\left(\frac{\partial V_z}{\partial r}\right)^2 + \left[r\frac{\partial}{\partial r}\left(\frac{V_\varphi}{r}\right)\right]^2\right\}^{-1/2}, \qquad (8)$$

where l_i is the mixing path length, $i = z, \varphi$.

Finally, the system (3)-(6) of $5N+1$ equations was integrated numerically by Runge-Kutta method.

3. RESEARCH RESULTS

Numerical results of the solution of the boundary value problem (3)-(6) were produced considering the following distributions of the sought variables for $z = 0$:

$$\begin{aligned} &U(r) = U_1 = 1,\ W(r) = W_1(r),\\ &T(r) = T_1 = 1,\ E(r) = E_1 = 1,\quad 0 \le r \le r_1,\\ &U(r) = U_2,\quad W(r) = W_2,\\ &T(r) = T_2,\quad E(r) = E_2,\quad r_1 < r \le 1. \end{aligned} \qquad (9)$$

The dimensionless value of the length of the region was taken as $z_0 = 2.2R_0$. The shape of the lateral surface was specified in two ways: either $R_0 = 1$, or $R(z) = 1 - 0.15z$. The flows were calculated in the range of parameters: $U_2 = 0.05 - 0.4$; $T_2 = 0.5 - 0.9$; $E_2 = 0.1$; $\sigma = 0.72$; $\pi_g = 6.45$; $\pi_T = 5754$; $\pi_w = 0 - 1.35$; $r_1 = 0.15; 0.33$; $N = 50$.

In most of the calculations the values used were $U_2 = 0.1$, $T_2 = 0.8$, $E_2 = 1$, $R_0 = 1$, $r_1 = 0.33$. The velocity profiles at these parameter values are shown in Fig. 2. In all cases, the main effect of the swirled flow is observed as the presence of a local minimum of the axial velocity for $r = 0$. This effect increases as the value of initial swirl increases from $\pi_w = 1$ to $\pi_w = 1.3$. For the values $\pi_w > 1.35$, calculation using parabolized equations is not possible. In this case, the full system of Navier-Stokes equations should be used.

In the considered problem, the lifting force has a significant effect on the process of flue gas mixing. Due to this, it is possible to increase the axial velocity of the gas flow through the pipe. For example, for the flow without swirl at $\pi_w = 0$ a small section $z \le 0.5$, the axial velocity of the flow increases by 1.5 times (Fig. 2, a). The action of lift force due to temperature differences can also contribute to the increase in flow velocity (Fig. 2, b). The addition of an initial swirl reduces this effect.

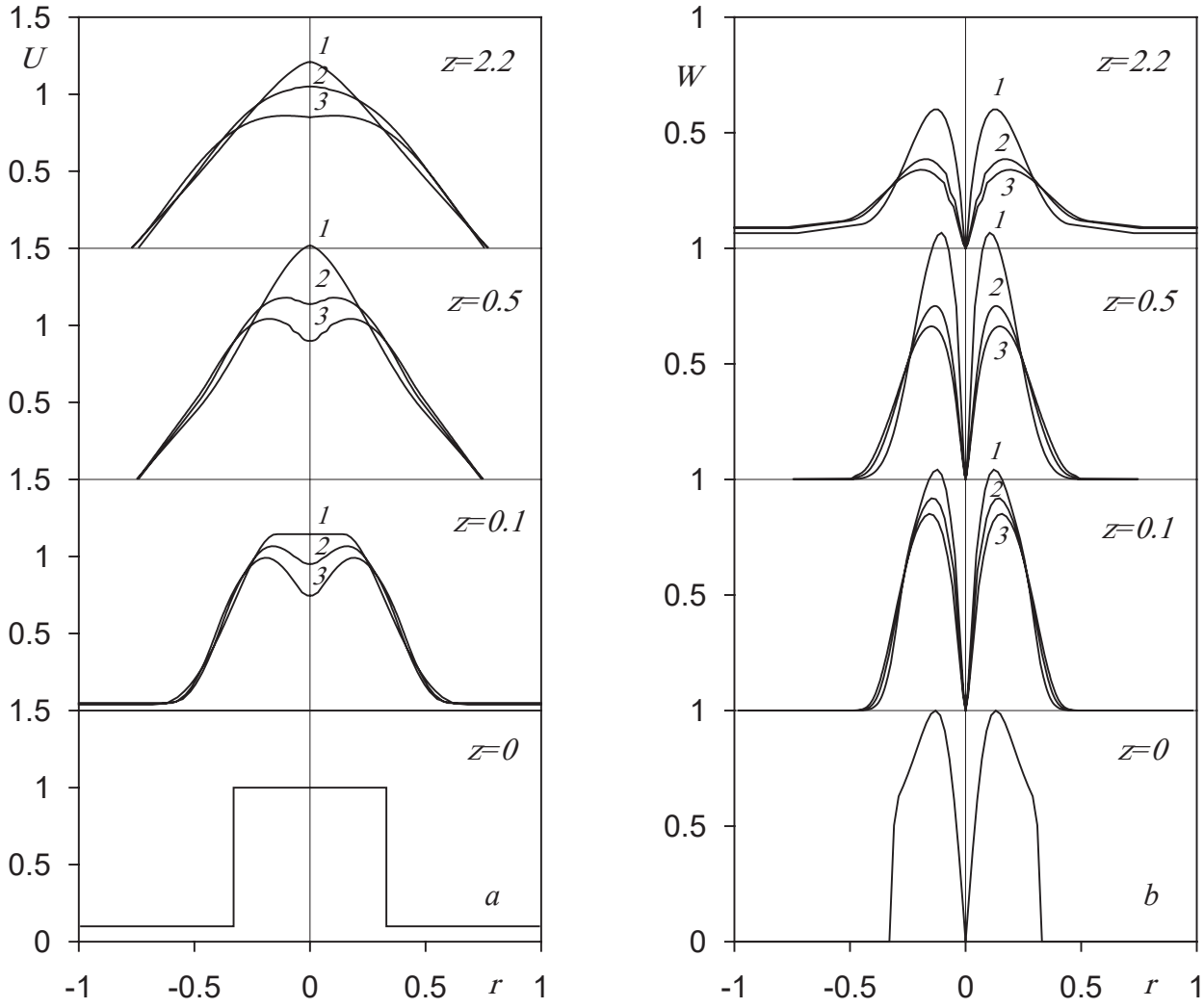

Figure 2. Axial U and azimuthal W velocity profiles at swirling $\pi_w = 0; 1; 1.3$ *(a)* $\pi_w = 0.2; 1; 1.3$ *(b) (curves 1-3)) in different cross-sections* $z = \text{const}$

With increasing temperature difference T_1 / T_2 for the internal jet of flue gas and external flow of warm air, the effect of the lifting force increases. Fig. 3, a shows the relation of axial velocity at $r = 0$ for different ratios of temperature difference, where $T_1 = 1$. The axial velocity maximum can increase more than 1.8 times the initial value (Fig. 3, a, curve 4). The lift force can also contribute to the increase in flow swirl. For example, the maximum azimuthal velocity $W_{\max}$ can increase by a factor of 1.3 compared to the initial value (Fig. 3, b).

Temperature distribution on the flow axis along the pipe for $r = 0$ is shown in Fig. 4, a. Due to mixing with warm air the flue gas temperature drops rather quickly. The initial swirl of the flow intensifies this process. A similar result is observed for the concentration distribution of harmful impurities. In the outlet section of the pipe the maximum concentration decreases more than 2 times (Fig. 4, b). This effect is extremely important with regard to the

environmental performance of the combined high-rise structure.

Fig. 5 shows characteristic pictures of the current lines. It can be seen that the current lines converge to the center rather quickly as the distance z increases. This data can be used for profiling the walls of the exhaust pipe in order to reduce the size of the erected structure, reduce material costs and increase the stability of the structure.

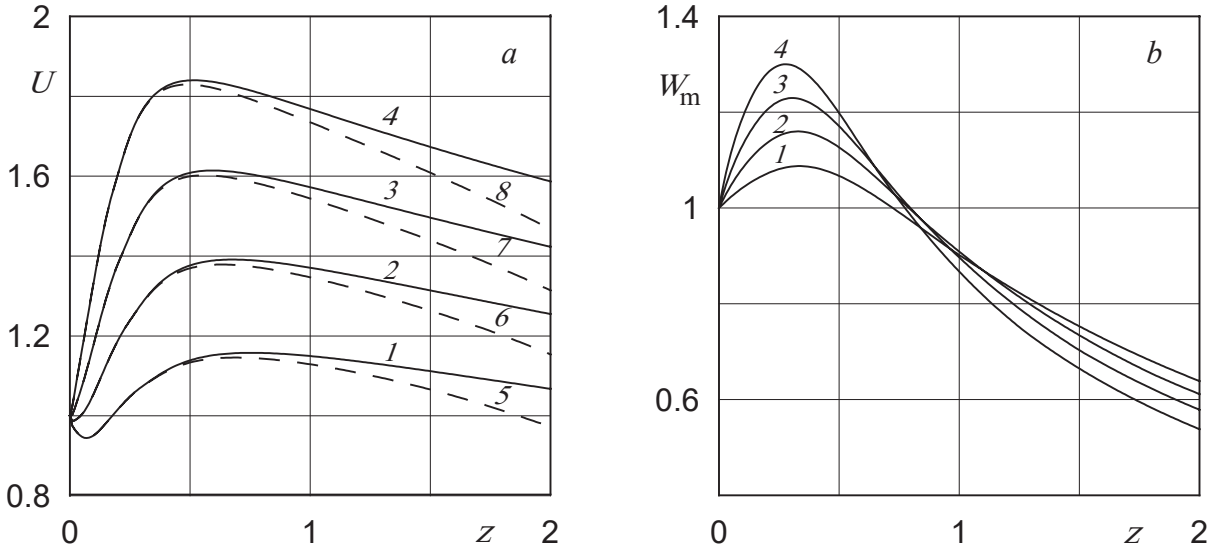

Figure 3. Distribution of axial velocity on axis $r = 0$ *for* $\pi_w = 1$ *(a) and maximum azimuthal velocity (b) for* $\pi_w = 0.2$*;* $T_2 = 0.8; 0.7; 0.6; 0.5$*;* $R(z) = 1$ *(curves 1–4),* $R(z) = 1 - 0.15z$ *(curves 5–8)*

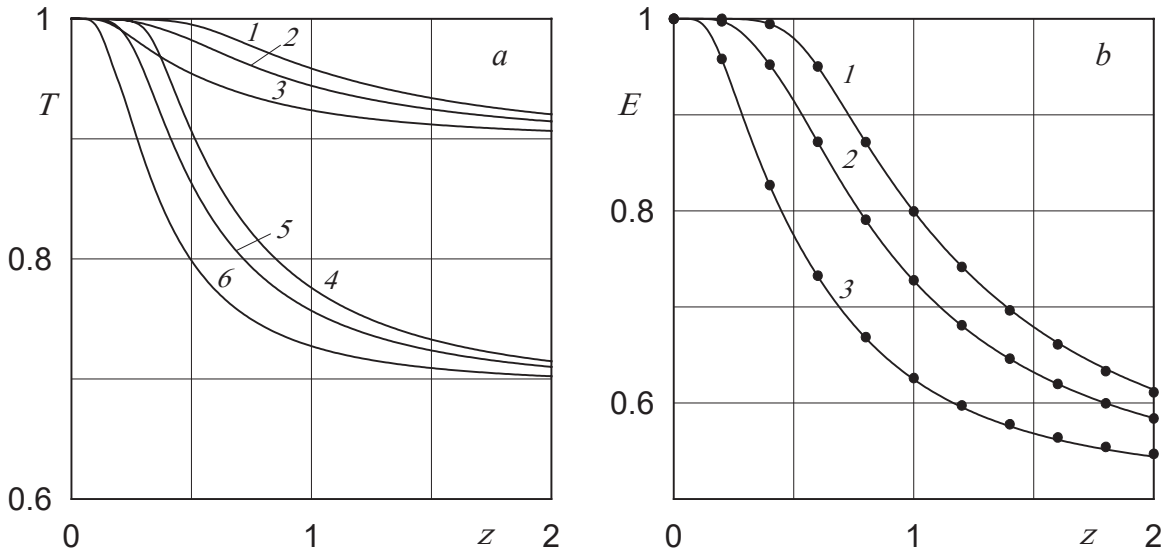

Figure 4. Temperature (a) and concentration (b) distribution on the axis $r = 0$ *for* $\pi_w = 0.2; 0.5; 1.3$*;* $T_2 = 0.8$ *(curves 1–3) and* $T_2 = 0.5$ *(curves 4–6)*

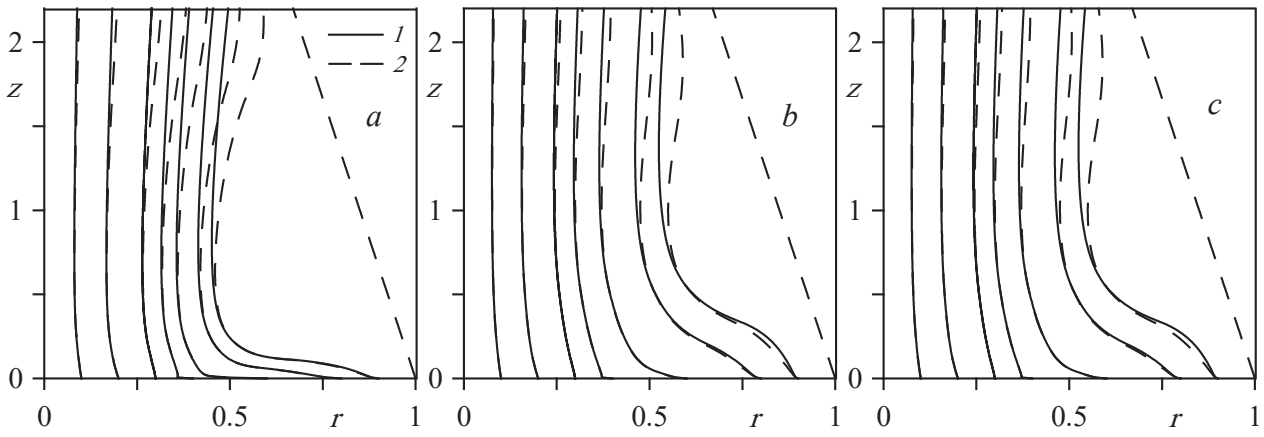

Figure 5. Current lines for T_2=0.8; r_1=0,33; U_2=0.1; 0.2; 0.3 (a, b, c), 1 – R(z)=1; 2 – R(z)=1–0.15z

4. CONCLUSIONS

The presented mathematical model and numerical calculation method allow obtaining necessary and detailed information on the character of flow in the exhaust stack of a combined high-rise building, temperature distribution and concentration of harmful impurities at the stack outlet. The initial swirling of the flue gas flow contributes to the improvement of gas mixing. However, excessively strong twist leads to undesirable flow inhibition and possible disintegration of swirl flow. The developed methodology allows to determine the maximum permissible value of the initial twist to eliminate such phenomenon. The obtained data of gas-dynamic flow pattern can serve as a basis for choosing the optimal shape of the pipe side surface in order to reduce the cost of the constructed structure.

REFERENCES

1. **Lucca-Negro O., O'Doherty T.** Vortex breakdown: a review // Progress in Energy and Combustion Science. 2001. V. 27. Pp. 431–481.
2. **Escudier M.P.** Vortex breakdown: observations and explanations // Progress in Aerospace Sciences. 1988. Vol. 25. № 2. Pp. 189-229.
3. **Wang Y., Xingjian Wang X., Yang V.** Evolution and transition mechanisms of internal swirling flows with tangential entry // Physics of Fluids. 2018. Vol. 30. 013601.
4. **Ogus G., Baelmans M., Vanierschot M.** On the flow structures and hysteresis of laminar swirling jets // Physics of Fluids. 2016. Vol. 28. 123604.
5. **Akhmetov V.K., Medvedev Yu.V., Shkadov V.Ya.** Effect of the Inertia Terms in Sliding Bearing Calculation Problems // Fluid Dynamics. 2014. Vol.49. №3. P.320-329.
6. **Orlandi P.** Two-dimensional and three-dimensional direct numerical simulation of co-rotating vortices // Physics of Fluids. 2007. Vol. 19. 013101.
7. **Akhmetov V.K.. Shkadov V.Ya.** Ustoychivost svobodnykh i ogranichennykh zakruchennykh techeniy s zonami retsirkulyatsii // Inzhenernaya fizika. 2008. № 6. 6–13 (in Russian).
8. **Oberleithner K., Paschereit C., Seele R., Wygnanski T.** Formation of turbulent vortex breakdown: intermittency, criticality, and global instability // AIAA Journal. 2012. Vol. 50. № 7. Pp. 1437–1452.
9. **Escudier M.P., Nickson A.K., Poole R.J.** Influence of outlet geometry on strongly swirling turbulent flow through a circular

tube // Physics of Fluids. 2006. Vol. 18. 125103.
10. **Mergheni M.A., Riahi Z., Sautet J.C., Nasrallah S.B.** Swirl effects on dynamics characteristics of a coaxial jet // Thermal Science. 2017. Vol. 21. № 6. Pp. 2543–2552.
11. **Alekseyenko S.V.. Shtork S.I.. Yusupov R.R.** Izotermicheskoye modelirovaniye aerodinamicheskoy struktury zakruchennogo techeniya v dvukhstupenchatom gorelochnom ustroystve // Izvestiya Tomskogo politekhnicheskogo universiteta. Inzhiniring georesursov. 2017. T. 328. № 7. 6–18 (in Russian).
12. **Mansouri Z., Aouissi M., Boushaki T.** A numerical study of swirl effects on the flow and flame dynamics in a lean premixed combustor // International journal of heat and technology. 2016. Vol. 34. № 2. Pp. 227-235.
13. **Kutateladze S.S.. Volchkov E.P.. Terekhov V.I.** Aerodinamika i teplomassoobmen v ogranichennykh vikhrevykh potokakh. Novosibirsk: Institut teplofiziki. 1987. 283 pages (in Russian).
14. **Lu X., Wang S., Sung H.G., Hiseh S.Y., Yang V.** Large-eddy simulation of turbulent swirling flow injected into dump chamber // Journal of Fluid Mechanics. 2005. Vol. 527. Pp. 171–195.
15. **Wang P., Bai X.S., Wessman M., Klingmann J.** Large eddy simulation and experimental studies of a confined turbulent swirling flow // Physics of Fluids. 2004. Vol. 16. № 9. Pp. 3306–3324.
16. **Rukes L., Sieber M., Paschereit C., Oberleithner K.** The impact of heating the breakdown bubble on the global mode of a swirling jet: experiments and linear stability analysis // Physics of Fluids. 2016. Vol. 28. 104102.
17. **Gallaire F., Ruith M., Meiburg E., Chomaz J., Huerre P.** Spiral vortex breakdown as a global mode // Journal of Fluid Mechanics. 2006. Vol. 549. Pp. 71–80.
18. **Blanco-Rodríguez F.J., Rodríguez-García J.O., Parras L., del Pino C.** Optimal response of Batchelor vortex // Physics of Fluids. 2017. Vol. 29. 064108.
19. **Yadav N.K., Samanta A.** The stability of compressible swirling pipe flows with density stratification // Journal of Fluid Mechanics. 2017. Vol. 823. Pp. 689–715.
20. **Delbende I., Rossi M.** Nonlinear evolution of a swirling jet instability // Physics of Fluids. 2005. Vol. 17. 044103.
21. **Akhmetov V.K.** Gidrodinamicheskaya ustoychivost kontrvikhrevykh techeniy // Gidrotekhnicheskoye stroitelstvo. 2018. № 2. 13–18 (in Russian).
22. **Shkadov V.Ya.** Nekotoryye metody i zadachi teorii gidrodinamicheskoy ustoychivosti // Trudy instituta mekhaniki MGU. 1973. № 25. 160 pages (in Russian).
23. **Kholpanov L.P.. Shkadov V.Ya.** Gidrodinamika i teplomassoobmen s poverkhnostyu razdela. M.: Nauka. 1990. 271 pages (in Russian).

СПИСОК ЛИТЕРАТУРЫ

1. **Lucca-Negro O., O'Doherty T.** Vortex breakdown: a review // Progress in Energy and Combustion Science. 2001. V. 27. Pp. 431–481.
2. **Escudier M.P.** Vortex breakdown: observations and explanations // Progress in Aerospace Sciences. 1988. Vol. 25. № 2. Pp. 189-229.
3. **Wang Y., Xingjian Wang X., Yang V.** Evolution and transition mechanisms of internal swirling flows with tangential entry // Physics of Fluids. 2018. Vol. 30. 013601.
4. **Ogus G., Baelmans M., Vanierschot M.** On the flow structures and hysteresis of laminar swirling jets // Physics of Fluids. 2016. Vol. 28. 123604.
5. **Akhmetov V.K., Medvedev Yu.V., Shkadov V.Ya.** Effect of the Inertia Terms

in Sliding Bearing Calculation Problems // Fluid Dynamics. 2014. Vol.49. №3. P.320-329.
6. **Orlandi P.** Two-dimensional and three-dimensional direct numerical simulation of co-rotating vortices // Physics of Fluids. 2007. Vol. 19. 013101.
7. **Ахметов В.К., Шкадов В.Я.** Устойчивость свободных и ограниченных закрученных течений с зонами рециркуляции // Инженерная физика. 2008. № 6. С. 6–13.
8. **Oberleithner K., Paschereit C., Seele R., Wygnanski T.** Formation of turbulent vortex breakdown: intermittency, criticality, and global instability // AIAA Journal. 2012. Vol. 50. № 7**.** Pp. 1437–1452.
9. **Escudier M.P., Nickson A.K., Poole R.J.** Influence of outlet geometry on strongly swirling turbulent flow through a circular tube // Physics of Fluids. 2006. Vol. 18. 125103.
10. **Mergheni M.A., Riahi Z., Sautet J.C., Nasrallah S.B.** Swirl effects on dynamics characteristics of a coaxial jet // Thermal Science. 2017. Vol. 21. № 6. Pp. 2543–2552.
11. **Алексеенко С.В., Шторк С.И., Юсупов Р.Р.** Изотермическое моделирование аэродинамической структуры закрученного течения в двухступенчатом горелочном устройстве // Известия Томского политехнического университета. Инжиниринг георесурсов. 2017. Т. 328. № 7. С. 6–18.
12. **Mansouri Z., Aouissi M., Boushaki T.** A numerical study of swirl effects on the flow and flame dynamics in a lean premixed combustor // International journal of heat and technology. 2016. Vol. 34. № 2. Pp. 227-235.
13. **Кутателадзе С.С., Волчков Э.П., Терехов В.И.** Аэродинамика и тепломассообмен в ограниченных вихревых потоках. Новосибирск: Институт теплофизики, 1987. 283 с.
14. **Lu X., Wang S., Sung H.G., Hiseh S.Y., Yang V.** Large-eddy simulation of turbulent swirling flow injected into dump chamber // Journal of Fluid Mechanics. 2005. Vol. 527. Pp. 171–195.
15. **Wang P., Bai X.S., Wessman M., Klingmann J.** Large eddy simulation and experimental studies of a confined turbulent swirling flow // Physics of Fluids. 2004. Vol. 16. № 9. Pp. 3306–3324.
16. **Rukes L., Sieber M., Paschereit C., Oberleithner K.** The impact of heating the breakdown bubble on the global mode of a swirling jet: experiments and linear stability analysis // Physics of Fluids. 2016. Vol. 28. 104102.
17. **Gallaire F., Ruith M., Meiburg E., Chomaz J., Huerre P.** Spiral vortex breakdown as a global mode // Journal of Fluid Mechanics. 2006. Vol. 549. Pp. 71–80.
18. **Blanco-Rodríguez F.J., Rodríguez-García J.O., Parras L., del Pino C.** Optimal response of Batchelor vortex // Physics of Fluids. 2017. Vol. 29. 064108.
19. **Yadav N.K., Samanta A.** The stability of compressible swirling pipe flows with density stratification // Journal of Fluid Mechanics. 2017. Vol. 823. Pp. 689–715.
20. **Delbende I., Rossi M.** Nonlinear evolution of a swirling jet instability // Physics of Fluids. 2005. Vol. 17. 044103.
21. **Ахметов В.К.** Гидродинамическая устойчивость контрвихревых течений // Гидротехническое строительство. 2018. № 2. С. 13–18.
22. **Шкадов В.Я.** Некоторые методы и задачи теории гидродинамической устойчивости // Труды института механики МГУ. 1973. № 25. 160 с.
23. **Холпанов Л.П., Шкадов В.Я.** Гидродинамика и тепломассообмен с поверхностью раздела. М.: Наука, 1990. 271 с.

Ахметов Вадим Каюмович, доктор технических наук, профессор кафедры информатики и прикладной математики Национального исследовательского Московского государственного строительного университета, 129337, г. Москва, Ярославское шоссе, д. 26, тел. +7(499) 183-59-94, e-mail: vadim.akhmetov@gmail.com

Vadim K. Akhmetov, Doctor of Science, Professor, Department of Computer Science and Applied Mathematics, Moscow State University of Civil Engineering, 26, Yaroslavskoe Shosse, Moscow, 129337, Russia, tel. +7(499) 183-59-94, e-mail: vadim.akhmetov@gmail.com

Шкадов Виктор Яковлевич, доктор физико-математических наук, профессор кафедры аэромеханики и газовой динамики механико-математического факультета Московского государственного университета им. М.В. Ломоносова, 119991, г. Москва, Ленинские горы, д. 1, tel. +7(495) 939-39-49, e-mail: shkadov@mech.math.msu.su

Viktor Y. Shkadov, Doctor of Sciences, Professor, Department of Aeromechanics and Gas Dynamics, Faculty of Mechanics and Mathematics, Lomonosov Moscow State University, 119991, Moscow, Leninskie Gory, 1, tel. +7(495) 939-39-49, e-mail: shkadov@mech.math.msu.su

DOI:10.22337/2587-9618-2024-20-1-68-80

COMPUTER MODELING OF ENERGY-EFFICIENT JOINTS OF WOOD COMPOSITE PANELS

Mikhail V. Lukin [1], Svetlana I. Roshchina [1], Anastasiya V. Lukina [1], Vladimir I. Rimshin [2]

[1] Vladimir State University named after Alexander and Nikolay Stoletovs, Institute of Architecture Construction and Energy Engineering, Vladimir, RUSSIA
[2] NRU Moscow State University of Civil Engineering, Moscow, RUSSIA

Abstract: High air permeability and the presence of thermal bridges at the junctions of wooden frame wall panels have a significant impact on the thermal balance of the building and its operational characteristics. The importance of improving the energy efficiency of nodal interfaces of panels with a wooden frame is undeniable.
To date, there is no single generally accepted method for calculating heat losses through nodal interfaces of panels with a wooden frame. Based on the analysis carried out, it is necessary to carry out calculations and measurements that allow creating this calculation methodology. To carry out numerical studies, a list of characteristics and parameters affecting their conduct is formulated: the influence of the thickness of a li-ear-discrete inclusion on the heat-protective properties of the panel docking unit; the thermal conductivity characteristics of the material used to fill linear-discrete inclusions affecting the heat flux density of the node interface; consideration of the influence of the outdoor temperature of air depending on different climatic zones on the density of heat flow. The dependences of the heat flux density on the "inner" surface of the experimental samples on the thermal conductivity coefficient of the material of the insulating insert, the width of the insulating insert and the outside air temperature were revealed and the nature of the temperature distribution on the "inner" surface of the prototypes was established. By calculating two-dimensional temperature fields in the cross section of the node, isofields of temperature distribution inside the structure, isofields of heat flux density and its direction, lines of temperature distribution and heat flux density along the inner and outer surfaces are obtained. It was found that the heat flux density in the ribs with heat-insulating inclusions is lower in comparison with solid wood parts by an amount from 13% to 52%.

Keywords: thermal engineering calculation, wooden panels, nodal interfaces, thermal conductivity, energy efficiency, thermal insulation dissections, specific losses, temperature, air permeability, thermal bridge, thermophysical parameters, temperature fields

КОМПЬЮТЕРНОЕ МОДЕЛИРОВАНИЕ ЭНЕРГОЭФФЕКТИВНЫХ СТЫКОВ ДЕРЕВОКОМПОЗИТНЫХ ПАНЕЛЕЙ

М.В. Лукин [1], С.И. Рощина [1], А.В. Лукина [1], В.И. Римшин [2]

[1] Владимирский государственный университет имени Александра Григорьевича и Николая Григорьевича Столетовых, Институт архитектуры, строительства и энергетики, г. Владимир, РОССИЯ
[2] НИУ Московский государственный строительный университет, г. Москва, РОССИЯ

Abstract: Высокая воздухопроницаемость и наличие тепловых мостов в местах соединений деревянных каркасных стеновых панелей оказывает значительное влияние на тепловой баланс здания и его эксплуатационные характеристики. Важность повышения энергоэффективности узловых сопряжений панелей с деревянным каркасом неоспорима. На сегодняшний день единой общепринятой методики расчета тепловых потерь через узловые сопряжения панелей с деревянным каркасом не существует. Исходя из проведенного анализа, необходимо провести расчеты и измерения, позволяющие создать данную методику расчета. Для проведения численных исследований сформулирован перечень характеристик и параметров, влияющих на их проведение: влияние толщины линейно-дискретного включения на теплозащитные свойства узла стыковки панелей; характеристики теплопроводности материала, применяемого для заполнения линейно-дискретных включений, влияющих на плотность теплового потока узлового сопряжения; учет влияния температуры наружного воздуха в зависимости

различных климатических зон на плотность теплового потока. Выявлены зависимости плотности теплового потока на «внутренней» поверхности опытных образцов от коэффициента теплопроводности материала теплоизолирующей вставки, ширины теплоизолирующей вставки и температуры наружного воздуха и установить характер распределения температуры на «внутренней» поверхности опытных образцов. Путём расчёта двухмерных температурных полей в поперечном сечении узла получены изополя распределения температуры внутри конструкции, изополя плотности теплового потока и его направленности, линии распределения температуры и плотности теплового потока по внутренней и наружной поверхностям. Установлено, что плотность теплового потока в рёбрах с теплоизолирующими включениями меньше по сравнению с цельнодеревянными деталями на величину от 13% до 52%.

Ключевые слова: теплотехнический расчет, деревянные панели, узловые сопряжения, теплопроводность, энергоэффективность, теплоизолирующие рассечки, удельные потери, температура, воздухопроницаемость, тепловой мост, теплофизические параметры, температурные поля

INTRODUCTION

Wood, as a structural material, has unsurpassed properties, being a natural renewable resource. The processability of processing, accessibility, high physical and mechanical properties, environmental friendliness make it possible to effectively use wood in various areas of the construction industry.

The issues of static modeling of heat transfer for thermal bridges of buildings are considered in [1-3], it is concluded that the proposed approach demonstrates a significant improvement over traditional modeling results. The dynamic calculation of heat fluxes considered in [4, 5] is analyzed over time to determine the step and for given boundary conditions: a sinusoidal change in internal temperature and a sharp or more realistic change in external temperature. Numerical characteristics of bridges are shown in [6], in particular, the method of infrared thermography, which is used to visualize thermal bridges, is presented for the first time, as well as a genuine additional experimental method that allows us to determine the quantitative aspects of heat loss through the shell. The authors of the article [7] model thermal bridges in three different approaches. Energy efficiency and thermal characteristics were studied in [8, 9], they proved that an accurate assessment of the availability and energy efficiency of buildings depends on the degree of use of the main components. Various methods of reducing the influence of thermal bridges are given in [10-12]. Heat transmission through the wall enclosure is considered in [13, 14] the heat transfer coefficient (U-value) of three LSF walls with different configurations is established, which is investigated on the basis of four different approaches: experimental laboratory measurements based on the thermal flowmeter method (HFM); 3D modeling by the finite element method (FEM) using the ANSYS software CFX ® ; 2D modeling based on FEM modeling using THERM software; analytical estimates based on the ISO 6946 procedure for constructing components with heterogeneous layers. The effect of connectors on the thermal characteristics of walls was considered in [15, 16], it was found that the increased distance and reduced length of connectors led to an improvement in thermal characteristics, which additionally indicated the need to study the effect of connectors on thermal characteristics. The life cycle assessment and thermal characteristics are given in [17, 18], the behavior of the wall plate during bending with various geometric parameters was experimentally investigated and a numerical model was created to study the thermal characteristics of the wall plate. Issues of improving thermal bridges in articles [19, 20], maps of temperature distribution in walls, their components and areas where walls intersect with other building structures were developed. These maps were used as an auxiliary tool for estimating the areas of zones affected by existing thermal bridges and for calculating R-values for these areas. New methods for predicting heat flows over a thermal bridge are discussed in [21, 22], studies show that existing approaches to

implementing the effect of thermal bridges do not correspond to the progress made in thermal insulation requirements, and the corresponding structure should be updated to better support efforts to achieve more rational and accurate results. Laboratory and full-scale non-destructive methods for assessing heat transmission in works [23, 24], in particular, the influence of the location of thermal insulation on its effectiveness in LSF facade walls is evaluated. For this purpose, several types of LSF walls are evaluated, namely cold, warm and hybrid construction. The influence of thermal bridges created by steel studs on the overall thermal characteristics of LSF walls is also evaluated. Calculations are performed using specialized finite element software (THERM). The prediction of heat transmission is given in [25, 26]. Evaluation of the effectiveness of thermal rupture strips in external walls is given in [27] it is proved that it is more effective to increase the thickness of thermal rupture strips (TBS) than their width. The energy characteristics of fire-resistant walls are shown in [28, 29]. A measurement method for quantifying the heat transmission coefficient is presented in [30], a new active method for determining the characteristics of a thermal bridge in situ is proposed. It generalizes the measurement of the thermal resistance of a homogeneous wall.

Numerical studies of composite structures are considered in papers [31…33]. Studies of the work of composite structures in frame wooden buildings were carried out in [34…36]. Engineering calculations of composite structures are considered in works [37…39], properties of composite materials in work 40.

Numerical studies were carried out in the Heat2D program by calculating two-dimensional temperature fields in the cross section of the node. The aim of the numerical studies was to evaluate the thermal properties of the nodal joint depending on the variable parameters. The calculations performed were preceded by a full-scale experiment and were carried out in the volume planned in the combination square.

The study was carried out in order to analyze the theoretical (calculated values) and practical (measured values) analysis of thermal bridges.

From the point of view of thermal conductivity, the paired rack formed by the joint of two panels is a linear heterogeneity of the panel material. When calculating the reduced resistance to heat transfer , it is necessary to take into account the influence of thermal bridges according to the formula:

$$R_0^{red} = \frac{1}{\frac{1}{R_0^{red}} + \sum l_j \psi_j + \sum n_k \chi_k} = \frac{1}{\sum a_i U_i + \sum l_j \psi_j + \sum n_k \chi_k} \quad (1)$$

where, R_0^{red} - is the area-averaged conditional resistance to heat transfer of a fragment of a heat–protective shell of a building or a dedicated enclosing structure, m^2 °S/W;

l_j – is the extent of linear inhomogeneity of the j-th type per 1 m^2 of a fragment of a heat-protective shell of a building, or a dedicated enclosing structure, m/m^2;

ψ_j – specific heat losses due to linear inhomogeneity of the j type, W/(m·oS);

n_k – the number of point inhomogeneities of the k- type per 1 m^2 of a fragment of the heat-shielding shell of a building, or a dedicated enclosing structure, pcs/m^2;

χ_k – specific heat losses due to point heterogeneity of the k type, W/°S;

a_i – the area of a flat structural element of the i – type, per 1 m^2 of a fragment of the heat-shielding shell of a building, or a dedicated enclosing structure, m^2/m^2.

$$a_i = \frac{A_i}{\sum A_i} \quad (2)$$

where A_i - is the area of the i-th part of the fragment, m^2;

U_i - is the heat transfer coefficient of the homogeneous i-th part of the fragment of the heat shield of the building (specific heat loss through a flat element of the i-th type), W /(m · ° C).

$$U_i = \frac{1}{R_{0,i}^{red}} \quad (3)$$

The essence of heat losses is taken into account in EN ISO 14683 "Thermal insulation of buildings" and is calculated by the linear heat transfer coefficient ψ [W/m×K] of the thermal bridge, which is obtained from the numerical determination of the two-dimensional coefficient of thermal coupling L^{2D} (i.e., the total heat flow through the component per linear meter divided by the temperature difference) of the component separating the two media under consideration. The linear thermal coupling of the frame -wall coupling coefficient ψ is obtained from the equation:

$$\psi = L^{2D} - \sum_{j=1}^{j} U_j \cdot I_j, \quad (4)$$

where L^{2D} - is the two-dimensional coefficient of thermal coupling, W/(m*K);
U_j- is the heat transfer coefficient of a one-dimensional element j, W/(m^2*K);
I_j - is the length of a one-dimensional element j, m.
When calculating the energy balance, thermal bridges can be considered standard. Buildings with high thermal protection, taking into account an increase in the heat transfer coefficient by 5%. Buildings with low thermal protection are a 10% increase in the heat transfer coefficient. If we want to calculate the energy demand for heating a building with almost zero energy consumption, it is necessary to specify each cold bridge.
Based on the review of regulatory documentation, it can be concluded that there is no method for calculating energy-efficient nodal interfaces of panels with a wooden frame. In this regard, the development of a method for calculating energy-efficient node interfaces of panels with a wooden frame is relevant.
The purpose of the work is to identify the calculated dependences of the heat flux density and to establish the nature of the temperature distribution on the inner and outer surfaces of the joint of wall panels, depending on variable factors: the thermal conductivity coefficient of the material of the insulating insert, the width of the insulating insert and the outdoor temperature.
The object of the study is the joints of the interface of wall wooden panels.
The subject of the study is the calculation of the energy parameters of the joints of wall panels.

METHODS

The Heat2D program uses a kind of finite-difference method - the control volume method to obtain a discrete analog of a stationary two-dimensional thermal conductivity problem. In this method, the calculated area is represented by the union of disjoint control volumes, each of which contains one nodal (calculated) point. To obtain a discrete analog, the differential equation of thermal conductivity is integrated for each control volume.
The resulting system of linear algebraic equations is solved by the method of exclusion of unknowns (Gauss method). Let's consider the main components of the method.
The process of two - dimensional heat transfer in a solid is described by the differential equation:

$$(\partial^2 t/\partial x^2 + \partial^2 t/\partial y^2) = Q \quad (5)$$

where Q is the source/heat drain, W/m^3.
The studied area of the two-dimensional section of the structure is divided into elementary platforms - rectangles so that each rectangle consists of one material. The center of each rectangle is taken as a node of the thermal grid. Thus, each grid node is surrounded by four neighboring ones, with which it is connected by thermal resistances equal to the resistances between the centers of the corresponding rectangles. The temperature at each node is the average temperature of an elementary rectangle.
So, in general terms, the area under study is replaced by its discrete analog, called a thermal grid, each node of which corresponds to a certain rectangle, and the thermal resistance to the interstitial connection.
Each node must maintain a balance of heat (energy), which is expressed by the

corresponding algebraic equation linking the heat flows coming into and out of the node. This equation can be obtained by integrating (5) over an elementary rectangle. As a result , we obtain the equation:

$$t_0(K_{01} + K_{02} + K_{03} + K_{04}) - t_1K_{01} - t_2K_{02} - t_3K_{03} - t_4K_{04} = q\Delta x\Delta y \quad (6)$$

Heat2D program, a system of linear algebraic equations is solved by an economical method of eliminating unknowns (the Gauss method) using a matrix system of equations with double precision inside the machine representation of numbers.

When calculating an axisymmetric temperature field, which is characterized by the fact that the temperature field does not change when the area under study is rotated around the vertical axis of symmetry OZ, the following differential equation is solved:

$$(\lambda/r)\ \partial(r\,\partial t/\partial r)/\partial r + \lambda\,\partial^2 t/\partial z^2 = 0 \quad (7)$$

where r is the distance from the axis of symmetry OZ.

So, if the axis of symmetry is to the left of a rectangle with a central node 0, then the resistance between points 1 and 0 can be expressed as follows:

$$R_{1-0} = (\ln(r/r1) + \ln(r_0/r))/(\lambda\Delta y) \quad (8)$$

where r_0, r_1 и $r = r_0 + \Delta x/2$ are the distances of the corresponding points to the axis of symmetry.

The scheme of finite-difference sampling of the node connection is shown in Figure 1.

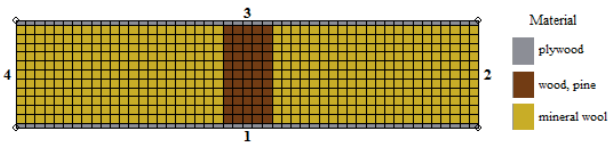

Figure 1. Scheme of finite-difference sampling of a node connection

where $K_{01}, K_{02}, K_{03}, K_{04}$ - are the conductivities of the interstitial connections of the grid.

In equation (6), the temperature t_0 of the central node is expressed in terms of the temperatures of neighboring nodes, whose values (if they are not located on the border) are also unknown. To find the temperature at any node, it is necessary to make equations of type (6) for each node and solve the resulting system of equations. In the

When implementing the numerical calculation, 12 types of wall panel joints were investigated [31-34]. The first letter of the marking is the type of joint (D – solid wood joint, T - joint with heat-insulating inclusion); the second digit is the value of negative outdoor temperature (-5, -20, -35 ° C); the third letter is the filling of the heat-insulating insert (V – air; E – extruded polystyrene foam; P – penofol); the last the figure is the width of the thermal insulation insert (5, 15 or 25 mm). An example of decoding the T-35-E-5 joint is a joint with a heat-insulating inclusion; the value of the negative outdoor temperature is 35 ° C; the filling of the thermal insulation insert is E – extruded polystyrene foam; the width of the thermal insulation insert is 5 mm.

RESULTS AND DISCUSSION

According to the results of calculations of thermal fields in the Heat2D program, isofields of temperature distribution inside the structure, isofields of heat flux density and its direction, lines of temperature distribution and heat flux density along the "inner" surface are obtained. The program also calculated the value of specific heat loss through linear thermal heterogeneity (wooden joint ribs), which directly takes into account heat loss in the junction when calculating the reduced heat transfer resistance.

As an example, the results of calculations of the joint of the T-35-E-5 panel in the software package are given. Figure 2 shows a finite element model of the junction of panels and an isofield of temperature distribution and heat flow. Figure 3 shows graphs of temperature and heat flow distribution, and Figure 4 shows 3-D graphs of their distribution.

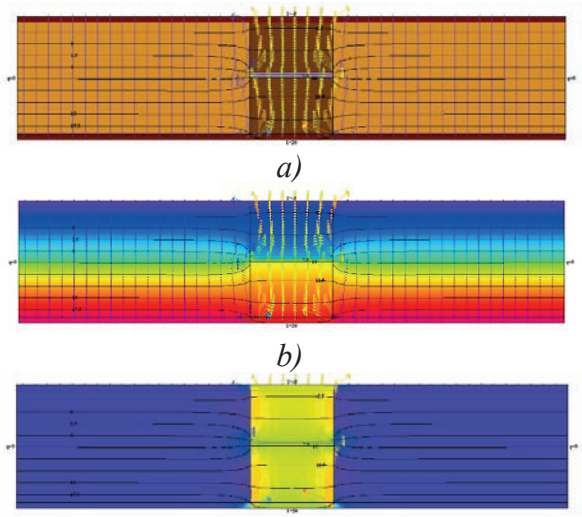

a)

b)

c)

Figure 2. Results of calculation of panel joints in the software package: a) finite element model of panel junction; b) isolines of temperature distribution over the section of the structure; c) isolines of heat flow distribution over the section of the structure

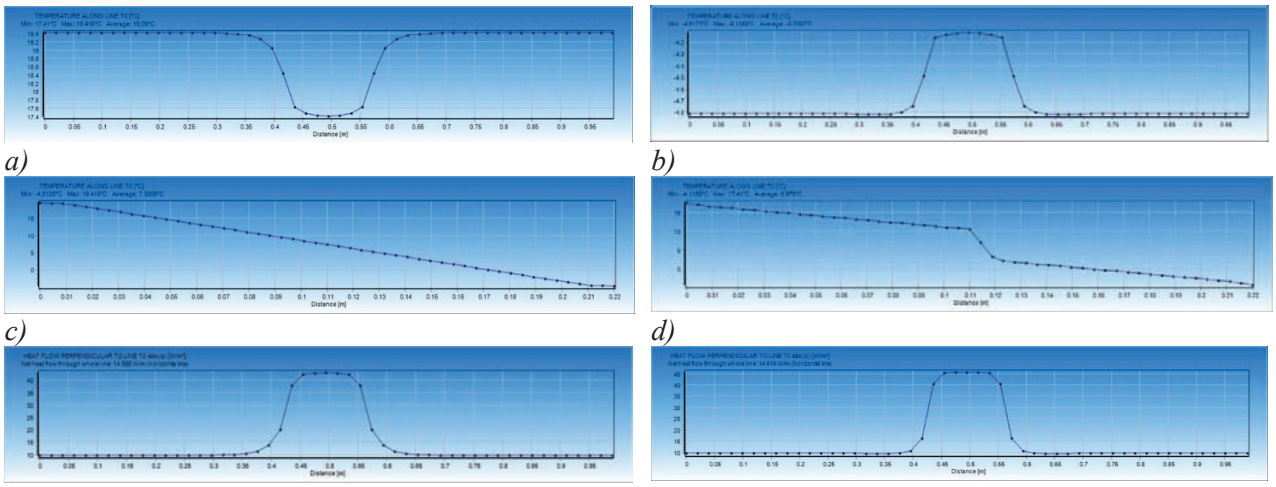

a) *b)*

c) *d)*

f) *g)*

Figure 3. Distribution charts: a), b) temperatures on the inner surface on the outer surface of the structure; c), d) by the cross section of the panels and by the cross section of the panels in the docking node; f), g) heat flow on the inner surface on the outer surface of the structure

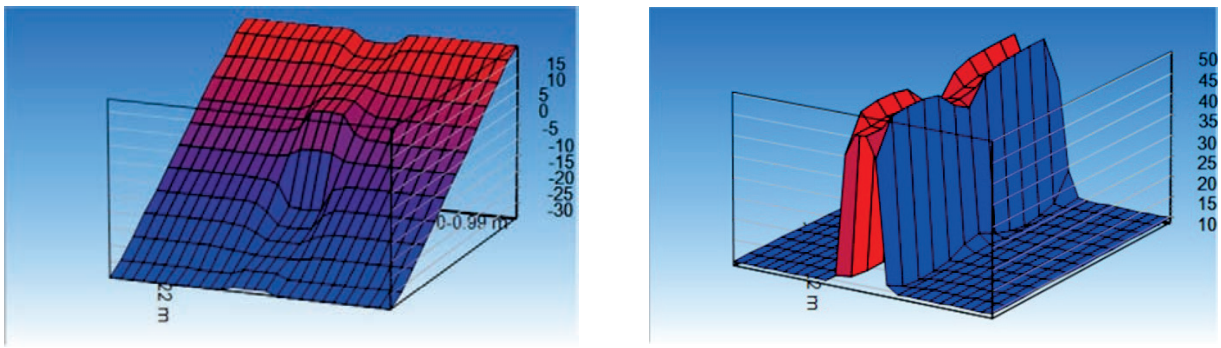

a) *b)*

Figure 4. 3-D distribution graphs on the inner surface of the structure: a) temperatures; b) heat flow

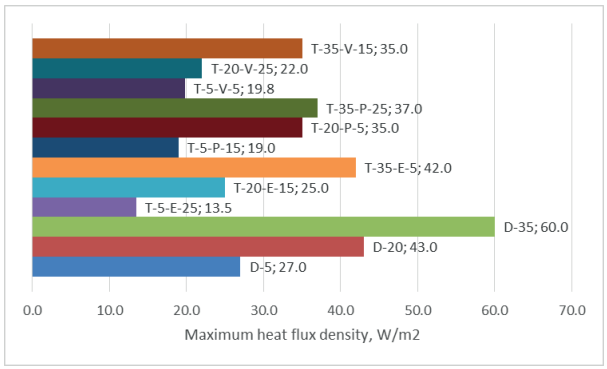

a)

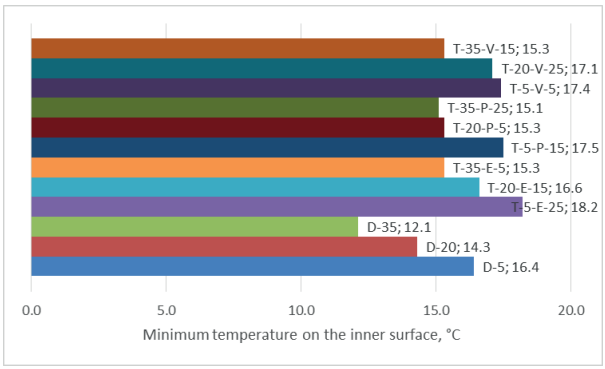

b)

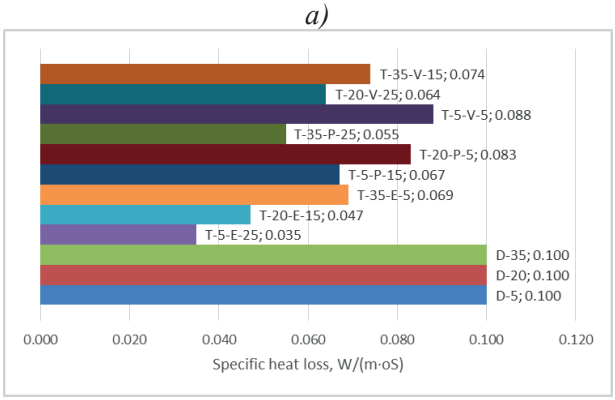

c)

Figure 5. Results of numerical research: a) Maximum heat flux density, W/m²; b) Minimum temperature on the inner surface, °C; c) Specific heat loss, W/(m·oS)

The shape of the graphs of the distribution of heat flux density and temperature along the inner face of the junction is the same for all variable parameters and differs only in peak values. The results of the numerical study are shown in the histograms of Figure 5.

Numerical values of the heat flux density, as well as the temperature on the inner surface of the enclosing structure for various combinations of variable parameters are given in Table 1 and 2, respectively.

Table 1. Heat flux density values for various combinations of variable parameters

Thermal conductivity coefficient of the material, W/(m*^{0}C)		Expanded polystyrene			Penofol			Air			Without insertion
Insert thickness, mm		5	15	25	5	15	25	5	15	25	
Outdoor temperature, ^{0}C	-5	19.5	16.0	13.5	22.0	19.0	17.0	19.8	16.1	13.6	27.0
	-20	31.0	25.0	22.0	35.0	31.0	27.0	32.0	25.5	22.0	43.0
	-35	42.0	34.0	29.5	49.5	42.0	37.0	44.0	35.1	30.0	60.0

Table 2. Temperature values on the inner surface of the structure for various combinations of variable parameters

Thermal conductivity coefficient of the material, W/(m*^{0}C)		Expanded polystyrene			Penofol			Air			Without insertion
Insert thickness, mm		5	15	25	5	15	25	5	15	25	
Outdoor temperature, ^{0}C	-5	17.4	17.9	18.2	17.1	17.5	17.8	17.4	18.1	18.2	16.4
	-20	15.7	16.6	17.1	15.3	16.0	16.4	15.8	16.6	17.1	14.3
	-35	15.3	15.4	16.1	13.2	14.4	15.1	14.3	15.3	16.1	12.1

CONCLUSIONS

Thus, based on the results of numerical studies of the energy efficiency of the joints of wall panels with a wooden frame, the following conclusions can be drawn:

1. Numerical calculations of the effect of dissections on the work of the nodal racks of wooden panels are carried out. The possibility of their use in node connection racks has been determined.
2. The dependences of the density of the heat flow passing through the linear thermal heterogeneity on the type of insulation used in the dissection, the width of the dissection and the outdoor temperature are determined.
3. By calculating two-dimensional temperature fields in the cross section of the node, isofields of temperature distribution inside the structure, isofields of heat flux density and its direction, lines of temperature distribution and heat flux density along the inner and outer surfaces are obtained.
4. The value of specific heat loss through linear thermal heterogeneity (wooden joint ribs) is calculated, which directly takes into account heat loss in the junction when calculating the reduced heat transfer resistance.
5. It was found that the heat flux density in the ribs with heat-insulating inclusions is less in comparison with solid wood parts by an amount from 13% to 52%.

GRATITUDE

The research was carried out within the state assignment in the field of scientific activity of the Ministry of Science and Higher Education of the Russian Federation (theme FZUN-2024-0004, state assignment of the VlSU).

REFERENCES

1. **Larbi A.** Ben Statistical modelling of heat transfer for thermal bridges of buildings // Energy and Buildings. 2005. № 9 (37). C. 945–951.
2. **Zhou S.-M.** [et al.]. Accurate global buckling simulation approach for composite walls with complex boundary conditions // Journal of Building Engineering. 2023. C. 105953.
3. **Carlos A. Moreno-Camacho, Jairo R. Montoya-Torresa, Anicia J., and Natacha G**. Sustainability Metrics for Real Case Applications of the Supply Chain Network Design Problem: A Systematic Literature Review. URL: https://www.sciencedirect.com/science/article/pii/S2352710221007518 (Accessed: 24.03.2023).

4. **Tadeu A.** [et al.]. Simulation of dynamic linear thermal bridges using a boundary element method model in the frequency domain // Energy and Buildings. 2011. № 12 (43). C. 3685–3695.
5. **Quinten J., Feldheim V.** Mixed equivalent wall method for dynamic modelling of thermal bridges: Application to 2-D details of building envelope // Energy and Buildings. 2019. (183). C. 697–712.
6. **Zalewski L.** [et al.]. Experimental and numerical characterization of thermal bridges in prefabricated building walls // Energy Conversion and Management. 2010. № 12 (51). C. 2869–2877.
7. **Ramalho de Freitas J., Grala da Cunha E**. Thermal bridges modeling in South Brazil climate: Three different approaches // Energy and Buildings. 2018. (169). C. 271–282.
8. **Soares N.** [et al.]. Energy efficiency and thermal performance of lightweight steel-framed (LSF) construction: A review // Renewable and Sustainable Energy Reviews. 2017. (78). C. 194–209.
9. **Santos P., Mateus D**. Experimental assessment of thermal break strips performance in load-bearing and non-load-bearing LSF walls // Journal of Building Engineering. 2020. (32).
10. **Höglund T., Burstrand H.** Slotted steel studs to reduce thermal bridges in insulated walls // Thin-Walled Structures. 1998. № 1–3 (32). C. 81–109.
11. **Martins C., Santos P., Silva L.S.** Da Lightweight steel-framed thermal bridges mitigation strategies: A parametric study // Journal of Building Physics. 2016. № 4 (39). C. 342–372.
12. **Santos P.** [et al.]. Thermal performance of lightweight steel framed wall: The importance of flanking thermal losses // Journal of Building Physics. 2014. № 1 (38). C. 81–98.
13. **Santos P**. [et al.]. Thermal transmittance of lightweight steel framed walls: Experimental versus numerical and analytical approaches // Journal of Building Engineering. 2019. (25).
14. **Kuo S., Chaorong Z., Xiaodong W.** Thermal performance and thermal transmittance prediction of novel light-gauge steel-framed straw walls - ScienceDirect [Electronic resource]. URL: https://www.sciencedirect.com/science/article/pii/S2352710223001523 (Accessed: 24.03.2023).
15. **Yu S**. [et al.]. Theoretical, experimental and numerical study on the influence of connectors on the thermal performance of precast concrete sandwich walls // Journal of Building Engineering. 2022. (57).
16. **Hallik J., Kalamees T.** The effect of flanking element length in thermal bridge calculation and possible simplifications to account for combined thermal bridges in well insulated building envelopes // Energy and Buildings. 2021. (252).
17. **Lin W., Liu X., Zhang T.** Indoor thermal and humid stratification and statistical distribution in ice arenas // Journal of Building Engineering. 2023. (67).
18. **Liu C.** [et al.]. A new demountable light-gauge steel framed wall: Flexural behavior, thermal performance and life cycle assessment // Journal of Building Engineering. 2022. (47).
19. **Kosny J., Christian J.E.** Thermal evaluation of several configurations of insulation and structural materials for some metal stud walls // Energy and Buildings. 1995. № 2 (22). C. 157–163.
20. **Romero M.J., Aguilar F., Vicente P.G.** Analysis of design improvements for thermal bridges formed by double-brick façades and intermediate slabs for nZEB residential buildings in Spain // Journal of Building Engineering. 2021. (44).
21. **Santos P., Lemes G., Mateus D.** Analytical methods to estimate the thermal transmittance of LSF walls: Calculation procedures review and accuracy comparison // Energies. 2020. № 4 (13).

22. **Theodosiou T.** [et al.]. Assessing the accuracy of predictive thermal bridge heat flow methodologies // Renewable and Sustainable Energy Reviews. 2021. (136).
23. **Soares N.** [et al.]. Laboratory and in-situ non-destructive methods to evaluate the thermal transmittance and behavior of walls, windows, and construction elements with innovative materials: A review // Energy and Buildings. 2019. (182). C. 88–110.
24. **Roque E., Santos P.** The effectiveness of thermal insulation in lightweight steel-framedwalls with respect to its position // Buildings. 2017. № 1 (7).
25. **Sun K., Zheng C., Wang X.** Thermal performance and thermal transmittance prediction of novel light-gauge steel-framed straw walls // Journal of Building Engineering. 2023. (67). C. 105973.
26. **Santos P., Lemes G., Mateus D.** Thermal transmittance of internal partition and external facade LSF walls: A parametric study // Energies. 2019. № 14 (12).
27. **Santos P., Lopes P., Abrantes D.** Thermal Performance of Load-Bearing, Lightweight, Steel-Framed Partition Walls Using Thermal Break Strips: A Parametric Study // Energies. 2022. № 24 (15).
28. **Perera D**. [et al.]. Energy performance of fire rated LSF walls under UK climate conditions // Journal of Building Engineering. 2021. (44).
29. **Angelis E. De, Serra E.** Light steel-frame walls: Thermal insulation performances and thermal bridges // Energy Procedia. 2014. (45). C. 362–371.
30. **François A.** [et al.]. In situ measurement method for the quantification of the thermal transmittance of a non-homogeneous wall or a thermal bridge using an inverse technique and active infrared thermography // Energy and Buildings. 2021. (233).
31. **Gribanov A.S., Rimshin V.I., Roshchina S.I.** Experimental investigations of composite wooden beams with local wood modification // IOP Conference Series: Materials Science and Engineering. 2019.
32. **Travush V.** [et al.]. Mechanical Safety and Survivability of Buildings and Building Structures under Different Loading Types and Impacts // Procedia Engineering. 2016. (164). C. 416–424.
33. **Fyodorov, V.S., Sidorov, V.N., Shepitko, E.S.** Computer simulation of composite beams dynamic behavior // Materials Science Forum. 2020. (974 MSF), C. 687–692.
34. Rimshin V. [et al.]. Multi-span composite beam // IOP Conference Series: Materials Science and Engineering. 2020.
35. **Rimshin V.I.** [et al.]. Improvement of strength and stiffness of components of main struts with foundation in wooden frame buildings // ARPN Journal of Engineering and Applied Sciences. 2018 13(11) 3851-3856.
36. **Roschina S.I.** [et al.]. Application of high glued wooden beams in the ceiling of buildings textile plants // Izvestiya Vysshikh Uchebnykh Zavedenii, Seriya Teknologiya Tekstil'noi Promyshlennosti. 2016.
37. **Rimshin V.** [et al.]. Regulatory support for the use of composite rod reinforcement in concrete structures//IOP Conference Series: Materials Science and Engineering. 2020 (896).
38. **Rimshin V.** [et al.]. Reinforced Concrete Vertical Structures Under a Gently Sloping Shell of Double Curvature Under the Influence of Progressive Collapse // Lecture Notes in Civil Engineering. 2022. (182). C. 577–587.
39. **Rimshin V.I.** [et al.]. Engineering Calculations of Acidifier Retaining Walls During Water Treatment Facilities Designing // Lecture Notes in Civil Engineering. 2022. (182). C. 55–73.
40. **Rimshin V.** [et al.]. Influence of Different Types of Aggregates on the Structural Properties of Fiber-Reinforced Concrete // Lecture Notes in Networks and Systems. 2022. (403 LNNS). C. 1467–1476.

СПИСОК ЛИТЕРАТУРЫ

1. **Ларби А.** Статистическое моделирование теплопередачи для тепловых мостов

зданий // Энергетика и здания. 2005. № 9 (37). С. 945-951.
2. **Чжоу С.-М**. [и др.]. Точный подход к моделированию глобальной потери устойчивости для композитных стен со сложными граничными условиями // Journal of Building Engineering. 2023. С. 105953.
3. **Карлос А. Морено-Камачо, Хайро Р. Монтойя-Торреса, Анисия Дж. и Наташа Г.** Показатели устойчивости для реальных применений проблемы проектирования сети цепочки поставок: Систематический обзор литературы. URL: https://www.sciencedirect.com/science/article/pii/S2352710221007518 (дата обращения: 24.03.2023).
4. **Тадеу А.** [и др.]. Моделирование динамических линейных тепловых мостов с использованием модели методом граничных элементов в частотной области // Энергетика и здания. 2011. № 12 (43). С. 3685-3695.
5. **Квинтен Дж., Фельдхайм В.** Метод смешанных эквивалентных стен для динамического моделирования тепловых мостов: применение к двумерным деталям ограждающих конструкций зданий // Энергетика и здания. 2019. (183). С. 697-712.
6. **Залевский Л.** [и др.]. Экспериментальная и численная характеристика тепловых мостиков в стенах сборных зданий // Преобразование энергии и управление. 2010. № 12 (51). С. 2869-2877.
7. **Рамальо де Фрейтас Х., Грала да Кунья Э.** Моделирование тепловых мостов в климате Южной Бразилии: три различных подхода // Энергетика и здания. 2018. (169). С. 271-282.
8. **Соареш Н.** [и др.]. Энергоэффективность и тепловые характеристики легких конструкций со стальным каркасом (LSF): обзор // Обзоры возобновляемой и устойчивой энергетики. 2017. (78). С. 194-209.
9. **Сантос П., Матеус Д**. Экспериментальная оценка эффективности термо-разрушающих полос в несущих и ненесущих стенах из LSF // Журнал строительной инженерии. 2020. (32).
10. **Хоглунд Т., Бурстранд Х.** Стальные шпильки с прорезями для уменьшения тепловых мостиков в изолированных стенах // Тонкостенные конструкции. 1998. № 1-3 (32). С. 81-109.
11. **Мартинс С., Сантос П., Сильва Л.С.** Стратегии смягчения последствий тепловых мостов с легким стальным каркасом: параметрическое исследование // Journal of Building Physics. 2016. № 4 (39). С. 342-372.
12. **Сантос П.** [и др.]. Тепловые характеристики легких стальных каркасных стен: важность снижения тепловых потерь по бокам // Журнал строительной физики. 2014. № 1 (38). С. 81-98.
13. **Сантос П.** [и др.]. Коэффициент теплопередачи легких стальных каркасных стен: экспериментальный в сравнении с численным и аналитическим подходами // Journal of Building Engineering. 2019. (25).
14. **Куо С., Чаоронг З., Сяодун В.** Прогноз тепловых характеристик и коэффициента теплопередачи новых соломенных стен со стальным каркасом малой толщины - ScienceDirect [Электронный ресурс]. URL: https://www.sciencedirect.com/science/article/pii/S2352710223001523 (дата обращения: 24.03.2023).
15. **Ю.С.** [и др.]. Теоретическое, экспериментальное и численное исследование влияния соединителей на тепловые характеристики сборных железобетонных многослойных стен // Journal of Building Engineering. 2022. (57).
16. **Халлик Дж., Каламис Т.** Влияние длины фланкирующего элемента при расчете теплового моста и возможные упрощения для учета комбинированных тепловых мостов в хорошо изолированных

ограждающих конструкциях зданий // Энергетика и здания. 2021. (252).
17. **Лин У., Лю Х., Чжан Т.** Тепловая и влажностная стратификация помещений и статистическое распределение на ледовых аренах // Журнал строительной инженерии. 2023. (67).
18. **Лю С.** [и др.]. Новая съемная стена из легкого стального каркаса: поведение при изгибе, тепловые характеристики и оценка жизненного цикла // Journal of Building Engineering. 2022. (47).
19. **Косны Дж., Кристиан Дж. Э**. Тепловая оценка нескольких конфигураций изоляционных и конструкционных материалов для некоторых металлических стен с шипами // Энергетика и здания. 1995. № 2 (22). С. 157-163.
20. **Ромеро М. Дж., Агилар Ф., Висенте П.Г**. Анализ конструктивных усовершенствований тепловых мостиков, образованных фасадами из двойного кирпича и промежуточными плитами для жилых зданий nZEB в Испании // Journal of Building Engineering. 2021. (44).
21. **Сантос П., Лемес Г., Матеус Д.** Аналитические методы оценки коэффициента теплопередачи стен LSF: обзор процедур расчета и сравнение точности // Энергия. 2020. № 4 (13).
22. **Теодосиу Т.** [и др.]. Оценка точности методик прогнозирования тепловых потоков по тепловому мосту // Обзоры возобновляемой и устойчивой энергетики. 2021. (136).
23. **Соареш Н.** [и др.]. Лабораторные и натурные неразрушающие методы оценки коэффициента теплопередачи и поведения стен, окон и строительных элементов с использованием инновационных материалов: обзор // Энергетика и здания. 2019. (182). С. 88-110.
24. **Роке Э., Сантос П.** Эффективность теплоизоляции в легких стенах со стальным каркасом в зависимости от их расположения // Здания. 2017. № 1 (7).
25. **Сунь К., Чжэн С., Ван Х.** Прогноз тепловых характеристик и коэффициента теплопередачи новых стен из соломы со стальным каркасом малого диаметра // Журнал строительной инженерии. 2023. (67). С. 105973.
26. **Сантос П., Лемес Г., Матеус Д.** Коэффициент теплопередачи внутренних перегородок и наружных фасадных стен LSF: параметрическое исследование // Энергия. 2019. № 14 (12).
27. **Сантос П., Лопес П., Абрантес Д.** Тепловые характеристики несущих легких перегородок со стальным каркасом с использованием терморазрывных полос: параметрическое исследование // Энергия. 2022. № 24 (15).
28. **Перера Д.** [и др.]. Энергетические характеристики огнестойких стен из LSF в климатических условиях Великобритании // Journal of Building Engineering. 2021. (44).
29. **Ангелис Э. Де, Серра Э.** Легкие стены из стального каркаса: теплоизоляционные характеристики и тепловые мостики // Energy Procedia. 2014. (45). С. 362-371.
30. **Франсуа А**. [и др.]. Метод измерения на месте для количественной оценки коэффициента теплопередачи неоднородной стены или теплового моста с использованием обратной методики и активной инфракрасной термографии // Энергетика и здания. 2021. (233).
31. **Грибанов А.С., Римшин В.И., Рощина С.И.** Экспериментальные исследования композитных деревянных балок с локальной модификацией древесины // Серия конференций IOP: Материаловедение и инженерия. 2019.
32. **Травуш В.** [и др.]. Механическая безопасность и живучесть зданий и строительных конструкций при различных типах нагрузок и воздействий // Procedia Engineering. 2016. (164). С. 416-424.
33. **Федоров В.С., Сидоров В.Н., Шепитько Е.С.** Компьютерное моделирование

динамического поведения композитных балок // Форум по материаловедению. 2020. (974 MSF), С. 687-692.
34. **Римшин В.** [и др.]. Многопролетная композитная балка // Серия конференций IOP: Материаловедение и инженерия. 2020.
35. **Римшин В.И.** [и др.]. Повышение прочности и жесткости элементов основных стоек с фундаментом в деревянных каркасных зданиях // ARPN Journal of Engineering and Applied Sciences. 2018 13(11) 3851-3856.
36. **Рощина С.И.** [и др.]. Применение высоких клееных деревянных балок в перекрытиях зданий текстильных предприятий // Известия высших учебных заведений, серия технология текстильной промышленности. 2016.
37. **Римшин, В.** [и др.]. Нормативное обеспечение применения композитной стержневой арматуры в бетонных конструкциях //Серия конференций IOP: Материаловедение и инженерия. 2020 (896).
38. **Римшин В**. [и др.]. Железобетонные вертикальные конструкции под пологой оболочкой двойной кривизны под воздействием прогрессирующего обрушения // Конспекты лекций по гражданскому строительству. 2022. (182). С. 577-587.
39. **Римшин В.И.** [и др.]. Инженерные расчеты подпорных стенок подкислителя при проектировании водоочистных сооружений // Конспекты лекций по гражданскому строительству. 2022. (182). С. 55-73.
40. **Римшин В.** [и др.]. Влияние различных типов заполнителей на структурные свойства фибробетона // Конспекты лекций по сетям и системам. 2022. (403 LNNS). С. 1467-1476.

Mikhail Vladimirovich Lukin, Candidate of Technical Sciences, Associate Professor of the Department of SC, Institute of Architecture, Construction and Energy, Vladimir State University named after Alexander Grigoryevich and Nikolai Grigoryevich Stoletov (VlSU), 87, Gorky str., Vladimir, 600000, Russian Federation, lukin_mihail_22@mail.ru.

Svetlana Ivanovna Roshchina, Doctor of Technical Sciences, Professor, Head of the Department of IC, Institute of Architecture, Construction and Energy, Vladimir State University of Alexander Grigoryevich and Nikolai Grigoryevich Stoletov (VlSU), 87, Gorky str., Vladimir, 600000, Russian Federation, rsi3@mail.ru.

Anastasia Vasilyevna Lukina, Candidate of Technical Sciences, Associate Professor of the Department of SC, Institute of Architecture, Construction and Energy, Vladimir State University of Alexander Grigoryevich and Nikolai Grigoryevich Stoletov (VlSU), 87, Gorky str., Vladimir, 600000, Russian Federation, pismo.33@yandex.ru.

Rimshin Vladimir Ivanovich, Doctor of Technical Sciences, Professor of the Department of Housing and Communal Complex of the Moscow State University of Civil Engineering, 26, Yaroslavskoye sh., Moscow, 129337, Russian Federation, v.rimshin@niisf.ru.

Михаил Владимирович Лукин, к.т.н., доцент кафедры СК, Институт архитектуры, строительства и энергетики, Владимирский государственный университет имени Александра Григорьевича и Николая Григорьевича Столетовых (ВлГУ), 87, ул. Горького, г. Владимир, 600000, Российская Федерация, lukin_mihail_22@mail.ru.

Светлана Ивановна Рощина, д.т.н., проф., зав. кафедрой СК, Институт архитектуры, строительства и энергетики, Владимирский государственный университет Александра Григорьевича и Николая Григорьевича Столетовых (ВлГУ), 87, ул. Горького, г. Владимир, 600000, Российская Федерация, rsi3@mail.ru.

Анастасия Васильевна Лукина, к.т.н., доцент кафедры СК, Институт архитектуры, строительства и энергетики, Владимирский государственный университет Александра Григорьевича и Николая Григорьевича Столетовых (ВлГУ), 87, ул. Горького, г. Владимир, 600000, Российская Федерация, pismo.33@yandex.ru.

Римшин Владимир Иванович, д.т.н., профессор кафедры Жилищно-коммунального комплекса НИУ Московского государственного строительного университета, 26, Ярославское ш., г. Москва, 129337, Российская Федерация, v.rimshin@niisf.ru.

.

International Journal for Computational Civil and Structural Engineering, 20(1) 81–87 (2024)

DOI:10.22337/2587-9618-2024-20-1-81-87

WAYS OF INCREASING OF LOADING CAPACITY OF THE REINFORCED CONCRETE SHALLOW SHELLS WITH A FLAT RECTANGULAR CONTOUR

Khanlar K. Seyfullayev [1], Gulnara Kh. Jabrayilova [2]

[1] Azerbaycan Scientific-Research Institut of Construction and Architecture. Baku, AZERBAIJAN
[2] Azerbaijan University of Architecture and Construction. Baku, AZERBAIJAN

Abstract: Shallow shells with variable curvature, prestressing contour and fixed above by horizontal reinforcing of two opposite contour elements are considered in the given article. These two offered ways practically produces non-moment state and increase loading capacity of the shallow shells several times. Method of definition of loading capacity of the shallow shells with a flat rectangular contour was worked out, and it's aim consists of that initial moment state before loss of loading capacity is described by nonlinear differential equations of the theory of the shallow shells. And then accentuating the main part of the solution of equations we receive the linear system of homogeneous differential equations with variable coefficients. The solution of the linearizated equations enables to define the forms of losing of loading capacity of shallow shells.

Key words: capacity, reinforced concrete, shallow shells, flat rectangular contour, non-moment, moment state, moment and to linear state, nonlinear and states moment state

СПОСОБЫ ПОВЫШЕНИЯ НЕСУЩЕЙ СПОСОБНОСТИ ПОЛОГИХ ЖЕЛЕЗОБЕТОННЫХ ОБОЛОЧЕК С ПРЯМОУГОЛЬНЫМ КОНТУРОМ

Х.К. Сейфуллаев [1], Г.Х. Джебраилова [2]

[1] Азербайджанский научно-исследовательский институт строительства и архитектуры, г. Баку, АЗЕРБАЙДЖАН
[2] Азербайджанский Архитектурный и Строительный Университет, г. Баку, АЗЕРБАЙДЖАН

Аннотация: В работе рассматриваются способы повышения несущей способности пологих железобетонных оболочек переменной кривизны с предварительно-напряженным контуром и закрепленных сверху горизонтальными арматурами двух противоположных контурных элементов. Эти два предложенных способа практически создают безмоментное состояние и повышают несущую способность пологих оболочек в несколько раз.

Ключевые слова: несущая способность, железобетон, пологие оболочки, плоский прямоугольный контур, безмоментное, моментное состояние, моментное и линейное состояние, нелинейное и моментное состояние

CONTENT OF THE WORK

Shallow shells are applied widely as covers of residential and public buildings due to small rise in a center and flat rectangular contour.

Rational usage of space constructions is reached by providing of their work in non-moment intense state.

As you know, loading capacity of the reinforced shallow shells is approximately defined by the method of limiting balance on the basis of experimental researches.

$$D\Delta^2 w - K_x \frac{\partial^2 \varphi}{\partial y^2} - K_y \frac{\partial^2 \varphi}{\partial x^2} + 2K_{xy} \frac{\partial^2 \varphi}{\partial x \partial y} - L(w, \varphi) = q$$

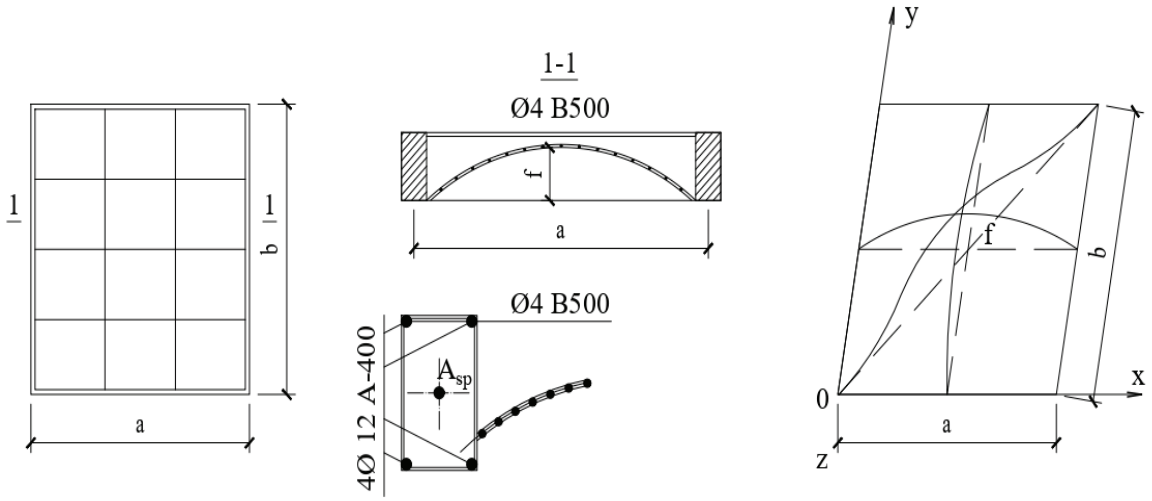

Here the following designations are accepted:
The initial intense state of the shallow shells with variable curvature is described by the following nonlinear differential equations:

$$\frac{1}{Eh}\Delta^2\varphi + K_x\frac{\partial^2 w}{\partial y^2} + K_y\frac{\partial^2 w}{\partial x^2} + 2K_{xy}\frac{\partial^2 w}{\partial x\partial y} + \\ +\frac{1}{2}L(w,w) = 0 \qquad (1)$$

D - cylindrical rigidity, v- is Poisson's ratio, Δ and L differential operators [5,6]:

$$D = K_0E_b\left(K_bI_{x,b} + nK_sI_{x,s}\right)$$
$$K_b = 1{,}5\left(1 - \frac{1}{3}K_0^2\right) - \gamma_{bl}\left(1 + \frac{K_0}{2}\right)(1 - K_0);$$
$$I_{x,b} = \frac{by^3}{3}$$
$$I_{x,s} = A_s(h_0 - y)^2 + \frac{\acute{\varepsilon}_s}{\varepsilon_{sl}}\acute{A}_s(y - \acute{a})^2;$$
$$K_s = \frac{\varepsilon_{sl}}{\varepsilon_s K_0}$$
$$K_0 = 1 \quad \text{and} \quad \gamma_{bl} = 1:$$
$$D_0 = E_b\left[\frac{by^3}{3} + nA_s(h_0 - y)^2\right]$$

The height of the compressed zone of concrete is determined by solving the following quadratic equation:

$$\xi^2 + 2n\mu_s\xi - 2n\mu_s = 0$$

here

$$\mu_s = \frac{A_s}{bh_0} \;\; ; \;\; n = \frac{E_s}{E_b}$$
$$D_p = K_0E_b\left(K_bI_{x,b} + nK_sI_{x,s}\right)$$

The height of the compressed zone of concrete during bending is determined by the formula [5,6]:

$$\xi = \frac{n_R\mu_s}{1 - K_0 - 0{,}5(1 - \gamma_{bl})(1 - K_0)}$$

where

$$n_R = \frac{R_s}{R_b} \;;\; K_s = \frac{\varepsilon_{sl}}{\varepsilon_s K_0} \;;\; \varepsilon_s = \varepsilon_{b2}\frac{h_0 - y}{y}$$
$$\Delta(\dots) = \frac{\partial^2(\dots)}{\partial x^2} + \frac{\partial^2(\dots)}{\partial y^2}$$
$$L(w,\varphi) = \frac{\partial^2 w}{\partial x^2}\frac{\partial^2\varphi}{\partial y^2} + \frac{\partial^2 w}{\partial y^2}\frac{\partial^2\varphi}{\partial x^2} \\ - 2\frac{\partial^2 w}{\partial x\partial y}\frac{\partial^2\varphi}{\partial x\partial y}$$

K_x, K_y, and K_{xy}- variable curvatures.
Equation of the middle surface of the shallow shells with a flat rectangular contour is accepted in the following form:

$$Z(x,y) = -\frac{16f}{a^2b^2}(ax - x^2)(by - y^2) \qquad (2)$$

The curvatures of the middle surface of the shells can be defined by the following formulas because of shallowness:

$$K_x = \frac{32f}{a^2b^2}(by - y^2): \qquad K_y = \frac{32f}{a^2b^2}(ax - x^2):$$
$$K_{xy} = -\frac{16f}{a^2b^2}(a - 2x)(b - 2y) \qquad (3)$$

The end conditions on a contour can be written in the form:
On line x=0 and x=a:

$$w = 0; \qquad \frac{\partial^3\varphi}{\partial x^3} + (2 + v)\frac{\partial^3\varphi}{\partial x\partial y^2} = \frac{Eh}{B_h}\varphi;$$
$$\frac{\partial^2 w}{\partial x^2} + v\frac{\partial^2 w}{\partial y^2} = 0;$$
$$\frac{\partial^2\varphi}{\partial x^2} - v\frac{\partial^2\varphi}{\partial y^2} = \frac{PEh}{E_bA_0}\left(1 - \frac{6e_0}{H}\right) \qquad (4)$$

The end conditions have the similar form on a contour along the line y=0 and y=b.
The bending forces of the shallow shells considerably are decreased in these end conditions.
The solution of the nonlinear differential equations with variable coefficients (1) presents large mathematical difficulties in these end conditions (4). Therefore the approximate method is used for the solution of the equations (1), which was developed in the work [2, 3], and the aim of which consists of the following:
The functions of stress and deflection are presented in the following form:

$$\varphi = \Phi(x, y) + \bar{\Phi}(x, y);$$
$$w = W(x, y) + \bar{W}(x, y) \qquad (5)$$

Here W and Φ functions of stress and deflection are appropriate to initial intense state of the shell. $\bar{\Phi}$ and $\bar{W}$ is the increase of these functions at the moment of losing the loading capacity of the shell, which are considered small.
Substituting ferreted functions (5) in this initial system of differential equations (1), neglecting the small members, we shall receive linear differential equations, from the solution of which the loading capacity of reinforced concrete shallow shells will be determined by the conditions of the loss of stability:

$$D\Delta^2\bar{W} - K_x\frac{\partial^2\bar{\Phi}}{\partial y^2} - K_y\frac{\partial^2\bar{\Phi}}{\partial x^2} + 2K_{xy}\frac{\partial^2\bar{\Phi}}{\partial x\partial y} +$$
$$+N_x^0\frac{\partial^2\bar{W}}{\partial x^2} + N_y^0\frac{\partial^2\bar{W}}{\partial y^2} + 2N_{xy}^0\frac{\partial^2\bar{W}}{\partial x\partial y} = 0,$$
$$\frac{1}{Eh}\Delta^2\bar{\Phi} + K_x\frac{\partial^2\bar{W}}{\partial y^2} + K_y\frac{\partial^2\bar{W}}{\partial x^2} + 2K_{xy}\frac{\partial^2\bar{W}}{\partial x\partial y} -$$
$$-\frac{1}{2}L(W, \bar{W}) = 0$$

Here N_x^0, N_y^0 and N_{xy}^0 are the initial membrane forces before losing the loading capacity of the reinforced concrete shallow shells, which are defined by the solution of the nonlinear differential equations and are considered known.
So, the problem of investigation of loading capacity of the shallow shells is led to integration of the nonlinear differential equations (1) and (6).
The nonlinear differential equations, describing the initial moment state, are is solved by us using small parameter method in the works [2, 3]
The geometrical sizes and reinforcing of the shallow shells are produced on the basis of calculation, which are received from solution of the equations (1), and then the loading capacity of considered design of the shell is checked up on the basis of the solution of the differential equations (6).
In practical calculations the initial intense state of the shallow shells, depending on the accuracy of calculation, the loading capacity of the reinforced shallow shells are accepted as following states:

a) Initial condition is non-moment state.

The initial differential equation is simplified in this case and accepts the form [1, 2]:

$$K_x\frac{\partial^2\Phi}{\partial y^2} - K_y\frac{\partial^2\Phi}{\partial x^2} + 2K_{xy}\frac{\partial^2\Phi}{\partial x\partial y} = -q \qquad (7)$$

The initial membrane forces N_x^0, N_y^0 and N_{xy}^0 are defined by solving of this equation through stress function by the known formulas Erie.

b) Initial condition is moment and to linear state.

The nonlinear differential operators are neglected in the initial differential equations (1)

and known differential equations of the theory of the shallow shells are received.

$$D\Delta^2 W - K_x\frac{\partial^2\Phi}{\partial y^2} - K_y\frac{\partial^2\Phi}{\partial x^2} + 2K_{xy}\frac{\partial^2\Phi}{\partial x\partial y} = q$$
$$\frac{1}{Eh}\Delta^2\Phi + K_x\frac{\partial^2 W}{\partial y^2} + K_y\frac{\partial^2 W}{\partial x^2} + 2K_{xy}\frac{\partial^2 W}{\partial x\partial y} = 0 \quad (8)$$

Solution of the differential equations (8) was received by many authors and is resulted in the literature [4].

c) Initial condition is nonlinear and moment state.

The initial equations up to the before critical state are described by the nonlinear equations (1). Solution of these nonlinear equations were indicated in the work [2,3] on the basis of a small parameter method. The solution of the considered problem is difficult in such setting a task. Therefore the gained results present the theoretical and practical interest in designing of the reinforced concrete shallow shells.

When the solution of the equations describing initial state of the shallow shells is found or known, then it is possible to find and investigate the loading capacity of the shell.

Differential equations (6) is large in appearance, form the point of view of initial nonlinear and moment state, and therefore it isn't given in this article.

Increasing of functions . $\bar{\Phi}$ and $\bar{W}$ describing the state in losing of loading capacity we shall accept in the following form:

$$\overline{W}(x,y) = \bar{B}_{mn}sin(\lambda_m x)sin(\mu_n y);$$

$$\bar{\Phi}(x,y) = \bar{A}_{mn}sin(\lambda_m x)sin(\mu_n y) - \sum_m \left\{\begin{matrix}\left[\frac{1}{\lambda_m^2} - \frac{vb^2}{2}\left(\frac{y^2}{b^2} - \frac{y}{b}\right)\right]X_m - \\ -\frac{Ehb^2}{2}\left(\frac{y^2}{b^2} - \frac{y}{b}\right)P_m\end{matrix}\right\} sin(\lambda_m x) -$$
$$-\sum_n\left\{\left[\frac{1}{\mu_n^2} - \frac{va^2}{2}\left(\frac{x^2}{a^2} - \frac{x}{a}\right)\right]\xi_n - \frac{Eha^2}{2}\left(\frac{x^2}{a^2} - \frac{x}{a}\right)\theta_n\right\} sin(\mu_n y) \quad (9)$$

$$\lambda_m = \frac{m\pi}{a}, \quad \mu_n = \frac{n\pi}{b}$$

The unary series in the function of stress (9) takes into account the influences of prestressing of the contour elements and horizontal reinforcing excluding horizontal displacements of the contour elements.

Substituting (9), received from (6), in the system of differential equations and then using end conditions (4), from the condition of a non-trivial solution of the received systems of algebraic equations, we'll receive the following in the general form:

$$q = \frac{1}{K(m,n)}\left(D\Delta_{mn}^2 + \frac{Eh\Delta_{kmn}^2}{\Delta_{mn}^2}\right) + P(m,n) + N(m,n) \quad (10)$$

As it is visible, the loading capacity of the shell depends on the form deformation at losing of stability. In varying ***m*** and ***n*** we find the least significance ***q*** and form of losing of loading capacity of the shell.

The offered method is general and it is possible in particular case to receive the known solutions for various classes of shells from it.

On the basis of the manual [4] the reinforced thin-walled shells are calculated on the action of an external load ***q*** on linear moment theory and then their designing and reinforcing are performed. In this case the significance of external load ***q*** should not exceed the significance of loading capacity $\boldsymbol{q_u}$.

For example, we'll consider a cylindrical shell, fixed above by horizontal reinforcing, providing immobility of the contour elements. In the considered example the prestressing of the contour elements are absent.

Initial state of the shell is non-moment. The initial up to critical state of the shell is described by the following equation:

$$\frac{1}{R}\frac{\partial^2\Phi}{\partial y^2} = -q. \qquad (11)$$

Decision of the equation (11) we accept in the form:

$$\Phi(x,y) = \sum_m \sum_n A_{mn} sin(\lambda_m x) sin(\mu_n y) - \\ - \sum_n \left[\frac{1}{\mu_n^2} - \frac{va^2}{2}\left(\frac{x^2}{a^2} - \frac{x}{a}\right)\right] \xi_n sin(\mu_n y) \qquad (12)$$

The coefficients of series of the solution (12) have the following significances satisfying the end conditions (4) and (11):

$$A_{mn} = \frac{16qR}{mn\pi^2\lambda_m^2} + \frac{4}{m\pi\lambda_m^2}\left(1 + v\frac{\lambda_m^2}{\mu_n^2}\right)\xi_n$$

$$\sum_m \frac{16\Delta_{mn}^{(2+v)}}{mn\pi^2\lambda_m^2} qR =$$

$$= \left[\frac{v(2+v)}{2} a\mu_n^2 - \sum_m \frac{4\Delta_{mn}^{(2+v)}}{n\pi\lambda_m^2}\left(1 + v\frac{\lambda_m^2}{\mu_n^2}\right)\right]\xi_n$$

$$\Delta_{mn}^{(2+v)} = \lambda_m^3 + (2+v)\lambda_m\mu_n^2$$

Differential equations for the determination of loading capacity (6) for considered case accept the following form:

$$D\Delta^2\overline{W} - \frac{1}{R}\frac{\partial^2\bar{\Phi}}{\partial y^2} - q\left\{\frac{\partial^2\overline{W}}{\partial x^2}\sum_m\sum_n a_{mn} sin(\lambda_m x)\, sin(\mu_n y) - \sum_n\left[1 - \frac{v\mu_n^2}{2}(x^2 - ax)\right]\xi_n sin(\mu_n y) + \right.$$
$$\frac{\partial^2\overline{W}}{\partial y^2}\left[v\sum \xi_n sin(\mu_n y) - \sum_m\sum_n a_{mn}\lambda_m^2 sin(\lambda_m x) sin(\mu_n y)\right] - 2\frac{\partial^2\overline{W}}{\partial x\partial y}\left[\frac{v\mu_n}{2}(2x - a)\xi_n cos(\mu_n y)\right] +$$
$$\left. + a_{mn}\lambda_m\mu_n cos(\lambda_m x) cos(\mu_n y)\right\} = 0, \qquad (13)$$

$$\frac{1}{Eh}\Delta^2\,\bar{\Phi} + \frac{1}{R}\frac{\partial^2\overline{W}}{\partial x^2} = 0$$

We accept the function of deflection $\overline{W}$ and stress $\bar{\Phi}$ in the form:

$$\overline{W} = \bar{B}_{mn} sin(\lambda_m x) sin(\mu_n y),$$
$$\bar{\Phi} = \bar{A}_{mn} sin(\lambda_m x) sin(\mu_n y). \qquad (14)$$

Substituting (14) in the (13) we find significances of the critical force or loading capacity of the shell.

It is very interesting that in the initial non-moment state the following state is realized:

$$N_x^0 = -qR; \quad N_y^0 = 0; \quad N_{xy}^0 = 0$$

Then the equation of stability accepts known form, indicated in the reference [3]. The significance of critical force:

$$q = \frac{1}{R\mu_n^2}\left(D\Delta_{mn}^2 + \frac{Eh\mu_n^2}{R^2\Delta_{mn}^2}\right),$$

$$\Delta_{mn}^2 = (\lambda_m^2 + \mu_n^2)^2$$

It is supposed that the cylindrical shell simply supported on the all contour, and the initial state is non-moment. Then in the initial state, the solution of the differential equation accepts the following form:

$$\Phi = \sum_m\sum_n qRa_{mn} sin(\lambda_m x)\, sin(\mu_n y)$$

and the critical force accepts following significances:

$$q = \frac{1}{K_0(m,n)}\left(D\Delta_{mn}^2 + \frac{Eh\mu_n^2}{R^2\Delta_{mn}^2}\right) \qquad (16)$$

m, n odd numbers.

The loading capacity of the cylindrical shallow shell determined by the formula (16) is a new solution and differs from the known formula

(15) by attendance *K(m,n)*, which expresses influence of the initial non-moment state on significance of loading capacity of the shell.
Certainly, in real terms of the work of the shell the above-mentioned intense state even with top horizontal reinforcing will not be realized. We have the following in the considered variant:

$$q = \frac{1}{K_0(m,n)}\left(D\Delta_{mn}^2 + \frac{Eh\mu_n^2}{R^2\Delta_{mn}^2}\right) + \\ +P(m,n) + N(m,n) \qquad (17)$$

Here, the second item takes into account the increasing of loading capacity of the cylindrical shallow shell because of producing of the condition with horizontal reinforcing.

CONCLUSION

So, we developed the new method of determination of loading capacity of the shallow shells on the basis of the geometrical nonlinear theory of the shallow shells. Methods of increasing of the loading capacity of the reinforced concrete shallow shells offered by us are very simple and will be easily realized in practice. They give an opportunity of their wide usage in housing construction as covers.

REFERENCES

1. **Kh.G. Seyfullayev.** On one method of research of loading capacity of the shallow shells large deflections (Russian). Collection of scientific works in mechanic, Baku, No. 4, pp. 3-6 (1994)
2. **Kh.G. Seyfullayev.** Stability of the reinforced concrete shallow shells under the action of a cross load at initial nonlinear moment state (Russian). Collection of scientific works in mechanic, Baku, No. 5, pp116-119 (1995)
3. **Kh.G. Seyfullayev.** Stability of circular cylindrical shells with variable thickness at moment-intense state (Russian). PMM, Vol.40, No.2, pp.376-383 (1976)
4. A manual on designing of the reinforced concrete space designs of covers (Russian).M. Gosstroyizdat, 1979
5. **G.Kh. Jabrayilova**. New method research on seismic resistance of bent reinforced concrete elements of the constructions that are based on a nonlinear deformation model**.** VII International conference "Seismology and engineerihg Seismology" dedicated to the 100th anniversary of the birth of the nationwide leader H. Aliyev., Baku 2023, pph. 59-69.
6. **G.Kh. Jabrayilova.** Solutions of problems of dynamics of bending reinforced concrete elements based on a nonlinear deformation model taking into account the long-term strength of concrete. Sciences of Europe (Praha, Czech Republic), vol 2, N 64 (2021), pp. 58-68.

СПИСОК ЛИТЕРАТУРЫ

1. **Х.К. Сейфуллаев.** Об одном методе исследования несущей способности пологих оболочек при больших прогибах. (Россия). Сборник научных работ по механике. (Россия). Баку, No 4, стр. 3-6 (1994).
2. **Х.К. Сейфуллаев**. Устойчивость пологих железобетонных оболочек под действием поперечной нагрузки при начальном моментном состоянии. (Россия). Сборник научных работ по механике. (Россия). Баку, No 5, стр.116-119 (1995).
3. **Х.К. Сейфуллаев**. Устойчивость круговых цилиндрических оболочек переменной толщины при моментном напряженном состоянии (Россия). ПМН, том 40, No 2, стр.376-383 (1976).
4. Руководство по проетированию железобетонных конструкций покрытия. (Россия). Госстройиздат, 1979 г.
5. **Г.Х. Джебраилова**. Новый метод исследования сейсмостойкости изгибаемых железобетонных элементов зданий на основе нелинейной деформационной модели механики. VII Международная

конференция "Сейсмология и инженерная сейсмология", посвященная 100-летию со дня рождения общенационального лидера Г.Алиева, Баку 2023, стр 59-56.

6. **Г.Х. Джебраилова**. Решения задач динамики изгибаемых железобетонных элементов на основе нелинейной деформационной модели с учетом длительной прочности бетона. Sciences of Europe (Praha, Czech Republic), vol 2, N 64 (2021), стр. 58-68

Seyfullayev Khanlar Kurban-Doktor of technical sciences, prof., Azerbaijan Scientific-Research Institute of Construction and Architecture, ASRICA, Fizuli street 65, Baku, 1014, Azerbaijan, xanlar.seyfullayev@mail.ru.

Jabrayilova Gulnara Khanlar- PhD, assos. Prof, dosent Azerbaijan University of Architecture and Construction, AzUAC, A. Sultanova street 5, 1073, Baku, Azerbaijan, gulnara.djebrailova@gmail.com.

Сейфуллаев Ханлар Курбан оглы- доктор технических наук, профессор, зав.отделом Азербайджанского научно-исследовательского института строительства и архитектуры, АзНИИСА.Улица Физули 65, Баку,1014,Азербайджан. xanlar.seyfullayev@mail.ru.

Джебраилова Гюльнара Ханлар кызы-кандидат технических наук, доцент кафедры механики, Азербайджанский Архитектурный и Строительный Университет, АзАиСУ. Улица А.Султанова 5, Баку, 1073, Азербайджан. gulnara.djebrailova@gmail.com.

DOI:10.22337/2587-9618-2024-20-1-88-97

OPTIMIZATION OF DESIGN OF THE FISH-SPAWNING PASS OF THE BAGAEVSKY HYDROELECTRIC COMPLEX USING NUMERICAL 2D MODELING

Vitaly V. Belikov, Natalya M. Borisova

Water Problems Institute of the Russian Academy of Sciences (WPI RAS), Moscow, RUSSIA

Abstract: The paper addresses numerical hydrodynamic modeling of water and sediment transport through the fish passage and spawning channel of the Bagaevsky hydroelectric complex on the Don River. The calculations are based on two-dimensional equations of shallow water and sediment transport implemented in the STREAM 2DCUDA software package. The paper gives recommendations on changing the longitudinal profile and configuration of the inlet section, as well as on increasing the roughness coefficient of the bottom and sides of the channel to ensure fish protection requirements.

Keywords: numerical modeling, shallow water equations, fish-spawning pass, flow rate, siltation, design optimization

ОПТИМИЗАЦИЯ КОНСТРУКЦИИ ПРОЕКТИРУЕМОГО РЫБОХОДНО-НЕРЕСТОВОГО КАНАЛА БАГАЕВСКОГО ГИДРОУЗЛА С ПОМОЩЬЮ ЧИСЛЕННОГО 2D-МОДЕЛИРОВАНИЯ

В.В. Беликов, Н.М. Борисова

Институт Водных проблем РАН (ИВП РАН), г. Москва, РОССИЯ

Аннотация: Рассматривается численное гидродинамическое моделирование пропуска воды и наносов через рыбоходно-нерестовый канал Багаевского гидроузла на р. Дон. В расчетах применяются двумерные уравнения мелкой воды и транспорта наносов, реализованные в программном комплексе STREAM 2DCUDA. Даются рекомендации по изменению продольного профилядна и конфигурации входного участка, а также по увеличению коэффициента шероховатости дна и бортов канала для обеспечения рыбоохранных требований.

Ключевыеслова: численное моделирование, уравнения мелкой воды, рыбоходно-нерестовый канал, скорость течения, заиление, оптимизация конструкции

INTRODUCTION

Bagayevsky hydroelectric power plant (BHPP) is a projected low-pressure hydroelectric power plant on the Don River in the Rostov region. The BHPP is located 4.4 km downstream of the inflow of the Manych River. The BHPP will ensure safe navigation conditions and the required track dimensions (80 m width, 4 m depth, 500 m radius of curvature) for unobstructed through passage of vessels along the Lower Don River during the entire navigation period.

Preliminary assessment of the consequences of the BHPP construction in terms of the fishery complex gives an extremely unfavorable forecast. The main reason for this is that the Bagayevskaya dam will cut off migration routes to fish spawning grounds. In order to overcome this problem, i.e., to separate the traffic flows of transport vessels and fish movement routes, a fish passage and spawning channel (FSC) of 5350 m length with a complex

configuration was designed separately from the navigable fairway (Fig. 1).

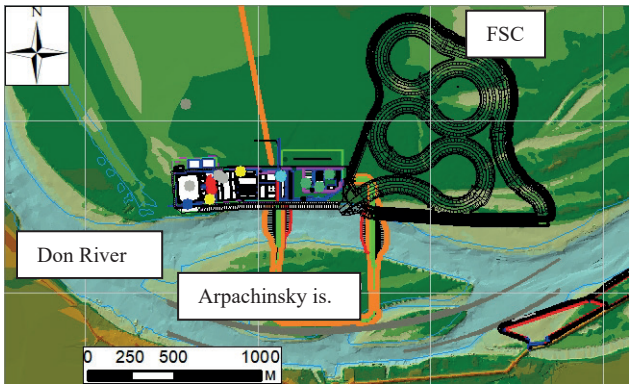

Figure 1. Scheme of the third stage of the BHPP construction period

The objective of this study is numerical modeling of FSC operation modes (Fig. 2) of the designed BHPP, determination of flow velocity characteristics along the length and width of the fish passage, forecasts of sediments at the fish passage channel and structures on it, selection of modes of hydraulic regulation of the channel.

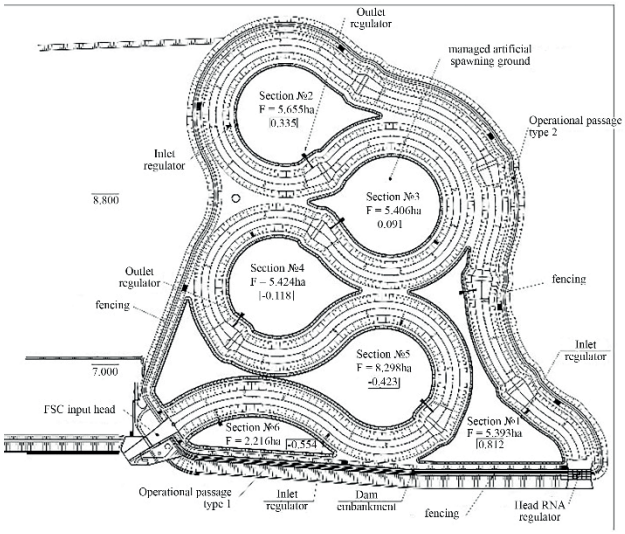

Figure 2. Schem Inlet regulatore of the FSC.

NUMERICAL HYDRODYNAMIC MODEL OF FSC

To calculate the hydrodynamic parameters of water flow and FSC siltation, we used the software package STREAM 2D CUDA [1], based on the original numerical algorithm for solving two-dimensional equations of shallow water on an uneven bottom. The latest version of STREAM 2D CUDA software package implements the new algorithm described in [2, 3]. The algorithm provides uniqueness and high accuracy of the solution in areas with complex bottom topography and hydraulic structures [4-6] and is parallelized on NVIDIA graphics processor with the use of CUDA technology to accelerate calculations. The algorithm, validation of the numerical model and numerous examples of applications to various problems of river hydraulics and hydrodynamics are also presented in the monograph [7].

Hybrid triangular-quadrangular meshes of irregular structure were used to build the FSC model. Such meshes are well adapted to the planned outlines of the calculation area and flow peculiarities. The schematization of the computational area on the slopes of dams, in artificial spawning reservoirs was carried out on the basis of a triangular grid with variable spacing. In the channel of the FSC, on its slopes, along the crests of dams, a quadrangular curvilinear grid was constructed (Fig. 3).

To construct a digital model of the FSC topography, the marks on the bottom of the spawning grounds, along the crests of the dams, the bottom of the inlet headrace and the head regulator of the FSC were entered from the provided drawings. Only two marks were given for the bottom of the FSC tract: at the inlet headrace -2.5 m and at the head regulator 0.25 m. Therefore, along the entire length of the FSC tract (≈5.3 km), the bottom marks were linearly interpolated between these two marks. As a result, the slope along the bottom of the RNA tract was ≈0.0005. The obtained DEM, interpolated on the computational grid, is presented in Fig. 4.

Since the calibration of this model is impossible due to the actual absence of the FSC object and its physical model in the hydraulic flume, the roughness coefficients in the calculation were initially assumed to be 0.025 for the bottom of the FSC tract, and 0.035 for the bottom of spawning

grounds, based on the experience of previous works on the bottom of the FSC tract, on the crests and slopes of dams.

The boundaries of the hydrodynamic model of the FSC are the head regulator and the inlet headrace. The main requirement for the functioning of the FSC is to allow fish passage from the lower reach of the BHPP through the FSC pathway to the upper reach. Therefore, velocities in the channel should not exceed 1.1 m/s.

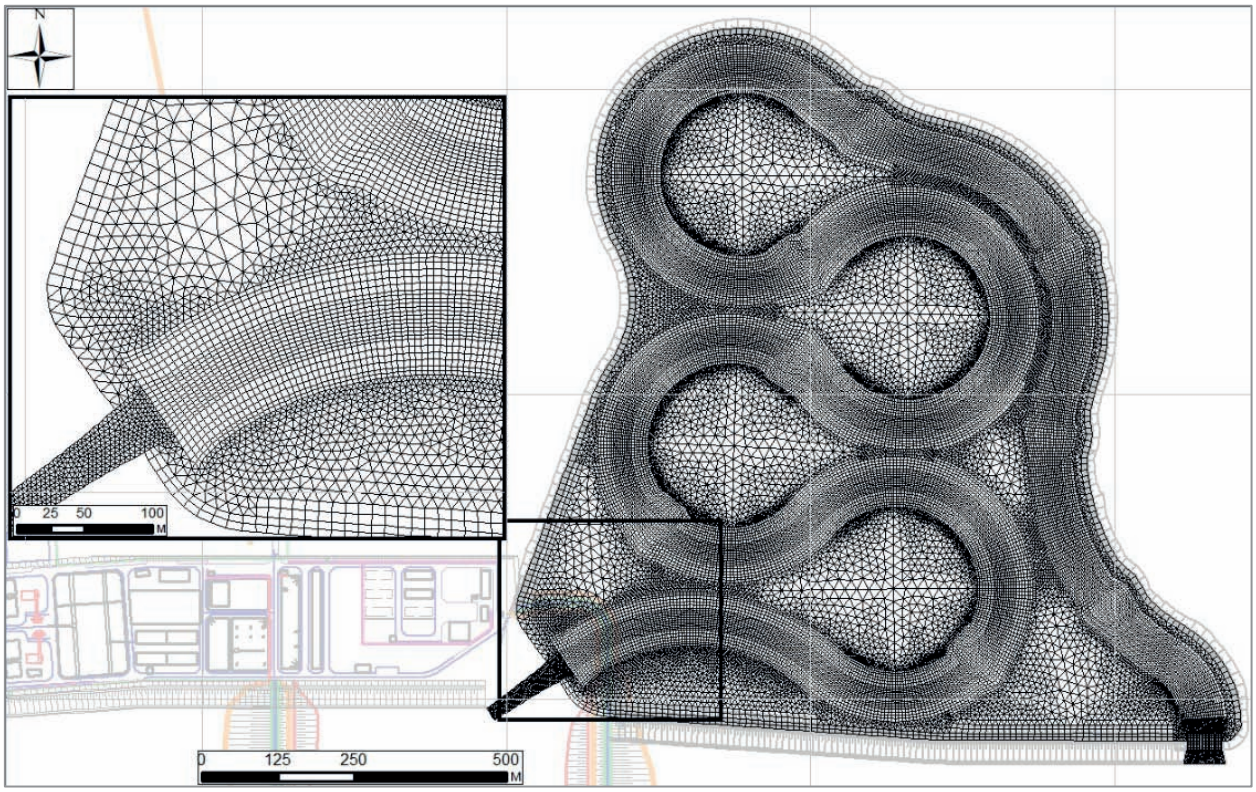

Figure 3. General view and fragment of the input section of the FSC calculation grid

CALCULATION RESULTS FOR LOW-WATER CONDITIONS

As a first computation, a low-water period was considered when the water level in the upstream BHPP was 2 m (head regulator) and in the downstream 0 m (inlet headrace). These water levels were set at the boundaries of the model and the calculation continued until "establishment", i.e., until the water discharge in the whole calculation area becomes the same and does not change anymore. For the case of the original bottom (Fig. 4), this calculation resulted in a flow rate of 82.35 m3/s in the FSC channel. The longitudinal profiles of water level and flow velocity are shown in Fig. 5. As a result, the water depth is ≈0.8 m greater at the inlet headrace compared to the depth at the head regulator, and the maximum velocity along the longitudinal channel is 1.3 m/s. This is higher than the maximum permissible maximum value of 1.1 m/s. Considering the unfinished junction of the head regulator and the FSC path, it became necessary to correct the initially proposed bottom variant.

The authors proposed a new variant of the bottom, in which changes occurred only in the marks along the FSC tract and at the junction of the head regulator with the FSC tract. The new version of the bottom mark of the FSC tract at the inlet header was taken -2 m, at the head regulator 0 m, and along the whole length of the RNA tract (≈5.3 km) the bottom marks changed linearly between these two. As a

result, the slope along the new bottom of the FSC tract decreased and became ≈0.00038. At the junction of the head regulator and the tract, the bottom elevation behind the gates was reduced to -4 m, and the head regulator elevation was gradually increased from 0.5 m to the tract elevation of 0 m (Fig. 6).

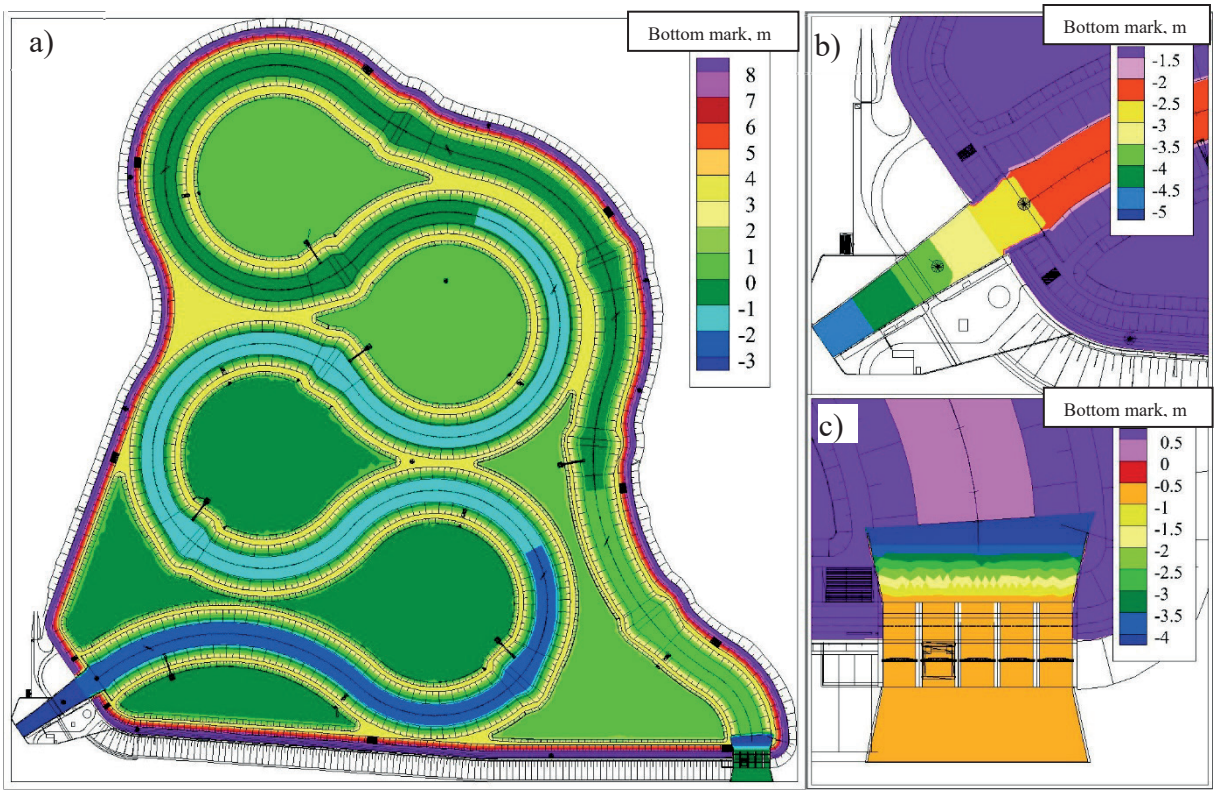

Figure 4. Initial topography of the FSC surface. General view (a), inlet header (b), head regulator (c)

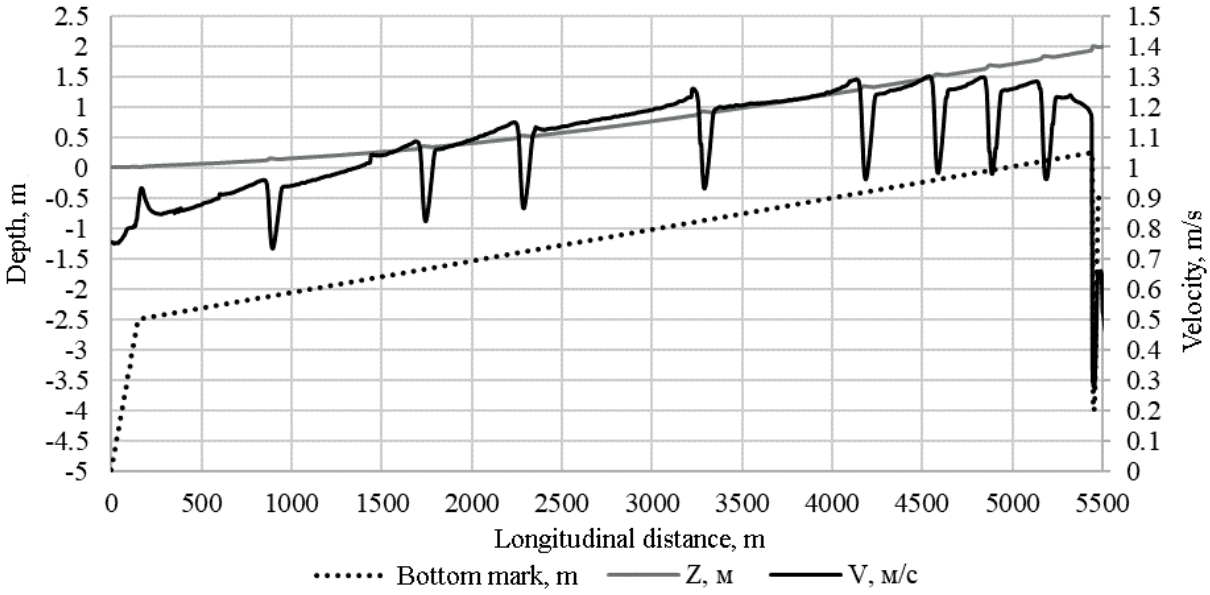

Figure 5. Longitudinal profiles of water level and flow velocity in the FSC under low-water conditions at the initial bottom

The same low water level case was recalculated on the edited FSC bottom, i.e., the water depth was set to 2 m in the upstream and 0 m in the downstream. Under these conditions, a constant flow rate of 88.44 m^3/s was established in the FSC. The difference of water depths at the FSC channel boundaries decreased to 6 cm. However, it should be noted that the maximum velocity in the channel remained 1.3 m/s, which is unacceptable for FSC functioning.

The next step was an attempt to reduce the velocity in the FSC channel by increasing the roughness coefficient along the bed and slopes of the FSC tract to 0.03 (corresponding to pebble backfilling of the bed and slopes). Under these conditions, a constant flow rate of 76.11 m^3/s was established in the FSC. The longitudinal profiles of water level and flow velocity are shown in Fig. 7 for two values of roughness coefficients in the channel 0.025 and 0.03. The water depth difference at the FSC channel boundaries decreased to 4 cm. The maximum velocity in the FSC channel decreased to 1.1 m/s.

It should be noted that the created numerical hydrodynamic model of the FSC allows to carry out further optimization of the fish passage design. For example, it allows to consider variable channel depth and variable lining roughness coefficient along the length of the channel. However, this requires clear criteria (restrictions) on the hydrodynamics of the flow (velocity, depth), formulated by the fish protection organization.

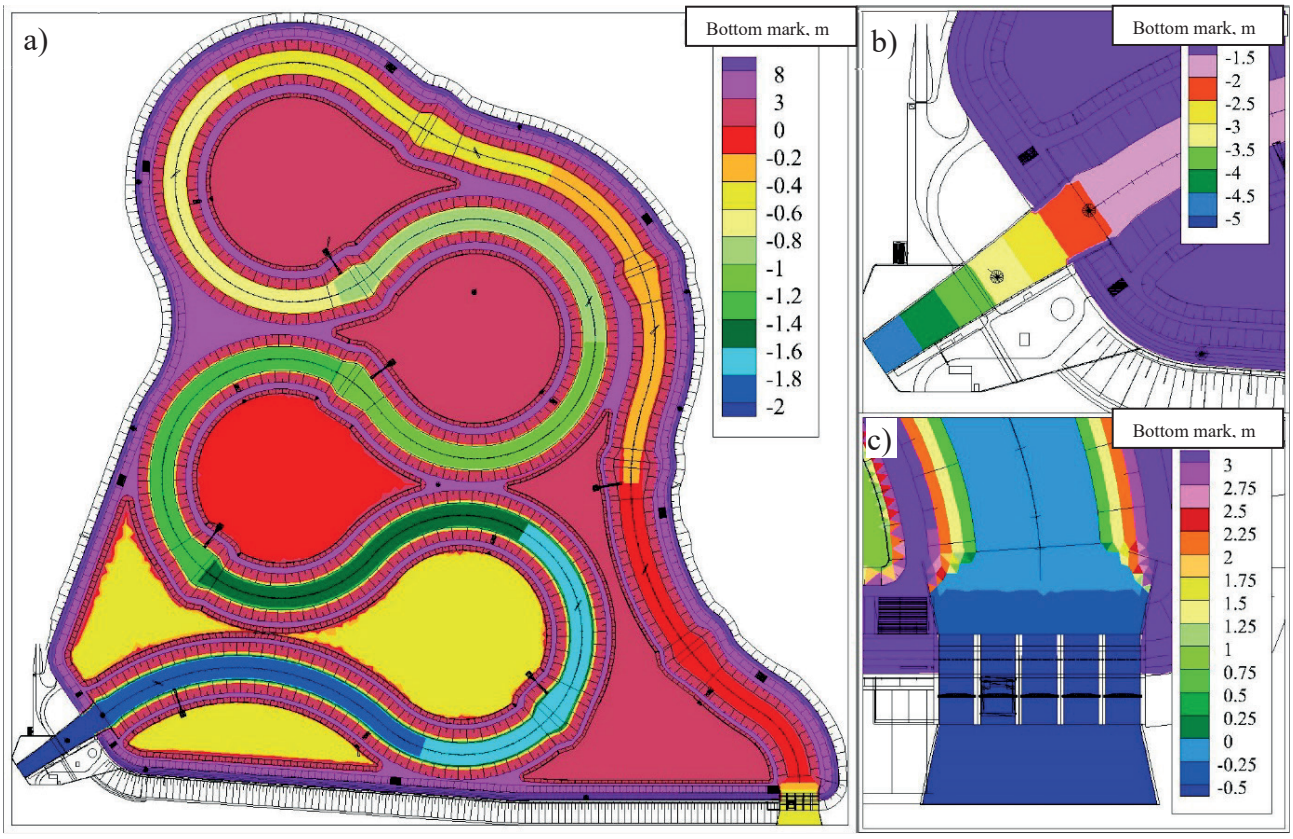

Figure 6. Edited topography of the FSC surface. General view (a), inlet header (b), head regulator (c)

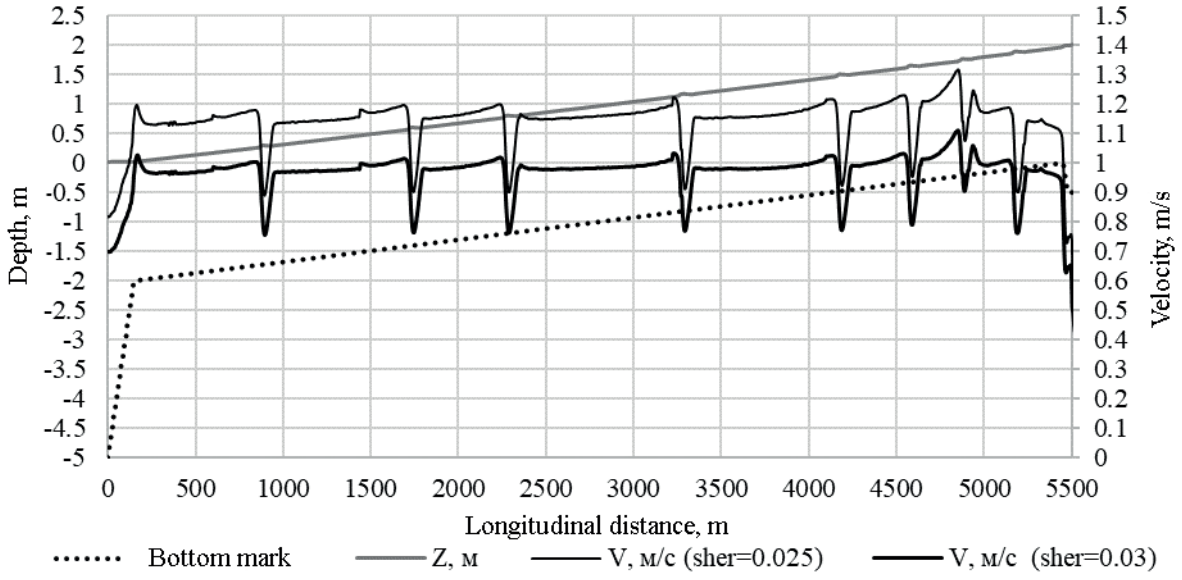

Figure 7. Longitudinal profiles of water level and flow velocity in the FSC under low-water conditions on the edited bottom

CALCULATIONS FOR 10% AND 1% SECURITY OF FLOOD

To run the calculations for 10% and 1% secured floods (7800 and 13200 m3/s respectively), it is necessary to set water level values in the upstream and downstream of the BHPP at the FSC. Based on the results of numerical hydrodynamic modeling of the BHPP in 2018. [8], the water levels at the BHPP FSC inlet and outlet were taken as 5.455 m and 5.56 m for the 10% flood security and 6.746 m and 6.815 m for the 1% flood security, respectively. These water levels were taken as boundary conditions for the FSC model at the newly edited bottom and with a roughness of 0.03 in the FSC channel. The calculation resulted in a flow rate of 223 m3/s for the 10% impaired flood and 229 m3/s for the 1% impaired flood in the FSC. The resulting longitudinal water levels and velocities are shown in Figures 8 and 9.

For the 10% and 1% floods, the entire FSC area inside the levees is flooded, as the FSC channel levees are 3.4 m high and overflow during floods. Swirling currents occur in the area of spawning grounds of Sections 1 and 5 (Figure 10).

FSC SILTATION CALCULATIONS

Calculation of FSC siltation was carried out for a flow rate of 10% probability. Water levels of 5.455 m and 5.56 m were set at the boundaries of the FSC, and a constant flow rate of 223 m^3/s was set in the FSC during the calculation process. As there are no data on the concentration of suspended sediment in the water flowing down the river (which is what will enter the FSC, as the inlet threshold is located 4 m above the river bottom), two options were considered: saturated water flow (natural (equilibrium) concentration of suspended sediment) and water flow with a given sediment concentration of 0.1 g/litre. The size of suspended sediment particles in both cases was assumed to be 0.05 mm. The results of the 18-day siltation calculation are shown in Fig. 11.

Regardless of the inlet concentration, the pattern of siltation is the same in both cases. The sediment is deposited on the head regulator upstream and downstream of the gates, then due to the high velocities in the channel of up to 0.9 m/s (see Fig. 10a), the sediment is not deposited in the channel of the FSC channel, but is deposited on the crest

of the slope of the FSC channel and the slopes of the bund dam, but a little further on, as velocities decrease, sediment begins to be deposited in the channel itself. In the calculated variants, sediment deposition with a given sediment concentration of 0.1 g/l showed more intensive siltation (the thickness of the siltation layer is approximately 2 times greater).

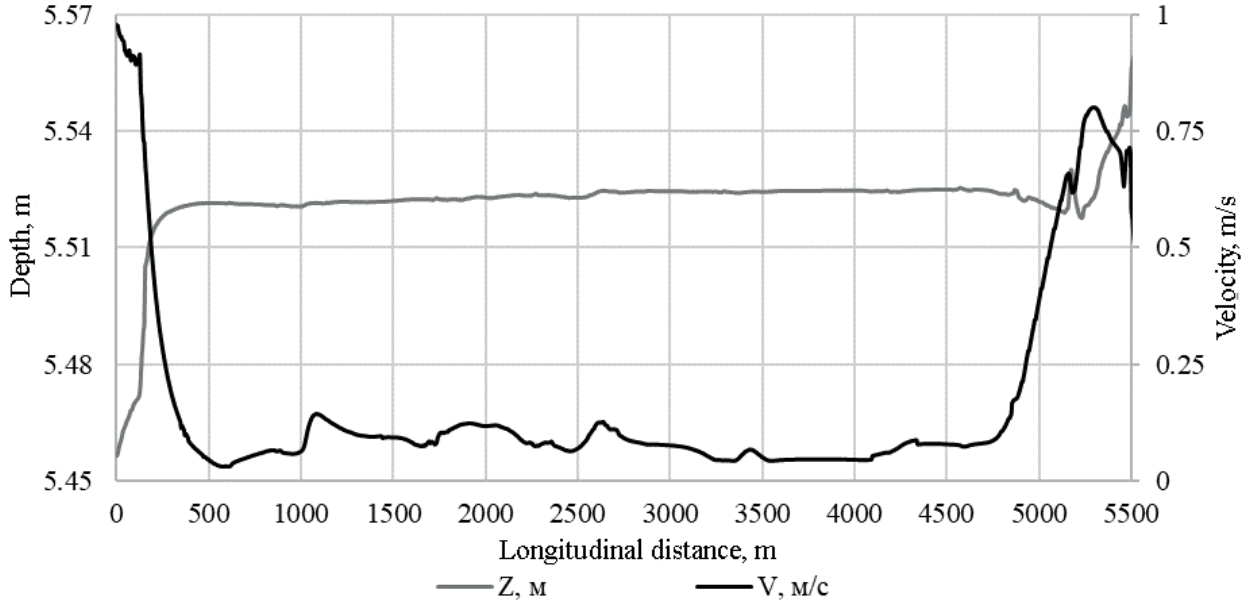

Figure 8. Longitudinal profiles of water level and FSC flow velocity during modeling of a 10% probability flood on the edited bottom with increased roughness in the channel

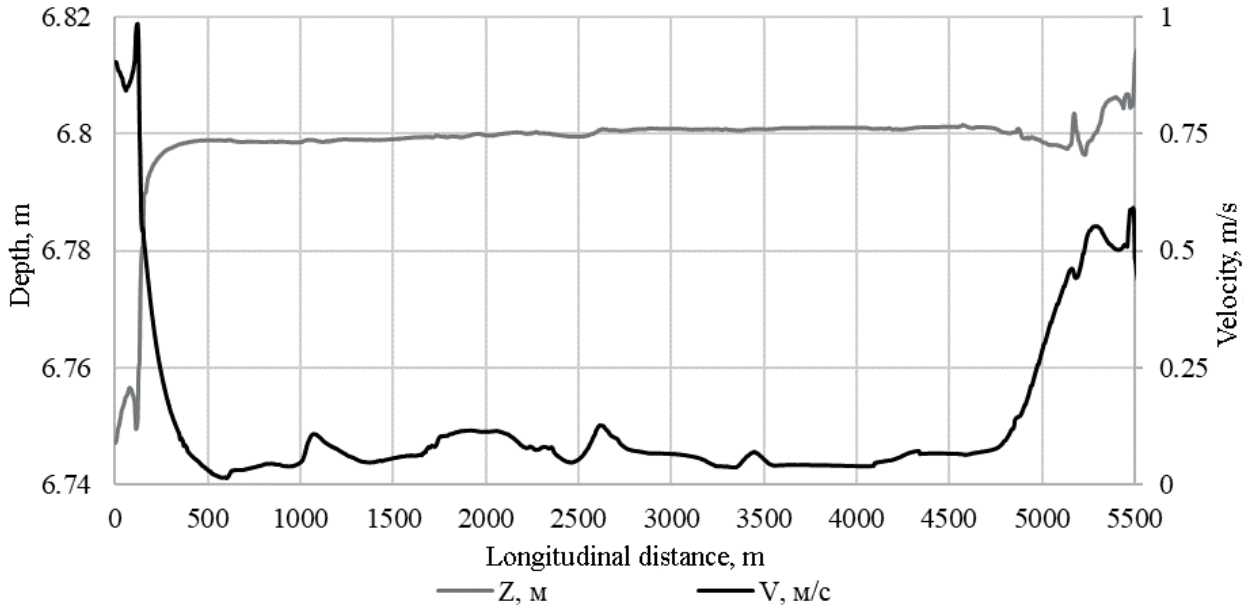

Figure 9. Longitudinal profiles of water level and FSC flow velocity during modeling of a 1% probability flood on the edited bottom with increased roughness in the channel

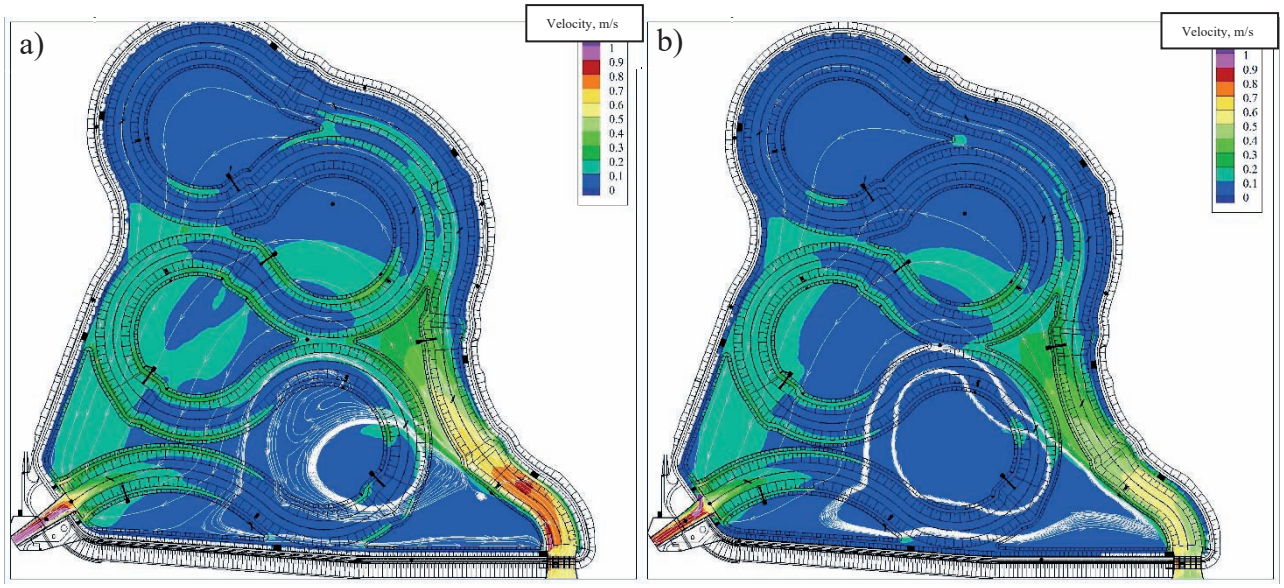

Figure 10. Water velocities and current lines in the FSC during simulations of a 10% (a) and 1% (b) secured flood on an edited bottom with increased roughness in the channel

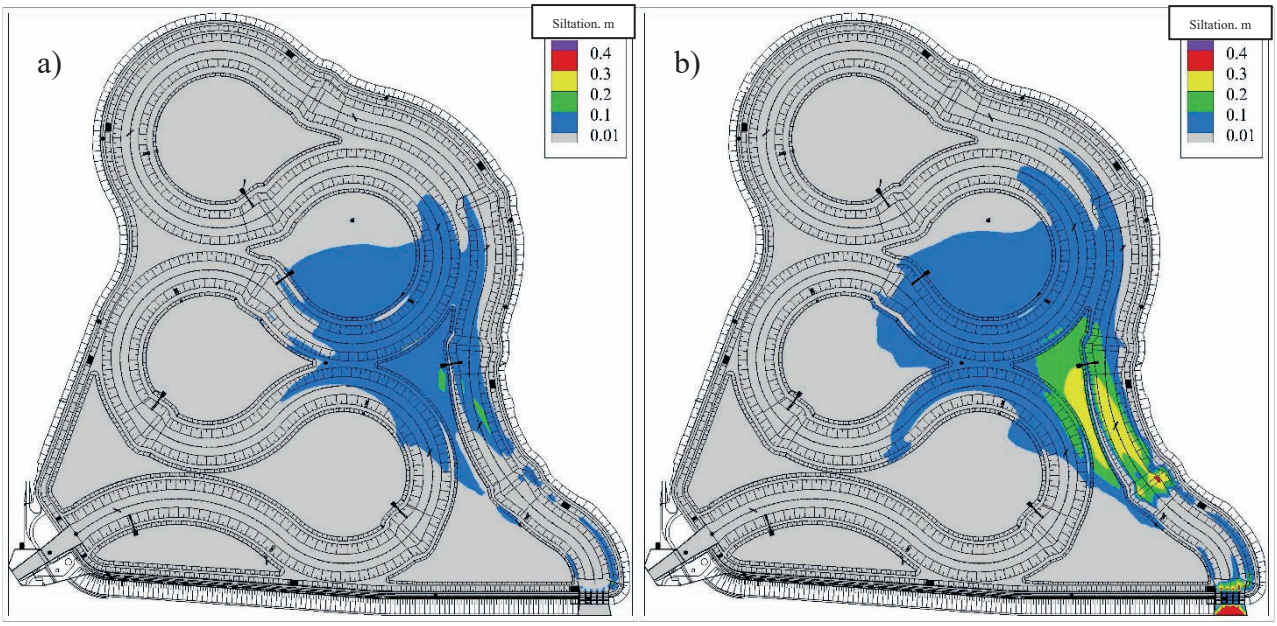

Figure 11. Siltation of the FSC in a simulated 10% flood event with natural sediment concentration at the inlet (a) and with an inlet sediment concentration of 0.1 g/l (b). 18 days

CONCLUSIONS

The article presents three variants of calculations for low-water conditions. The first calculation was performed for the design version of the FSC, reconstructed according to the drawings. It turned out that the maximum velocity in the fish passage channel exceeds 1.3 m/s, the flow depth along the length of the channel is essentially uneven, and a smooth junction between the bottom marks of the head regulator of the FSC and the inlet section of the channel is not ensured. When the model was corrected, the hydraulic parameters of the FSC improved, the depths along the

length were equalized, but the maximum velocity decreased insufficiently. Then the calculation was performed with a slightly increased roughness coefficient of 0.03 in the channel. At such roughness maximum flow velocities in the FSC do not exceed 1.1 m/s, total water flow rate in the channel was 76.11 m^3/s, water depth in the channel was 2.0 m with fluctuations of several centimeters.

For the last variant, calculations of hydraulic operation of FSC in 10% and 1% floods were performed. For these modes, the flow rates through the FSC are very close, equal to 223 m^3/s and 229 m^3/s, respectively. In the case of the 10% and 1% floods, the entire FSC area inside the levees is flooded, as the FSC channel levees are 3.4 m high and overflow during floods. Swirling currents occur in the area of the spawning grounds of Sections 1 and 5. Current velocities in the FSC channel do not exceed 1 m/s. However, there are localized zones with slightly higher velocities in the areas of the head regulator and inlet headrace. Siltation calculations have shown insignificant (0.1-0.2 m layer) siltation in some sections, which can be easily eliminated after flooding.

Based on the obtained modeling results, it is recommended to change the slope of the channel bottom in comparison with the design slope, to improve the junction of the FSC head regulator with the channel inlet section, to create a coating of the channel bottom and sides providing increased roughness of 0.03 Manning (e.g., bottom vegetation in the channel or filling the bottom and sides with pebbles with a diameter of 0.1 m).

ACKNOLEDGEMENT

The study was carried out within the framework of the State assignment of the IWP RAS (theme FMWZ-2022-0003 "Development of numerical models of hydrological, hydrodynamic and hydrochemical processes in water bodies and their catchment areas, creation of technologies based on the developed models to support decisions in the field of water security for information modernization of the Russian economic sector").

REFERENCES

1. **Aleksyuk A.I., Belikov V.V.** STREAM 2D CUDA software for calculation of currents, bottom deformations and pollution transfer in open streams using ComputeUnifiedDeviceArchitecture technologies (on NVIDIA graphics processors). // Certificate of State Registration of Computer Programs No. 2017660266 dated 20.09.2017.
2. **Aleksyuk A.I., Belikov V.V.** Modeling of shallow water currents with shallowing areas and bottom breaks // Journal of computational mathematics and mathematical physics, 2017. T. 57. № 2. C. 316-338.
3. **Aleksyuk A.I., Belikov V.V**. Simulation of shallow water flows with shoaling areas and bottom discontinuities // Comput. Math. Math. Phys., 2017, Vol. 57, No.2, pp. 318-339. doi:10.1134/S0965542517020026
4. **A.I. Aleksyuk, V.V. Belikov** The uniqueness of the exact solution of the Riemann problem for the shallow water equations with discontinuous bottom // Journal of Computational Physics, vol. 390, pp. 232-248, Aug.2019. https://doi:10.1016/j.jcp.2019.04.001
5. **Aleksyuk A.I., Malakhov M.A., Belikov V.V.** The exact Riemann solver for the shallow water equations with a discontinuous bottom // Journal of Computational Physics. 2022, vol. 450, p. 110801, 2022, doi: 10.1016/j.jcp.2021.110801
6. **Aleksyuk, A.I., Malakhov, M.A., Belikov, V.V.** Riemann problem solver for shallow water equations with a discontinuous bottom // Certificate of state registration of computer program №2020660617, 2020.
7. **Belikov V.V., Aleksyuk A.I.** Models of shallow water in problems of river hydrodynamics. MOSCOW: RAS, 2020. - 346 p.
8. **Belikov V.V., Borisova N.M., Aleksyuk A.I., Rumyantsev A.B., Glotko A.V., Shurukhin L.A.** Hydraulic justification of the Bagaevsky hydrosystem project with the application of numerical hydrodynamic modeling // Hydrotechnical Construction, 2018, No.5, p.19-35.

СПИСОК ЛИТЕРАТУРЫ

1. **Алексюк А.И., Беликов В.В.** Программный комплекс STREAM 2D CUDA для расчета течений, деформаций дна и переноса загрязнений в открытых потоках с использованием технологий ComputeUnifiedDeviceArchitecture (на графических процессорах NVIDIA). // Свидетельство о государственной регистрации программ для ЭВМ № 2017660266 от 20.09.2017
2. **Алексюк А.И., Беликов В.В.** Моделирование течений мелкой воды с областями обмеления и разрывами дна // Журнал Вычисл. матем. и матем. физ., 2017 г. Т. 57. № 2. С. 316-338.
3. **Aleksyuk A.I., Belikov V.V.** Simulation of shallow water flows with shoaling areas and bottom discontinuities // Comput. Math. Math. Phys., 2017, Vol. 57, No.2, pp. 318–339. doi:10.1134/S0965542517020026
4. **A.I. Aleksyuk, V.V. Belikov** The uniqueness of the exact solution of the Riemann problem for the shallow water equations with discontinuous bottom // Journal of Computational Physics, vol. 390, pp. 232-248, Aug.2019. https://doi:10.1016/j.jcp.2019.04.001
5. **Aleksyuk A.I., Malakhov M.A., Belikov V.V.** The exact Riemann solver for the shallow water equations with a discontinuous bottom // Journal of Computational Physics. 2022, vol. 450, p. 110801, 2022, doi: 10.1016/j.jcp.2021.110801
6. **Алексюк А.И., Малахов М.А., Беликов В.В.** Решатель задачи Римана для уравнений мелкой воды с разрывным дном // Свидетельство о государственной регистрации программы для ЭВМ №2020660617, 2020.
7. **Беликов В.В., Алексюк А.И.** Модели мелкой воды в задачах речной гидродинамики. М.: РАН, 2020. – 346 с.
8. **Беликов В.В., Борисова Н.М., Алексюк А.И., Румянцев А.Б., Глотко А.В., Шурухин Л.А.** Гидравлическое обоснование проекта Багаевского гидроузла с применением численного гидродинамического моделирования // Гидротехническое строительство, 2018, №5, с.19-35.

Vitaly V. Belikov, Doctor of Technical Sciences, Head of Laboratory of Numerical Hydrodynamic Modelling; Water Problems Institute of the Russian Academy of Sciences; 3, Gubkinst., Moscow, 119333, Russia; e-mail: belvv@bk.ru.

Natalya M. Borisova, Candidate of Science in Physics and Mathematics, senior researcher; Water Problems Institute of the Russian Academy of Sciences; 3, Gubkinst., Moscow, 119333, Russia; e-mail:borisovanm@mail.ru.

Беликов Виталий Васильевич, доктор технических наук, главный научный сотрудник, заведующий лабораторией численного гидродинамического моделирования; Институт водных проблем Российской академии наук; 119333, Москва, ул. Губкина, 3; e-mail: belvv@bk.ru.

Борисова Наталья Михайловна, кандидат физико-математических наук, старший научный сотрудник; Институт водных проблем Российской академии наук; 119333, Москва, ул. Губкина, 3; e-mail: borisovanm@mail.ru.

DOI:10.22337/2587-9618-2024-20-1-98-108

BEARING CAPACITY OF T-BEAMS WITH A FLANGE MADE OF HIGH-STRENGTH CONCRETE AND LONGITUDINAL REINFORCEMENT OF CLASS A500C

Yuriy F. Rogatnev, Oleg O. Sokolov, Oleg E. Perekalskiy, M.M. Jawid Hasani

Voronezh State Technical University, Voronezh, RUSSIA

Abstract: Experimental and numerical studies of the bearing capacity and deformation of T-beams with a flange made of high-strength concrete and longitudinal reinforcement of class A500C with a web made of concrete of ordinary strength were carried out on prototypes of beams and numerical models. The beams being tested are considered at different percentages of reinforcement. The calculation scheme of the beams corresponded to a four-point bend.

As a result of experimental and numerical studies, the nature of the destruction of beams, their deformation and the nature of cracking are determined. Experimental and numerical relationships of relative deflections on relative bending moments are obtained. A comparative analysis of the values of the bearing capacity and the relative height of the compressed zone of the beams, obtained experimentally, numerically and according to SP 63.13330.2018, was carried out. The nature of the distribution of deformations in concrete of normal section of beams at different levels of loading is determined.

Keywords: T-beam, flange made of high-strength concrete, longitudinal reinforcement of class A500C, load-bearing capacity, deformation

НЕСУЩАЯ СПОСОБНОСТЬ БАЛОК ТАВРОВОГО ПРОФИЛЯ С ПОЛКОЙ ИЗ ВЫСОКОПРОЧНОГО БЕТОНА И ПРОДОЛЬНОЙ АРМАТУРОЙ КЛАССА А500С

Ю.Ф. Рогатнев, О.О. Соколов, О.Е. Перекальский, М.М. Джавид Хасани

Воронежский государственный технический университет, г. Воронеж, РОССИЯ

Аннотация: Экспериментальные и численные исследования несущей способности и деформативности балок таврового профиля с полкой из высокопрочного бетона и продольной арматурой класса А500С с ребром из бетона обычной прочности проведены на опытных образцах балок и численных моделях. Исследуемые балки рассмотрены при различных процентах армирования Расчетная схема балок соответствовала четырехточечному изгибу.

В результате проведения экспериментальных и численных исследований определен характер разрушения балок, их деформации и характер трещинообразования. Получены экспериментальные и численные зависимости относительных прогибов от относительных изгибающих моментов. Проведен сравнительный анализ значений несущей способности и относительной высоты сжатой зоны балок, полученных экспериментально, численно и по СП 63.13330.2018. Выявлен характер распределения деформаций в бетоне нормального сечения балок при различных уровнях нагружения

Ключевые слова: тавровая балка, полка из высокопрочного бетона, продольное армирование класса А500С, несущая способность, деформативность

INTRODUCTION

High-strength concrete is an efficient material with exceptional mechanical properties. The use of high-strength concrete makes it possible to obtain high values of bearing capacity and stiffness for beams [1–6]. However, high-strength concrete in the tension zone does not affect the bearing capacity. Therefore, in order to reduce material consumption and increase the efficien-

cy of using the mechanical properties of construction materials, high-strength concrete should be used in the compressed zone of the beam, and in the tension zone, concrete of a class that would ensure compatibility with longitudinal reinforcement.

Studies of rectangular cross-section beams with high-strength concrete in the compressed zone have proven their effectiveness.[7–9] However, there are no studies of similar T-beams. In view of the fact that the T- cross section is less material-intensive and most used in split single-span reinforced concrete structures, it is a promising task to study reinforced concrete T- beams with a flange of high-strength concrete.

MODELS AND METHODS

Experimental studies were carried out on single-span beams. The size of the web is 60 x 100 mm, the flange are 240 x 20 mm, the span is 1200 mm, the total length of the beam is 1400 mm, the boundary of the two layers runs along the border of the flange and the web, respectively, the height of the upper layer of high-strength concrete is 20 mm. Steel rebar of class B500 with a diameter of 6 mm was used as transverse reinforcement. The transverse rebar enters the flange by 10 mm, thus performing the function of dowel bars and ensuring the joint operation of the two layers. To combine the reinforcement into a flat frame, mounting steel rebar of class B500 with a diameter of 6 mm was used. The studies were carried out on beams with a percentage of longitudinal reinforcement of 0.7–3.5%. Class of longitudinal rebar is A500C. In order to ensure the joint operation of the longitudinal rebar and the web, anchor devices in the form of steel angles were welded to the longitudinal rebar. The design and calculation scheme of the beam are shown in fig. 1

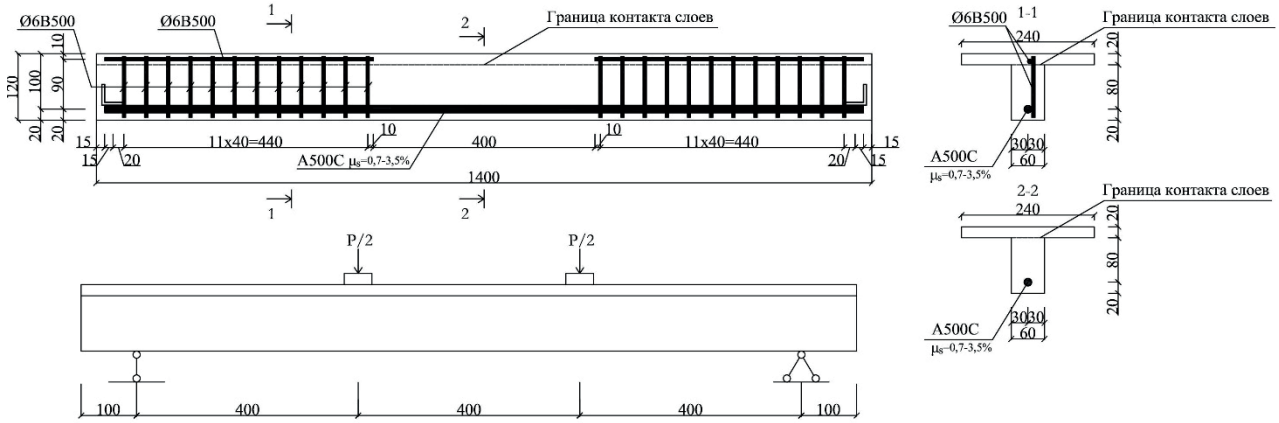

Figure 1 – Design and calculation scheme of beams

The control of the main mechanical characteristics of concrete and rebar was carried out by testing control samples of concrete prisms with a size of 70x70x280mm, in accordance with STST 24452-80 "Methods for determining prism strength, modulus of elasticity and Poisson's ratio", and reinforcing bars in accordance with STST 12004-81 "Reinforcing steel. Tensile test methods. The test results are shown in table 1, 2.

Table 1. Basic parameters of beams

Beam code	Working section height h_0, mm	Longitudinal reinforcement diameter d_s, mm	Percentage of longitudinal reinforcement μ_s	Compressive strength of high-strength concrete $R_{1b,n}$, MPa	Compressive strength of concrete of second layer, $R_{2b,n}$, MPa
DTB -1	100	8	0,70%	94,64	22,3
DTB -2	95	10	1,10%	94,64	22,3
DTB -3	99	12	1,60%	82,5	23,25
DTB -4	92	14	2,10%	82,5	23,25
DTB -5	102	16	2,80%	88,48	41,07
DTB -6	97	18	3,50%	86,3	41,07

The beams were tested on an INSTRON 600 kN hydraulic press (fig. 2). To determine the stress-strain state of the beams, the relative deformations of the normal section were recorded. The correlation of the load level, values of relative deformations and deflections is provided by the multi-channel measuring system MGCplus. The layout of strain gauges and deflection meter is shown in figure 2.

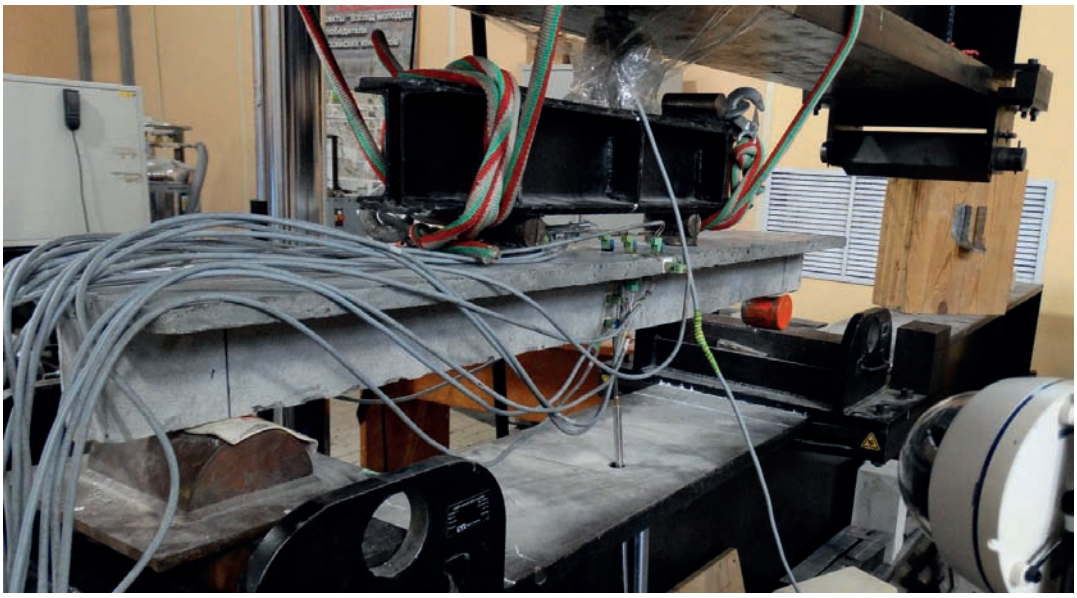

Figure 2 –General view of experiments on the beams

Table 2. Mechanical characteristics of A500C rebar

Rebar diameter, mm	Yield strength σ_y, MPa	Elastic modulus E_s, MPa	Deformation at yield strength ε_{s0}, %	Deformation corresponding to the end of the yield platform ε_{s2}, %
8	758,9	220921	0,34	2,5
10	610,9	206510	0,31	2,5
12	580,5	205470	0,32	2,5
14	551,2	210160	0,28	2,5
16	618,4	197210	0,3	2,5
18	580,6	213200	0,31	2,5

Finite element analysis (FEA) of beams, taking into account the nonlinear properties of materials, was performed using the «ANSYS 2022 R2» software package (fig. 3). Eight-node finite elements (FE) of the Solid 65 type were chosen for the finite elements of the concrete body. In this type of FE, the Willam-Warnke concrete strength criterion is implemented.[10] Reinforcing frame modeled with Beam 188 linear finite elements.

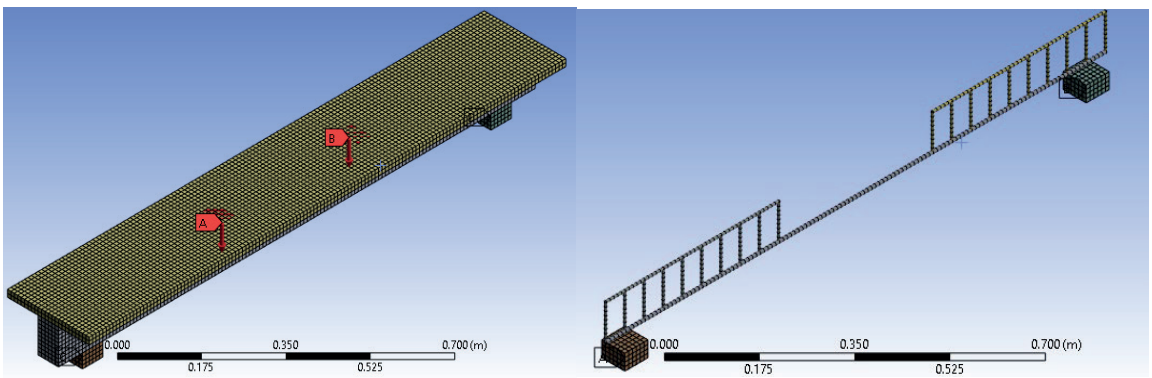

Figure 3 – General view of the numerical model

Table 3. Analysis of test results and numerical simulation of beams

Beam code	Ultimate bending moment, kN·m		Relative deflection		Relative height of compressed zone			Limiting relative height of the compressed zone, ξ_R
	$M_{ult,EXP}$	$M_{ult,ANSYS}$	$f_{ult,EXP}/l_0$	$f_{ult,ANSYS}/l_0$	X_{EXP}/h_0	x_{ANSYS}/h_0	X_{SP}/h_0	
DTB-1	2,71	3,48	1/154	1/146	0,13	0,18	0,02	0,23
DTB -2	4,42	4,56	1/166	1/184	0,13	0,18	0,02	0,26
DTB -3	6,44	6,26	1/169	1/191	0,2	0,196	0,03	0,26
DTB -4	7,88	7,98	1/152	1/165	0,26	0,199	0,05	0,28
DTB -5	11,85	12,12	1/149	1/141	0,18	0,2	0,06	0,25
DTB -6	13,91	13,92	1/133	1/141	0,15	0,2	0,08	0,27

RESEARCH RESULTS AND THEIR ANALYSIS

The destruction of all beams occurred after the occurrence of stresses in the rebar corresponding to the yield strength. The relative deflection, at the time of failure, significantly exceeded the maximum allowable - 1/123 of the span (SP 20.133330.2016 "Loads and Impacts") and was in the range of 1/15–1/55 of the span. A large scatter of values is associated with different types of destruction. In the beam DTB-1, the destruction is caused by the achievement of stress reinforcement equal to the limit of tensile strength. DTB-2 and DTB-3 were destroyed with crushing of concrete in the compressed zone above the web. The destruction of DTB-4 - DTB-6 was local in nature and was caused by a split of the flange overhang.

Beam tests were accompanied by the development of normal and oblique cracks. The development of normal cracks took place along the height of the web with the transition to the lower part of the flange overhang and exit to the end part of the flange overhang. Horizontal shear cracks between the layers before the occurrence of stresses in the rebar corresponding to the normative tensile resistance were not determined. In beams DTB-4 - DTB-6 at the later stages of testing, the transformation of inclined cracks into horizontal ones was observed at the point of contact of the two layers. Also in these beams, horizontal cracks were found on the surface at the place of the future split of the flange overhang.

Beam tests were accompanied by the development of normal and oblique cracks. The development of normal cracks took place along the height of the web with the transition to the lower part of the flange overhang and exit to the end part of the flange overhang. Horizontal shear cracks between the layers before the occurrence of stresses in the rebar corresponding to the normative tensile resistance were not determined. In beams DTB-4 - DTB-6 at the later stages of testing, the transformation of inclined cracks into horizontal ones was observed at the point of contact of the two layers. Also in these beams, horizontal cracks were found on the surface at the place of the future split of the flange overhang.

The discrepancy between the experimental and numerical values of the bearing capacity is 1.27% - 28.6%. The greatest discrepancy between the results was found in the beam with the percentage of reinforcement μs=0.7% and corresponded to 28.6%. In the rest of the beams, the discrepancy between the values of the bearing capacity was in the range of 1.27%–3.08%. The values of the relative height of the compressed zone according to SP 63.13330.2018 «Concrete and reinforced concrete structures» are in the range of 0.02–0.08. The values of the relative height of the compressed zone were experimentally established in the range of 0.13-0.26 and did not exceed the values of the

boundary height of the compressed zone according to SP 63.13330.2018 for each individual beam. The numerical values of the relative height of the compressed zone have a smaller divergence from the experimental ones and are in the range of 0.18–0.2.

An analysis of the relationships between relative deflection and relative bending moment (fig.6-8) allows us to determine two levels of stabilization of deflection values - during cracking and when the bearing capacity is exhausted. In finite element analysis (FEA), the relationship between stresses and relative strains in rebar and concrete is determined by a double-line strain diagram. The main parametric points of the diagrams are determined in accordance with SP 63.13330.2018 «Concrete and reinforced concrete structures» according to the test results of control samples. Deformation at yield strength of reinforcement is determined by expression (1) SP 63.13330.2018 «Concrete and reinforced concrete structures»:

$$\varepsilon_0 = \sigma_y / E_s \qquad (1)$$

where, ε_0 – relative deformation corresponding to the yield strength of reinforcement; σ_y – stress corresponding to the yield strength of reinforcement; E_s – elastic modulus of rebar.

In connection with the use of a double-line diagram of steel rebar deformation in the numerical model, the divergence of deflection values at M_{ult} was 5%–13.04%. It is possible to improve the convergence of results by using more complex charts.

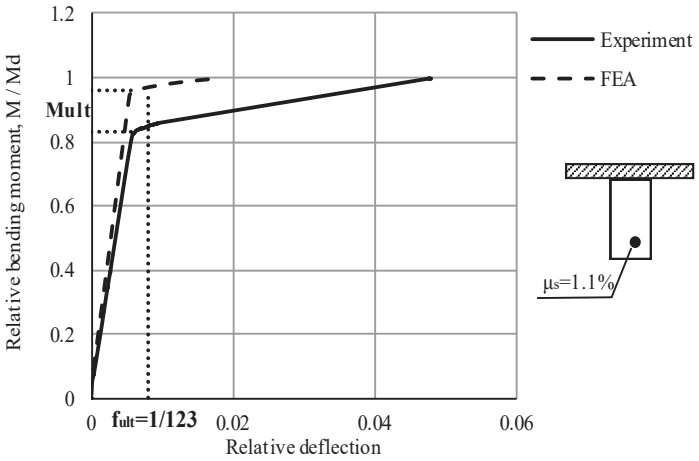

Figure 4. Relationship between relative deflection and relative bending moment for a beam with reinforcement percentage μ=1,1%

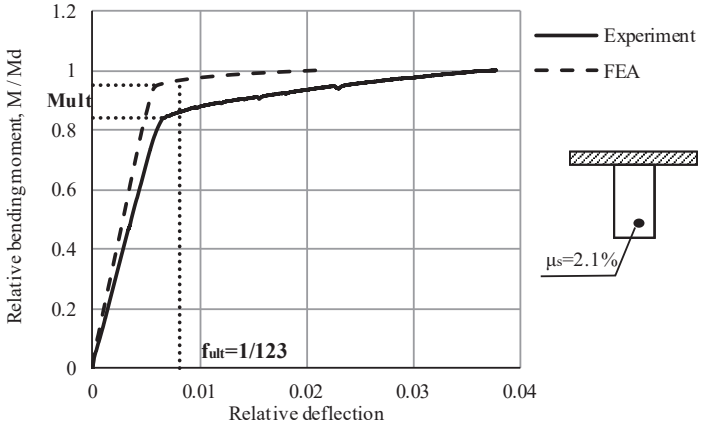

Figure 5. Relationship between relative deflection and relative bending moment for a beam with reinforcement percentage μ=2,1%

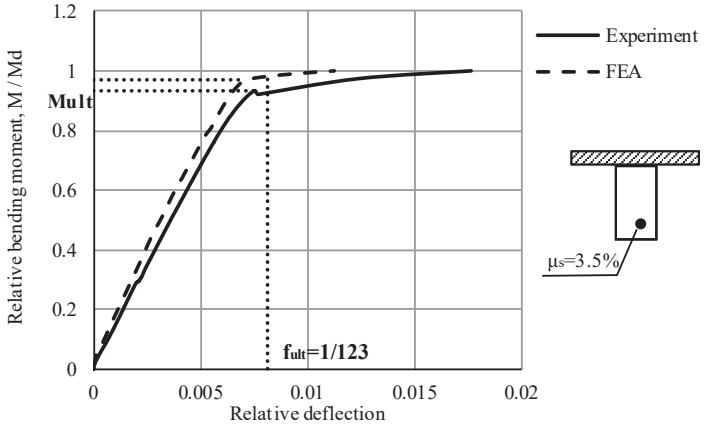

Figure 6. Relationship between relative deflection and relative bending moment for a beam with reinforcement percentage μ=3,5%

The limiting relative strain of a double-line diagram of rebar deformation - ε_2 has a value of $25 \cdot 10^{-3}$, and the stress, at a given point in the diagram, corresponds to the yield strength of the rebar. In this connection, the numerical values of the breaking moment and the corresponding deflection of the beam are lower than the experimental values. Graphs (fig. 4-6) make it possible to make sure that with an increase in the percentage of reinforcement, the relative deflection corresponding to the breaking moment decreases.

The nature of concrete deformations in samples with a reinforcement percentage of 0.7% and 1.1% at the border of adjacent layers there are gaps in the nature of the development of relative deformations (fig. 7). A similar nature of deformations corresponds to the development of deformations in composite structures [11–15]. The nature of the development of concrete deformations along the height of the section, obtained by calculating the FEM at M_{crc}, has a linear form due to the conjugation of two layers by rigid nodes. At the stage of loading M_{ult}, the lower layer is subject to cracking, and the nature of deformations in the compressed zone of normal section has a linear form (fig. 8). The nature of the development of deformations at M_{ult}, obtained by the calculation of the FEM, contains a deviation from the linear law.

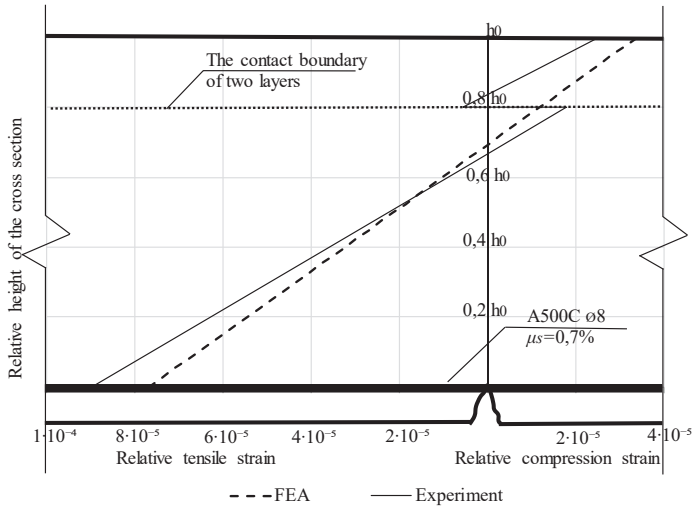

Figure 7. The nature of deformations in concrete of normal section of a beam with a percentage of reinforcement μ=0,7% at Mcrc

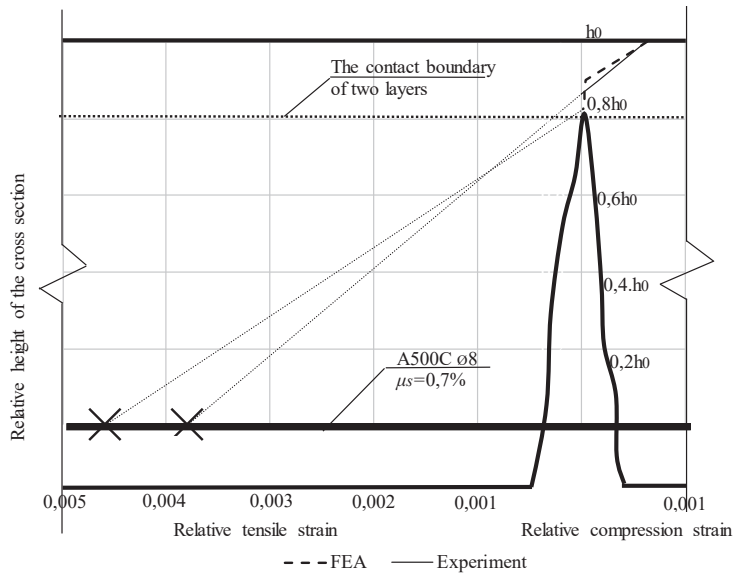

Figure 8. The nature of deformations in concrete of normal section of a beam with a percentage of reinforcement μ=0,7% at Mult

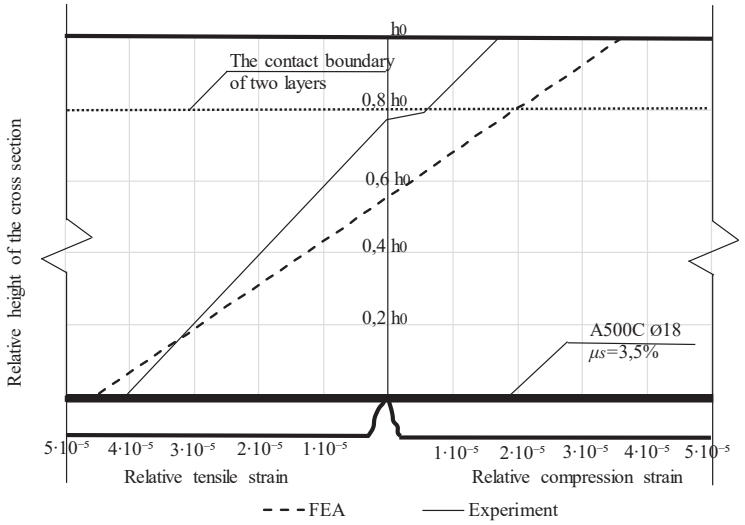

Figure 9. The nature of deformations in concrete of normal section of a beam with a percentage of reinforcement μ=3,5% at Mcrc

In samples with a reinforcement percentage of 1.6%–3.5%, the gap in the values of relative deformations of concrete was qualitatively different and can be caused by the presence of different-modulus materials of adjacent layers in the boundary of the compressed zone of the normal section of the beam [11]. With a bending moment equal to M_{ult}, the boundary of the compressed zone did not go beyond the contact surface of the two layers, and the diagram had a linear form. The distribution of concrete deformations, obtained in the calculation of the FEM, at M_{crc} had a linear form (fig. 9). At M_{ult} , according to the FEM calculation, the compressed zone included the outermost fibers of the second layer, in connection with which a pattern with a rupture of deformations was obtained, which is caused by the presence of different-modulus materials of adjacent layers in the boundary of the compressed zone of the normal section of the beam (fig. 10).

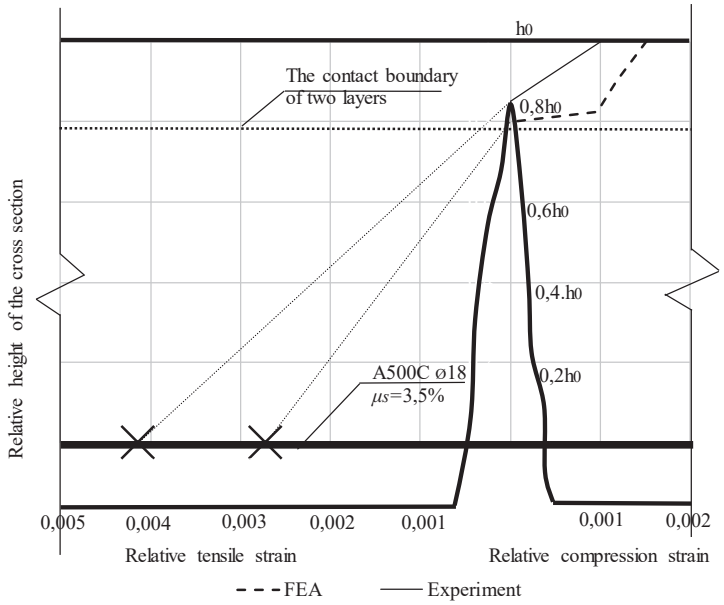

Figure 10. The nature of deformations in concrete of normal section of a beam with a percentage of reinforcement μ=3,5% at Mult

ACKNOWLEDGMENTS

The experimental studies have been carried out using the facilities of the Collective Research Center named after Professor Yu. M. Borisov, Voronezh State Technical University, which is partly supported by the Ministry of Science and Education of the Russian Federation, Project No. 075-15-2021-662.

CONCLUSIONS

As a result of experimental and numerical studies of the bearing capacity and deformation of beams, it has been established that the method for determining the relative height of the compressed zone according to SP 63.13330.2018 «Concrete and reinforced concrete structures» requires clarification in the case of calculating T-beams with a flange of high-strength concrete and longitudinal reinforcement A500C. It was also found that the numerical values of the bearing capacity have acceptable convergence not for all percentages of reinforcement, and the nature of the distribution of deformations in concrete does not correspond to the experimental data. In this connection, it is necessary to develop a method for calculating T-beams with high-strength concrete in the flange and longitudinal reinforcement A500C, which would allow with the necessary accuracy to determine the relative height of the compressed zone and the bearing capacity of the beams at various percentages of reinforcement, as well as to determine a reliable picture of the nature of deformations in concrete beams by section height.

REFERENCES

1. **Wang D.H., Ju Y.Z., Zheng W.Z.** (2017), Strength of reactive powder concrete beam-column joints reinforced with high-strength (HRB600) bars under seismic loading, Strength of Materials, Springer New York LLC, Vol. 49, No. 1, pp. 139–151.
2. **Wang J., Morikawa H., Kawaguchi T.** (2013), Influence of strengthening by ultra high strength fiber reinforced concrete panels on shear resisting mechanism and bond-slip behavior of low strength RC members, The international conference on sustainable construction materials and technologies, Vol. 2013-August.

3. **Wang J., Morikawa H., Kawaguchi T.** (2015), Shear strengthening of RC beams using ultra-high-strength fiber-reinforced concrete panels, Magazine of Concrete Research, Vol. 67, P. 1–12.
4. **Chu L., Liu J., Zhao J.** (2021), Normal Section Bearing Capacity of Partial Steel Fiber Reinforced High Strength Concrete Shear Wall, Yingyong Jichu yu Gongcheng Kexue Xuebao/Journal of Basic Science and Engineering. Editorial Board of Journal of Basic Science and, Vol. 29, No. 1, pp. 147–160.
5. **Elsanadedy H.M. et al.** (2021), Hybrid UHPC/NSM CFRP strips vs. traditional systems for flexural upgrading of RC beams – Experimental and FE study Composite Structures. Elsevier Ltd, Vol. 261.
6. **Andrzej L., Sadowska-Buraczewska B., Tomaszewicz** (2005), A. Experimental and numerical analysis of flexural composite beams with partial use of high strength/high performance concrete, Journal of Civil Engineering and Management,Vol. 11. P. 115–120.
7. **Potapov Yu.B., Rogatnev Yu.F., Panfilov D.V., Javid M.M**. (2015), Experimental studies of the bearing capacity of normal sections of reinforced concrete bending elements with class A600 reinforcement, Scientific Bulletin of the Voronezh State University of Architecture and Civil Engineering, Construction & Architecture, No. 2 (38), pp. 16–24.
8. **Potapov Yu.B., Barabash D.E., Rogatnev Yu.F., Panfilov D.V., Javid M.M.** (2016), Calculation of deflections of reinforced concrete bending elements with a top layer of high-quality concrete, Vestnik Mscu.. No. 3, P. 26–36.
9. **Rogatnev Yu.F., Ivanov Yu.V., Sokolov O.O.** (2020), Numerical modeling of the stress-strain state of a tee-section element with high-strength concrete in a compressed zone under short-term load, News of higher educational institutions. Construction, No. 9 (741), P. 36–47.
10. **Willam K.J., Warnke E.P.** (1975), Constitutive model for the triaxial behavior of concrete, Proceedings, international association for bridge and structural engineering, Vol. 19, P. 1–30.
11. **Kolchunov V.I., Panchenko L.A.** (1999), Calculation of composite thin-walled structures, Moscow, DIA Publishing House, 281 p.
12. **Kolchunov V.I., Skobeleva E.A., Gornostaev S.I.** (2006), Experimental studies of deformation and crack resistance of composite structures, Proceedings of the Orel State Technical University. Series: Construction and Transport, No. 1–2. pp. 12-16.
13. **Kolchunov V.I., Skobeleva E.A., Korzhavykh A.I.** (2009), The calculation of the deformation of reinforced concrete frames with elements of a composite section, Academia. Architecture & Construction, No. 4. P. 74-78.
14. **Fedorov V.S., Bashirov Kh.Z., Kolchunov V.I.** (2014), Elements of the theory of calculation of reinforced concrete composite structures, Academia. Architecture & Construction, No. 2. P. 116-118.
15. **Foraboschi P.** (2009), Analytical Solution of two-Layer Beam Taking into Account Nonlinear Interlayer Slip, Journal of Engineering Mechanics-asce - J ENG MECH-ASCE, Vol. 135.

СПИСОК ЛИТЕРАТУРЫ

1. **Wang D.H., Ju Y.Z., Zheng W.Z.** (2017), Strength of reactive powder concrete beam-column joints reinforced with high-strength (HRB600) bars under seismic loading, Strength of Materials, Springer New York LLC, Vol. 49, No. 1, pp. 139–151.
2. **Wang J., Morikawa H., Kawaguchi T.** (2013), Influence of strengthening by ultra high strength fiber reinforced concrete panels on shear resisting mechanism and bond-slip behavior of low strength RC members, The international conference on sustainable construction materials and technologies, Vol. 2013-August.

3. **Wang J., Morikawa H., Kawaguchi T.** (2015), Shear strengthening of RC beams using ultra-high-strength fiber-reinforced concrete panels, Magazine of Concrete Research, Vol. 67, P. 1–12.
4. **Chu L., Liu J., Zhao J.** (2021), Normal Section Bearing Capacity of Partial Steel Fiber Reinforced High Strength Concrete Shear Wall, Yingyong Jichu yu Gongcheng Kexue Xuebao/Journal of Basic Science and Engineering. Editorial Board of Journal of Basic Science and, Vol. 29, No. 1, pp. 147–160.
5. **Elsanadedy H.M. et al.** (2021), Hybrid UHPC/NSM CFRP strips vs. traditional systems for flexural upgrading of RC beams – Experimental and FE study Composite Structures. Elsevier Ltd, Vol. 261.
6. **Andrzej L., Sadowska-Buraczewska B., Tomaszewicz** (2005), A. Experimental and numerical analysis of flexural composite beams with partial use of high strength/high performance concrete, Journal of Civil Engineering and Management,Vol. 11. P. 115–120.
7. **Потапов Ю.Б., Рогатнев Ю.Ф., Панфилов Д.В., Джавид М.М.** (2015), Экспериментальные исследования несущей способности нормальных сечений железобетонных изгибаемых элементов с арматурой класса А600, Научный Вестник Воронежского Государственного Архитектурно-Строительного Университета. Строительство и Архитектура № 2 (38). С. 16–24.
8. **Потапов Ю.Б., Барабаш Д.Е., Рогатнев Ю.Ф., Панфилов Д.В., Джавид М.М.** (2016), Расчет прогибов железобетонных изгибаемых элементов с верхним слоем из высококачественного бетона // Вестник Мгсу. № 3. С. 26–36.
9. **Рогатнев Ю.Ф., Иванов Ю.В., Соколов О.О.** (2020), Численное моделирование напряженно-деформированного состояния элемента таврового сечения с высокопрочным бетоном в сжатой зоне при кратковременной нагрузке, Известия Высших Учебных Заведений. Строительство, № 9 (741). Р. 36–47.
10. **Willam K.J., Warnke E.P.** (1975), Constitutive model for the triaxial behavior of concrete, Proceedings, international association for bridge and structural engineering, Vol. 19, P. 1–30.
11. **Колчунов В.И., Панченко Л.А.** (1999), Расчет составных тонкостенных конструкций. Москва: Издательство АСВ, 281 с.
12. **Колчунов В.И., Скобелева Е.А., Горностаев С.И.** .(2006), Экспериментальные исследования деформирования и трещиностойкости составных конструкций, Известия Орловского Государственного Технического Университета. Серия: Строительство И Транспорт, № 1–2. С. 12-16.
13. **Колчунов В.И., Скобелева Е.А., Коржавых А.И.** .(2009), К расчету деформативности железобетонных рам с элементами составного сечения, Academia. Архитектура И Строительство, № 4. С. 74-78.
14. **Федоров В.С., Баширов Х.З., Колчунов В.И.** .(2014), Элементы теории расчета железобетонных составных конструкций, Academia. Архитектура И Строительство № 2. С. 116-118.
15. **Foraboschi P.** (2009), Analytical Solution of two-Layer Beam Taking into Account Nonlinear Interlayer Slip, Journal of Engineering Mechanics-asce - J ENG MECH-ASCE, Vol. 135.

Rogatnev Yuriy Fedorovich, «Voronezh State Technical University», Voronezh, Russia, Candidate of technical sciences, Associate Professor of the department of Building Constructions, Footings and Foundations named after Prof. Yu.M. Borisov. E-mail: yrogatnev@yandex.ru

Рогатнев Юрий Федорович, ФГБОУ ВО «Воронежский государственный технический университет», г. Воронеж, Россия, кандидат технических наук, доцент кафедры строительных конструкций оснований и фундаментов им. проф. Ю.М. Борисова. E-mail: yrogatnev@yandex.ru

Sokolov Oleg Olegovich, «Voronezh State Technical University», Voronezh, Russia, assistant of the department of Building Constructions, Footings and Foundations named after Prof. Yu.M. Borisov. E-mail: osokolov@vgasu.vrn.ru

Perekalskiy Oleg Evgenievich, «Voronezh State Technical University», Voronezh, Russia, Candidate of technical sciences, Associate Professor of the department of Building Constructions, Footings and Foundations named after Prof. Yu.M. Borisov. E-mail: perekalskiy@mail.ru

Jawid Hasani Mohammad Mahdi, «Voronezh State Technical University», Voronezh, Russia, Candidate of technical sciences, Associate Professor of the department of Building Constructions, Footings and Foundations named after Prof. Yu.M. Borisov. E-mail: mahdi.jawid21@yandex.ru

Соколов Олег Олегович, ФГБОУ ВО «Воронежский государственный технический университет», г. Воронеж, Россия, ассистент кафедры строительных конструкций оснований и фундаментов им. проф. Ю.М. Борисова. E-mail: osokolov@vgasu.vrn.ru

Перекальский Олег Евгеньевич, ФГБОУ ВО «Воронежский государственный технический университет», г. Воронеж, Россия, кандидат технических наук, доцент кафедры строительных конструкций оснований и фундаментов им. проф. Ю.М. Борисова. E-mail: perekalskiy@mail.ru

Джавид Хасани Мохаммад Махди, ФГБОУ ВО «Воронежский государственный технический университет», г. Воронеж, Россия, кандидат технических наук, доцент кафедры строительных конструкций оснований и фундаментов им. проф. Ю.М. Борисова. E-mail: mahdi.jawid21@yandex.ru

International Journal for Computational Civil and Structural Engineering, 20(1) 109–115 (2024)

DOI:10.22337/2587-9618-2024-20-1-109-115

STUDY OF DYNAMIC CHARACTERISTICS OF HYBRID TITANIUM-POLYMER COMPOSITE MATERIALS

Arseniy V. Babaytsev, Sergey S. Lopatin, Fedor A. Nasonov

Moscow Aviation Institute (National Research University), Moscow, RUSSIA

Abstract: Low specific weight and high mechanical strength (especially at elevated temperatures) of titanium and its alloys make them very valuable aviation materials. In the field of aircraft construction and aircraft engine production, titanium is increasingly replacing aluminum and stainless steel. At present, aircraft developers are restructuring the whole material science concept of aircraft construction, actively involving and using various types of composite materials based on titanium alloys. Combined with the properties of titanium, FML composites based on titanium have greater stiffness, impact resistance, heat resistance, and corrosion resistance especially compared to similar aluminum-based materials. The paper investigates the dynamic characteristics of hybrid titanium-polymer composite materials (TPCM) based on titanium alloy BT-23 and fiberglass with a brief presentation of the main characteristics of prepregs. The process of manufacturing specimens for testing including heat treatment, ply laying scheme and reinforcement scheme in two variants is described. The results of experimental studies of natural frequencies and damping coefficient by the method of free damped oscillations in free oscillations of TPCM plates are presented. The tests are carried out on a specially designed unit with a triangulation sensor in the variant of vertical loading. Two identical specimens with different overall dimensions are tested.Each specimen was tested with a different amplitude. Five tests were conducted for each amplitude. The physical constants of the specimens were pre-determined in static tests. The natural frequencies and damping coefficients for the titanium-polymer composite specimens were found.

Keywords: titanium-polymer composites, natural frequencies; vibrations; TPCM; damping coefficient; layered composites

ИССЛЕДОВАНИЕ ДИНАМИЧЕСКИХ СВОЙСТВ ГИБРИДНОГО ТИТАН-ПОЛИМЕРНОГО КОМПОЗИЦИОННОГО МАТЕРИАЛА

А.В. Бабайцев, С.С. Лопатин, Ф.А. Насонов

Московский авиационный институт (национальный исследовательский университет), г. Москва, РОССИЯ

Аннотация: Малый удельный вес и высокая механическая прочность (особенно при повышенных температурах) титана и его сплавов делают их весьма ценными авиационными материалами. В области самолетостроения и производства авиационных двигателей титан все больше вытесняет алюминий и нержавеющую сталь. В настоящее время разработчики авиатехники перестраивают всю материаловедческую концепцию строительства самолетов, активно привлекая и используя различные виды композиционных материалов на основе титановых сплавов. В сочетании со свойствами титана композиционные материалы FML на его основе обладают большей жёсткостью, ударостойкостью, термостойкостью, коррозионной стойкостью особенно по сравнению с аналогичными материалами на основе алюминия. В работе исследуются динамические характеристики гибридных титан-полимерных композиционных материалов (ТПКМ) на основе титанового сплава ВТ-23 и стеклопластика с кратким приведением основных характеристик препрегов. Описан процесс изготовления образцов, для испытаний включая термообработку, схема укладки слоёв и схема армирования в двух вариантах. Представлены результаты экспериментальных исследований собственных частот и коэффициента демпфирования по методу свободных затухающих колебаний при свободных колебаниях пластин ТПКМ. Испытания проводятся на специально сконструированной установке с триангуляционным датчиком в варианте вертикального нагружения. Испытываются два однотипных образца с разными габаритными размерами. Каждый образец испытывался с различной амплитудой. Для каждой амплитуды проводилось по 5 испытаний. Физические константы образцов предварительно определены в

статических испытаниях. Найдены собственные частоты и коэффициенты демпфирования для образцов титан-полимерного композиционного материала.

Ключевые слова: сферическая композитная оболочка; контактная задача; теория многокомпонентного анизотропного сухого трения

INTRODUCTION

The study of dynamic characteristics is one of the main points for compiling a complete picture of the properties of materials in various branches of engineering, especially hybrid titanium-polymer composites or metal-fiber laminate (FML). A number of articles [1-6] investigated a wide range of issues devoted to various stages of creation, study of properties and characteristics, metal-polymer materials based on titanium [6]. These materials have high corrosion resistance and strength in combination with low density, as well as paramagnetic properties and are widely used in aviation, space technology, shipbuilding. Special attention has been paid to the research and development of metal polymers based on thin sheets of titanium alloys VT20 and VT23M [1-6]. Compared to similar materials based on aluminum, TPKM has advantages in thermal conductivity, since the thermal conductivity of titanium is 13 times less than that of aluminum [1]. Traditional titanium alloys have high mechanical characteristics, but all possibilities are currently exhausted to increase their strength and reduce density, especially in comparison with foreign analogs, β-alloys, which have a complex alloying system and contain scarce and expensive elements (e.g., alloys SP-700, Beta CEZ). This is another advantage of TPKM.

The layup configuration can be different depending on the working conditions and the task to be performed. Composite materials based on titanium are widely used in helicopter main rotor blade spar, in Mi 26 tail rotor blade spar, in Mi-26 stabilizer spar, in Mi-2 tail rotor blade, which have special requirements related to rigidity, strength, thermal insulation. One of the main tasks was to determine the dynamic characteristics of such material: natural frequencies, bending stiffness and damping coefficients, to build a mathematical model based on the plate for prediction in the design of structural elements of aircraft operating under conditions of high-frequency vibration loading. This paper investigates the dynamic characteristics of titanium-polymer composite material based on titanium alloy BT-23 by the method of free damped oscillations [7-8].

MATERIALS AND METHODS

A promising material among metal composite laminates is a laminate based on titanium and glass or carbon fibers. The use of titanium increases the stiffness of the composite compared to the metal composite material based on aluminum alloys and has high corrosion resistance, including in aggressive environments [9-10]. The use of different thickness and different number of metal and composite layers or different arrangement of fibers allows to change the properties of such material, as well as other types of metal composite laminate [11-12]. For high flight speeds, titanium FML(TPCMs) have high heat resistance and can withstand working surface temperatures where they are used up to 300°C. TPCMs are mainly used in regions where high temperatures and high fracture toughness are required. In addition to these advantages, TPKMs have high fracture toughness, high impact resistance and low density.

This paper investigates samples from hybrid titanium-polymer composite material (TPCM) based on titanium alloy BT-23, which are metal plates produced by vacuum-autoclave method after assembly of layered billet packages. Table 1 gives the characteristics of the materials used in the test. Figure 1 shows the samples of titanium-polymer composite material. Two types of TPCM specimens with dimensions

280mm x 20mm x 0.8mm and 180mm x 10mm x 0.8mm cut from one plate by guillotine were investigated.

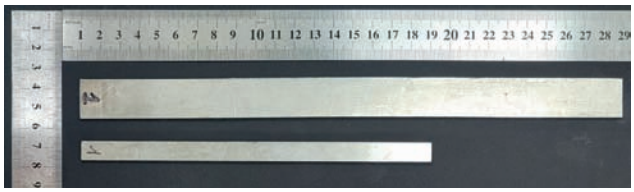

Figure 1. The types of TPCM samples under study are from the top a sample measuring 280mm x 20mm x 0.8mm and from the bottom a sample measuring 180mm x 10mm x 0.8mm

Table 1. Material Characteristics

Material	ρ, kg/m^3	E, GPa	Tensile strength, MPa
BT-23	4570	100-110	980
ВПС-37К10	1700-1800	42/11,5	1500/75
ВСК-14-2м	1780	3,7	92

To form the samples, a monolithic panel with dimensions of 500 x 250 mm was manufactured. Three layers of titanium foil of high-strength deformable titanium alloy VT-23 0.08 mm thick, between which alternate layers of fiberglass plastic based on prepreg KMKS-2m.120.T60. Fig. 2 shows the laying scheme of TPKM layers. Table 2 shows the scheme of laying and reinforcement of the material.

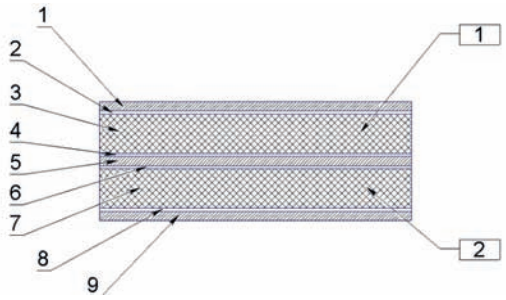

Figure 2. Layout scheme of TPKM layers. On the left 1,5,9-VT23, foil; 2,4,6,8-layer VK-25; 3,6-KMKS-2m.120.T60. On the right laying package 1 and 2

Table 2. Layout and reinforcement scheme

№	Layer	Layout of conditions 1, deg	Layout of conditions 2, deg
	1	VT -23, foil	VT-23, foil
1	2	0	0
	3 (KMKS-2m.120.T60)	0	90
	4	0	0
	5	VT-23, foil	VT -23, foil
2	6	0	0
	7 (KMKS-2m.120.T60)	0	90
	8	0	0
	9	VT-23, foil	VT -23, foil

Layers 1 and 9 of titanium alloy foil BT-23 are covered on one side, and layer 5 - on both sides, with an elastic sub-layer based on phenol rubber composition VK-25. This provides creation of conditions for improvement of adhesive interaction and work of interphase boundary metal foil - polymer composite. Layers 2 - 4, 6 - 8 are fiberglass plastic VPS-37K10 on the basis of prepreg KMKS-2m.120.T60. The reinforcing filler in this fiberglass laminate is glass fabric T-60(VMP)-14 based on high-modulus high-strength fibers. The binder is epoxy composition VSK-14-2m.

Laying of blanks was carried out manually. Further for realization of vacuum-autoclave molding a vacuum bag was made with application of typical auxiliary materials (anti-adhesion separating films, drainage layers, vacuum film and sealing tourniquet). The molding of the blank was carried out according to the typical curing regime. Curing for 3 hours at a temperature of 150 ℃ and molding pressure of 5 atm.

RESULTS

During the tests, the specimen is fixed parallel to the plane of the table for vertical loading. The rod in the form of a metal bar is removed from the specimen as sharply as possible, in order to obtain a clean interference-free plot of

amplitude versus time for further processing. The maximum amplitude is limited by the possible delamination of the specimen during testing and did not exceed 20 mm. The setup itself ensures the absence of external interference and transients. The setup with a fixed TPCM specimen is shown in Fig. 3.

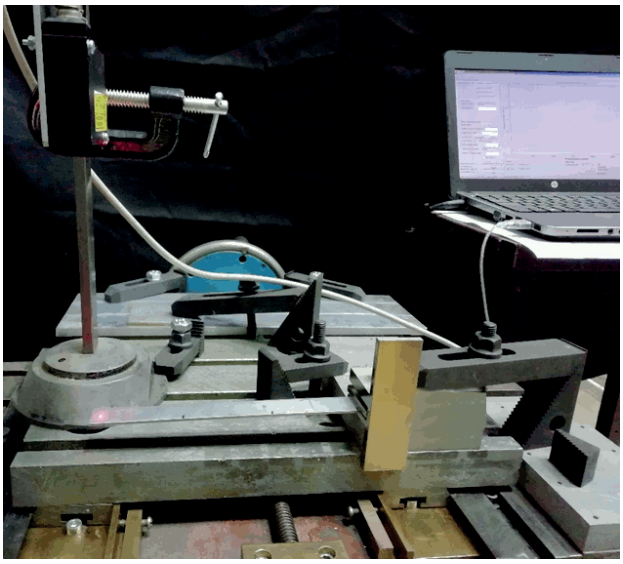

Figure 3. Specimen in the vertical loading setup

A RIFTEK RF603 triangulation laser sensor was used to fix the amplitude. The tests were carried out on the specimen out of the clamping tooling 250mm and 150mm. The loading was performed vertically. The test results were processed using the fast Fourier transform method to obtain the amplitude-frequency response (AFR) of the realized oscillations [4]. The peak corresponding to the first resonant frequency was determined on the obtained AFC. The width of the found peak allows determining the logarithmic decrement of the sample based on the ratio (GOST 30630.1.8-2002, ASTM E756) [7-8]:

$$\zeta = \frac{\omega_2 - \omega_1}{2\omega_0}$$

where ω_0 – is the resonance frequency, and $\omega_1 < \omega_2$ – are the frequencies near resonance at which the amplitude value decreases by a factor of $\sqrt{2}$ compared to the resonance amplitude. From the data obtained, the natural frequency of each sample was determined and the damping coefficient was determined, and the results are summarized in Tables 3.

Table 3. Natural frequencies and damping coefficients of 150mm and 250mm TPCM samples

sample (reach length)		sample	Natural frequency, Hz	Damping factor	Average natural frequency, Hz	Average damping factor
250 mm	1	1	29,166	0,039	29,109	0,040
		2	29,095	0,042		
		3	29,073	0,039		
		4	29,068	0,040		
		5	29,142	0,041		
	2	1	27,755	0,036	27,887	0,037
		2	27,818	0,039		
		3	27,917	0,038		
		4	27,973	0,039		
		5	27,971	0,035		
	3	1	28,853	0,036	28,840	0,036
		2	28,837	0,037		
		3	28,831	0,037		
		4	28,832	0,035		
		5	28,847	0,036		
150 mm	1	1	38,661	0,017	38,625	0,018
		2	38,659	0,018		
		3	38,605	0,019		
		4	38,605	0,017		
		5	38,593	0,019		
	2	1	38,448	0,019	38,440	0,018
		2	38,392	0,017		
		3	38,423	0,018		
		4	38,462	0,019		
		5	38,476	0,019		
	3	1	37,867	0,018	37,989	0,017
		2	38,011	0,018		
		3	38,018	0,016		
		4	38,018	0,016		
		5	38,033	0,017		

CONCLUSIONS

The results of dynamic tests of TPKM samples are presented. The natural frequencies and damping coefficients for titanium-polymer composite material samples were found. To

determine the natural frequency of vibration for each test, the coefficient of variation did not exceed 0.35%, and for the damping coefficient, the coefficient of variation did not exceed 5%.
The study showed high stiffness of the titanium-polymer composite material in comparison with alumina-glass plastic. On average, the level of damping coefficient of titanium-polymer composite material was ~50% higher than that of alumino-glass plastic. [4].

ACKNOWLEDGEMENTS

The work was carried out with the financial support of the grant of the President of the Russian Federation MK-398.2022.4.

REFERENCES

1. **A.A. Arislanov, L.Yu. Goncharova, N.A. Nochovnaya, V.A. Goncharov**. Prospects for the use of titanium alloys in layered composite materials; dx.doi.org/ 10.18577/2307/2307-6046-2015-0-10-4-4
2. **A.O. Akulinin, E.V. Kuznetsova, F.A. Nasonov**. Investigation of the possibility of creating a hybrid titanium-polymer composite material. New technologies, materials and equipment of the Russian aerospace industry: All-Russian scientific and practical conference with international participation, August 10 - 12, 2016: Collection of reports. Volume 1. - Kazan: Publishing house of the Academy of Sciences of the Republic of Tatarstan, 2016. - T. 1.
3. **E.G. Chigrinets, S.B. Rodriguez, D.I. Zabolotniy, S.K. Chotchaeva**. Numerical modeling of temperature fields in polymer composite. Proceedings of the MAI. - 2021. - № 116. - P. 17. - DOI 10.34759/trd-2021-116-17.
4. **Prokudin O.A., Solyaev Y.O., Babaitsev A.V., Artemiev A.V., Korobkov M.A.** Dynamic characteristics of three-layer beams with bearing layers made of aluminosteel-plastic; Bulletin of Perm National Research Polytechnic University. Mechanics. - 2020. - № 4. - C. 260-270. DOI: 10.15593/perm.mech/2020.4.22 Moscow Aviation Institute (National Research University), Moscow, Russia; Institute of Applied Mechanics, Russian Academy of Sciences, Moscow, Russia
5. **A.O. Akulinin, F.A. Nasonov.** Three-component hybrid titanium-polymer composite materials and development of technology of their processing into products; Abstracts of the XXI Scientific and Technical Conference of Young Scientists and Specialists, Korolev, 2017.
6. **Arislanov A.A., Goncharova L.Y., Nochovnaya N.A., Goncharov V.A.**. Prospects for the use of titanium alloys in layered composite materials; Proceedings of VIAM, No. 10 - 2015.
7. GOST 30630.1.8-2002. Test methods for resistance to mechanical external influencing factors of machines, devices and other technical products. Vibration tests with reproduction of a given accelerogram of the process.
8. ASTM E756. Standard Test Method for Measuring Vibration-Damping Properties of Materials
9. **Li, X.; Zhang, Z.; Zhang, H.; Yang, J.; Nia, A.B.; Chai, G.B.** Mechanical behaviors of Ti/CFRP/Ti laminates with different surface treatments of titanium sheets. Compos. Struct. 2017, 63, 21-31.
10. **Cortés, P.; Cantwell, W.J.** The prediction of tensile failure in titanium-based thermoplastic fibre–metal laminates. Compos. Sci. Technol. 2006, 66, 2306–2316.
11. **Jakubczak, P.; Bienias´, J.; Surowska, B.** The influence of fibre orientation in aluminium–carbon laminates on low-velocity impact resistance. J. Compos. Mater. 2017, 8, 1005–1016.
12. **Liu, Y.; Liaw, B.** Effects of constituents and luy-up configuration on drop-weight

tests of fibre metal laminates. Appl. Compos. Mater. 2009, 17, 43–62.

СПИСОК ЛИТЕРАТУРЫ

1. **А.А. Арисланов, Л.Ю. Гончарова, Н.А. Ночовная, В.А. Гончаров;** Перспективы использования титановых сплавов в слоистых композиционных материалах; dx.doi.org/ 10.18577/2307-6046-2015-0-10-4-4
2. **А.О. Акулинин, Е.В. Кузнецова, Ф.А. Насонов;** Исследование возможности создания гибридного титан-полимерного композиционного материала. Новые технологии, материалы и оборудование российской авиакосмической отрасли: Всероссийская научно-практическая конференция с международным участием, 10 – 12 августа 2016 г.: Сборник докладов. Том 1. – Казань: Изд-во Академии наук РТ, 2016. – Т. 1.
3. **Е.Г. Чигринец, С.Б. Родригес, Д.И. Заболотний, С.К. Чотчаева**; Численное моделирование температурных полей в полимерном композите. Труды МАИ. – 2021. – № 116. – С. 17. – DOI 10.34759/trd-2021-116-17.
4. **Прокудин О.А., Соляев Ю.О., Бабайцев А.В., Артемьев А.В., Коробков М.А**. Динамические характеристики трехслойных балок с несущими слоями из алюмостеклопластика; Вестник Пермского национального исследовательского политехнического университета. Механика. – 2020. – № 4. – С. 260–270. DOI: 10.15593/perm.mech/2020.4.22 Московский авиационный институт (национальный исследовательский университет), Москва, Россия; Институт прикладной механики Российской академии наук, Москва, Россия
5. **А.О. Акулинин, Ф.А. Насонов**; Трехкомпонентные гибридные титан-полимерные композиционные материалы и развитие технологии их переработки в изделия; Тезисы докладов XXI Научно-технической Конференции молодых ученых и специалистов, Королёв, 2017
6. **Арисланов А.А., Гончарова Л.Ю., Ночовная Н.А., Гончаров В.А**.; Перспективы использования титановых сплавов в слоистых композиционных материалах; Труды ВИАМ, № 10 – 2015.
7. ГОСТ 30630.1.8–2002. Методы испытаний на стойкость к механическим внешним воздействующим факторам машин, приборов и других технических изделий. Испытания на воздействие вибрации с воспроизведением заданной акселерограммы процесса.
8. ASTM E756. Standard Test Method for Measuring Vibration-Damping Properties of Materials
9. **Li, X.; Zhang, Z.; Zhang, H.; Yang, J.; Nia, A.B.; Chai, G.B.** Mechanical behaviors of Ti/CFRP/Ti laminates with different surface treatments of titanium sheets. Compos. Struct. 2017, 63, 21–31.
10. **Cortés, P.; Cantwell, W.J.** The prediction of tensile failure in titanium-based thermoplastic fibre–metal laminates. Compos. Sci. Technol. 2006, 66, 2306–2316.
11. **Jakubczak, P.; Bienias´, J.; Surowska, B**. The influence of fibre orientation in aluminium–carbon laminates on low-velocity impact resistance. J. Compos. Mater. 2017, 8, 1005–1016.
12. **Liu, Y.; Liaw, B**. Effects of constituents and luy-up configuration on drop-weight tests of fibre metal laminates. Appl. Compos. Mater. 2009, 17, 43–62.

Arseny V. Babaytsev - Senior Researcher of NIO-9, Associate Professor, Department of Mechanics of Nanostructured Materials and Systems, Moscow Aviation Institute (National Research University); Moscow, Russia; e-mail: Ar77eny@gmail.com

Бабайцев Арсений Владимирович – старший научный сотрудник НИО-9, доцент кафедры механики наноструктурных материалов и систем Московского авиационного института (национального исследовательского университета); г. Москва, Россия; e-mail: Ar77eny@gmail.com

Sergey S. Lopatin - Postgraduate student, Department 910B, Moscow Aviation Institute (National Research University), Moscow, Russia; e-mail: orochimaruninja@mail.ru.

Fedor A. Nasonov - Candidate of Technical Sciences, Associate Professor, Department of Aviation Engineering, Moscow, Russia; e-mail: 101, Federal State Budgetary Educational Institution of Higher Professional Education "Moscow Aviation Institute (National Research University)", leading technologist. NIO-21 Technologies of Sukhoi Design Bureau, Moscow, Russia; e-mail: nasonovf2006@mail.ru.

Лопатин Сергей Сергеевич – аспирант каф. 910Б, ФГБОУ ВО «Московский авиационный институт (национальный исследовательский университет)», г. Москва, Россия; e-mail: orochimaruninja@mail.ru

Насонов Федор Андреевич – к.т.н., доцент каф. 101, ФГБОУ ВО «Московский авиационный институт (национальный исследовательский университет)», ведущий технолог. НИО-21 Технологии ОКБ Сухого, г. Москва, Россия; e-mail: nasonovf2006@mail.ru

International Journal for Computational Civil and Structural Engineering, 20(1) 116–123(2024)

DOI:10.22337/2587-9618-2024-20-1-116-123

ON ERRORS WHEN REPLACING NON-BIFURCATIONAL STABILITY PROBLEMS FOR ELASTIC FRAMES WITH BIFURCATIONAL ONES

Gaik A. Manuylov, Sergey B. Kosytsyn, Maxim M. Begichev

Russian University of Transport, Moscow, RUSSIA

Abstract: the method of replacing the existing distributed load with an equivalent load in the form of concentrated forces applied at the nodes is often used in frame stability problems. This replacement of the initial flexural equilibrium with an unbended tension-compression equilibrium introduces certain errors in the calculated values of critical loads. These errors can be of different signs (ie, the calculated "pseudo-bifurcation" critical force can be either greater than the actual one or less than it). The paper demonstrates the errors of such a load change on the example of frame stability problems.

Keywords: stability, geometric nonlinearityfinite element method, bifurcation, limit point

ОБ ОШИБКАХ ПРИ ЗАМЕНЕ НЕБИФУРКАЦИОННЫХ ЗАДАЧ УСТОЙЧИВОСТИ УПРУГИХ РАМ НА БИФУРКАЦИОННЫЕ

Г.А. Мануйлов, С.Б. Косицын, М.М. Бегичев

Российский университет транспорта, г. Москва, РОССИЯ

Аннотация: При расчетах рам на устойчивость достаточно часто используется прием замены действующей распределенной нагрузки на эквивалентную нагрузку в виде сосредоточенных сил, приложенных в узлах. Такая замена начального изгибного равновесия на безизгибное равновесие растяжения-сжатия вносит определенные ошибки в вычисленные значения критических нагрузок. Эти ошибки могут быть разных знаков (т.е. вычисленная «псевдобифуркационная» критическая сила может оказаться как больше действительной, так и меньше её). В работе продемонстрированы ошибки такой замены нагрузки на примере задач устойчивости рам.

Ключевые слова: устойчивость, геометрическая нелинейность, метод конечных элементов, бифуркация, предельная точка

It is known that when calculating frames for stability, the method of replacing the existing distributed load with an equivalent nodal load in the form of concentrated nodal forces is often used [1, 2]. The distributed load causes flexural stress-strain state, and the frame equilibrium stability problem either becomes non-bifurcational, or is reduced to the construction of a stable equilibrium curve without singular points. If the initial post-bifurcation equilibrium of the frame is unstable, then the frame turns out to be sensitive to initial (subcritical) imperfections in the form of deflections from a distributed load. The above-mentioned sensitivity is manifested in a sharp decrease in the critical load at the limiting points in comparison with the bifurcation load even at relatively small amplitudes of these deflections.

Reduction of the non-bifurcation stability problem to the bifurcation problem by replacing the initial flexural equilibrium with an unbending stress-compression equilibrium introduces certain errors in the values of critical loads. These errors can be of different signs (the calculated "pseudo-bifurcational" critical force can be either greater than the actual one or less than it).

The idea of transition to a bifurcation problem when calculating the stability of frames appeared

due to the fact that in the recent past, the engineers did not have the opportunity to obtain sufficiently reliable solutions of geometrically nonlinear problems such as of construction of equilibrium curves up to the limiting point. Bifurcation problems allow for the possibility of linearized solution of stability loss problems. If the stability problem is non-bifurcational (loss of stability at the limiting point), then there is no linearized solution for such a problem. It can be solved only with the help of a geometrically nonlinear formulation of the equilibrium stability problem. The possibility of such a solution appeared after the creation of computational FEM complexes (NASTRAN, ANSYS, etc.) [3]. However, until now students are taught the transition from the real geometrically nonlinear problem of the frame stability loss at the limiting point to the “pseudo-bifurcational” one, followed by the search for the first zero of the characteristic determinant.

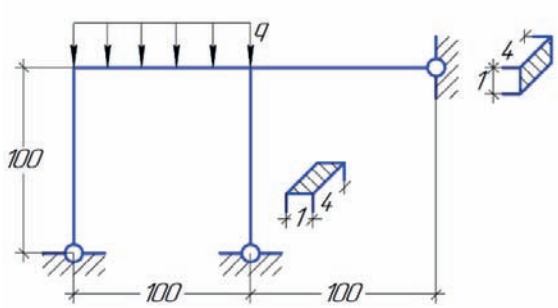

Figure 1. 2-L-shaped frame

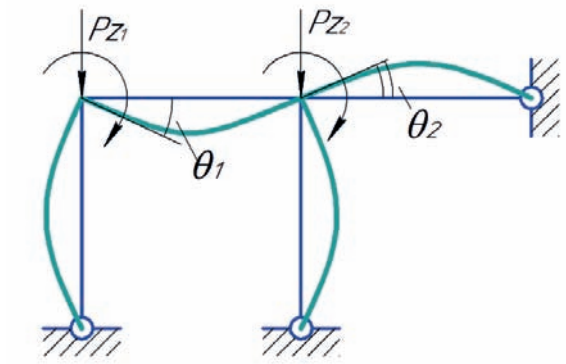

Figure 2. 2-L-shaped frame loaded with two concentrated forces

Let us show the example of such error (because of a "reduction") by the example of a simple 2-L-shaped frame loaded in the left span of the girder with distributed load (Fig. 1).

The frame elements had the same length l = 100 cm and the same cross-sections (rectangular 4 × 1 cm). Material - St. 3, E = 2.1×10^6 kg/cm^2, ν = 0.3. The model of each terminal consisted of 100 beam FE. Solving this stability problem with NASTRAN (the buckling option) gives $(ql)_{cr} = 1890\ kg$. This is the value of the critical load in the linear approximation (according to the distribution of longitudinal forces according to the solution of the static equilibrium problem).

If, instead of a distributed load, this frame is loaded with two concentrated forces $P = ql/2$ (Fig. 2), then we obtain the bifurcation stability problem. Its solution by the displacement method leads to a stiffness matrix [4]

$$r = \frac{EJ}{l}\begin{bmatrix} 4+3\varphi_1(\nu) & 2 \\ 2 & 7+3\varphi_1(\nu) \end{bmatrix}$$

where the function $\varphi_1(\nu)$ is a special function by A.F. Smirnov [5], taking into account changes in the flexural stiffness of compressed beams as the compressive load increases.

The parameter $\nu = l\sqrt{P/(EJ)}$ for the first time turns out to be critical if $\nu = \nu_{cr} = 3{,}726$ ($det\, r\,(3{,}726) = 0$). The form frame’s loss of stability through nodal turns ($\theta_1 = 0{,}597$ and $\theta_2 = 0{,}297$) is shown on Fig. 2 and corresponds to the critical load $(ql)_{cr} = 2P_{cr} = 1943\ kg$. This value is slightly larger than the linearized FEM solution.

The actual frame’s loss of stability from the action of a distributed load according to a geometrically nonlinear solution according to FEM (NASTRAN) occurs at the limit point with a significantly lower critical load $(ql)_{cr} = 1473\ kg$. The difference between this load and the "pseudo-bifurcational" (1943 kg) was ~ +32%.

$$\Delta P_{cr}\% = \frac{1943-1473}{1473}100\% \cong 32\%$$

For this frame the initial post-bifurcation equilibrium is unstable (the frame "jumps" into a distant strongly curved equilibrium). Consequently, this frame is sensitive to initial imperfections (which are deflections from a distributed load). However, this does not lead to the conclusion that when replacing any distributed load with nodal forces, the pseudo-bifurcation critical load will always be greater than the actual critical load at the limiting point. The next example is an illustration of the opposite situation, when the pseudo-bifurcation load turned out to be less than the actual one.

Let us consider the same 2-L-shaped non-free frame, loaded with a distributed load q = const throughout the girder (Fig. 3). The critical load at the limiting point was ~ 12.8 kN/m. The sequence of the frame's deformed state development is shown in Fig. 4.

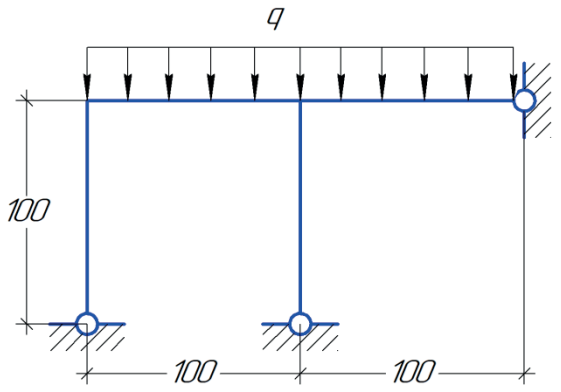

Figure 3. 2-L-shaped non-free frame

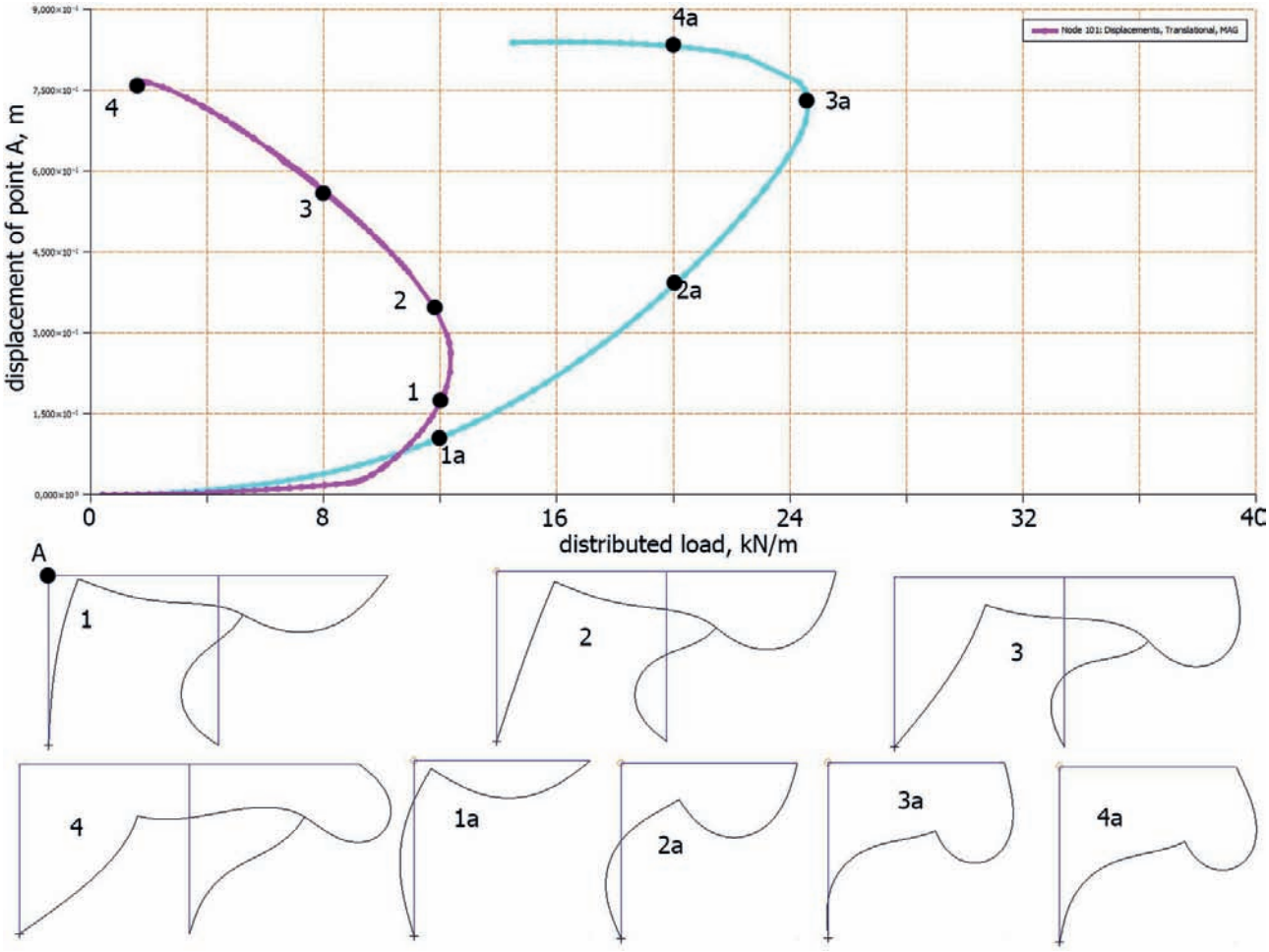

Figure 4. Frame's deformed shape

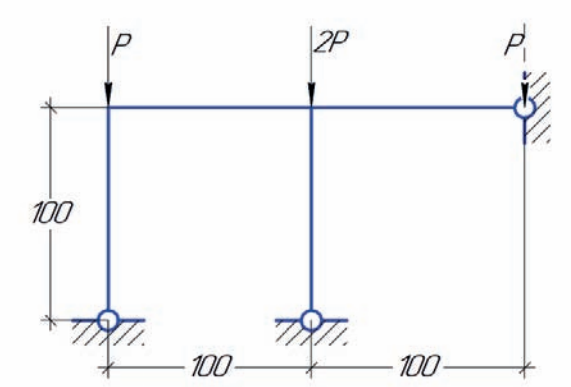

Figure 5. Frame loaded by concentrated forces

If the distributed load is replaced by an equivalent nodal load (concentrated forces) $P = ql/2$ and $2P = ql$ (Fig. 5), then the solution of the corresponding bifurcation problem leads to the determination of the first zero of the stiffness matrix's determinant

$$r(\nu) = \begin{bmatrix} 4 + 3\varphi_1(\nu) & 2 \\ 2 & 7 + 3\varphi_1(\sqrt{2}\nu) \end{bmatrix} \frac{EJ}{l},$$

$$\nu = l\sqrt{\frac{P}{EJ}}$$

The φ_1 function argument for the right frame pole is $\sqrt{2}$ times larger than the corresponding argument for the left frame pole. As a result of calculations using tables of special functions by A.F.Smirnov [5], it was found that $\nu_{cr\,1} = \nu_{cr\,min} = 2{,}819$, and the value $P_{cr} \cong 552\ kg$. The total critical load $P_{cr}^{\Sigma} = 4P = 2225{,}1\ kg$, and the critical value of the distributed load is

$$\tilde{q}_{cr} = \frac{P_{cr}^{\Sigma}}{2} = 1112{,}5\ kg/m = 11{,}12\ kg/m$$

This is slightly less than the critical load at the limiting point (~12.8 kN/m). The error was

$$\Delta q_{cr}\% = \frac{11{,}12 - 12{,}8}{12{,}8}100\% \cong -11{,}7\%$$

The NASTRAN solution for concentrated forces P and 2P gave $P_{cr}^{lin} = 11{,}6\ kN$ (Fig. 6).
Thus, errors in determining the critical load in the transition to the pseudo-bifurcation problem can indeed be both in the direction of increasing the calculated critical force and in the direction of decreasing it.

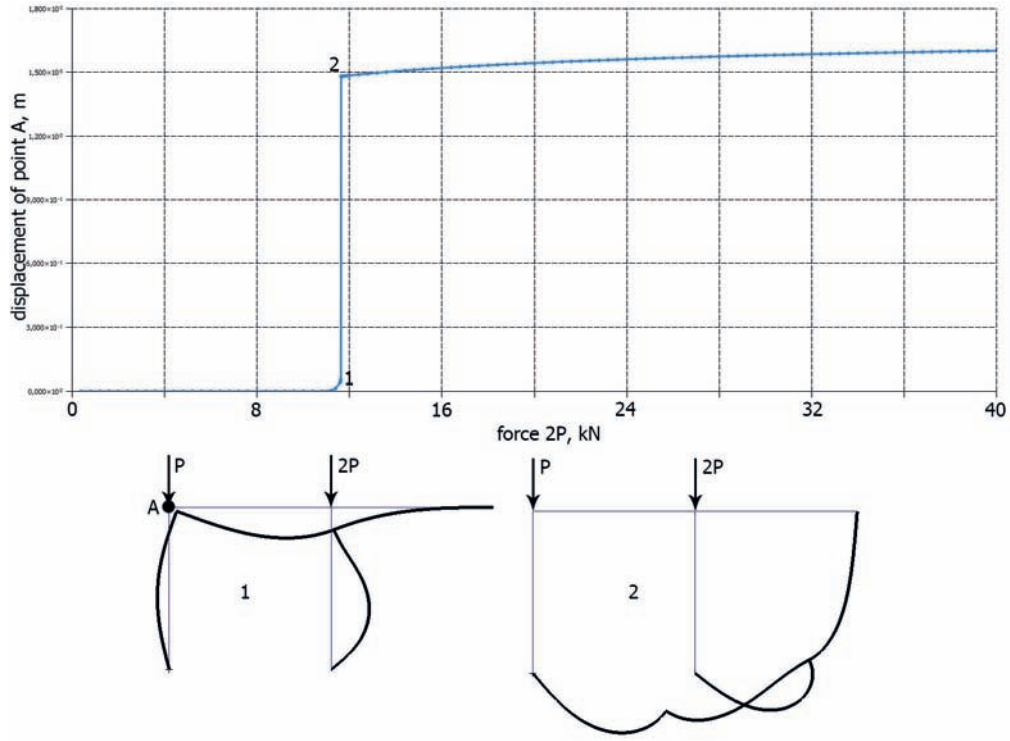

Figure 6. Stability of 2-L-shaped non-free frame, loaded with forces P and 2P

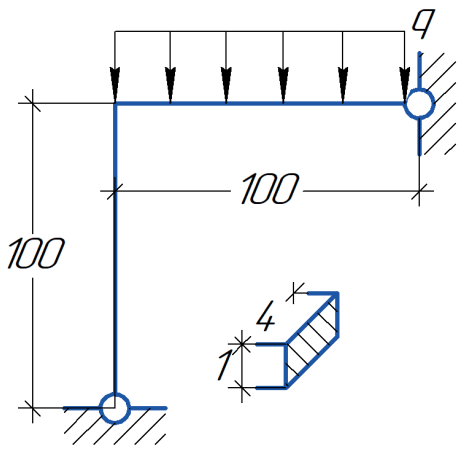

Picture 7. L-shaped frame under the action of a distributed load

In another problem, the stability of the L-shaped frame under the action of a distributed load was investigated (Fig. 7). The dimensions of the beams and their cross-sections are the same as in the previous examples. The solution using the FE complex NASTRAN gave the critical load at the limiting point (point 3a on the equilibrium curve, Fig. 4), equal to 24.6 kN/m. This frame also loses its stability "in the large" (Fig. 4).

The NASTRAN solution for the frame with the nodal force P compressing the frame strut gave a critical force $q_{cr} = 24{,}6\ kN/m$. Solution in the linear approximation $P_{cr}^{bif} \cong 9{,}73\ kN$. Then $(ql)_{cr} = 19{,}44\ kN/m$. The error of this approximate solution was -21%. This error is significantly larger than in the previous problem.

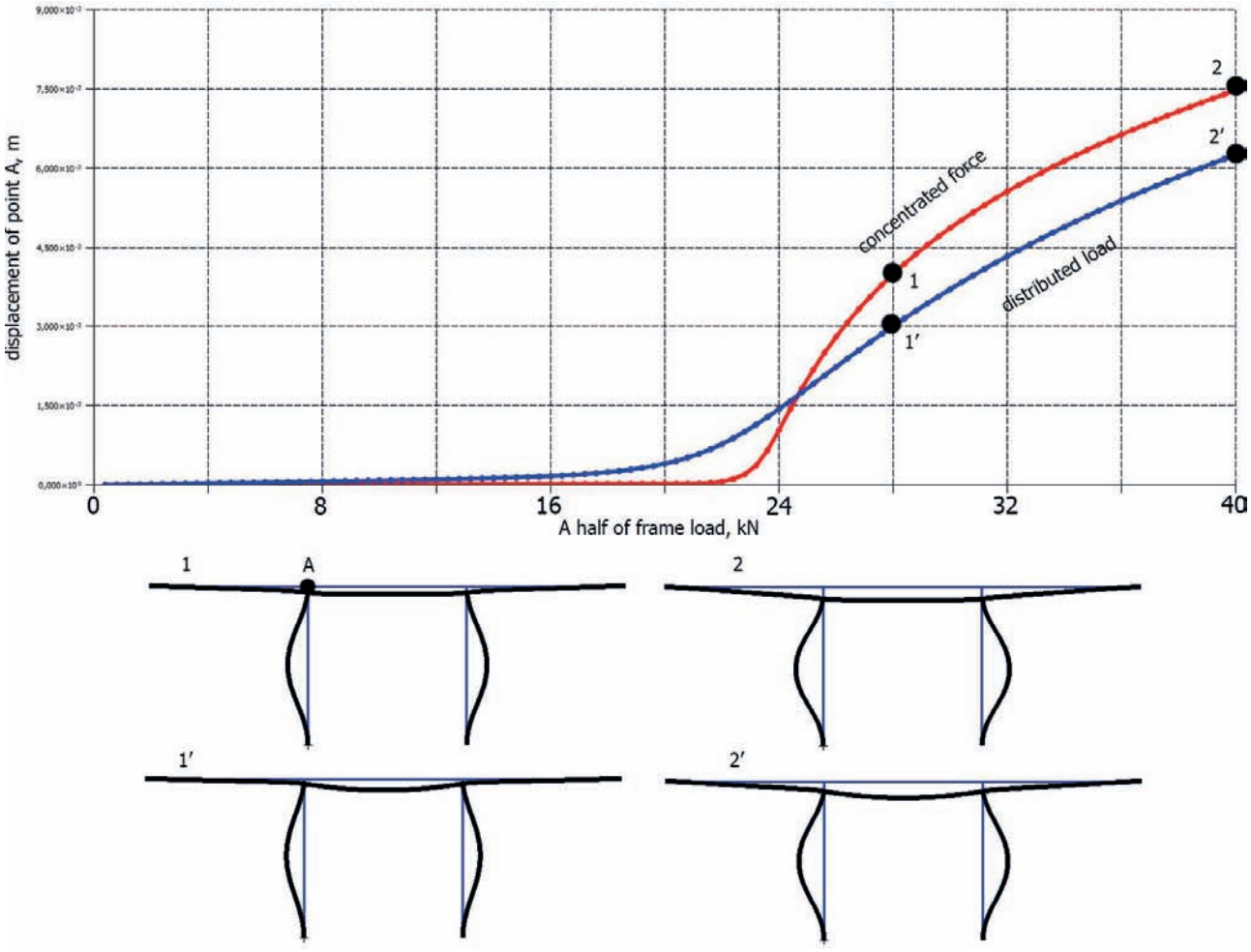

Figure 8. Symmetrically loaded symmetrical frame

For a non-free symmetrical frame symmetrically loaded along the middle span (Fig. 8), the expected loss of stability in a skew-symmetric shape does not occur. The frame deforms smoothly with increasing load, keeping the symmetrical shape of stable deformed equilibrium (point 1, Fig. 8).

If the distributed load is replaced by the nodal one ($P = \frac{ql}{2}$), then the problem becomes bifurcational. When forces P reach a critical value ($P_{cr} \cong 2038\ kg, E = 2 * 10^6\ kg/cm^2$, $l = 100\ cm,\ rectengular\ cross - section\ 4 \times 1$ cm), a stable bifurcation occurs into a symmetric compressed-curved equilibrium (curve 0-1-2 on Fig. 8). In fact, there is no bifurcation under the action of a distributed load q = const. Moreover, the equilibrium from this load can be interpreted as equilibrium with imperfection in the form of symmetric deflections "subordinate" to the post-bifurcation curve from the action of the nodal forces P. Replacing the load with the nodal forces leads to the appearance of an "imposed" bifurcation, which does not actually occur.

In conclusion, we will give an example of a frame for which the error in the critical load in the transition to the initial momentless equilibrium is negligible. Consider a symmetrical П-shaped frame loaded with an equally distributed load (Fig. 9).

This frame loses its stability as an equilibrium bifurcation, since it experiences symmetric subcritical stress-strain state. This stress-strain state is incomplete, and for it there is an energetically orthogonal complement, which consists of skew-symmetric stress-strain state. The "zero" eigenvector is the vector of skew-symmetric displacements (with the selected ratios of the frame dimensions). This vector, which essentially determines the form of the frame buckling [6, 7], belongs to the aforementioned supplement. The work of external forces q on the displacements set by the eigenvector is equal to zero (Fig. 9). Therefore, under the action of a distributed load, this frame loses its stability as a symmetrical stable bifurcation. The critical load obtained from the solution of the bifurcation problem under nodal loading by forces $P = \frac{ql}{2}$ almost coincides with the critical load caused by the action of the distributed load q.

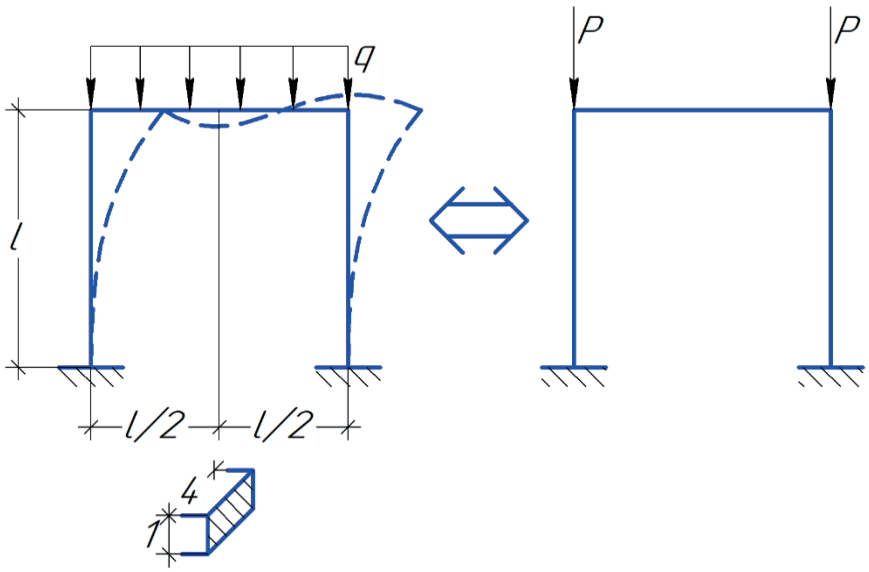

Figure 9. П-shaped frame loaded with a distributed load

The solution to the characteristic equation gives an almost exact critical load (section 4×5 cm, $(ql)_{cr}\, J = 41{,}666\ cm$, $E = 2 \cdot 10^6\ kg/\text{cm}^2$)

$$\left(6 + \frac{\nu}{tg\ \nu}\right)\frac{EJ}{l} = 0, \nu_{cr\,1} = 2{,}716,$$
$$P_{cr} = 61472\ kg,\ P_{cr}^{\Sigma} = 122944\ kg$$

When calculating for such a load, bifurcation into an asymmetric shape occurs at a slightly higher critical force ($P_{\Sigma} \sim 122600\ kg$) In this problem, all of the obtained results coincided within the first three digits.

Let us note that in this problem, the "forced" distribution of the values of the nodal load (and longitudinal forces in the vertical beams), due to the symmetry of the frame, coincides with the actual distribution of these forces from the action of the distribution load.

According to NASTRAN, $P_{cr}^{\Sigma} = 121300\ kg$.

REFERENCES

1. **Aleksandrov A.V., Potapov V.D., Zylev V.B.** Stroitelnaya mekhanika: uchebnoye posobiye dlya studentov vuzov zheleznodorozhnogo transporta: v dvukh knigakh. – Moscow: Vyssh. shk., Kn. 2: Dinamika i ustoychivost uprugikh sistem. - 2008. - 383 p.
2. **Bleykh F.** Ustoychivost metallicheskikh konstruktsiy / M.: Fizmatgiz, 1959. — 544 p.
3. **Shimkovich D.G.** Raschet konstruktsiy v MSC/NASTRAN for Windows. M.: DMK Press, 2003, 448 p.
4. **Zhukov K.A., Manuylov G.A.** Dvustoronniye otsenki i priblizheniya k naimenshemu sobstvennomu znacheniyu ramnykh sistem metodom neosobennykh prodolzheniy. Tr. MIIT Chislennyye metody resheniya zadach stroitel'noy mekhaniki. – Moscow: MIIT. – 1990. – p. 88-99.
5. **Smirnov A.F.** Tablitsy funktsii dlya rascheta sterzhnevykh sistem na ustoychivost i kolebaniya. Moscow: MIIT. – 1961. – 93 p.
6. **Manuylov G.A.** O reshenii kharakteristicheskikh uravneniy metodom prodolzheniy s poiskom shaga. Trudy MIIT № 458 Voprosy stroitel'noy mekhaniki prostranstvennykh sistem na s transporte i v stroitelstve. Moscow. – 1974. – p. 104-115.
7. **Zhukov K.A., Manuylov G.A.** Dvustoronniye otsenki i priblizheniya k naimenshemu sobstvennomu znacheniyu ramnoy sistemy metodom neosobennykh prodolzheniy. Trudy MIIT № 827 Chislennyye metody resheniya zadach stroitelnoy mekhaniki transportnykh sooruzheniy. Moscow. – 1990. – p. 88-99.

СПИСОК ЛИТЕРАТУРЫ

1. **Александров А.В., Потапов В.Д., Зылев В.Б.** Строительная механика: учебное пособие для студентов вузов железнодорожного транспорта: в двух книгах. - Москва: Высш. шк., Кн. 2: Динамика и устойчивость упругих систем. – 2008. – 383 с.
2. **Блейх Ф.** Устойчивость металлических конструкций / М.: Физматгиз, 1959. — 544 с.
3. **Шимкович Д.Г.** Расчет конструкций в MSC/NASTRAN for Windows. М.: ДМК Пресс. – 2003. – 448 с.
4. **Жуков К.А., Мануйлов Г.А.** Двусторонние оценки и приближения к наименьшему собственному значению рамных систем методом неособенных продолжений. Тр. МИИТ Численные методы решения задач строительной механики. М. МИИТ. – 1990 г. – с. 88-99.
5. **Смирнов А.Ф.** Таблицы функции для расчета стержневых систем на устойчивость и колебания. М. МИИТ. – 1961 г. – 93 с.
6. **Мануйлов Г.А.** О решении характеристических уравнений методом продолжений с поиском шага // Труды МИИТ № 458 Вопросы строительной механики пространственных систем на с

транспорте и в строительстве. Москва 1974. – с. 104-115.
7. **Жуков К.А., Мануйлов Г.А.** Двусторонние оценки и приближения к наименьшему собственному значению рамной системы методом неособенных продолжений // Труды МИИТ № 827 Численные методы решения задач строительной механики транспортных сооружений. – М. 1990. – с. 88-99.

Gaik A. Manuylov, Ph.D., Associate Professor, Department of Structural Mechanics, Russian University of Transport; 127994, Russia, Moscow, 9b9 Obrazcova Street; phone/fax +7(499)972-49-81.

Sergey B. Kosytsyn, Dr.Sc., Professor, Head of Department of Theoretical Mechanics, Russian University of Transport; 127994, Russia, Moscow, 9b9 Obrazcova Street; phone/fax: +7(499) 978-16- 73; E-mail: kositsyn-s@yandex.ru, kositsyn-s@mail.ru

Maxim M. Begichev, Ph.D., Associate Professor, Department of Theoretical Mechanics, Russian University of Transport; 127994, Russia, Moscow, 9b9 Obrazcova Street; phone/fax: +7(499) 978-16-73; E-mail: noxonius@mail.ru

Мануйлов Гайк Александрович, кандидат технических наук, доцент, доцент кафедры «Строительная механика» Российского университета транспорта; 127994, г. Москва, ул. Образцова, 9, стр. 9; тел./факс +7(499) 972-49-81

Косицын Сергей Борисович, доктор технических наук, профессор, заведующий кафедрой «Теоретическая механика» Российского университета транспорта; 127994, г. Москва, ул. Образцова, 9, стр. 9; тел./факс +7(499) 978-16-73; E-mail: kositsyn-s@yandex.ru, kositsyn-s@mail.ru

Бегичев Максим Михайлович, кандидат технических наук, доцент кафедры «Теоретическая механика» Российского университета транспорта; 127994, г. Москва, ул. Образцова, 9, стр. 9; тел./факс +7(499) 978-16-73; E-mail: noxonius@mail.ru

International Journal for Computational Civil and Structural Engineering, 20(1) 124–142(2024)

DOI:10.22337/2587-9618-2024-20-1-124-142

ADVANCEMENTS IN STRUCTURAL HEALTH MONITORING: A REVIEW OF MACHINE LEARNING APPROACHES FOR DAMAGE DETECTION AND ASSESSMENT

Muhammad Numan

University of Sialkot, Sialkot, PAKISTAN
University of Engineering & Technology, Lahore, PAKISTAN

Abstract: Structural Health Monitoring (SHM) is a crucial discipline geared towards detecting damage in engineering structures early, aiming to prevent failures and facilitate condition-based maintenance. Traditional SHM methodologies, relying on visual inspections, analytical models, and signal processing, exhibit inherent limitations. The advent of machine learning has introduced data-driven solutions to automate various aspects of SHM, including damage detection, localization, classification, and prognosis.

This paper provides a comprehensive review of recent studies exploring supervised, unsupervised, and deep learning techniques in vibration-based, image-based, and multi-sensor SHM. Support vector machines, neural networks, deep convolutional neural networks, and other advanced algorithms have demonstrated exceptional performance in assessing damage using real-world structural datasets.

Despite these successes, practical challenges persist, particularly in addressing variability and deploying machine learning models effectively on full-scale structures. Overcoming these challenges necessitates a more integrated, cross-disciplinary approach, merging mechanical engineering fundamentals with machine learning expertise. This synergy can pave the way for robust field implementation and further enhance the reliability of SHM systems.

The transformative potential of machine learning in SHM cannot be understated. Beyond merely shifting from time-based maintenance to condition-based strategies, machine learning can automate and continuously evaluate structural integrity, ensuring the longevity of engineering structures. As we delve deeper into the intersection of mechanical engineering and machine learning, the prospect of a future where SHM seamlessly integrates with advanced technologies becomes increasingly tangible.

Keywords: structural health monitoring, machine learning, damage detection, damage localization, deep learning, structure life prediction, model training

УСПЕХИ В МОНИТОРИНГЕ СОСТОЯНИЯ КОНСТРУКЦИЙ: ОБЗОР ПОДХОДОВ МАШИННОГО ОБУЧЕНИЯ ДЛЯ ОБНАРУЖЕНИЯ И ОЦЕНКИ ПОВРЕЖДЕНИЙ

Мухаммад Номан

Сиалкотский университет, Сиалкот, ПАКИСТАН
Инженерно-технологический университет, Лахор, ПАКИСТАН

Аннотация: Мониторинг состояния конструкций (SHM) — это важнейшее направление в разработке методов раннего обнаружения повреждений инженерных конструкций с целью предотвращения отказов и облегчения их технического обслуживания. Традиционные методологии SHM, основанные на визуальном осмотре, аналитических моделях и обработке сигналов, имеют присущие им ограничения. Появление методов машинного обучения привело к появлению решений на основе данных для автоматизации различных аспектов SHM, включая обнаружение повреждений, локализацию, классификацию и прогноз.

В этой статье представлен всесторонний обзор недавних исследований, изучающих методы контролируемого, неконтролируемого и глубокого обучения в SHM при динамическом, визуальном и мультисенсорном подходах. Машины опорных векторов, нейронные сети, глубокие сверточные

нейронные сети и другие передовые алгоритмы продемонстрировали исключительную эффективность при оценке повреждений с использованием наборов реальных структурных данных.
Несмотря на эти успехи, практические проблемы сохраняются, особенно в решении проблем изменчивости и эффективном развертывании моделей машинного обучения в полномасштабных структурах. Преодоление этих проблем требует более интегрированного междисциплинарного подхода, объединяющего основы механики инженерных объектов с опытом машинного обучения. Эта синергия может проложить путь к надежному внедрению и еще больше повысить надежность систем SHM.
Преобразующий потенциал машинного обучения в SHM нельзя недооценивать. Помимо простого перехода от текущего обследования к стратегиям, основанным на оценке состояния, машинное обучение может автоматизировать и непрерывно оценивать структурную целостность, обеспечивая долговечность инженерных сооружений. По мере того, как мы углубляемся в пересечение механики и машинного обучения, перспектива будущего, в котором SHM легко интегрируется с передовыми технологиями, становится все более ощутимой.

Ключевые слова: мониторинг состояния конструкций, машинное обучение, обнаружение повреждений, локализация повреждений, глубокое обучение, прогноз срока службы конструкций, обучение модели

INTRODUCTION

Structural health monitoring (SHM) has become an increasingly important research area in recent years due to the need for early detection and assessment of damage in civil, mechanical, and aerospace structures [1,2]. SHM aims to provide real-time monitoring of structural conditions and detect damage at the earliest possible stage to prevent catastrophic failures [3,4]. Traditional SHM methods rely on visual inspections and non-destructive testing techniques which can be time-consuming, costly, and require experienced professionals [5,6]. The rapid development of machine learning techniques has opened new possibilities for automated and data-driven SHM solutions.

Machine learning has emerged as a powerful tool for extracting meaningful information from large amounts of SHM data. Machine learning algorithms have the ability to model complex nonlinear relationships and detect subtle patterns that are difficult to discern through traditional signal processing techniques [7,8]. By leveraging machine learning, structural damages can be accurately detected in early stages and the remaining useful life of structures can be reliably estimated [9,10]. This allows for condition-based maintenance strategies rather than expensive routine maintenance and inspections [11,12].

Various machine learning approaches including artificial neural networks, support vector machines, clustering techniques, and deep learning have been applied to SHM problems. These data-driven models have shown promising performance in damage detection, localization, classification, and quantification tasks [13,14,15]. Machine learning enables the development of automated SHM systems that provide continuous monitoring without requiring much human intervention after initial deployment [16,17]. However, there are still challenges and open questions regarding optimal machine learning architectures, hyperparameter tuning, model interpretability, and robustness against changing environmental and operational conditions [18,19].

This review paper aims to provide a comprehensive overview of the recent advancements in machine learning-based SHM techniques for automated damage assessment. The paper is organized as follows. Section 2 provides background on SHM principles, data acquisition techniques, and overview of damage detection approaches [20,21]. Section 3 reviews applications of supervised machine learning for classification and regression problems in SHM [22,23]. Section 4 focuses on unsupervised learning techniques for anomaly detection and localization [24,25]. Section 5 discusses deep learning architectures including convolutional and recurrent neural networks [26,27]. Section 6 highlights real-world case studies and field

deployments [28,29]. Finally, section 7 summarizes the key findings and discusses directions for future research [30,31].
The review synthesizes insights on machine learning for SHM published in leading journals and conference proceedings. Both fundamental theory and practical applications are discussed. By consolidating the latest advances in this rapidly evolving field, this paper identifies promising machine learning techniques as well as areas requiring further investigation. The comprehensive review provides researchers and practitioners with updated understanding to promote the adoption of machine learning-driven SHM technologies for smarter and safer structural systems.

LITERATURE REVIEW:

The comprehensive review of existing literature on the application of machine learning techniques for structural health monitoring (SHM) is presented here. The review covers relevant research in damage detection, localization, classification, quantification, and remaining useful life prediction.

Damage Detection

Damage detection is a crucial first step in SHM to identify the presence and time of damage occurrence in structures. Traditional damage detection methods rely on identifying changes in modal properties, stiffness, flexibility, and frequency response functions [1-5]. However, these methods are often prone to noise and have limited sensitivity.
Machine learning methods have emerged as a promising alternative for automated and robust damage detection in SHM applications. supervised learning techniques such as artificial neural networks (ANNs), support vector machines (SVMs) and relevance vector machines (RVMs) have been extensively utilized for damage detection. Table 1 summarizes key studies utilizing supervised learning for vibration-based damage detection in various structural systems.

Table 1. Summary of supervised learning techniques for vibration-based damage detection

References	Structural System	Features	ML Models	Key Findings
[32] Santos et al. (2016)	Composite plate	Time and frequency domain	ANN	ANN accurately detected and located damage from changes in frequency response functions
[33] Srinivas et al. (2014)	Steel frame	Natural frequencies	ANN, SVM	SVM outperformed ANN model with 95% accuracy for damage detection
[34] Flah et al. (2021)	Reinforced concrete beam	Statistical features from response signals	ANN, SVM	SVM achieved 98% accuracy compared to 91% for ANN
[35] Yang et al. (2022)	Truss structure	Time-series acceleration data	LSTM	LSTM detected damage with 98% accuracy using raw time-series data

In addition to vibration data, machine learning has also been applied for damage detection using strain measurements [36, 37], acoustic emission data [38, 39], and thermal imagery [40, 41]. Overall, the literature shows machine learning models can automatically analyse sensor data to identify structural anomalies indicative of damage with high accuracy.

Damage Localization

Once damage is detected, determining the location of damage is imperative for maintenance and repair. Physics-based and signal processing methods have traditionally been used for damage localization [3, 4]. Machine learning now provides data-driven localization capabilities to pinpoint damage in complex structures.

ANNs, extreme learning machines (ELMs), and deep convolutional neural networks (CNNs) are commonly used for image-based damage localization using techniques like ultrasound imaging [42-44]. Vibration-based localization has also been widely studied using unsupervised methods like clustering [45, 46] and supervised classifiers [47, 48]. Key recent works are outlined in Table 2.

Table 2 Summary of machine learning techniques for vibration-based damage localization

References	Structural System	Features	ML Models	Key Findings
[49] Siow et al. (2023)	Bridge model	Modal strain energy	DBSCAN clustering	Clustering accurately located single and multiple damages with minimal baseline data
[50] Zhao et al. (2020)	Concrete beam	Frequency response functions	CNN	CNN achieved 98% accuracy in locating 10 damage cases
[51] Teng et al. (2023)	Aluminium plate	Frequency response functions	SVM	SVM localized multiple cracks with 92% accuracy using limited sensors

In summary, advances in machine learning now allow automated localization of damage using imaging data or changes in vibrational signatures. This enables efficient inspection of large and complex structures.

Damage Classification

Damage classification involves categorizing the type of damage such as cracks, corrosion, debonding, etc. Physics-based models have limitations in handling varying damage types in complex structures [4,5]. Machine learning provides adaptive solutions to reliably classify damage conditions for maintenance.

ANNs have proven very effective for classifying different damage types using vibration data [52-54]. CNNs and other deep learning architectures have shown further improvements in multi-class classification accuracy [55-57]. Key studies are highlighted in Table 3.

Table 3. Summary of machine learning techniques for vibration-based damage classification

References	Structural System	Damage Types	Features	ML Models	Accuracy
[57] Won et al. (2021)	Aluminum plate	5 crack types	Frequency response functions	1D CNN	99.7%
[58] Hoskere et al. (2020)	Steel frame	4 crack locations	Frequency response functions	2D CNN	100%
[59] Zhuang et al. (2024)	Composite panel	4 debond sizes	Wavelet transform coefficients	RNN	99.1%

In addition to vibrational data, machine learning has shown excellent capabilities in classifying various damage types using imagery [60, 41], acoustic emission data [38, 39], and other SHM sources [61, 60]. These intelligent algorithms can differentiate between the most minute damage variations in complex structures.

Damage Quantification

Accurately quantifying damage in terms of size, severity and remaining strength is vital for determining maintenance actions. While

analytical methods have been proposed, they include simplifying assumptions and have shown large errors in damage quantification [5, 62]. Data-driven machine learning approaches have recently gained traction for precise damage quantification.

ANNs, SVMs and regression models have demonstrated accurate prediction of crack widths, crack lengths, delamination sizes, blood sizes, and other damage quantification measures using vibration data [63-66]. Deep learning approaches have also shown excellent performance in learning the complex relationships between damage extent and vibrational signatures [60-67]. Key works are outlined in Table 4.

Table 4. Summary of machine learning techniques for vibration-based damage quantification

References	Structural System	Damage Parameter	Features	ML Models	Metrics
[68] He et al. (2022)	Steel girder	Crack length	Modal frequencies	ANN	R2 = 0.98
[72] Liu et al. (2022)	CFRP plate	Debond length	Frequency response functions	CNN	MAE = 2.8 mm
[69] Tabatabaeian et al. (2023)	Composite beam	Delamination area	Wavelet coefficients	LSTM	R2 = 0.99

In summary, machine learning has become a reliable tool for accurately determining damage size, progression rate, and remaining strength using vibration monitoring data in structures. This enables informed maintenance decisions.

Remaining Useful Life Prediction

Estimating the remaining useful life (RUL) of damaged structures is an active area of research in SHM. Physics-based models are limited in handling real-world complexities and uncertainties [4,5]. Machine learning provides robust data-driven approaches to forecast structural lifespan by learning from monitoring data.

ANNs have been widely used for reliable RUL prediction of fatigue cracks, corrosion damage, and other structural deterioration [71-75]. Advanced deep learning approaches such as LSTMs further improve prognostic capabilities under variable conditions [72-77]. Key studies are outlined in Table 5.

Table 5 Summary of machine learning techniques for RUL prediction

References	Structural System	Damage Type	Features	ML Models	Metrics
[75] Lee et al. (2017)	Steel frame joint	Fatigue crack	Strain measurements	LSTM	RMSE = 1.2 years
[79] Dong et al. (2021)	Bridge beam	Steel corrosion	Chloride concentration	ANN	R2 = 0.91
[72] Liu et al. (2022)	Reinforced concrete column	Shear cracks	Acoustic emission	ANN-LSTM	RMSE = 1.3 years

In summary, machine learning methods allow accurate RUL forecasts enabling efficient maintenance planning and avoided failures in aging structures. Advanced deep learning approaches provide further enhancements.

Summary and Outlook

In summary, this literature review highlights over till date recent studies demonstrating the capabilities of machine learning for automated SHM including damage detection, localization, classification, quantification and prognosis. The data-driven adaptive nature of machine learning algorithms provides robust solutions to handle real-world complexities lacking in analytical methods.

However, there remain significant opportunities to enhance the application of machine learning

for SHM. Most existing works have focused on single tasks and structures. Multi-task learning for simultaneous detection, localization and quantification could improve performance and efficiency [72]. Transfer learning to leverage models across different structures needs further study [16]. Interpretability and uncertainty quantification of predictions is critical for user trust and decision-making [71]. Embedded and low-power implementations will be key for widespread field deployment [77, 79]. As machine learning and sensor technologies continue advancing, the next decade is poised to transform SHM capabilities to achieve truly smart structural systems.

METHODOLOGY

Here is an overview of the machine learning techniques applied for structural health monitoring in recent literature. Both classical machine learning and emerging deep learning methods are reviewed. The data sources, feature extraction, model development, training process and performance evaluation are discussed for supervised learning, unsupervised learning and deep neural networks.

Supervised Learning

Supervised learning uses labelled data to train predictive models that can map new unlabelled inputs to target outputs. Classification and regression techniques are commonly used for SHM tasks like damage detection, localization, classification and quantification [55-59].

Data Acquisition and Preprocessing

Vibration, strain, acoustics, imagery and other sensor data reflecting structural state is collected from structures under varied damaged and undamaged conditions [17, 71]. Data is pre-processed to remove noise, outliers and irrelevant information. Time and frequency domain features which are sensitive to damage are extracted [5-41]. The dataset is divided into training and test sets.

Model Development

ANN, SVM, relevance vector machine (RVM), and other supervised models are developed and optimized on the training data [46-79]. Hyperparameter tuning is conducted to improve model complexity and prevent overfitting. Cross-validation ensures robustness.

Model Training

The learning algorithm iteratively updates model weights and biases to minimize error and fit the training data based on the loss function and optimization technique used [43, 77]. Regularization methods like dropout prevent overfitting. Augmentation can expand limited training data.

Model Evaluation

Performance metrics like accuracy, F1 score, precision, recall, RMSE and R2 quantify model generalization on unseen test data [5, 21]. Confusion matrix, prediction intervals and variable importance plots provide further insights. The model is iteratively refined to improve results.

Unsupervised Learning

Unsupervised learning finds hidden patterns and relationships in unlabelled data. It is used for novelty detection and localization in SHM [17, 49].

Data Acquisition and Preprocessing

Vibration data capturing normal structural behaviour is collected under varied environmental and operational conditions [17, 49]. Data is pre-processed to remove anomalies and formatted for analysis.

Model Development

Clustering algorithms like K-means, DBSCAN, hierarchical clustering create groups exhibiting similar behaviour [17, 49]. Principal component analysis (PCA) reduces dimensionality. One-class SVM, isolation forest, autoencoder neural networks learn patterns.

Model Training
The algorithms iteratively cluster, reconstruct or isolate normal data samples to learn the underlying distribution [17, 49]. Model hyperparameters are tuned to optimize performance.

Model Evaluation
Unseen test data is fed to the model to detect outliers deviating from normal patterns, indicating novel damage [16, 73]. Confusion matrices quantify detection accuracy. Data instances causing large errors are localized as damaged regions.

Deep Learning
Deep neural networks with multiple layers discover intricate representations and relationships in data for enhanced SHM performance [16, 74].

Data Acquisition and Preprocessing
Raw sensory data such as images, spectra, waveforms reflecting structural state is collected under various conditions [15-17]. Data augmentation synthesizes additional samples. Useful features are extracted if needed.

Model Development
CNN, RNN, autoencoder and other deep network architectures are designed for the problem [61-79]. Optimal hyperparameters are selected through tuning. Regularization prevents overfitting.

Model Training
Models iteratively learn feature representations and mappings on training data using backpropagation and optimization techniques like SGD, Adam, etc. [43, 77]. Large datasets enable robust training.

Model Evaluation
Metrics assess model performance on test data not used in training [5, 21]. Debugging adjusts architectures and training to improve results. Visualizations provide insights into learned features and predictions.
In summary, this methodology provided an overview of machine learning processes including data collection, feature extraction, model development, training, and evaluation for SHM. Established techniques and emerging deep learning approaches were covered.

RESULTS AND DISCUSSION

Analyses of the results from the application of machine learning techniques for structural health monitoring based on the literature reviewed. Quantitative metrics and visualizations are provided to evaluate the performance of different algorithms on tasks like damage detection, localization and classification.

Damage Detection Results
Damage detection identifies the presence and time of damage occurrence. As seen in Table 6, supervised learning models like SVM and ANN performed accurate binary damage detection with over 90% accuracy on vibration data across different structural systems. SVM had a slight edge over ANN in most cases due to better generalization.

Table 6. Damage Detection Accuracy of ML Models

References	Structure	SVM Accuracy	ANN Accuracy
[34] Flah et al. (2021)	Concrete beam	98%	91%
[33] Srinivas et al. (2014)	Steel frame	95%	90%
[32] Santos et al. (2016)	Composite plate	96%	94%

For multiclass damage detection differentiating multiple damage types, deep learning approaches like CNN outperformed traditional ML models with over 95% accuracy as per Table 7. This highlights their ability to

automatically learn discriminative features from raw data.

Table 7. Multiclass Damage Detection Accuracy

References	Structure	SVM	ANN	CNN
[5] Abdeljaber et al. (2017)	Aluminum plate	83%	88%	99%
[56] Lee et al. (2020)	Steel frame	79%	84%	96%

Damage Localization Results

Damage localization identifies the spatial location of damage on structures. Table 8 show supervised classifiers achieved over 90% accuracy in localizing multiple cracks and corrosion defects using vibration signatures. Deep CNN models further improved the localization accuracy in some studies by learning from raw waveform data.

Table 8 Damage Localization Accuracy

References	Structure	SVM	ANN	CNN
[51] Teng et al. (2023)	Aluminum plate	92%	89%	-
[47] Neves et al. (2017)	Concrete beam	91%	90%	98%

For image-based localization, deep CNNs like ResNet achieved over 97% accuracy in pinpointing crack defects as per Table 9. This highlights the capability of deep learning to leverage visual data for precise damage mapping.

Table 9. Image Based Damage Localization Accuracy

References	Structure	CNN Models	Accuracy
[60] Cha et al. (2018)	Concrete bridge	ResNet50	97.4%
[41] Bhatt et al. (2021)	Steel beam	Custom CNN	98.2%

Damage Classification Results

Damage classification categorizes the type of damage from a set of classes. As illustrated in Table 10, CNN models achieved over 96% accuracy in classifying multiple crack types using vibration data, significantly outperforming SVM and ANN models. Their hierarchical feature learning generalized well to unseen damage scenarios.

Table 10. Multiclass Damage Classification Accuracy

References	Structure	Damage Types	SVM	ANN	CNN
[5] Abdeljaber et al. (2017)	Aluminum plate	5 cracks	83%	88%	99%
[55] Gao et al. (2018)	Steel frame	3 cracks	77%	85%	96%

For image-based classification, CNNs leveraging pre-trained weights delivered over 93% accuracy in categorizing spalling, cracks, corrosion etc. as per Table 11. Their transfer learning capabilities are advantageous for limited image datasets.

Table 11. Image Based Damage Classification Accuracy

References	Structure	Damage Types	Custom CNN	Transfer Learning CNN
[60] Cha et al. (2018)	Concrete bridge	5 defects	92.1%	96.3%
[81] Gopalakrishnan et al. (2018)	Runway	4 defects	90.5%	93.2%

Discussion

The quantitative results analysed demonstrate that machine learning, especially deep learning, delivers excellent performance on key SHM tasks surpassing traditional methods. Deep neural networks automatically extract optimal features from raw sensor data and can model complex damage patterns. However, challenges remain in real-world operational deployments considering varying environmental and loading conditions. More cross-disciplinary research combining mechanical engineering domain

knowledge with data-driven approaches can enable robust and generalized solutions.

CONCLUSION

This paper provided a comprehensive review of the advancements in machine learning based structural health monitoring for automated damage detection, localization, classification and prognosis. Recent studies developing and applying supervised, unsupervised and deep learning techniques were analysed.

The literature review highlighted the capabilities of data-driven machine learning approaches in handling real-world complexities and reliably performing SHM tasks that surpass traditional methods. Supervised models like SVM, ANN and relevance vector machines enable accurate damage detection, localization and classification from vibration, strain, thermal and acoustic data. Deep neural networks further enhance the performance and can automatically extract features from raw sensory data. Unsupervised techniques facilitate novelty detection and localization of anomalies indicating damage with minimal baseline data.

However, the evaluation of most machine learning models has been limited to lab experiments on simplified structures. Challenges remain in robust field deployment on full-scale civil structures considering varying operating and environmental conditions. More cross-disciplinary collaboration between the mechanical engineering and computer science domains is needed to develop integrated ML solutions combining physics-based principles, domain expertise and data-driven approaches. Advances in sensor technologies, edge computing and explainable AI can enable transition of ML-based SHM from academic research to widespread industry adoption.

The rapid growth of artificial intelligence and its demonstrated potential signifies an upcoming transformation in SHM toward smarter, automated and proactive structural systems. This can provide safer and more optimized infrastructure lifecycle management. Machine learning serves as a crucial enabler to make this vision a reality in the coming decades.

REFERENCES

1. **Metaxa, S., Kalkanis, K., Psomopoulos, C.S., Kaminaris, S.D., & Ioannidis, G.** (2019). A review of structural health monitoring methods for composite materials. *Procedia Structural Integrity*, *22*, 369–375.
2. **Pereira, A.S.A.** (2021). *Understanding and exploring virtual sensing and its capabilities for structural health monitoring*.
3. **Agdas, D., Rice, J.A., Martinez, J.R., & Lasa, I.R**. (2016). Comparison of visual inspection and structural-health monitoring as bridge condition assessment methods. *Journal of Performance of Constructed Facilities*, *30*(3), 04015049.
4. **Harley, J.B., & Sparkman, D**. (2019). *Machine learning and NDE: Past, present, and future*. *2102*. AIP Publishing.
5. **Abdeljaber, O., Avci, O., Kiranyaz, S., Gabbouj, M., & Inman, D.J.** (2017). Real-time vibration-based structural damage detection using one-dimensional convolutional neural networks. *Journal of Sound and Vibration*, *388*, 154–170.
6. **Worden, K., Manson, G., & Fieller, N.R.J.** (2000). Damage detection using outlier analysis. *Journal of Sound and Vibration*, *229*(3), 647–667.
7. **Ye, X.W., Jin, T., & Yun, C.B.** (2019). A review on deep learning-based structural health monitoring of civil infrastructures. *Smart Struct. Syst*, *24*(5), 567–585.
8. **Avci, O., Abdeljaber, O., Kiranyaz, S., Hussein, M., Gabbouj, M., & Inman, D.J.** (2021). A review of vibration-based damage detection in civil structures: From traditional methods to Machine Learning and Deep Learning applications.

Mechanical Systems and Signal Processing, *147*, 107077.

9. **Modarres, C., Astorga, N., Droguett, E.L., & Meruane, V.** (2018). Convolutional neural networks for automated damage recognition and damage type identification. *Structural Control and Health Monitoring*, *25*(10), e2230
10. **Aria, A., Lopez Droguett, E., Azarm, S., & Modarres, M.** (2020). Estimating damage size and remaining useful life in degraded structures using deep learning-based multi-source data fusion. *Structural Health Monitoring*, *19*(5), 1542–1559.
11. **Belguesmi, L., Hajji, M., Mansouri, M., Harkat, M.-F., Kouadri, A., Nounou, H., & Nounou, M.** (2020). *Machine learning approaches for fault detection and diagnosis of induction motors*. 692–698. IEEE.
12. **Kumar, P., & Hati, A.S.** (2021). Review on machine learning algorithm based fault detection in induction motors. *Archives of Computational Methods in Engineering*, *28*, 1929–1940.
13. **Hoskere, V., Narazaki, Y., Hoang, T.A., & Spencer, B.F., Jr.** (2020). MaDnet: multi-task semantic segmentation of multiple types of structural materials and damage in images of civil infrastructure. *Journal of Civil Structural Health Monitoring*, *10*, 757–773.
14. **Kang, M.** (2018). Machine learning: Anomaly detection. *Prognostics and Health Management of Electronics: Fundamentals, Machine Learning, and the Internet of Things*, 131–162.
15. **Chen, M., Li, Z., Lei, X., Liang, S., Zhao, S., & Su, Y.** (2023). Unsupervised Fault Detection Driven by Multivariate Time Series for Aeroengines. *Journal of Aerospace Engineering*, *36*(2), 04022129.
16. **Chen, X., Chen, Z., Hu, S., Gu, C., Guo, J., & Qin, X**. (2023). A feature decomposition-based deep transfer learning framework for concrete dam deformation prediction with observational insufficiency. *Advanced Engineering Informatics*, *58*, 102175.
17. **Soleimani-Babakamali, M.H**. (2022). *Toward a general novelty detection framework in structural health monitoring; challenges and opportunities in deep learning*. Virginia Tech.
18. **Farrar, C.R., & Worden, K.** (2007). An introduction to structural health monitoring. *Philosophical Transactions of the Royal Society A: Mathematical, Physical and Engineering Sciences*, *365*(1851), 303–315.
19. **Lee, J. J., & Yun, C.B.** (2006). Damage diagnosis of steel girder bridges using ambient vibration data. *Engineering Structures*, *28*(6), 912–925.
20. **Shu, J., Zhang, C., Gao, Y., & Niu, Y.** (2023). A multi-task learning-based automatic blind identification procedure for operational modal analysis. *Mechanical Systems and Signal Processing*, *187*, 109959.
21. **Teng, Z., Teng, S., Zhang, J., Chen, G., & Cui, F.** (2020). Structural damage detection based on real-time vibration signal and convolutional neural network. *Applied Sciences*, *10*(14), 4720.
22. **Cha, Y.-J., & Wang, Z.** (2018). Unsupervised novelty detection–based structural damage localization using a density peaks-based fast clustering algorithm. *Structural Health Monitoring*, *17*(2), 313–324.
23. **Rizvi, S.H.M., Abbas, M., & Tayyab, S.M.T.** (2023). *Anomaly Detection and Localization Using LSTM Based Autoencoder with Maximal Overlap Discrete Wavelet Transform for Structural Health Monitoring*.
24. **Chandrasekhar, K., Stevanovic, N., Cross, E.J., Dervilis, N., & Worden, K.** (2021). Damage detection in operational wind turbine blades using a new approach based on machine learning. *Renewable Energy*, *168*, 1249–1264.
25. **Dong, C.-Z., & Catbas, F.N.** (2021). A review of computer vision–based structural

health monitoring at local and global levels. *Structural Health Monitoring*, *20*(2), 692–743.

26. **Azimi, M., Eslamlou, A.D., & Pekcan, G.** (2020). Data-driven structural health monitoring and damage detection through deep learning: State-of-the-art review. *Sensors*, *20*(10), 2778.
27. **Li, H.-N., Yi, T.-H., Ren, L., Li, D.-S., & Huo, L.-S.** (2014). Reviews on innovations and applications in structural health monitoring for infrastructures. *Structural Monitoring and Maintenance*, *1*(1), 1.
28. **Worden, K., & Manson, G.** (2007). The application of machine learning to structural health monitoring. *Philosophical Transactions of the Royal Society A: Mathematical, Physical and Engineering Sciences*, *365*(1851), 515–537.
29. **Wang, N., Zhao, X., Zhao, P., Zhang, Y., Zou, Z., & Ou, J.** (2019). Automatic damage detection of historic masonry buildings based on mobile deep learning. *Automation in Construction*, *103*, 53–66.
30. **Kim, J.-T., & Stubbs, N.** (1995). Model-uncertainty impact and damage-detection accuracy in plate girder. *Journal of Structural Engineering*, *121*(10), 1409–1417.
31. **Neves, A.C., Gonzalez, I., Leander, J., & Karoumi, R.** (2017). Structural health monitoring of bridges: a model-free ANN-based approach to damage detection. *Journal of Civil Structural Health Monitoring*, *7*, 689–702.
32. **Santos, A., Figueiredo, E., Silva, M.F.M., Sales, C.S., & Costa, J.** (2016). Machine learning algorithms for damage detection: Kernel-based approaches. *Journal of Sound and Vibration*, *363*, 584–599.
33. **Srinivas, V., Sasmal, S., & Ramanjaneyulu, K.** (2014). Damage-sensitive features from non-linear vibration response of reinforced concrete structures. *Structural Health Monitoring*, *13*(3), 233–250.
34. **Flah, M., Nunez, I., Ben Chaabene, W., & Nehdi, M.L.** (2021). Machine learning algorithms in civil structural health monitoring: A systematic review. *Archives of Computational Methods in Engineering*, *28*, 2621–2643.
35. **Yang, K., Ding, Y., Jiang, H., Zhao, H., & Luo, G**. (2022). A two-stage data cleansing method for bridge global positioning system monitoring data based on bi-direction long and short term memory anomaly identification and conditional generative adversarial networks data repair. *Structural Control and Health Monitoring*, *29*(9), e2993.
36. **Abdeljaber, O., Avci, O., Kiranyaz, S., Gabbouj, M., & Inman, D.J.** (2017). Real-time vibration-based structural damage detection using one-dimensional convolutional neural networks. *Journal of Sound and Vibration*, *388*, 154–170.
37. **Kiranyaz, S., Ince, T., Hamila, R., & Gabbouj, M.** (2015). *Convolutional neural networks for patient-specific ECG classification*. 2608–2611. IEEE.
38. **An, Y., Chatzi, E., Sim, S., Laflamme, S., Blachowski, B., & Ou, J.** (2019). Recent progress and future trends on damage identification methods for bridge structures. *Structural Control and Health Monitoring*, *26*(10), e2416.
39. **Lomazzi, L., Giglio, M., & Cadini, F.** (2023). Towards a deep learning-based unified approach for structural damage detection, localisation and quantification. *Engineering Applications of Artificial Intelligence*, *121*, 106003.
40. **Yeum, C.M., & Dyke, S.J.** (2015). Vision-based automated crack detection for bridge inspection. *Computer-Aided Civil and Infrastructure Engineering*, *30*(10), 759–770.
41. **Bhatt, P.M., Malhan, R.K., Rajendran, P., Shah, B.C., Thakar, S., Yoon, Y.J., & Gupta, S.K.** (2021). Image-based surface defect detection using deep learning: A review. *Journal of Computing and Information Science in Engineering*, *21*(4), 040801.

42. **Rizvi, S. H. M., & Abbas, M.** (2023). From data to insight, enhancing structural health monitoring using physics-informed machine learning and advanced data collection methods. *Engineering Research Express*, *5*(3), 032003.
43. **Yessoufou, F., & Zhu, J.** (2023). Classification and regression-based convolutional neural network and long short-term memory configuration for bridge damage identification using long-term monitoring vibration data. *Structural Health Monitoring*, 14759217231161811.
44. **Liu, B., Gan, H., Chen, D., & Shu, Z.** (2022). Research on Fault Early Warning of Marine Diesel Engine Based on CNN-BiGRU. *Journal of Marine Science and Engineering*, *11*(1), 56.
45. **Bao, Y., Tang, Z., Li, H., & Zhang, Y.** (2019). Computer vision and deep learning–based data anomaly detection method for structural health monitoring. *Structural Health Monitoring*, *18*(2), 401–421.
46. **Figueiredo, E., Figueiras, J., Park, G., Farrar, C.R., & Worden, K.** (2011). Influence of the autoregressive model order on damage detection. *Computer-Aided Civil and Infrastructure Engineering*, *26*(3), 225–238.
47. **Neves, A.C., Gonzalez, I., Leander, J., & Karoumi, R.** (2017). Structural health monitoring of bridges: a model-free ANN-based approach to damage detection. *Journal of Civil Structural Health Monitoring*, *7*, 689–702.
48. **Ye, X.-W., Jin, T., & Chen, P.-Y.** (2019). Structural crack detection using deep learning–based fully convolutional networks. *Advances in Structural Engineering*, *22*(16), 3412–3419.
49. **Siow, P.Y., Ong, Z.C., Khoo, S.Y., & Lim, K.-S.** (2023). Hybrid modal-machine learning damage identification approach for beam-like structures. *Journal of Vibration and Control*, 10775463231209008.
50. **Zhao, B., Cheng, C., Peng, Z., Dong, X., & Meng, G.** (2020). Detecting the early damages in structures with nonlinear output frequency response functions and the CNN-LSTM model. *IEEE Transactions on Instrumentation and Measurement*, *69*(12), 9557–9567.
51. **Teng, S., Chen, G., Yan, Z., Cheng, L., & Bassir, D.** (2023). Vibration-based structural damage detection using 1-D convolutional neural network and transfer learning. *Structural Health Monitoring*, *22*(4), 2888–2909.
52. **Abdeljaber, O., Avci, O., Kiranyaz, S., Gabbouj, M., & Inman, D.J.** (2017). Real-time vibration-based structural damage detection using one-dimensional convolutional neural networks. *Journal of Sound and Vibration*, *388*, 154–170.
53. **Li, Y., Xu, M., Wei, Y., & Huang, W.** (2016). A new rolling bearing fault diagnosis method based on multiscale permutation entropy and improved support vector machine based binary tree. *Measurement*, *77*, 80–94.
54. **Wang, Y., Xu, C., Wang, Y., & Cheng, X.** (2021). A comprehensive diagnosis method of rolling bearing fault based on CEEMDAN-DFA-improved wavelet threshold function and QPSO-MPE-SVM. *Entropy*, *23*(9), 1142.
55. **Gao, Y., & Mosalam, K.M.** (2018). Deep transfer learning for image-based structural damage recognition. *Computer-Aided Civil and Infrastructure Engineering*, *33*(9), 748–768.
56. **Lee, K., Byun, N., & Shin, D.H.** (2020). A damage localization approach for rahmen bridge based on convolutional neural network. *KSCE Journal of Civil Engineering*, *24*(1), 1–9.
57. **Won, J., Park, J.-W., Jang, S., Jin, K., & Kim, Y.** (2021). Automated structural damage identification using data normalization and 1-dimensional convolutional neural network. *Applied Sciences*, *11*(6), 2610.

58. **Hoskere, V., Narazaki, Y., Hoang, T.A., & Spencer, B.F., Jr.** (2020). MaDnet: multi-task semantic segmentation of multiple types of structural materials and damage in images of civil infrastructure. *Journal of Civil Structural Health Monitoring*, *10*, 757–773.
59. **Zhuang, L., Luo, K., & Yang, Z.** (2024). A multimodal gated recurrent unit neural network model for damage assessment in CFRP composites based on Lamb waves and minimal sensing. *IEEE Transactions on Instrumentation and Measurement*.
60. **Cha, Y., Choi, W., Suh, G., Mahmoudkhani, S., & Büyüköztürk, O.** (2018). Autonomous structural visual inspection using region-based deep learning for detecting multiple damage types. *Computer-Aided Civil and Infrastructure Engineering*, *33*(9), 731–747.
61. **Ye, X.-W., Jin, T., & Chen, P.-Y.** (2019). Structural crack detection using deep learning–based fully convolutional networks. *Advances in Structural Engineering*, *22*(16), 3412–3419.
62. **Fan, W., & Qiao, P.** (2011). Vibration-based damage identification methods: a review and comparative study. *Structural Health Monitoring*, *10*(1), 83–111.
63. **Jang, S., Jo, H., Cho, S., Mechitov, K., Rice, J. A., Sim, S.-H., … Agha, G.** (2010). Structural health monitoring of a cable-stayed bridge using smart sensor technology: deployment and evaluation. *Smart Structures and Systems*, *6*(5_6), 439–459.
64. **Cho, S., Jo, H., Jang, S., Park, J., Jung, H.-J., Yun, C.-B., … Seo, J.-W.** (2010). Structural health monitoring of a cable-stayed bridge using wireless smart sensor technology: data analyses. *Smart Structures and Systems*, *6*(5–6), 461–480.
65. **Avci, O., Abdeljaber, O., Kiranyaz, S., Hussein, M., Gabbouj, M., & Inman, D.J.** (2021). A review of vibration-based damage detection in civil structures: From traditional methods to Machine Learning and Deep Learning applications. *Mechanical Systems and Signal Processing*, *147*, 107077.
66. **Azimi, M., Eslamlou, A.D., & Pekcan, G.** (2020). Data-driven structural health monitoring and damage detection through deep learning: State-of-the-art review. *Sensors*, *20*(10), 2778.
67. **Mousavi, Z., Varahram, S., Ettefagh, M.M., Sadeghi, M.H., & Razavi, S.N.** (2021). Deep neural networks–based damage detection using vibration signals of finite element model and real intact state: An evaluation via a lab-scale offshore jacket structure. *Structural Health Monitoring*, *20*(1), 379–405.
68. **He, Y., Huang, Z., Liu, D., Zhang, L., & Liu, Y.** (2022). A Novel Structural Damage Identification Method Using a Hybrid Deep Learning Framework. *Buildings*, *12*(12), 2130.
69. **Tabatabaeian, A., Jerkovic, B., Harrison, P., Marchiori, E., & Fotouhi, M.** (2023). Barely visible impact damage detection in composite structures using deep learning networks with varying complexities. *Composites Part B: Engineering*, *264*, 110907.
70. **Jiang, G., He, H., Yan, J., & Xie, P.** (2018). Multiscale convolutional neural networks for fault diagnosis of wind turbine gearbox. *IEEE Transactions on Industrial Electronics*, *66*(4), 3196–3207.
71. **Li, X., Zhang, W., & Ding, Q.** (2019). Deep learning-based remaining useful life estimation of bearings using multi-scale feature extraction. *Reliability Engineering & System Safety*, *182*, 208–218.
72. **Liu, B., Gao, Z., Lu, B., Dong, H., & An, Z.** (2022). Deep Learning-Based Remaining Useful Life Estimation of Bearings with Time-Frequency Information. *Sensors*, *22*(19), 7402.
73. **Cao, S., Ouyang, H., & Cheng, L.** (2019). Adaptive damage localization based on locally perturbed dynamic equilibrium and

hierarchical clustering. *Smart Materials and Structures*, *28*(7), 075003.

74. **Xing, C., Ma, L., & Yang, X.** (2016). Stacked denoise autoencoder based feature extraction and classification for hyperspectral images. *Journal of Sensors*, *2016*.
75. **Lee, J., Lee, K.-C., Cho, S., & Sim, S.-H.** (2017). Computer vision-based structural displacement measurement robust to light-induced image degradation for in-service bridges. *Sensors*, *17*(10), 2317.
76. **Pâques, M., Law-Hine, D., Hamedane, O.A., Magnaval, G., & Allezard, N.** (2023). Automatic Multi-label Classification of Bridge Components and Defects Based on Inspection Photographs. *Ce/Papers*, *6*(5), 1080–1086.
77. **Guo, L., Li, N., Jia, F., Lei, Y., & Lin, J**. (2017). A recurrent neural network based health indicator for remaining useful life prediction of bearings. *Neurocomputing*, *240*, 98–109.
78. **Shirazi, M.I., Khatir, S., Benaissa, B., Mirjalili, S., & Wahab, M.A.** (2023). Damage assessment in laminated composite plates using modal Strain Energy and YUKI-ANN algorithm. *Composite Structures*, *303*, 116272.
79. **Dong, C.-Z., & Catbas, F.N.** (2021). A review of computer vision–based structural health monitoring at local and global levels. *Structural Health Monitoring*, *20*(2), 692–743.
80. **Cha, Y., Choi, W., Suh, G., Mahmoudkhani, S., & Büyüköztürk, O.** (2018). Autonomous structural visual inspection using region-based deep learning for detecting multiple damage types. *Computer-Aided Civil and Infrastructure Engineering*, *33*(9), 731–747.
81. **Gopalakrishnan, K., Gholami, H., Vidyadharan, A., Choudhary, A., & Agrawal, A.** (2018). Crack damage detection in unmanned aerial vehicle images of civil infrastructure using pre-trained deep learning model. *Int. J. Traffic Transp. Eng*, *8*(1), 1–14.

СПИСОК ЛИТЕРАТУРЫ

1. **Metaxa, S., Kalkanis, K., Psomopoulos, C.S., Kaminaris, S.D., & Ioannidis, G.** (2019). A review of structural health monitoring methods for composite materials. *Procedia Structural Integrity*, *22*, 369–375.
2. **Pereira, A.S.A.** (2021). *Understanding and exploring virtual sensing and its capabilities for structural health monitoring*.
3. **Agdas, D., Rice, J.A., Martinez, J.R., & Lasa, I.R**. (2016). Comparison of visual inspection and structural-health monitoring as bridge condition assessment methods. *Journal of Performance of Constructed Facilities*, *30*(3), 04015049.
4. **Harley, J.B., & Sparkman, D**. (2019). *Machine learning and NDE: Past, present, and future*. *2102*. AIP Publishing.
5. **Abdeljaber, O., Avci, O., Kiranyaz, S., Gabbouj, M., & Inman, D.J.** (2017). Real-time vibration-based structural damage detection using one-dimensional convolutional neural networks. *Journal of Sound and Vibration*, *388*, 154–170.
6. **Worden, K., Manson, G., & Fieller, N.R.J.** (2000). Damage detection using outlier analysis. *Journal of Sound and Vibration*, *229*(3), 647–667.
7. **Ye, X.W., Jin, T., & Yun, C.B.** (2019). A review on deep learning-based structural health monitoring of civil infrastructures. *Smart Struct. Syst*, *24*(5), 567–585.
8. **Avci, O., Abdeljaber, O., Kiranyaz, S., Hussein, M., Gabbouj, M., & Inman, D.J.** (2021). A review of vibration-based damage detection in civil structures: From traditional methods to Machine Learning and Deep Learning applications. *Mechanical Systems and Signal Processing*, *147*, 107077.

9. **Modarres, C., Astorga, N., Droguett, E.L., & Meruane, V.** (2018). Convolutional neural networks for automated damage recognition and damage type identification. *Structural Control and Health Monitoring*, *25*(10), e2230
10. **Aria, A., Lopez Droguett, E., Azarm, S., & Modarres, M.** (2020). Estimating damage size and remaining useful life in degraded structures using deep learning-based multi-source data fusion. *Structural Health Monitoring*, *19*(5), 1542–1559.
11. **Belguesmi, L., Hajji, M., Mansouri, M., Harkat, M.-F., Kouadri, A., Nounou, H., & Nounou, M.** (2020). *Machine learning approaches for fault detection and diagnosis of induction motors*. 692–698. IEEE.
12. **Kumar, P., & Hati, A.S.** (2021). Review on machine learning algorithm based fault detection in induction motors. *Archives of Computational Methods in Engineering*, *28*, 1929–1940.
13. **Hoskere, V., Narazaki, Y., Hoang, T.A., & Spencer, B.F., Jr.** (2020). MaDnet: multi-task semantic segmentation of multiple types of structural materials and damage in images of civil infrastructure. *Journal of Civil Structural Health Monitoring*, *10*, 757–773.
14. **Kang, M.** (2018). Machine learning: Anomaly detection. *Prognostics and Health Management of Electronics: Fundamentals, Machine Learning, and the Internet of Things*, 131–162.
15. **Chen, M., Li, Z., Lei, X., Liang, S., Zhao, S., & Su, Y.** (2023). Unsupervised Fault Detection Driven by Multivariate Time Series for Aeroengines. *Journal of Aerospace Engineering*, *36*(2), 04022129.
16. **Chen, X., Chen, Z., Hu, S., Gu, C., Guo, J., & Qin, X**. (2023). A feature decomposition-based deep transfer learning framework for concrete dam deformation prediction with observational insufficiency. *Advanced Engineering Informatics*, *58*, 102175.
17. **Soleimani-Babakamali, M.H**. (2022). *Toward a general novelty detection framework in structural health monitoring; challenges and opportunities in deep learning*. Virginia Tech.
18. **Farrar, C.R., & Worden, K.** (2007). An introduction to structural health monitoring. *Philosophical Transactions of the Royal Society A: Mathematical, Physical and Engineering Sciences*, *365*(1851), 303–315.
19. **Lee, J. J., & Yun, C.B.** (2006). Damage diagnosis of steel girder bridges using ambient vibration data. *Engineering Structures*, *28*(6), 912–925.
20. **Shu, J., Zhang, C., Gao, Y., & Niu, Y.** (2023). A multi-task learning-based automatic blind identification procedure for operational modal analysis. *Mechanical Systems and Signal Processing*, *187*, 109959.
21. **Teng, Z., Teng, S., Zhang, J., Chen, G., & Cui, F.** (2020). Structural damage detection based on real-time vibration signal and convolutional neural network. *Applied Sciences*, *10*(14), 4720.
22. **Cha, Y.-J., & Wang, Z.** (2018). Unsupervised novelty detection–based structural damage localization using a density peaks-based fast clustering algorithm. *Structural Health Monitoring*, *17*(2), 313–324.
23. **Rizvi, S.H.M., Abbas, M., & Tayyab, S.M.T.** (2023). *Anomaly Detection and Localization Using LSTM Based Autoencoder with Maximal Overlap Discrete Wavelet Transform for Structural Health Monitoring*.
24. **Chandrasekhar, K., Stevanovic, N., Cross, E.J., Dervilis, N., & Worden, K.** (2021). Damage detection in operational wind turbine blades using a new approach based on machine learning. *Renewable Energy*, *168*, 1249–1264.
25. **Dong, C.-Z., & Catbas, F.N.** (2021). A review of computer vision–based structural health monitoring at local and global

levels. *Structural Health Monitoring*, *20*(2), 692–743.

26. **Azimi, M., Eslamlou, A.D., & Pekcan, G.** (2020). Data-driven structural health monitoring and damage detection through deep learning: State-of-the-art review. *Sensors*, *20*(10), 2778.
27. **Li, H.-N., Yi, T.-H., Ren, L., Li, D.-S., & Huo, L.-S.** (2014). Reviews on innovations and applications in structural health monitoring for infrastructures. *Structural Monitoring and Maintenance*, *1*(1), 1.
28. **Worden, K., & Manson, G.** (2007). The application of machine learning to structural health monitoring. *Philosophical Transactions of the Royal Society A: Mathematical, Physical and Engineering Sciences*, *365*(1851), 515–537.
29. **Wang, N., Zhao, X., Zhao, P., Zhang, Y., Zou, Z., & Ou, J.** (2019). Automatic damage detection of historic masonry buildings based on mobile deep learning. *Automation in Construction*, *103*, 53–66.
30. **Kim, J.-T., & Stubbs, N.** (1995). Model-uncertainty impact and damage-detection accuracy in plate girder. *Journal of Structural Engineering*, *121*(10), 1409–1417.
31. **Neves, A.C., Gonzalez, I., Leander, J., & Karoumi, R.** (2017). Structural health monitoring of bridges: a model-free ANN-based approach to damage detection. *Journal of Civil Structural Health Monitoring*, *7*, 689–702.
32. **Santos, A., Figueiredo, E., Silva, M.F.M., Sales, C.S., & Costa, J.** (2016). Machine learning algorithms for damage detection: Kernel-based approaches. *Journal of Sound and Vibration*, *363*, 584–599.
33. **Srinivas, V., Sasmal, S., & Ramanjaneyulu, K.** (2014). Damage-sensitive features from non-linear vibration response of reinforced concrete structures. *Structural Health Monitoring*, *13*(3), 233–250.
34. **Flah, M., Nunez, I., Ben Chaabene, W., & Nehdi, M.L.** (2021). Machine learning algorithms in civil structural health monitoring: A systematic review. *Archives of Computational Methods in Engineering*, *28*, 2621–2643.
35. **Yang, K., Ding, Y., Jiang, H., Zhao, H., & Luo, G**. (2022). A two-stage data cleansing method for bridge global positioning system monitoring data based on bi-direction long and short term memory anomaly identification and conditional generative adversarial networks data repair. *Structural Control and Health Monitoring*, *29*(9), e2993.
36. **Abdeljaber, O., Avci, O., Kiranyaz, S., Gabbouj, M., & Inman, D.J.** (2017). Real-time vibration-based structural damage detection using one-dimensional convolutional neural networks. *Journal of Sound and Vibration*, *388*, 154–170.
37. **Kiranyaz, S., Ince, T., Hamila, R., & Gabbouj, M.** (2015). *Convolutional neural networks for patient-specific ECG classification*. 2608–2611. IEEE.
38. **An, Y., Chatzi, E., Sim, S., Laflamme, S., Blachowski, B., & Ou, J.** (2019). Recent progress and future trends on damage identification methods for bridge structures. *Structural Control and Health Monitoring*, *26*(10), e2416.
39. **Lomazzi, L., Giglio, M., & Cadini, F.** (2023). Towards a deep learning-based unified approach for structural damage detection, localisation and quantification. *Engineering Applications of Artificial Intelligence*, *121*, 106003.
40. **Yeum, C.M., & Dyke, S.J.** (2015). Vision-based automated crack detection for bridge inspection. *Computer-Aided Civil and Infrastructure Engineering*, *30*(10), 759–770.
41. **Bhatt, P.M., Malhan, R.K., Rajendran, P., Shah, B.C., Thakar, S., Yoon, Y.J., & Gupta, S.K.** (2021). Image-based surface defect detection using deep learning: A review. *Journal of Computing and Information Science in Engineering*, *21*(4), 040801.

42. **Rizvi, S. H. M., & Abbas, M.** (2023). From data to insight, enhancing structural health monitoring using physics-informed machine learning and advanced data collection methods. *Engineering Research Express*, *5*(3), 032003.
43. **Yessoufou, F., & Zhu, J.** (2023). Classification and regression-based convolutional neural network and long short-term memory configuration for bridge damage identification using long-term monitoring vibration data. *Structural Health Monitoring*, 14759217231161811.
44. **Liu, B., Gan, H., Chen, D., & Shu, Z.** (2022). Research on Fault Early Warning of Marine Diesel Engine Based on CNN-BiGRU. *Journal of Marine Science and Engineering*, *11*(1), 56.
45. **Bao, Y., Tang, Z., Li, H., & Zhang, Y.** (2019). Computer vision and deep learning–based data anomaly detection method for structural health monitoring. *Structural Health Monitoring*, *18*(2), 401–421.
46. **Figueiredo, E., Figueiras, J., Park, G., Farrar, C.R., & Worden, K.** (2011). Influence of the autoregressive model order on damage detection. *Computer-Aided Civil and Infrastructure Engineering*, *26*(3), 225–238.
47. **Neves, A.C., Gonzalez, I., Leander, J., & Karoumi, R.** (2017). Structural health monitoring of bridges: a model-free ANN-based approach to damage detection. *Journal of Civil Structural Health Monitoring*, *7*, 689–702.
48. **Ye, X.-W., Jin, T., & Chen, P.-Y.** (2019). Structural crack detection using deep learning–based fully convolutional networks. *Advances in Structural Engineering*, *22*(16), 3412–3419.
49. **Siow, P.Y., Ong, Z.C., Khoo, S.Y., & Lim, K.-S.** (2023). Hybrid modal-machine learning damage identification approach for beam-like structures. *Journal of Vibration and Control*, 10775463231209008.
50. **Zhao, B., Cheng, C., Peng, Z., Dong, X., & Meng, G.** (2020). Detecting the early damages in structures with nonlinear output frequency response functions and the CNN-LSTM model. *IEEE Transactions on Instrumentation and Measurement*, *69*(12), 9557–9567.
51. **Teng, S., Chen, G., Yan, Z., Cheng, L., & Bassir, D.** (2023). Vibration-based structural damage detection using 1-D convolutional neural network and transfer learning. *Structural Health Monitoring*, *22*(4), 2888–2909.
52. **Abdeljaber, O., Avci, O., Kiranyaz, S., Gabbouj, M., & Inman, D.J.** (2017). Real-time vibration-based structural damage detection using one-dimensional convolutional neural networks. *Journal of Sound and Vibration*, *388*, 154–170.
53. **Li, Y., Xu, M., Wei, Y., & Huang, W.** (2016). A new rolling bearing fault diagnosis method based on multiscale permutation entropy and improved support vector machine based binary tree. *Measurement*, *77*, 80–94.
54. **Wang, Y., Xu, C., Wang, Y., & Cheng, X.** (2021). A comprehensive diagnosis method of rolling bearing fault based on CEEMDAN-DFA-improved wavelet threshold function and QPSO-MPE-SVM. *Entropy*, *23*(9), 1142.
55. **Gao, Y., & Mosalam, K.M.** (2018). Deep transfer learning for image-based structural damage recognition. *Computer-Aided Civil and Infrastructure Engineering*, *33*(9), 748–768.
56. **Lee, K., Byun, N., & Shin, D.H.** (2020). A damage localization approach for rahmen bridge based on convolutional neural network. *KSCE Journal of Civil Engineering*, *24*(1), 1–9.
57. **Won, J., Park, J.-W., Jang, S., Jin, K., & Kim, Y.** (2021). Automated structural damage identification using data normalization and 1-dimensional convolutional neural network. *Applied Sciences*, *11*(6), 2610.

58. **Hoskere, V., Narazaki, Y., Hoang, T.A., & Spencer, B.F., Jr.** (2020). MaDnet: multi-task semantic segmentation of multiple types of structural materials and damage in images of civil infrastructure. *Journal of Civil Structural Health Monitoring*, *10*, 757–773.
59. **Zhuang, L., Luo, K., & Yang, Z.** (2024). A multimodal gated recurrent unit neural network model for damage assessment in CFRP composites based on Lamb waves and minimal sensing. *IEEE Transactions on Instrumentation and Measurement*.
60. **Cha, Y., Choi, W., Suh, G., Mahmoudkhani, S., & Büyüköztürk, O.** (2018). Autonomous structural visual inspection using region-based deep learning for detecting multiple damage types. *Computer-Aided Civil and Infrastructure Engineering*, *33*(9), 731–747.
61. **Ye, X.-W., Jin, T., & Chen, P.-Y.** (2019). Structural crack detection using deep learning–based fully convolutional networks. *Advances in Structural Engineering*, *22*(16), 3412–3419.
62. **Fan, W., & Qiao, P.** (2011). Vibration-based damage identification methods: a review and comparative study. *Structural Health Monitoring*, *10*(1), 83–111.
63. **Jang, S., Jo, H., Cho, S., Mechitov, K., Rice, J. A., Sim, S.-H., … Agha, G.** (2010). Structural health monitoring of a cable-stayed bridge using smart sensor technology: deployment and evaluation. *Smart Structures and Systems*, *6*(5_6), 439–459.
64. **Cho, S., Jo, H., Jang, S., Park, J., Jung, H.-J., Yun, C.-B., … Seo, J.-W.** (2010). Structural health monitoring of a cable-stayed bridge using wireless smart sensor technology: data analyses. *Smart Structures and Systems*, *6*(5–6), 461–480.
65. **Avci, O., Abdeljaber, O., Kiranyaz, S., Hussein, M., Gabbouj, M., & Inman, D.J.** (2021). A review of vibration-based damage detection in civil structures: From traditional methods to Machine Learning and Deep Learning applications. *Mechanical Systems and Signal Processing*, *147*, 107077.
66. **Azimi, M., Eslamlou, A.D., & Pekcan, G.** (2020). Data-driven structural health monitoring and damage detection through deep learning: State-of-the-art review. *Sensors*, *20*(10), 2778.
67. **Mousavi, Z., Varahram, S., Ettefagh, M.M., Sadeghi, M.H., & Razavi, S.N.** (2021). Deep neural networks–based damage detection using vibration signals of finite element model and real intact state: An evaluation via a lab-scale offshore jacket structure. *Structural Health Monitoring*, *20*(1), 379–405.
68. **He, Y., Huang, Z., Liu, D., Zhang, L., & Liu, Y.** (2022). A Novel Structural Damage Identification Method Using a Hybrid Deep Learning Framework. *Buildings*, *12*(12), 2130.
69. **Tabatabaeian, A., Jerkovic, B., Harrison, P., Marchiori, E., & Fotouhi, M.** (2023). Barely visible impact damage detection in composite structures using deep learning networks with varying complexities. *Composites Part B: Engineering*, *264*, 110907.
70. **Jiang, G., He, H., Yan, J., & Xie, P.** (2018). Multiscale convolutional neural networks for fault diagnosis of wind turbine gearbox. *IEEE Transactions on Industrial Electronics*, *66*(4), 3196–3207.
71. **Li, X., Zhang, W., & Ding, Q.** (2019). Deep learning-based remaining useful life estimation of bearings using multi-scale feature extraction. *Reliability Engineering & System Safety*, *182*, 208–218.
72. **Liu, B., Gao, Z., Lu, B., Dong, H., & An, Z.** (2022). Deep Learning-Based Remaining Useful Life Estimation of Bearings with Time-Frequency Information. *Sensors*, *22*(19), 7402.
73. **Cao, S., Ouyang, H., & Cheng, L.** (2019). Adaptive damage localization based on locally perturbed dynamic equilibrium and

hierarchical clustering. *Smart Materials and Structures*, *28*(7), 075003.

74. **Xing, C., Ma, L., & Yang, X.** (2016). Stacked denoise autoencoder based feature extraction and classification for hyperspectral images. *Journal of Sensors*, *2016*.
75. **Lee, J., Lee, K.-C., Cho, S., & Sim, S.-H.** (2017). Computer vision-based structural displacement measurement robust to light-induced image degradation for in-service bridges. *Sensors*, *17*(10), 2317.
76. **Pâques, M., Law-Hine, D., Hamedane, O.A., Magnaval, G., & Allezard, N.** (2023). Automatic Multi-label Classification of Bridge Components and Defects Based on Inspection Photographs. *Ce/Papers*, *6*(5), 1080–1086.
77. **Guo, L., Li, N., Jia, F., Lei, Y., & Lin, J**. (2017). A recurrent neural network based health indicator for remaining useful life prediction of bearings. *Neurocomputing*, *240*, 98–109.
78. **Shirazi, M.I., Khatir, S., Benaissa, B., Mirjalili, S., & Wahab, M.A.** (2023). Damage assessment in laminated composite plates using modal Strain Energy and YUKI-ANN algorithm. *Composite Structures*, *303*, 116272.
79. **Dong, C.-Z., & Catbas, F.N.** (2021). A review of computer vision–based structural health monitoring at local and global levels. *Structural Health Monitoring*, *20*(2), 692–743.
80. **Cha, Y., Choi, W., Suh, G., Mahmoudkhani, S., & Büyüköztürk, O.** (2018). Autonomous structural visual inspection using region-based deep learning for detecting multiple damage types. *Computer-Aided Civil and Infrastructure Engineering*, *33*(9), 731–747.
81. **Gopalakrishnan, K., Gholami, H., Vidyadharan, A., Choudhary, A., & Agrawal, A.** (2018). Crack damage detection in unmanned aerial vehicle images of civil infrastructure using pre-trained deep learning model. *Int. J. Traffic Transp. Eng*, *8*(1), 1–14.

Engr. *Muhammad Numan*
Lecturer, University of Sialkot (Postal Code: 51310), Sialkot, Punjab, Pakistan; Numan.zaheer007@gmail.com; Muhammad.numan@uskt.edu.pk; +92-302-7204931

DOI:10.22337/2587-9618-2024-20-1-143-153

FILTRATION AND TEMPERATURE REGIME OF A FROZEN-TYPE SOIL DAM IN THE CRYOLITHOZONE

Nikolay A. Aniskin, Stanislav A. Sergeev, Ilia A. Bokov

National Research Moscow State University of Civil Engineering, Moscow, RUSSIA

Abstract. In this paper, the solution of a joint temperature filtration problem is considered in relation to a soil dam in a cryolithozone. The dam is designed according to one of the principles adopted for the design and construction of structures in such climatic conditions. A description of the methodology used is given. Using the PLAXIS software package, a numerical solution to the problem was obtained, taking into account the phased construction of the structure, repair and reconstruction of the structure caused by the occurrence of an emergency situation after rapid filling of the reservoir. The obtained results of solving the temperature filtration problem revealed problems with ensuring the "frozen" regime of the structure and the need to take additional measures for this.

Keywords: cryolithozone, frozen type dam, temperature filtration problem, numerical solution, finite element method

FUNDING. The research was funded by the National Research Moscow State University of Civil Engineering (grant for fundamental and applied scientific research, project No. 29-392/130).

ФИЛЬТРАЦИОННО-ТЕМПЕРАТУРНЫЙ РЕЖИМ ГРУНТОВОЙ ПЛОТИНЫ МЕРЗЛОГО ТИПА В КРИОЛИТОЗОНЕ

Н.А. Анискин, С.А. Сергеев, И.А. Боков

Национальный исследовательский Московский государственный строительный университет, г. Москва, РОССИЯ

Аннотация. В данной работе рассматривается решение совместной температурно-фильтрационной задачи применительно к грунтовой плотине в условиях криолитозоны. Плотина запроектирована по одному из принципов, принятых для проектирования и строительства сооружений в таких климатических условиях. Дается описание использованной методики. С использованием программного комплекса PLAXIS получено численное решение задачи с учетом поэтапного возведения сооружения, ремонта и реконструкции сооружения, вызванными возникновением аварийной ситуации после быстрого наполнения водохранилища. Полученные результаты решения температурно-фильтрационной задачи выявили проблемы с обеспечение «мерзлого» режима сооружения и необходимости принятия для этого дополнительных мер.

Ключевые слова: криолитозона, плотина «мерзлого» типа, температурно-фильтрационная задача, численное решение, метод конечных элементов

Финансирование. Данная работа была поддержана грантом 2024 года на проведение фундаментальных и прикладных научных исследований (НИР/НИОКР) научными коллективами НИУ МГСУ, проект № 29-392/130.

INTRODUCTION

In this paper, the solution of a joint temperature filtration problem is considered in relation to an soil dam in a cryolithozone. The dam is designed according to one of the principles adopted for the design and construction of structures in such climatic conditions. A description of the methodology used is given. Using the PLAXIS software package, a numerical solution to the problem was obtained, taking into account the phased construction of the structure, repair and reconstruction of the structure caused by the occurrence of an emergency situation after rapid filling of the reservoir. The obtained results of solving the temperature filtration problem revealed problems with ensuring the "frozen" regime of

the structure and the need to take additional measures for this.

The rapid development of the territories of Russia belonging to the cryolithozone caused the need for the construction of hydraulic structures for various purposes in the second half of the twentieth century. Today, hydraulic works for water management, energy, reclamation and environmental purposes in large numbers (more than 1000) have been erected in permafrost territories [1-3]. As a rule, a hydraulic works includes a water support structure in the form of a soil dam and a spillway. The operability of an underground water supply structure in a cryolithozone is largely ensured by its temperature and filtration regime [4]. The practice of designing, erecting and operating such structures made it possible to formulate the basic principles of construction set out in the scientific literature and regulatory documents [4-7]. During the construction of groundwater dams on permafrost soils, two possible principles of the structure are accepted, the choice of which depends on the design and technological features of the dam, engineering and geocrylological conditions and the possibility of purposeful changes in soil properties [4-7].

In accordance with the 1st principle, the soils of the base are preserved in a frozen state during construction and operation, and the thawed soils of the anti-filtration elements of the dam and the base are frozen before operation and filling of the reservoir, when the effect of the filtration flow begins. The frozen state of these soils should be maintained throughout the entire period of operation [4-7]. In the practice of hydraulic engineering, such dams are called "frozen" type dams. In this case, the frozen soil mass of the dam is waterproof and performs the functions of an anti-filtration device that excludes filtration. High antifiltration and strength properties of frozen soils are the basis for ensuring the stability of frozen dams. The frozen state of the dam and foundation soils during operation can be ensured by natural freezing or artificial freezing of soils [4-7].

The second principle assumes that the permafrost soils of the base and the groundwater support structure are in a thawed or thawing state (with their preliminary thawing before the start of construction or with their possible thawing during operation) [4-7]. On the basis of principle 2, "melt" type dams are designed and erected. In this case, an obstacle to the filtration flow is an array of thawed soils – in the form of anti-filtration devices of the dam and the base, as well as part of the bottom prism. It provides filtration in the structure within acceptable limits: filtration flow, gradients and velocities do not exceed the limit values, the stability of the structure is ensured [4-7].

In practice, a soil dam is often a combination of frozen and thawed structures in separate sections of the reservoir [4-7]. The complex temperature and filtration regime of the "ground dam-base" complex should ensure both local and general filtration and static stability of the structure.

When designing groundwater dams in the cryolithozone, the main issue is the forecast of their temperature and humidity regime or their geocrylological condition. It is necessary to ensure a quasi-stable state of the soil structure array, its base and sides, ensuring the stability of the structure as a whole and its filtration efficiency. The complexity of the problem being solved is due to the need to jointly solve several interrelated tasks: temperature, filtration, determination of the stress-strain state and stability of the structure and foundation. In addition, during construction and operation, under the influence of external factors, the condition of the dam and foundation soils changes over time: a part of the soil is undergoing a transition from a thawed state to a frozen one and back. At the same time, the properties of soils change, which must be taken into account in calculations. Design miscalculations caused by errors in accounting for the temperature and filtration state of the structure can lead to an emergency situation up to its destruction [8-11].

In this paper, we consider the solution of a non-stationary joint temperature filtration problem for a soil dam in the permafrost zone. The results of the numerical solution using the PLAXIS software package are presented. An analysis and conclusions are made based on the results obtained and the forecast of the dam condition.

METHODS

The solution of the considered joint temperature-filtration problem for modeling the processes of transition of dam and foundation soils from a frozen state to a thawed state and vice versa is reduced to solving a differential equation that takes into account the processes of heat and mass transfer, taking into account the phase transitions of the soil [12-13].

$$\left(\rho_m c_{pm} + L_w \Theta \frac{\partial \Theta_u}{\partial T}\right)\frac{\partial T}{\partial t} + \rho_w c_{pw} V_x \frac{\partial T}{\partial x} = \lambda_m \left(\frac{\partial^2 T}{\partial x^2} + \frac{\partial^2 T}{\partial y^2}\right) \quad (1)$$

where T is the temperature of the medium; t is time; x, y are the coordinates of the coordinate system; ρ, c_p, λ – are density, heat capacity and thermal conductivity, respectively (the designations of the indices m and w relate to soil and water), V_x is the component of the velocity of the filtration flow, determined by the Darcy formula:

$$V_x = -K\frac{dH}{dx} \quad (2)$$

where K is the coefficient of filtration of the dam or foundation soil, H is the filtration pressure.

The value $L_w\Theta\ (\partial\Theta_u/\partial T)$ on the left side of equation (1) determines the amount of heat released or absorbed as a result of phase transitions of the soil (transition from thawed to frozen state or vice versa).The value L_w is the latent heat of melting ice, Θ is the volume content of water in the pores of the soil, $\partial\Theta_u/\partial T$ is the change in the content of unfrozen water in the pores of the soil when the temperature of the medium changes. Phase transitions occur when the temperature changes in a certain range (approximately from -1 ° C to 0 ° C).

For areas of the computational domain where there is no filtration flow, the differential equation (1) is simplified and can be written as [12]:

$$\rho_m c_{pm}\frac{\partial T}{\partial t} = \lambda_m\left(\frac{\partial^2 T}{\partial x^2} + \frac{\partial^2 T}{\partial y^2}\right) \quad (3)$$

To determine the filtration flow rates included in equation (1), it is necessary to solve the filtration problem, which for the case of water-saturated soils is described by the basic differential equation of filtration theory using known boundary and initial conditions [14-15]:

$$\frac{\partial}{\partial x}\left(K_x\frac{\partial H}{\partial x}\right) + \frac{\partial}{\partial y}\left(K_y\frac{\partial H}{\partial y}\right) - \mu\frac{\partial H}{\partial t} = 0 \quad (4)$$

where $H=f\ (x,\ y,\ t)$ is the desired pressure function in the computational domain, varying in time t; K_x, K_y, are the filtration coefficients in the directions of the coordinate axes X, Y; μ is the coefficient of soil water recovery.

A large number of Russian and foreign researchers have devoted themselves to solving joint temperature and filtration problems, taking into account heat and mass transfer and phase transitions. Analytical methods for solving some particular problems have been used [16-18], and, especially in recent years, numerical methods using the finite difference method [19-20] and the finite element method [21-23].

Temperature and filtration calculations were carried out by the finite element method using the PLAXIS 2D software package. The calculation of filtration in a non-saturated zone is based on models describing the hydraulic behavior of unsaturated soils. When calculating in the PLAXIS 2D PC, one of the most common and proven models was used – the Van Genuchten model [24-25], the main equation of which relates water saturation to pressure as follows:

$$S(\phi_p) = S_{res} + (S_{sat} - S_{res})\left[1 + (g_a|\phi_p|)^{g_n}\right]^{g_c}, \quad (5)$$

where $\phi_p = -\frac{p_w}{\gamma_w}$ and p_w is the pore suction pressure, is the specific gravity of the pore liquid, S_{res} is the residual water saturation, which characterizes the part of the liquid remaining in the pores even with high suction, S_{sat} may be less than one, since the pores may also be occupied by gas, g_a is a parameter characterizing the amount of gas that has penetrated into the soil, g_n is a parameter characterizing the rate of water discharge from the soil, $g_c = \frac{(1-g_n)}{g_n}$ – parameter used in the general Van Genuchten equation.

Further, the paper presents some results of numerical solutions of the joint temperature filtration problem for the considered object.

RESEARCH OBJECT

The object of research in this work is a soil dam as part of a hydroelectric complex that creates a reservoir to provide technical water supply to the facilities of the Srednebotuobinsk oil and gas condensate field. The hydraulic works is located in the Republic of Sakha (Yakutia), 130 km from the city of Mirny. The climate of the area is sharply continental, characterized by long, harsh winters (from October to April) and short summers. The coldest month of the year is January with an average monthly air temperature of minus 29.7°C. On some days, the air temperature can drop to minus 60 °C. The absolute minimum air temperature was recorded in December – minus 59.6 °C. The distribution of average monthly temperatures throughout the year is shown in Table 1.

Table 2.1 Average monthly and annual air temperatures (°C)

Statiom	I	II	III	IV	V	VI	VII	VIII	IX	X	XI	XII	Год
Dorozhniy	-29,7	-26,1	-15,8	-4,7	5,3	14,2	16,9	13,2	5,0	-5,8	-21,1	-29,0	-6,5

The annual course of soil surface temperature is basically similar to the annual course of air temperature. The lowest soil surface temperature is observed in January - February (minus 32.8 °C), the highest in July (21.7 °C).

The earthen bulk dam is designed according to the First principle of construction on an ever-frozen foundation, that is, as a "frozen" type dam. The maximum height of the dam is 14 m with a crest mark of 354 m, the width along the crest is 12 m, the length along the axis of the dam is 628 m, the laying of the upper slope is 1:3.5, the lower slope above the berm is 1:3, the laying of the lower slope below the berm is 1:2.5. The calculated transverse profile of the dam is shown in Figure 1.

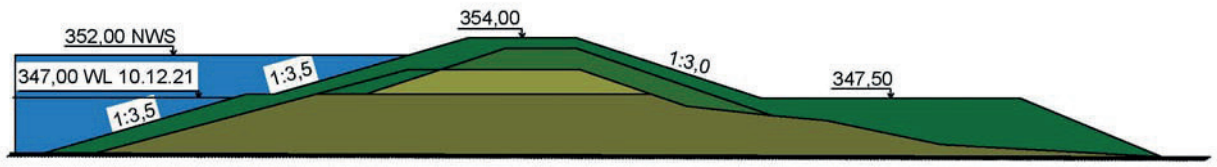

Figure 1. Calculated cross-section of a soil dam

The dam was built according to the project in 2016 and put into operation in 2017. In May 2017, 15 days after the intensive filling of the reservoir, a partial destruction of the dam occurred with the formation of a through hole 5-7 m wide. After the accident, repairs and reconstruction of the structure were carried out. The profile of the dam was increased due to additional filling of the soil. The crest of the dam is reinforced with a filling of rocky soil 0.6 m thick. From the side of the upstream, a layer of coarse-grained rocky soil with a thickness of up to 2.5 m is poured along the upper slope, which performs the function of protecting the dam body from cryogenic cracking, wave and ice effects, increases the stability of the upper slope, and also protects the heaving soils of the dam body from thawing. The side prism on the downstream side is reinforced with rock filling, 0.5 m thick. Additionally, to increase the stability of the lower slope of the dam, a berm is arranged at 346.7 m, with a width of 30.0 m. The profile of the dam before and after reconstruction is shown in Fig. 1.

PROBLEM STATEMENT

Calculations of the predicted temperature and filtration regime of the dam were performed by the finite element method using a PLAXIS 2D PC. The calculated area of one of the sections of the dam (7 in total were considered), broken down into finite elements of a triangular shape, is shown in Fig. 2.

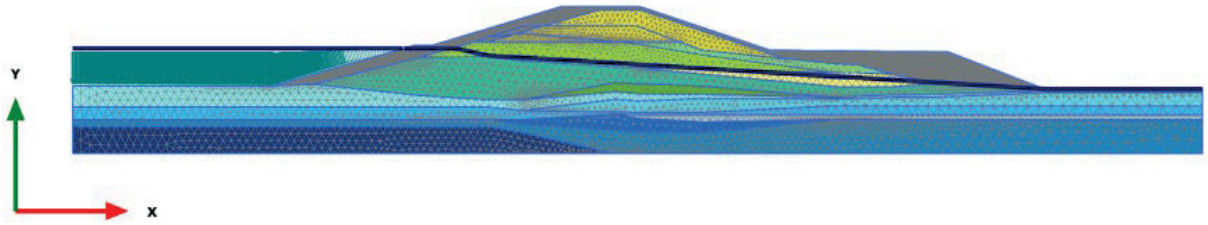

Figure 2. Computational domain of the numerical model

The physical and mechanical characteristics of the soils of the base and body of the existing dam were adopted based on the analysis of materials from engineering and geological surveys performed at the facility.

The depth of the calculated area is assumed to be equal to the depth of penetration of temperatures of an annual amplitude equal to 15 m, obtained on the basis of field observations. The width of the calculated area was selected based on the condition that it had no effect on the calculation results: an increase in the calculated area towards the upper and lower reaches from the dam profile is assumed to be twice the height of the structure.

The boundary conditions for solving the problem were set as follows. For filtration calculations on the lateral surfaces of the base and on the lower boundary of the calculated area, the condition of absence of flow along the normal to these surfaces was set: $\partial H/\partial n=0$, where H is the filtration pressure. The values of the corresponding filtration pressures were set along the surface of the base and part of the upper and lower slopes below the water levels of the upper and lower reaches.

For the non-stationary calculation of the temperature distribution, the corresponding boundary conditions were set in the model. Along the lateral boundaries of the model, a condition is assigned for the absence of heat flow normal to the surface $(\partial T/\partial n=0)$.

The lower boundary is assigned an average annual temperature value at a depth of zero annual amplitudes, equal to -0.75 ° C, taken into account in accordance with field observations at the facility. The conditions of convective heat exchange were set on the upper surface of the base and dam on contact with air, and the water temperature on contact with water. Changes in air temperature at each calculated time were taken in accordance with temperature change graphs (for air - Table 1).

When solving the problem, the process of constructing the initial profile of the dam was modeled with its subsequent reconstruction in accordance with the schedule and the scheme of phased construction.

RESULTS

As a result of calculations of the temperature and humidity regime of the dam-base system, temperature distributions in the calculated region for the corresponding time points were obtained. The time interval from the beginning of the construction of the structure was considered, including the stages of the construction of the initial profile, filling of the reservoir, discharge of the reservoir after an emergency, stages of reconstruction, refilling of the reservoir and the operational period until the end of 2025. Some results are presented in Fig. 3-5.

The temperature field of the ground dam (initial profile) and the base at the time of April 15, 2018 (after the emergency and emptying of the reservoir) is shown in Fig. 3, a. At this point in time, the dam body and base are completely frozen, the temperature ranges from -0.75 °C in the depth of the base to -4.5 °C at the surface foundations and dams.

In July 2018, after filling the reservoir to the UMO mark (347.0 m), the warming effect of water and positive air temperatures affects. This leads to the formation of a through zone of thawed soils along the surface of the calculated area with a depth of up to 2.0-2.5 meters (Fig. 3, b).

In the future, the temperature and humidity regime is formed by the constant warming effect of the reservoir and variable air temperatures throughout the year (Table 1).

Figure 4 shows the results obtained at the time points of January 15 and July 15, 2023 (before the start of reconstruction). It can be noted that the degradation of the frozen zone continues both in the ground dam and in the base under it.

After the completion of the reconstruction of the dam and filling of the reservoir to the NWS (352.0 m) in July 2024, the effect of the warming effect on the slope and the base under the reservoir remains, the depth of the thawed zone increases to 8 m. A through-thawing zone is observed in the body of the dam to a depth below the NWS.

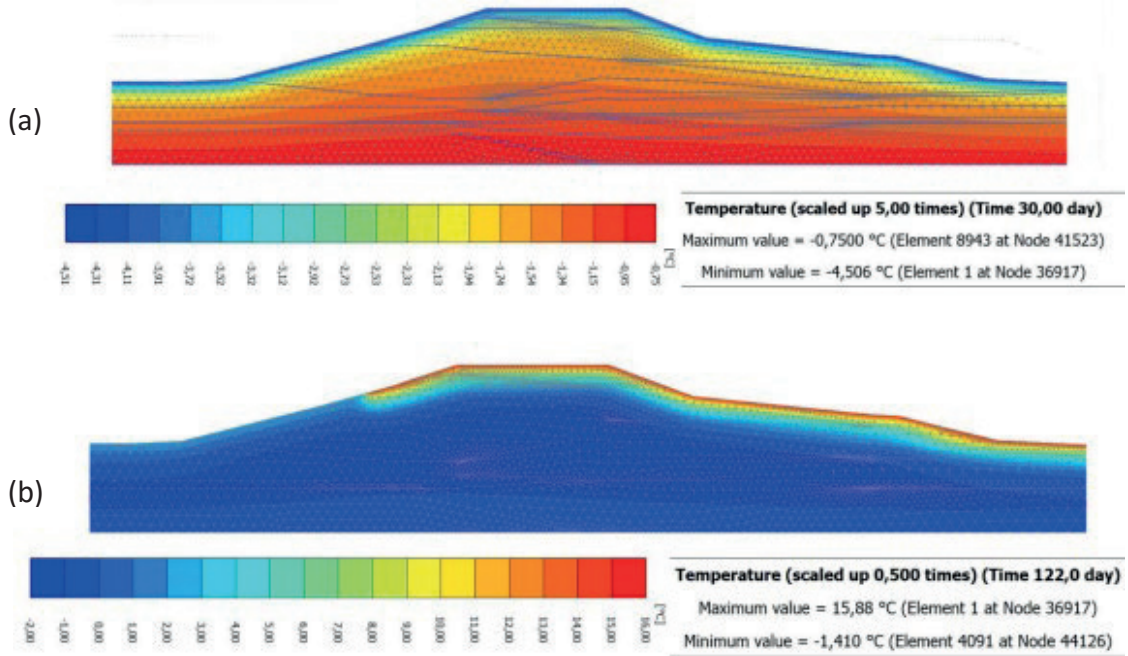

Figure 3. Temperature distribution in an underground dam in 2018: a - on April 15; b – on July 15 (after filling the reservoir to the dead storage level mark)

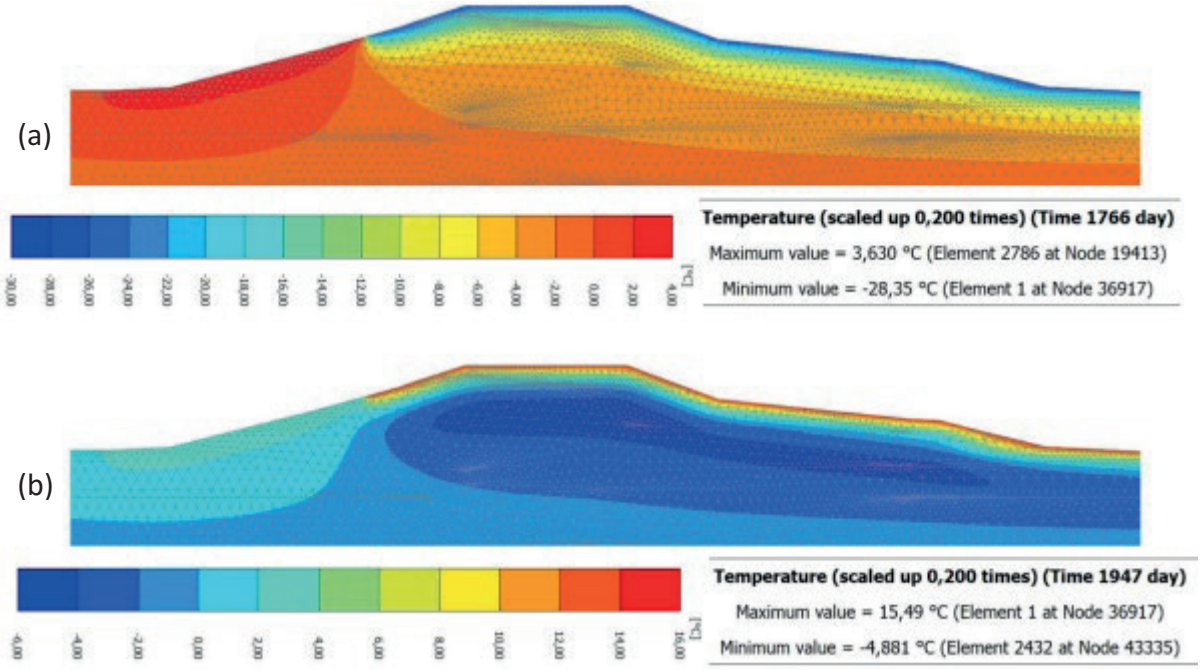

Figure 4. Temperature distribution in a soil dam in 2023: a - on January 15; b – on July 15

A similar picture has been obtained for 2025. If at the time of January 15, 2025 (Fig. 5, a) the frozen zone is restored from the base to the crest of the dam, which ensures the operability of the structure, then on July 15 (Fig. 5, b) in the zone at the crest of the dam, the thawing zone falls below the NWS mark, which violates the principle of operation of the "frozen" dam kind.

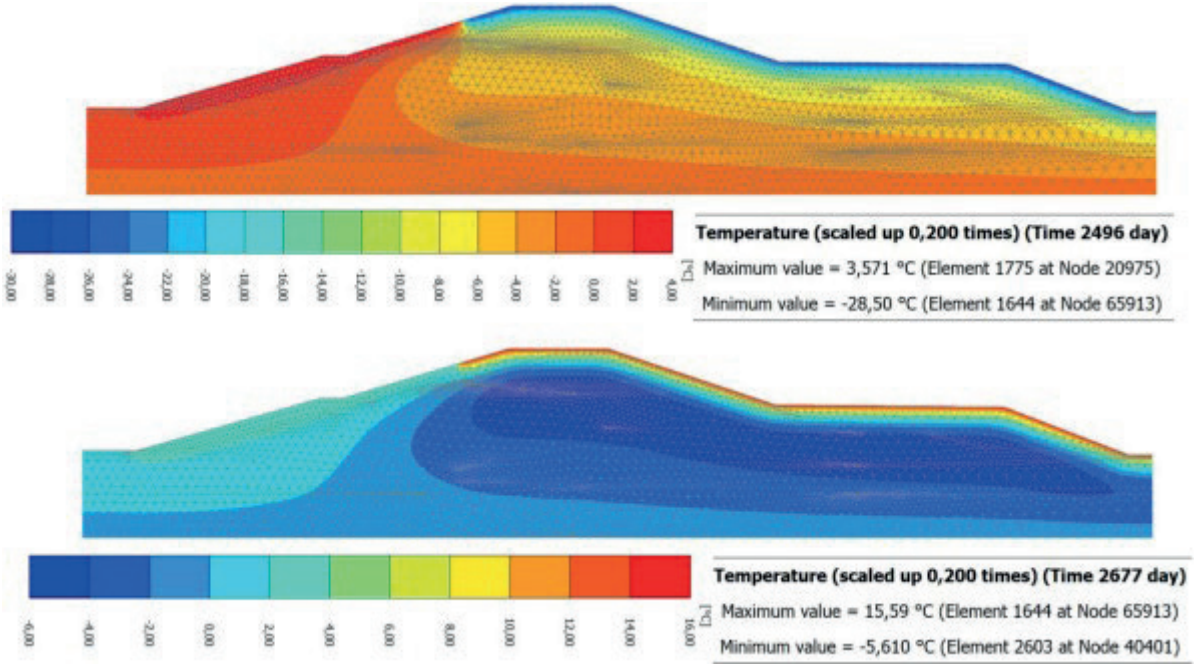

Figure 5. Temperature distribution in a soil dam in 2025: a - on January 15; b – on July 15

In the process of further operation, the situation is likely to worsen.

To ensure the necessary temperature and humidity regime for a "frozen" type dam, it is necessary to consider options for solving the problem. In particular, it is possible to propose an additional outline of the soil in the area near the crest of the dam, or the installation of a permafrost curtain, which will exclude thawing of the zone at the crest of the dam in the summer [26].

CONCLUSIONS

1. In this paper, the PLAXIS 2D software package was used for numerical modeling based on the forecast of the temperature and humidity regime of the soil dam-base system, which allowed taking into account many active factors and influences. This allowed us to get a reliable detailed picture.
2. The calculations took into account non-stationary filtration, which is based on the introduction of time-dependent hydraulic boundary conditions, water levels, non-zero time interval and filtration parameters of soils, as well as the effect of non-stationary heat flow.
3. In the temperature filtration calculation, it was assumed that there is no filtration through frozen soils. The temperature of the beginning of freezing of the soil was taken on the basis of data from engineering and geological surveys.
4. Based on the results of numerical modeling of temperature and filtration calculations, temperature distributions were obtained for the period of commencement of operation (from April 2018 to July 2023) and reconstruction of the dam from July 2023 to July 2025. Based on the results obtained, it can be concluded that a warming effect is observed during the reconstruction and initial operation of the dam from the upstream water and positive air temperatures to the upper slope of the dam and the base of the reservoir, reaching a depth of 8 m after filling the reservoir with water by 2022. and continuing until 2025.
5. The results of numerical modeling of temperature and filtration calculations showed that after filling the reservoir to the dead storage level and NWS marks in the warm season (5 months a year), a thawing zone appears in the dam body below the NWS mark, which makes it possible for water to filter freely through the dam body. Such a temperature-filtration regime is unacceptable when designing and operating a "frozen" type dam.
6. As a recommendation to ensure the necessary temperature and filtration regime, additional soil loading can be proposed in the area close to the crest of the dam, which will increase its thermal insulation, or the installation of a permafrost curtain.

REFERENCES

1. **Biyanov G.F., Kogodovsky O.A., Makarov V.I.** Soil dams on permafrost. Yakutsk: IMZ SO of the USSR Academy of Sciences, 1989. 152 p.
2. **O.B. Andersland and B. Ladanyi.** An Introduction to Frozen Ground Engineering. Chapman & Hall, New York, USA. 1994.
3. **Zhang R.V.** Hydrosystems in the Arctic zone of Russia. Cryosphere of the Earth. 2016;20(4): 79-92
4. **Zhang R.V.** Geocryological principles of operation of groundwater dams in the cryolithozone in a changing climate// Fundamental Research. – 2014. – No. 9-2. – pp. 288-296;
5. **Zhang R.V.** Temperature regime and stability of low-pressure waterworks and groundwater channels in the cryolithozone. Yakutsk: IMZ SB RAS, 2002. – 207 p.
6. SP 25.13330.2020 "SNiP 2.02.04-88 Foundations and foundations on permafrost soils"
7. SP 39.13330.2012 "Dams made of ground materials"
8. **Barabanova S.E**. Cases of damage to hydraulic structures and measures to ensure safety // Hydraulic engineering construction. - 1995. – No. 3. – pp. 24-27.
9. **M. Foster, R. Fell and M. Spannagle.** The statistics of embankment dam failures and

accidents. Canadian Geotechnical Journal, Volume 37, pages 1000-1024, 2000.

10. **Gulyi S.A**. Analysis of the work of a dam that switched from frozen to thawed type of operation (on the example of the ArGRES dam) on the Myaunje River // Problems of engineering permafrost: proceedings of the IX International Symposium (Mirny, Russia, September 3-7, 2011). – Yakutsk: Publishing House URAN IMZ SB RAS, 2011. – S. 238 – 242.
11. **Olovin B.A. Medvedev B.A.** Dynamics of the temperature field of the Vilyuyskaya HPP dam. Novosibirsk: Nauka, 1980. 48 p.
12. **Goldin A.L., Rasskazov L.N.** Design of ground dams. M.; Publishing House of the DIA, 2001.
13. **Sobol S.V., Februlev A.V.** Temperature regime of filtering taliks at the base of the hydroelectric complex and the shores of the reservoir. News of universities. Construction, 1992.- No.5-6, pp. 106-110.
14. **Polubarinova-Kochina P.Ya.** Theory of groundwater movement. State Publishing House of Technical and Theoretical Literature, Moscow, 1952.
15. Development of research on the theory of filtration in the USSR // Institute of Hydrodynamics of the SB Academy of Sciences of the USSR, VNIIG named after B.E.Vedeneev. Research Institute of Natural Gases. M. “Science".
16. **V.I. Vasiliev, Yu.G. Danilov, I.S. Eremeev, V.V. Popov, G.G. Tsypkin, Yu. Song, Zhao Yendong** Comparison of mathematical models of heat and mass transfer in soils.- NEFU BULLETIN, 2013, volume 10, No. 4, pp. 5-10
17. **Krylov D.A.** Mathematical modeling of temperature fields taking into account phase transitions in the cryolithozone.- Science and Education: Electronic Scientific Publication, Bauman Moscow State Technical University, El no. FS 77 - 48211. ISSN 1994-0408, http://technomag.edu.ru/doc/354740.html
18. **Alexey A. Korshunov. and Sergey P. Doroshenko. and Alexander L. Nevzorov** The Impact of Freezing-thawing Process on Slope Stability of Earth Structure in Cold Climate.- Advances in Transportation Geotechnics 3 . The 3rd International Conference on Transportation Geotechnics (ICTG 2016) Volume 143, 2016, Pages 682–688
19. **Gorokhov E.N., Fevralev A.V.** Calculation of the heat-filtration regime of the interface of earthen and concrete structures of the type “HPP-earth dam” or “spillway-earth dam”. Energeticheskoe stroi tel'stvo. 1984;(11):45-47
20. **E.N. Gorokhov, I.S. Sobol, V.I. Loginov, E.A. Gnetov** A virtual model of the temperature-cryogenic regime of the base and subsidence of the reservoir bed in the cryolithozone / // Privolzhsky Scientific Journal / Nizhegorod. gosudarstvenny architectury-builds. un-T. – Nizhny Novgorod, 2013. – No. 4. – pp. 39-49.
21. **Lai Yuanming, Liu Songyu, U Ziwang, Wu Yaping, G & Konrad, J.M**. (2002) Numerical simulation for the coupled problem of temperature and seepage fields in cold region dams. J. Hydraul. Res. 40(5), 631–635.
22. **A. Kamanbedast and A. Delvari** Analysis of Earth Dam: Seepage and Stability Using Ansys and Geo-Studio Software.- World Applied Sciences Journal 17 (9): 1087-1094, 2012 ISSN 1818-4952
23. **Trapeznikov A., Becker A., Isaeva E., Tsimbelman N., Chernova T.** Numerical modeling of the thermal regime of the frozen-type embankment dam of the Anadyr hydrosystem. FEFU: School of Engineering Bulletin. 2022 ;(50):81-93. (In Russ.). https://doi.org/10.24866/2227-6858/2022-1/81-93
24. **Van Genuchten, M.Th.** 1980. A closed form equation for predicting the hydraulic conductivity of unsaturated soils. Soil Sci. Soc. Am. J. 44:892-989.
25. **Mualem, Y.** A new model for predicting the hydraulic conductivity of unsaturated porous media. Water Resour. Res. 1976; 12(3), Pp. 513–522. DOI: 10.1029/WR012i003p00513

26. **N. Aniskin, A. Antonov** Simulation model of thermal-seepage regime of thawing dams with permafrost curtain// IOP Conf. Series: Journal of Physics: Conf. Series 1425 (2020) 012076. doi:10.1088/1742-6596/1425/1/012076

СПИСОК ЛИТЕРАТУРЫ

1. **Биянов Г.Ф., Когодовский О.А., Макаров В.И.** Грунтовые плотины на вечной мерзлоте. – Якутск: ИМЗ СО АН СССР, 1989. – 152 с.
2. **O.B. Andersland and B. Ladanyi.** An Introduction to Frozen Ground Engineering. Chapman & Hall, New York, USA. 1994.
3. **Zhang R.V.** Hydrosystems in the Arctic zone of Russia. Cryosphere of the Earth. 2016; 20(4): 79-92
4. **Чжан Р.В.** Геокриологические принципы работы грунтовых плотин в криолитозоне в условиях меняющегося климата// Фундаментальные исследования. – 2014. – № 9-2. – С. 288-296; URL: http://www.fundamental-research.ru/ru/article/view?id=34841 (дата обращения: 19.10.2016).
5. **Чжан Р.В.** Температурный режим и устойчивость низконапорных гидроузлов и грунтовых каналов в криолитозоне. Якутск: ИМЗ СО РАН, 2002. – 207 с.
6. СП 25.13330.2020 «СНиП 2.02.04-88 Основания и фундаменты на вечномерзлых грунтах»
7. СП 39.13330.2012 «Плотины из грунтовых материалов»
8. **Барабанова С.Е**. Случаи повреждений гидротехнических сооружений и меры по обеспечению безопасности // Гидротехническое строительство. – 1995. – № 3. – С. 24–27.
9. **M. Foster, R. Fell and M. Spannagle**. The statistics of embankment dam failures and accidents. Canadian Geotechnical Journal, Volume 37, pages 1000-1024, 2000.
10. **Гулый С.А.** Анализ работы плотины, перешедшей с мерзлого на талый тип эксплуатации (на примере плотины АрГРЭС) на р. Мяундже // Проблемы инженерного мерзлотоведения: материалы IX Международного симпозиума (г. Мирный, Россия, 3-7 сентября 2011г.). – Якутск: Изд-во УРАН ИМЗ СО РАН, 2011. – С. 238 – 242.
11. **Оловин Б.А. Медведев Б.А.** Динамика температурного поля плотины Вилюйской ГЭС. – Новосибирск: Наука, 1980. – 48 с.
12. **Гольдин А.Л., Рассказов Л.Н.** Проектирование грунтовых плотин. М.; Изд. АСВ, 2001.
13. **Соболь С.В., Февралев А.В.** Температурный режим фильтрующих таликов в основании гидроузла и берегах водохранилища. Известия ВУЗов. Строительство, 1992.- №5-6, с. 106-110.
14. **Полубаринова-Кочина П.Я.** Теория движения грунтовых вод. Гос. Издательство технико-теоретической литературы, М., 1952.
15. Развитие исследований по теории фильтрации в СССР // Институт гидродинамики СО АН СССР, ВНИИГ им. Б.Е.Веденеева. ВНИИ Природных газов. М. “Наука”.
16. **В.И. Васильев, Ю.Г. Данилов, И.С. Еремеев, В.В. Попов, Г.Г. Цыпкин, Юйжуй Сун, Чжао Яндун** Сравнение математических моделей тепломассо-переноса в почвогрунтах.- ВЕСТНИК СВФУ, 2013, том 10, № 4, с. 5-10
17. **Крылов Д.А.** Математическое моделирование температурных полей с учетом фазовых переходов в криолитозоне.- Наука и образование: Электронное научное издание, ФГБОУ ВПО «МГТУ им. Н.Э.Баумана, Эл № ФС 77 - 48211. ISSN 1994-0408, http://technomag.edu.ru/doc/354740.html
18. **Alexey A. Korshunov. and Sergey P. Doroshenko. and Alexander L. Nevzorov** The Impact of Freezing-thawing Process on Slope Stability of Earth Structure in Cold Climate.- Advances in Transportation Geotechnics 3 . The 3rd International

Conference on Transportation Geotechnics (ICTG 2016) Volume 143, 2016, Pages 682–688
19. **Gorokhov E.N., Fevralev A.V.** Calculation of the heat-filtration regime of the interface of earthen and concrete structures of the type “HPP-earth dam” or “spillway-earth dam”. Energeticheskoe stroi tel'stvo. 1984;(11):45-47
20. **Е.Н. Горохов, И.С. Соболь, В.И. Логинов, Е.А. Гнетов** Виртуальная модель температурно-криогенного режима основания и оседания ложа водохранилища в криолитозоне / // Приволжский научный журнал / Нижегор. гос. архитектур.-строит. ун-т. – Нижний Новгород, 2013. – № 4. – С. 39-49.
21. **Lai Yuanming, Liu Songyu, U Ziwang, Wu Yaping, G & Konrad, J.M.** (2002) Numerical simulation for the coupled problem of temperature and seepage fields in cold region dams. J. Hydraul. Res. 40(5), 631–635.
22. **A. Kamanbedast and A. Delvari** Analysis of Earth Dam: Seepage and Stability Using Ansys and Geo-Studio Software.- World Applied Sciences Journal 17 (9): 1087-1094, 2012 ISSN 1818-4952
23. **Trapeznikov A., Becker A., Isaeva E., Tsimbelman N., Chernova T.** Numerical modeling of the thermal regime of the frozen-type embankment dam of the Anadyr hydrosystem. FEFU: School of Engineering Bulletin. 2022 ;(50):81-93. (In Russ.). https://doi.org/10.24866/2227-6858/2022-1/81-93
24. **Van Genuchten,** M.Th. 1980. A closed form equation for predicting the hydraulic conductivity of unsaturated soils. Soil Sci. Soc. Am. J. 44:892-989.
25. **Mualem, Y.** A new model for predicting the hydraulic conductivity of unsaturated porous media. Water Resour. Res. 1976; 12(3), Pp. 513–522. DOI: 10.1029/WR012i003p00513
26. **N. Aniskin, A. Antonov** Simulation model of thermal-seepage regime of thawing dams with permafrost curtain// IOP Conf. Series: Journal of Physics: Conf. Series 1425 (2020) 012076. doi:10.1088/1742-6596/1425/1/012076

Aniskin Nikolay Alexeyevich, Professor, DSc, Acting Director of the Institute of Hydrotechnical and Power Engineering (IGES) of the National Research Moscow State University of Civil Engineering (NRU MGSU), 129337, Russia, Moscow, Yaroslavskoe shosse, 26, phone +7 (495) -287-49-14 ext. 14-19, e-mail: Aniskin@mgsu.ru

Sergeev Stanislav Alexeyevich, PhD, Associate Professor of the Department of Hydraulics and Hydraulic Engineering, Researcher at the Scientific and Educational Center "Geotechnics" of the National Research Moscow State University of Civil Engineering (NRU MGSU), 129337, Russia, Moscow, Yaroslavskoe shosse, 26, phone +7 (495) -287-49-14 ext. 14-19, e-mail: SergeevSA@mgsu.ru

Bokov Ilia Alexeyevich, student of the Institute of Hydrotechnical and Power Engineering (IGES) of the National Research Moscow State University of Civil Engineering (NRU MGSU), 129337, Russia, Moscow, Yaroslavskoe shosse, 26, phone +7 (495) -287-49-14 ext. 14-19, e-mail: ibokov111111@gmail.com

Анискин Николай Алексеевич, профессор, доктор технических наук, исполняющий обязанности директора Института гидротехнического и энергетического строительства (ИГЭС) Национального исследовательского Московского государственного строительного университета (НИУ МГСУ), 129337, г. Москва, Ярославское ш., д. 26, тел. +7 (495)-287-49-14 доб.14-19. e-mail: Aniskin@mgsu.ru

Сергеев Станислав Алексеевич, кандидат технических наук, доцент кафедры «Гидравлики и гидротехнического строительства», научный сотрудник Научно-образовательного центра «Геотехника» Национального исследовательского Московского государственного строительного университета (НИУ МГСУ) 129337, г. Москва, Ярославское ш., д. 26, тел. +7 (495)-287-49-14 доб.14-19 e-mail: SergeevSA@mgsu.ru

Боков Илья Алексеевич, студент Института гидротехнического и энергетического строительства (ИГЭС) Национального исследовательского Московского государственного строительного университета (НИУ МГСУ), 129337, г. Москва, Ярославское ш., д. 26, тел. +7 (495)-287-49-14 доб.14-19. e-mail: ibokov111111@gmail.com

International Journal for Computational Civil and Structural Engineering, 20(1) 154–161(2024)

DOI:10.22337/2587-9618-2024-20-1-154-161

TAKING INTO ACCOUNT MOISTURE IN INCREASING THE ACCURACY OF CALCULATING HEAT LOSSES OF A BUILDING

Kirill P. Zubarev

National Research Moscow State University of Civil Engineering, Moscow, RUSSIA
Research Institute of Building Physics of Russian Academy of Architecture and Construction Sciences, Moscow, RUSSIA
RUDN University, Moscow, RUSSIA

Abstract: A discrete-continuous approach was applied to the moisture transfer equation, which made it possible to obtain an analytical solution for the moisture potential. The new method was applied to study the unsteady-state moisture regime of the facade heat-insulating composite system with expanded polystyrene insulation and aerated concrete base. It was found that the mass moisture content of building materials achieved in the walls during the period of operation is lower than the mass moisture content used in construction regulations, which makes it possible to increase the accuracy of calculating the transmission heat losses of the building. Calculations of heat losses of a two-storey building in the climatic conditions of Moscow (Russia) showed a decrease in the heating system load by 5 %, and the reduction in heat losses for specific premises of the building ranged from 3.6 to 7 %.

Keywords: building envelope, effect of moisture on thermal conductivity, heat and moisture transfer, mathematical model, discrete-continuous approach

УЧЕТ ВЛАЖНОСТИ В ПОВЫШЕНИИ ТОЧНОСТИ РАСЧЕТА ТЕПЛОВЫХ ПОТЕРЬ ЗДАНИЯ

К.П. Зубарев

Национальный исследовательский Московский государственный строительный университет, г. Москва, РОССИЯ
Научно-исследовательский институт строительной физики Российской академии архитектуры и строительных наук, г. Москва, РОССИЯ
Российский университет дружбы народов, г. Москва, РОССИЯ

Аннотация: К уравнению влагопереноса применен дискретно-континуальный подход, позволивший получить аналитическое решение для потенциала влажности. Новый метод был применен для исследования нестационарного влажностного режима системы фасадной теплоизоляционной композиционной с утеплителем из пенополистирола и основанием из газобетона. Было получено, что массовая влажность строительных материалов, достигаемая в стенах за период эксплуатации ниже массовой влажности, используемой в нормативных документах по строительству, что дает возможность повысить точность расчета трансмиссионных тепловых потерь здания. Расчеты тепловых потерь двухэтажного здания в климатических условиях г. Москвы (Россия) показали снижение нагрузки на систему отопления на 5 %, а для конкретных помещений здания снижения тепловых потерь составило от 3.6 до 7 %.

Ключевые слова: ограждающая конструкция здания, влияние влаги на теплопроводность, тепло- и влагоперенос, математическая модель, дискретно-континуальный подход

1. INTRODUCTION

1.1. The role of moisture in construction

The moisture regime of building envelopes is a highly sophisticated scientific problem in construction. Research on distribution of moisture over the thickness of fences has a huge applied relevance [1]. From a medical point of view, wet building material is a breeding ground for bacteria, which can cause various human diseases, such as asthma and allergy. A change in moisture content of a building material directly affects its

thermal conductivity and the heat-shielding shell of the building. Errors in assessing moisture state of building fences can lead to condensation and mold on the internal surfaces of building envelopes, as well as waterlogging of the wall material, which is directly related to the durability of the building [2,3].

1.2. Influence of moisture on heat losses of a building

It is a common knowledge that moisture content rise of a building material causes an increase in its thermal conductivity, which negatively affects thermal protection of buildings [4–7].

The dependence of thermal conductivity on moisture is described by the formula [4–7]:

$$\lambda_w = \lambda_0 + w \cdot \Delta\lambda_w. \quad (1)$$

where λ_w is a coefficient of thermal conductivity of the material at moisture w, W/(m·ºC); w is mass moisture content of the material, kg/kg; λ_0 is a thermal conductivity coefficient of dry material, W/(m·ºC); $\Delta\lambda_w$ is change in the thermal conductivity of the material when its mass moisture changes by 1 %, W/(m·ºC ·%).

There is a variety of methods for calculating the heat loss of a building.

In the general case, heat losses of the building premises are a sum of transmission and infiltration heat losses:

$$Q = Q_{tr} + Q_{inf}. \quad (2)$$

where Q is total heat loss of the building premise, W; Q_{tr} are transmission heat losses of the building premise, W; Q_{inf} is infiltration heat loss of the building premise, W.

Transmission heat losses through a certain enclosing structure are estimated using the following expression [4–7]:

$$Q_{tr} = k \cdot F \cdot \Delta t \cdot n \cdot (1 + \sum \beta). \quad (3)$$

where k is a heat transfer coefficient, W/(m^2·ºC); F is a heat transfer surface area, m^2; Δt is a temperature difference on different sides of the building envelope ºC; n is a coefficient that depends on the position of the building envelope in relation to the outer air, ºC; β are additional heat losses that are dependent on the orientation of the building envelope over the cardinal points.

The heat transfer coefficient in equation (3) is the reciprocal of the reduced resistance to heat transfer [4–7]:

$$k = \frac{1}{R_{act}}. \quad (4)$$

where R_{act} is reduced heat transfer resistance, m^2·ºC/(W).

The reduced resistance to heat transfer of the enclosing structure of the building wall is calculated with the formula [4–7]:

$$R_{act} = \frac{1}{\frac{1}{R_{con}} + \sum l_j \cdot \psi_j + \sum n_k \cdot \chi_k}. \quad (5)$$

where R_{con} is conditional heat transfer resistance, (m^2·ºC)/W; $l_j \cdot \psi_j$ are specific heat losses through a linear thermal inhomogeneity of the j-th type, W/(m^2·ºC); $n_k \cdot \chi_k$ are specific heat losses through point thermal inhomogeneity of the k-th type, W/(m^2·ºC).

Conditional resistance of heat transfer for the outer wall of the building is determined by the formula [4–7].:

$$R_{con} = \frac{1}{\frac{1}{\alpha_{in}} + \sum \frac{\delta_i}{\lambda_i} + \frac{1}{\alpha_{ext}}}. \quad (6)$$

where α_{in} is a coefficient of heat transfer between outer air and the outer surface of the wall, (m²·ºC)/W; α_{ext} is a coefficient of heat transfer between the indoor air of the room and the inner surface of the wall, (m²·ºC)/W; δ_i is the thickness of i-th material of the wall, m; λ_i is a coefficient of thermal conductivity of the i-th material of the wall, W/(m·ºC).

So, an increment of the calculation accuracy of mass moisture content w in the building wall will make the thermal conductivity coefficients of building materials by equation (1) more precise, which according to equations (2)-(6) will refine the heat loss of the building.

2. THE PROBLEM

Assessment of the impact of the building material operational humidity determined using the proposed method on the heat losses of the building.

3. MATERIALS AND METHODS

The mathematical model for the joint moisture transfer of vaporous and liquid moisture was proposed by V.G. Gagarin and V.V. Kozlov. V.G. Gagarin derived a necessary and sufficient condition for the potentiality of a vector field during the water vapor and liquid transfer, which thereafter allowed V.G. Gagarin and V.V. Kozlov to develop a formula for the moisture potential F [8]:

$$F(w,t) = E_t(t)\cdot\varphi(w) + \frac{1}{\mu}\int_0^w \beta(\zeta)\,d\zeta. \qquad (7)$$

where F is moisture potential, Pa; E_t is saturated water vapor pressure, Pa; φ is relative air humidity, %; μ is vapor permeability coefficient, *kg/(m·s·Pa)*; β is moisture conductivity coefficient, kg/(m · s · kg/kg), which depends on moisture, t is temperature, $^{\circ}C$; w is material moisture , % by weight (1 kg/kg = 100 % by weight).

Moisture transfer differential equation based on the moisture potential F can be formulated as:

$$\frac{\partial F(w,t)}{\partial \tau} = \left(\frac{1}{\mu}\beta(w) + \frac{\partial\varphi(w)}{\partial w}E_t(t)\right)\frac{\mu}{\gamma_0}\frac{\partial^2 F(w,t)}{\partial x^2}. \qquad (8)$$

The equation (7) can be solved in the following form using discrete-continuous approach [9–11]:

$$\overline{F} = p\cdot\left(\left(E_t\cdot A\right)^{-2}\cdot e^{E_t\cdot A\cdot\tau} - \tau\cdot\left(E_t\cdot A\right)^{-1} - \left(E_t\cdot A\right)^{-2}\right)\cdot \cdot \overline{L} + \left(E_t\cdot A\right)^{-1}\left(e^{E_t\cdot A\cdot\tau} - E\right)\cdot\overline{B} + e^{E_t\cdot A\cdot\tau}\cdot\overline{F}_0. \qquad (9)$$

4. RESULTS AND DISCUSSION

4.1. Application of a discrete-continuous approach to assess the unsteady-state moisture regime of a facade heat-insulating composite system with external plaster layers

The developed method for assessing the unsteady-state moisture regime was applied to study the facade heat-insulating composite system with external plaster layers with a 300 mm thick aerated concrete base and 120 mm thick expanded polystyrene insulation built in Moscow.

The change in the mass humidity of the building envelope along the wall thickness is presented (Figure 1).

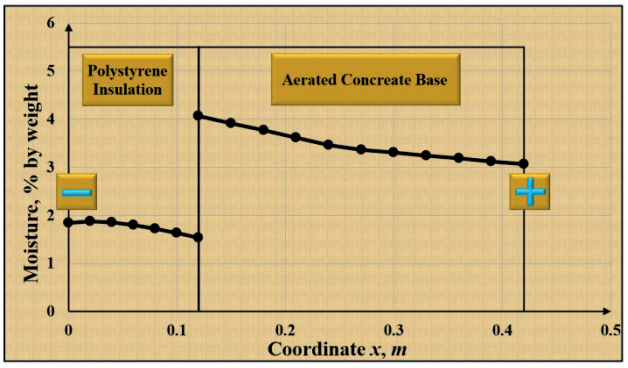

Figure 1. Change in the mass moisture content of the building envelope across the wall thickness

The change in the humidity of the insulation layer during the year was obtained according to the proposed method for assessing the unsteady-state moisture regime (Figure 2).

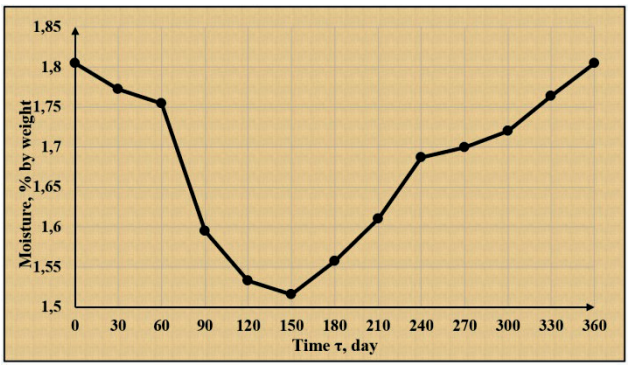

Figure 2. Change in the moisture of the insulation layer during the year according to the proposed method for assessing the unsteady-state moisture regime

As a result of the research, it was discovered that maximum moisture for the facade heat-insulating composite system with aerated concrete base and expanded polystyrene insulation will be observed at the beginning of January (Figure 2), which corresponds to the maximum temperature difference on different sides of the fence. This result is explained by the low inertia of the insulation layer. Consequently, it was discovered that for facade heat-insulating composite systems, the period of maximum moisture differs from the period of maximum moisture for enclosing structures that do not contain insulation.

4.2. Comparison of the operational moisture of the building wall obtained using the discrete-continuous approach with standard values

To evaluate the effect of the proposed method, the operating humidity was compared according to the proposed method for assessing the unsteady-state moisture regime with the values given in the official regulatory document Set of Rules 50.13330.2012 "Thermal protection of buildings" (Russian regulatory document).

The construction of the wall illustrated in Figure 1 was taken for the study.

Comparison of the operational moisture of a building wall with a base made of aerated concrete (aerated concrete layer thickness 0.3 m) and expanded polystyrene insulation (insulation layer thickness 0.12 m) obtained using the proposed calculation method based on a discrete-continuous approach with standard values (Table 1) was carried out.

As we can see from Table 1, the actual values of the operating moisture content of building materials obtained by the proposed formula are significantly lower than the moisture content of building materials taken according to the standards. According to the formula (1), a decrease in the mass moisture content of building material leads to a decrease in its thermal conductivity. Thus, it gives a possibility to save energy when determining the exact amount of mass moisture in the building envelope materials by taking into account the refined thermal conductivity coefficient.

Table 1. Comparison of the operational humidity of a building wall with aerated concrete base and expanded polystyrene insulation obtained using the proposed calculation method based on a discrete-continuous approach with standard values

Material	Regulatory values for operating humidity, % by weight	The result of calculating the unsteady-state moisture regime according to the proposed formula (9), % by weight
Aerated concrete	12.0	3.4
Expanded polystyrene	10.0	1.8

4.3. Increasing energy savings by improving the calculation accuracy of heat losses of a building

To assess the reduction of heat losses in the building envelope, two calculations of heat losses were made for a two-storey cottage building in Moscow (Russia). The first calculation was carried out at standard values of humidity, whereas the second one was carried

out in agreement with the calculated values that were obtained during the modeling of the non-stationary state of the enclosing structure of the building wall (Table 1).
The temperature of the coldest five-day period was set as the outside temperature according to the climatological data of the construction area.

Comparison of the composition of the transmission heat losses of the wall of a cottage house building according to the standard values and according to the proposed method for defining the unsteady-state moisture regime with the aid a discrete-continuous approach is presented (Figure 3).

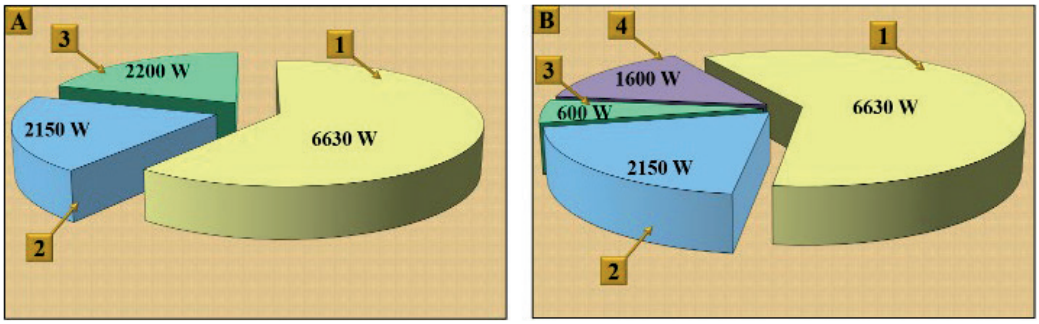

Figure 3. Comparison of the transmission heat losses composition of the wall of the cottage house building: A – distribution of heat losses in the wall obtained in the calculation at the moisture content of materials taken according to the standard values; B – distribution of heat losses in the wall that were obtained when making calculations at the values of the moisture content of materials determinated from the results of the assessment of the unsteady-state moisture regime (1 – heat losses of the wall along the surface of the wall through dry material; 2 – heat losses of the wall through heat engineering inhomogeneities; 3 – heat losses of the wall due to moisture; 4 – energy saving achieved by taking into account the unsteady-state moisture regime)

As may be inferred from Figure 3, taking into account the unsteady-state moisture regime led to energy savings of 1600 W due to a decrease in transmission heat losses.
Transmission heat losses through building walls are not the only source of building heat losses. In order to estimate the overall reduction of heat losses in the total costs of the building for heating and ventilation, it is also essential to determine the transmission heat losses through the floor, ceiling, windows and doors of the building as well as heat losses for heating the infiltrated air.
The comparison of the results of the calculations of heat losses at the moisture content of the building wall materials taken according to standard values as well as at the moisture content of the building wall materials gained from the results of the assessment of the unsteady-state moisture regime using the proposed method is presented (Table 2).

Table 2. Comparison of the results of heat loss calculations at the moisture content of the building wall materials taken according to standard values as well as at the moisture content of the building wall materials gained from the results of the assessment of the unsteady-state moisture regime using the given method is presented

Building envelopes	Heat loss according to the standard humidity values, *W*	Heat loss according to the calculated humidity values, *W*
Walls	10980	9380
Windows	8470	8470
Roof coating	3030	3030
Doors	1070	1070
Floor	1405	1405
Infiltration	6075	6075
Total heat losses	31030	29430

Thus, for the building under consideration, energy saving when calculating heat losses by taking into account the unsteady-state moisture regime of the building wall using the method for calculating the unsteady-state moisture regime suggested in this article is 1600 W (5%).

To illustrate the reduction of heat losses in each separate room, a plan of the second floor of a two-storey cottage house is presented with heat losses calculated at the temperature of the coldest period of five days (figure 4).

As can be noticed from Figure 4, the reduction of heat losses of the building is large for each room and can be presented as a table 3.

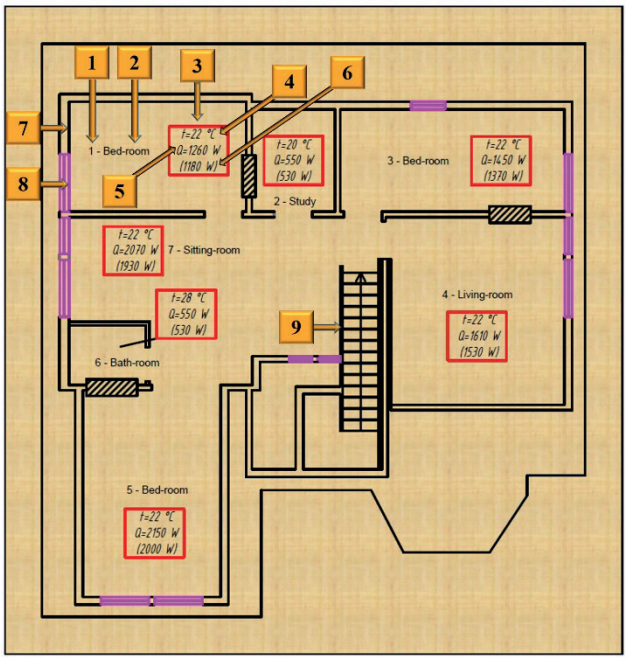

Figure 4. Plan of the second floor of a two-storey cottage house with heat losses calculated at the temperature of the coldest period of five days (1 – room number; 2 – purpose of the room; 3 – table with parameters of the room; 4 – indoor air temperature in the room during cold season (winter); 5 – heat loss of the room determined at the normative humidity of the building materials of the wall; 6 – heat losses of the room at the moisture content of the building materials of the wall determined by the calculation of the unsteady-state moisture regime; 7 – the outer wall of the building; 8 – the window of the building; 9 – stairs)

Table 3. Reduction of heat losses due to the assessment of the unsteady-state moisture regime by the suggested method

No.	Room name	Heat loss according to the standard humidity values, *W*	Heat loss according to the calculated humidity values, *W*	Percentage of heat loss reduction, %
1	Bedroom	1260	1180	6.3
2	Study	550	530	3.6
3	Bedroom	1450	1370	5.5
4	Living-room	1610	1530	5.0
5	Bedroom	2150	2000	7.0
6	Bathroom	550	530	3.6
7	Sitting-room	2070	1930	6.8

As is obvious from Table 3, the actual heat losses obtained during the modelling are from 3.6 to 7.0 % less than those calculated for different rooms from, which is significant when projecting buildings.

5. CONCLUSIONS

The assessment of the unsteady-state moisture regime made allows us to make a conclusion that moisture content in the thickness of the building envelope materials is lower than is accepted according to regulatory documents. The energy saving of the building was assessed by applying the proposed methodology by calculating heat losses of the building. Comparative calculations for the studied two-storey building showed a total reduction of the building's heat demand for heating and ventilation in the amount of 5 %. At once, the reduction of heat loss can reach from 3.6 to 7 % depending on the room.

REFERENCES

1. **Zaborova D., Musorina T.** Environmental and energy-efficiency considerations for selecting building envelopes //

Sustainability. 2022, Vol. 14, No. 10. P. 5914.
2. **Kotlyarova E.** Improving the methodology for assessing the level of environmental safety of urban areas as the basis of their life cycle // E3S Web of Conferences, 2023, Vol. 389, No. 09062.
3. **Kotlyarova E.** Basic Scientific Principles of Improving the Methodology for the Assessment of the Level of Environmental Safety of Urbanized Territories // AIP Conference Proceedings, 2023, Vol. 2560, No. 020010.
4. **Gamayunova O., Gumerova E., Miloradova N.** Smart glass as the method of improving the energy efficiency of high-rise buildings // E3S Web of Conferences, 2018, Vol. 33, No. 02046.
5. **Gamayunova O., Radaev A., Petrichenko M., Shushunova N.** Energy audit and energy efficiency of modular military towns // E3S Web of Conferences, 2019, Vol. 110, No. 01088.
6. **Zaborova D., Vieira G., Musorina T., Butyrin A.** Experimental study of thermal stability of building materials // Advances in Intelligent Systems and Computing. Cham, 2018, Vol. 692 pp. 482-489.
7. **Vieira G.B., Petrichenko M.R., Musorina T.A., Zaborova D.D.** Behavior of a hollowed-wood ventilated façade during temperature changes // Magazine of Civil Engineering, 2018, Vol. 79, No. 3, pp. 103-111.
8. **Gagarin V.G., Kozlov V.V., Zubarev K.P.** Determination of maximum moisture zone on enclosing structures. // Cold Climate HVAC 2018: Sustainable Buildings in Cold Climates, 2019, pp. 925-932.
9. **Zubarev K.P.** Derivation of the equation of unsteady-state moisture behaviour in the enclosing structures of buildings using a discrete-continuous approach // International Journal for Computational Civil and Structural Engineering, 2021, Vol. 17, No. 4, – pp. 83-90.
10. **Sidorov V.N. Matskevich S.M.** Discrete-analytical solution of the unsteady-state heat conduction transfer problem based on the finite element method. // IDT 2016 - Proceedings of the International Conference on Information and Digital Technologies 2016. 2016, pp. 241-244.
11. **Zolotov A.B., Mozgaleva M.L., Akimov P.A., Sidorov V.N.** Ob odnom diskretno-kontinualnom podkhode k resheniyu odnomernoy zadachi teploprovodnosti [About one discrete-continual method of solution of one-dimensional heat conductivity problem]. // Academia. Architecture and Construction (Academia. Arkhitektura i stroitelstvo), Iss. 3, 2010, pp. 287-291.

СПИСОК ЛИТЕРАТУРЫ

1. **Zaborova D., Musorina T.** Environmental and energy-efficiency considerations for selecting building envelopes // Sustainability. 2022, Vol. 14, No. 10. P. 5914.
2. **Kotlyarova E.** Improving the methodology for assessing the level of environmental safety of urban areas as the basis of their life cycle // E3S Web of Conferences, 2023, Vol. 389, No. 09062.
3. **Kotlyarova E.** Basic Scientific Principles of Improving the Methodology for the Assessment of the Level of Environmental Safety of Urbanized Territories // AIP Conference Proceedings, 2023, Vol. 2560, No. 020010.
4. **Gamayunova O., Gumerova E., Miloradova N.** Smart glass as the method of improving the energy efficiency of high-rise buildings // E3S Web of Conferences, 2018, Vol. 33, No. 02046.
5. **Gamayunova O., Radaev A., Petrichenko M., Shushunova N.** Energy audit and energy efficiency of modular military towns // E3S Web of Conferences, 2019, Vol. 110, No. 01088.

6. **Zaborova D., Vieira G., Musorina T., Butyrin A.** Experimental study of thermal stability of building materials // Advances in Intelligent Systems and Computing. Cham, 2018, Vol. 692 pp. 482-489.
7. **Vieira G.B., Petrichenko M.R., Musorina T.A., Zaborova D.D.** Behavior of a hollowed-wood ventilated façade during temperature changes // Magazine of Civil Engineering, 2018, Vol. 79, No. 3, pp. 103-111.
8. **Gagarin V.G., Kozlov V.V., Zubarev K.P.** Determination of maximum moisture zone on enclosing structures. // Cold Climate HVAC 2018: Sustainable Buildings in Cold Climates, 2019, pp. 925-932.
9. **Zubarev K.P.** Derivation of the equation of unsteady-state moisture behaviour in the enclosing structures of buildings using a discrete-continuous approach // International Journal for Computational Civil and Structural Engineering, 2021, Vol. 17, No. 4, – pp. 83-90.
10. **Sidorov V.N. Matskevich S.M.** Discrete-analytical solution of the unsteady-state heat conduction transfer problem based on the finite element method. // IDT 2016 - Proceedings of the International Conference on Information and Digital Technologies 2016. 2016, – pp. 241-244.
11. **Золотов А.Б., Мозгалева М.Л., Акимов П.А., Сидоров В.Н.** Об одном дискретно-континуальном подходе к решению одномерной задачи теплопроводности. // Academia. Архитектура и строительство, Iss. 3, 2010, pp. 287-291.

Zubarev Kirill Pavlovich, Ph.D. (Candidate of Engineering Sciences), Associate Professor, Associate Professor at the Department of General and Applied Physics of the Moscow State University of Civil Engineering, 129337, Moscow, Yaroslavskoe shosse, 26; Lecturer at the Department of Heat and Gas Supply and Ventilation of the Moscow State University of Civil Engineering, 129337, Moscow, Yaroslavskoe shosse, 26; Senior Researcher at the Laboratory of Building Thermal Physics of the Research Institute of Building Physics of Russian Academy of Architecture and Construction Sciences, 127238, Moscow, Lokomotivny proezd, 21; Associate Professor at the Department of Civil Engineering, Academy of Engineering, the Peoples' Friendship University of Russia (RUDN University) 117198, Moscow, st. Miklukho-Maclaya, 6; Leading Researcher at the Scientific Center of Engineering and Construction Technologies, Academy of Engineering, the Peoples' Friendship University of Russia (RUDN University) 117198, Moscow, st. Miklukho-Maclaya, 6; e-mail.: zubarevkirill93@mail.ru

Зубарев Кирилл Павлович, кандидат технических наук, доцент, доцент кафедры общей и прикладной физики Национального исследовательского Московского государственного строительного университета 129337, г. Москва, Ярославское шоссе, 26; преподаватель кафедры теплогазоснабжения и вентиляции Национального исследовательского Московского государственного строительного университета 129337, г. Москва, Ярославское шоссе, 26; старший научный сотрудник лаборатории строительной теплофизики Научно-исследовательского института строительной физики Российской академии архитектуры и строительных наук 127238, г. Москва, Локомотивный проезд, 21; доцент департамента строительства инженерной академии Российского университета дружбы народов 117198, г. Москва, ул. Миклухо-Маклая, 6; ведущий научный сотрудник научного центра техники и технологий строительства Российского университета дружбы народов 117198, г. Москва, ул. Миклухо-Маклая, 6; e-mail.: zubarevkirill93@mail.ru

DOI:10.22337/2587-9618-2024-20-1-162-170

THE EFFECT OF MODIFYING ADDITIVES ON THE PERFORMANCE PROPERTIES OF SLAG-ALKALI BINDERS AND CONCRETES

Zhambul T. Aimenov [1], Askar J. Aimenov [1], Vladimir T. Yerofeyev [2], Linar S. Sabitov [3], Yana A. Sanyagina [4]

[1] M. Auezov South Kazakhstan Research University, Shymkent, KAZAKHSTAN,
[2] National Research Moscow State University of Civil Engineering, Moscow, RUSSIA,
[3] Kazan Federal University, Kazan, RUSSIA,
[4] Scientific Research Institute of Structural Physics of the Russian Academy of Sciences, Moscow, RUSSIA

Abstract: The results of the analysis and generalization of research on the problem of using man-made industrial waste for the production of composite slag-alkali binders and concretes based on them are presented. The disposal of industrial man-made waste and their use in the production of composite binders are issues of global importance. Therefore, much attention is paid to this issue in the industrialized countries of the world.The influence of waste products from the enrichment of polymetallic ores – carbonate-barium tailings on the performance properties (strength, water absorption, density, etc.) of composite slag-alkali binders and concretes based on them has been studied. Various methods of introducing modifying additives into the composition of composite slag-alkali binders and concretes based on them have been investigated. The optimal amount of introduction of modifying additives into the composition of composite slag–alkali binders - waste of carbonate-barium tailings and an efficiency indicator for the effect on the activity of concrete, depending on the type of alkaline component and hardening conditions, has been established. The methods of conducting experimental work to determine the operational properties of slag-alkali binders and concretes based on them are presented.

Keywords: waste of carbonate-barium tailings, composite slag-alkali binders, modifying additives, strength, water absorption, density

ВЛИЯНИЕ МОДИФИЦИРУЮЩИХ ДОБАВОК НА ЭКСПЛУАТАЦИОННЫЕ СВОЙСТВА ШЛАКОЩЕЛОЧНЫ ХВЯЖУЩИХ И БЕТОНОВ

Ж.Т. Айменов [1], А.Ж. Айменов [1], В.Т. Ерофеев [2], Л.С. Сабитов [3], Я.А. Санягина [4]

[1] Южно-Казахстанский исследовательский университет им. М. Ауэзова, г. Шымкент, КАЗАХСТАН,
[2] Национальный исследовательский Московский государственный строительный университет, г.Москва, РОССИЯ,
[3]Казанский Федеральный Университет, г. Казань, РОССИЯ,
[4]Научно-исследовательский институт строительной физики РААСН, г.Москва, РОССИЯ

Аннотация: Приведены результаты анализа и обобщения исследований по проблеме использования техногенных отходов промышленности для производства композиционных шлакощелочных вяжущих и бетонов на их основе. Утилизация промышленных техногенных отходов и их использование в производстве композиционных вяжущих является вопросами глобального значения. Поэтому в промышленно развитых странах мира этому вопросууделяется большое внимание. Изучено влияние отходов производства обогащения полиметаллических руд – карбонатно-бариевых хвостов на эксплуатационные свойства (прочность, водопоглощение, плотность и др.) композиционных шлакощелочных вяжущих и бетонов на их основе. Исследованы различные способы введениямодифицирующих добавок в состав композиционных шлакощелочных вяжущих и бетонов на их основе. Установлено оптимальное количество введения в состав композиционных шлакощелочных вяжущих модифицирующих добавок – отходов карбонатно-бариевых хвостов и показатель эффективности по влиянию на активность бетона, в зависимости от вида

щелочного компонента и условий твердения. Приведены методики проведения экспериментальных работ по определению эксплуатационных свойств шлакощелочных вяжущих и бетонов на их основе.

Ключевые слова: отходы карбонатно-бариевых хвостов, композиционные шлакощелочные вяжущие, модифицирующие добавки, прочность, водопоглощение, плотность

1. INTRODUCTION

The problem of effective utilization of technogenic industrial waste has great importance due to the continuous growth of industrial production and consumption of natural mineral raw materials. Insufficiency and irreplaceability of deposits of natural raw materials, complication of mining and geological conditions of occurrence of ore bodies and rise in cost of their extraction, negative influence on the environment of accumulated technogenic wastes is an actual problem. Therefore, the application of industrial technogenic wastes in the production of composite materials is today the most important research questions of scientists.

The volumes of accumulated industrial wastes of production are significant in the Russian Federation and Kazakhstan, and their wide application for production of composite slag-alkali binders and concretes on their basis is expedient, and it requires their immediate accounting on a par with natural mineral resources. Development of composite cement and slag-alkali binders and concretes on the basis of industrial technogenic wastes promotes systematic and more intensive involvement of various types of technogenic mineral formations in the production process [1,2,3,4,5,5,6,7].

Currently, only an insignificant share of industrial anthropogenic waste in Russia and Kazakhstan is used in the production of construction materials. The widespread use of industrial waste in production turnover will allow to increase energy and resource saving on a large scale due to cost savings on exploration, extraction and processing of mineral raw materials. Application of accumulated technogenic industrial wastes (mining wastes, ashes of thermal power plants, phosphorus, metallurgical, steelmaking slags, non-ferrous metallurgy slags, alkaline-containing industrial wastes, etc.) as a component of cement is the main direction of modern development of cement industry both in Russia and Kazakhstan.

At present, construction science and practice have accumulated a huge positive experience in the field of application of industrial wastes in the production of construction and silicate materials, but they have not been properly applied in production. In cement industry this direction includes development and research of glass- and slag-alkaline binders and concretes. In recent years, their new varieties have been obtained [7,8,9,10,11,12]. At the same time, alkaline-activated binders are very often proposed to replace cement and other binders [13,14,15]. They are formed by the reaction of aluminosilicate material with an alkaline agent such as sodium hydroxide [16,17]. The advantage of alkaline binders is that their use can reduce carbon dioxide emissions by up to 80% [18]. The use of alkaline binders can also reduce the cost of production of composite materials [19,20], reduce the heat of hydration [21] and strengthen the filler-matrix interface [13,19,22].

Research work on the production and study of composite slag-alkali binders with local mineral additives and concrete on their basis in recent years are conducted in the Research Institute of "Natural and Technical Sciences" at M. Auezov SKIU [11,12,23,24].

2. METHODS AND MATERIALS

Preparation and testing of composite slag-alkali binders was carried out in accordance with technical conditions TU 67-1020-89 "Slag-alkali binder. Technical conditions".

The made specimen beams were stored for 3 days in molds with the covered top surface in air-dry conditions, then unplugged and stored in normal-moisture conditions until testing. Testing of binder specimen beams was carried out

according to the accelerated method: specimen beams were made in accordance with the requirements of GOST 310.4-81 "Methods of determining the compressive and bending strength", taking into account the above changes, not earlier than 4 hours and not later than 12 hours after preparation. After manufacturing the specimens were subjected to heat and humidity treatment (HHT) in molds according to the regime 3+6+3 h at the temperature of isothermal heating 95±5 ºC. The specimens were subjected to testing one day after manufacturing.

For determination of construction-technical characteristics of concrete on the basis of CSB we used GOST 10180-90 "Methods of determination of strength by control samples", GOST 12730.0-78, GOST 12730.4-78 for determination of concrete density, GOST 12730.3 for determination of water absorption and characteristics of concrete porosity. For the grinding of different compositions of CSB and slag we used mills: Ml-1, Aktivator-4 m and SVM-3.

3. RESEARCH RESULTS

This section provides the results of research on the use of electro thermo phosphorus slags for the production of salt-slag binders. These include binders based on electro thermo phosphorus slags and natural salts (sulfates, chlorides, nitrites of alkaline and alkaline-earth metals) obtained by autoclave treatment of compositions [11].

The presence of ions CI- and SO-4 in the composition of salt-slag binders limits their application for the manufacture of reinforced concrete structures, as evidenced by the results of studies of corrosion of steel in concrete [25,26]. In these experiments it is shown that without special protection of steel reinforcement salt-slag concrete autoclave curing, prepared on salts of sodium sulfate, carnallite, magnesium chloride, can be used only at a relative humidity of up to 60%. In order to reduce corrosion of steel reinforcement, the same and other authors proposed to introduce into the composition of such concrete deficient and expensive additives of two substituted sodium orthophosphate and potassium bichromate, which does not solve the issue of their widespread practical application.

Currently, there is a deficit of conditioned alkaline components for the production of slag-alkali binders and concrete in Kazakhstan due to the lack of their production. Therefore, for production of composite slag-alkali binders and concretes various alkaline-containing wastes of technological processes and productions (for example, metallurgical and chemical industries) are used.

In particular, a very promising multi-tonnage alkali containing waste for production of slag-alkali concrete, especially in the region of Central Asia, is sodosulfate mixture - a waste of caprolautam production of Chirchik PO "Elektrokhimprom" (annual output is 14 million tons). The waste is a complex product of chemical composition: sodium sulfate - 30...35 %; sodium carbonate - 50...55 % and sodium chloride 10...15 %. 15 %. The research of the possibility of using this waste in the production of slag-alkali concrete has been devoted to a small number of works so far. The authors of works [23,24] showed the possibility of obtaining slag-alkali binders of grades 300, 400 on the basis of mixtures of sodium salts, weak and strong acids. On the basis of the developed binders the author obtained slag-alkali expanded clay concrete of grades 250, 400 with an average density of 1400, 1800 kg/m, respectively. The study of frost resistance and duration of reinforcement preservation in slag-alkali expanded clay concretes showed that the investigated characteristics of such concretes are most influenced by the type of alkaline component and the density of its solution [23].

Corrosion of reinforcement in slag-alkali expanded clay concrete is caused by penetration of stimulant ions CI^- and SO^-_4. The samples showed rust spots and the degree of corrosion of reinforcement in concrete was estimated at 3 points. The authors [23,25] recommend the introduction of $NaNO_2$ corrosion inhibitors or lowering the density of sodium sulphate carbonate solution to 1050 kg/m^3.

Despite the fact that the paper [12] noted the influence of the type and density of the alkaline component on the physical and mechanical properties of concrete. However, there is no systematized data on the optimization of the structure of concrete on soda-sulfate mixture, as well as there is no information on some construction and technical characteristics of heavy slag-alkali concrete in relation to different types of construction.

The influence of different methods of carbonate-barium tailings (CBBT) additive introduction on the performance properties of slag-alkali concrete was investigated. Studies were conducted using Portland cement clinker, phosphorus slag, modifying additive of waste carbonate-barium tailings and aqueous solution of soda-sulfate mixture. In the first case phosphorus slag and additive waste-carbonate-barium tailings were subjected to separate grinding to the residue on the sieve 008 10 % (300 m^2/kg on PSX-12). In the second case phosphorus slag, Portland cement clinker and waste carbonate-barium tailings - together. The joint grinding of the components of CSB was carried out for the time required for grinding without additive, grinding fineness up to Sud 300 m^2/kg. The obtained results are shown in Figure 1.

Compared to separate milling, co-milling is more efficient. The milled CSB compositions obtained by separate and joint grinding methods show higher activity results and have a wider range of "possible" and "effective" replacement of carbonate-barium tailings waste with modifying additive, higher density by 1.7 % and lower water absorption by 9.8 % as compared to unmilled samples. At separate grinding of components (the amount of Portland cement clinker is accepted - 5 % Const) the range of replacement of phosphorus slag by modifying additive of waste carbonate-barium tailings, in which the composition on CSB is not inferior to additive-free, is 4-6 %. At joint grinding of CSB constituents this area increases up to 10 % and it is possible to get a binder with increased activity in comparison with control compositions. It is established that, depending on the type of hardening and alkaline component in comparison with the control composite compositions of CSB on phosphorus slag, modifying additive of waste carbonate-barium tailings of Portland cement clinker, obtained by joint dispersion, have higher activity by 60.0-70.0 MPa.

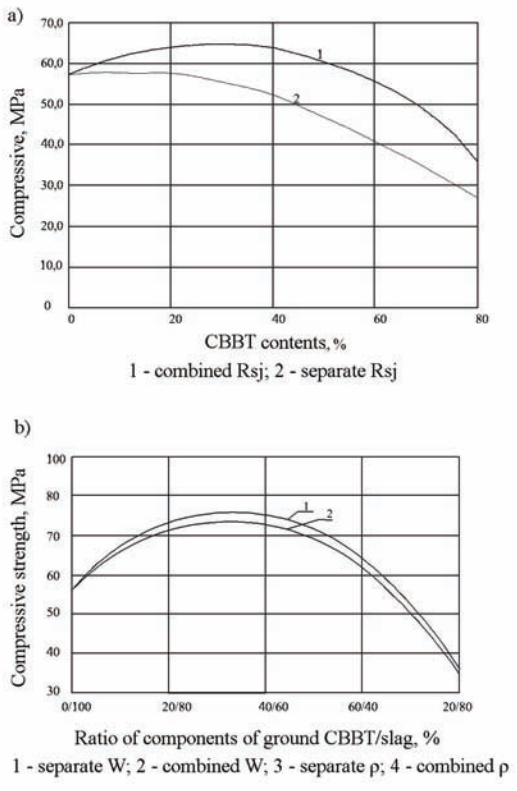

Figure 1. Dependences of strength (a), density and water-absorption (b) of CSB stone on the content of waste carbonate-barium tailings and the method of additive introduction

Introduction of a modifying additive of waste carbonate-barium tailings at co-milling with phosphorus slag gives a great effect, it is achieved for the following reasons. From the results of the study, it is known that Portland cement clinker is crushed lighter than phosphoric slag and at the same time is crushed to Sud 1.2 times more than phosphoric slag. When co-milling with a modifying additive of waste - carbonate-barium tailings to Sud 300 m^2/kg, particles of phosphoric slag are not ground and have a size in the composition of CSB than in a sample of pure phosphoric slag with the same grinding fineness.

We cannot exclude the possibility of interaction of waste carbonate-barium tailings in the solid

phase and the formation of aggregates or "complexes", doped as a result of breaking and compensation of bonds on the surface-active particles, changes in their curvature and relief, and the formation of new mechanical bonds.

Based on the experimental results, the combined milling of phosphorus slag, Portland cement clinker and modifying additive of waste - carbonate-barium tailings to produce CSB was accepted in further studies.

The activity of CSB samples and concrete on their basis was determined on the samples made on the basis of phosphorus slag, Portland cement clinker and with modifying additive of waste carbonate-barium tailings, aqueous solutions of soda-sulfate mixture and soda ash, after TVO (mode 4+3+6+3 h at the temperature of isothermal heating 95±5 P.). Fine milled CSB with modifying addition of waste carbonate-barium tailings is 300 m^2/kg. The results of the study are presented in the form of Figure 2. It follows from the data of the figure that fluctuations in the composition of additives do not significantly affect the level of activity of CSB stone with modifying additive of waste carbonate-barium tailings. The content of modifying additive of carbonate-barium tailings waste has a great influence on the strength. The content of carbonate-barium tailings additive in the composite binder is 10 % regardless of the nature of the alkaline component

When using soda ash, the strength increase was 22,1-26,1 %, soda-sulfate mixtures - 19,2-20,4 %. Introduction of carbonate-barium tailings waste modifying additive up to 10 % into CSB composition allows to obtain equal strength cement stone CSB with modifying additive of carbonate-barium tailings waste in comparison with non-additive one. In CSB, increasing the content of carbonate-barium tailings waste modifying additive up to 15 % reduces the activity of cement stone samples. CSB with carbonate-barium tailings waste additive on soda ash - 32,2-38,2 % and on soda-sulfate mixture - 31,3-39,2 %. At the optimum content of modifying additive of carbonate-barium tailings waste - 10 % efficiency index on the effect on the strength of stone obtained by co-milling up to 600 m2/kg depending on the type of alkaline component and curing conditions is in the range of 1.2-1.41.

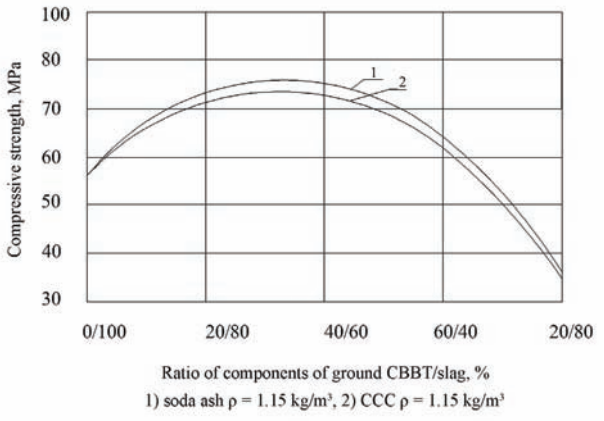

Figure 2. Influence of type and content of milled CBBT on the strength of CSB stone specimens after TVO, made on aqueous solutions, %

4. CONCLUSIONS

1. It is established that the amount of modifying additive of carbonate-barium tailings waste has a great influence on the strength, with the content in the composite binder being 10% regardless of the nature of the alkaline component.

2. It is determined that for CSB compositions without additive and with additives the dependences of properties are described by minimum regularities with maximum values of average density and strength and minimum values of water absorption in the area of grinding fineness 6,0-7,0 m^2/kg irrespective of the nature of alkaline component and curing conditions.

REFERENCES

1. **Erofeev V.T., Rodin A.I., Bochkin V.S., Yakunin V.V., Ermakov A.A.** Lightweight geopolymers made of mineral wool production waste // Magazine of Civil Engineering. 2020. 93(1). Pp. 3–12.
2. **Erofeev V.T., Rodin A.I., Yakunin V.V., Tuvin M.N.** Structure, composition and properties of geopolymers from mineral

wool waste // Magazine of Civil Engineering. 2019. 90(6). Pp. 3–14.

3. **Erofeev V.T., Rodin A.I., Kravchuk A. S., Kaznacheev S.V., Zaharova E.A.** Biostable silicic rock-based glass ceramic foams // Magazine of Civil Engineering. 2018. 84(8). Pp. 48–56.
4. **Erofeev V.T., Rodin A.I., Yakunin V.V., (...), Bochkin V. S., Chegodajkin A.M.** Alkali-activated slag binders from rockwool production wastes // Magazine of Civil Engineering. 2018. 82(6). Pp. 219–227.
5. **Yusupova A.A., Akhmetova R.T., Treshchev A.A., (...), Shafigullin L.N., Lakhno A.A.** Production and investigation of properties of sulfide composite materials based on technogenic sulfur waste with titanium chloride as an activator // Research Journal of Pharmaceutical, Biological and Chemical Sciences. 2016. 7(6). Pp. 1614–1619.
6. **Bulgakov A., Erofeev V., Bogatov A., Smirnov V., Schach, R.** Innovative production technology of binding and building composite materials on the basis of glass wastes // Insights and Innovations in Structural Engineering, Mechanics and Computation. – Proceedings of the 6th International Conference on Structural Engineering, Mechanics and Computation, SEMC. 2016. Pp. 1583–1586.
7. **Ajmenov A.ZH., Ajmenov ZH.T., Sarsenbaev B.K.** Kompozicionnye vyazhushchie s ispol'zovaniem syr'evyh resursov Kazahstana // Vestnik KazNA-EN. № 1. 2019. S. 8–9.
8. **Urhanova L.A., Balhanova E.D.** Poluchenie kompozicionnyh alyumosilikatnyh vyazhushchih na osnove vulkanicheskih porod // Stroitel'nye materialy. 2006. S.51-53.
9. **Rahimov R.Z. Magdeev U.H. YArmakovskij V.N.** Ekologiya, nauchnye dostizheniya i innovacii v proizvodstve stroitel'nyh materialov na osnove i s primeneniem tekhnogennogo syr'ya / M-ly mezhd. kongressa «Nauka i innovacii v stroitel'stve SIB-2008», Sovremennye problemy stroitel'nogo materialovedeniya i tekhnologii. 2008. S.441-448.
10. **Rahimova N.R.** Kompozicionnye shlkoshchelochnye vyazhushchie, rastvory i betony na ih osnove // Nauch-nyj vestnik VGASU. Stroitel'stvo i arhitektu-ra. 2008. №4(12). S.110–118. (in Russian).
11. **Sarsenbaev B.K., Estemesov Z.A., Ajmenov ZH.T., Sarsenbaev N.B., Ajmenov A.ZH.** SHlakoshchelochnye vyazhushchie i betony // SHymkent: Izd-vo YUKGU im. M. Aueezova, 2016. 360 s. (in Russian).
12. **Bischembaew W., Sarsenbaew B., Altaewa S., Imanaliew K.** Strukturbildung von Alkalischlacken – Bindemitteln auf Basis von Djambulischer Schlacken // 16. internationale Baustofftagung. Ibausil. Weimar 2006. Tagungsbericht-Band 1. S.1 Pp.1153 – 1155. (in Russian).
13. **Aydin S., Baradan B.,** Engineering properties of reactive powder concrete without portland cement, ACI Mater. J. 110 (6) (2013) 619–627.
14. **Alharbi Y.R., Abadel A.A., Salah A.A., Mayhoub O.A., Kohail M.,** Engineering properties of alkali activated materials reactive powder concrete, Construct. Build. Mater. 271.
15. **Mayhoub O.A.,. Nasr E.S.A.R, Ali Y., Kohail M.** Properties of slag based geopolymer reactive powder concrete, Ain Shams Engineering Journal. 12 (1) Pp.99–105.
16. **Bouikni A, Swamy R. N, Bali A.** Durability properties of concrete containing 50 % and 65 % slag. Constr. Build. Mater. 2009.
17. **Caldarone M.A**. High-Strength Concrete. A practical guide. – 2009.
18. **Pacheco-Torgal F., Abdollahnejad Z., Camoes A.F., Jamshidi M., Ding Y**. Durability of alkali-activated binders: a clear advantage over Portland cement or an unproven issue // Construct. Build. Mater. 2012. 30. Pp. 400–405.
19. **Bajpai R., Choudhary K., Srivastava A., Sangwan K.S., Singh M.** Environmental im-

pact assessment of fly ash and silica fume based geopolymer concrete. 2020. 254.

20. **So H.S., Yi J.B., Khulgadai J., So S.Y.** Properties of strength and pore structure of reactive powder concrete exposed to high temperature // ACI Mater J 2014.
21. **Ollivier J. P, Maso J. C., Bourdette B.** Interfacial transition zone in concrete // Adv. Cem. Based Mater. 1995.
22. **Scrivener KL, Crumbie AK, Laugesen P.** The interfacial transition zone (ITZ) between cement paste and aggregate in concrete. Interface Sci 2004.
23. **Ajmenov A.ZH., Ajmenov ZH.T. Sarsenbaev B.K.,** Razrabotka sostavov betonov na osnove kompozicionnyh cementov s dobavkoj othodov karbonatnobarievyh hvostov // Vestnik KazNA-EN. № 1. S. 56–58.
24. **Ajmenov ZH.T., Ajmenov A.ZH., Sarsenbaev B.K. Sarsenbaev N.B.** Proizvodstva maloklinkernyh tonkomolotyh cementov na osnove othodov gornometallurgicheskih predpriyatij // Sb. tr. Mezhd. nauchno-prakt, konf «Innovacii v oblasti estestvennyh nauk kak osnova eksportoorintirovannoj industrializacij Kazahstana» 2019. S. 216–222. (in Russian).
25. **Ajmenov A.ZH., Zajnudinov A.K., Tasbolatov K.M., Kiizbaj A.K.** Korroziya armatury v betonah na os-nove maloklinkernyh tonkomolotyh cementov iz prirodnyh i tekhnogennyh napolnitelej // Vest-nik Kazahskoj golovnoj arhitekturnostroitel'noj akademii. Nauchnyj zhurnal. № 3. 2016. S. 77–83. (in Russian).
26. **Krishan A., Rimshin V., Erofeev V., Kurbatov V., Markov S.** The energy integrity resistance to the destruction of the long-term strength concrete // Procedia Engineering. 2015, 17(1). Pp. 211–217. (in Russian).

СПИСОК ЛИТЕРАТУРЫ

1. **Erofeev V.T., Rodin A.I., Bochkin V.S., Yakunin V.V., Ermakov A.A.** Lightweight geopolymers made of mineral wool production waste // Magazine of Civil Engineering. 2020. 93(1). Pp. 3–12.
2. **Erofeev V.T., Rodin A.I., Yakunin V.V., Tuvin M.N.** Structure, composition and properties of geopolymers from mineral wool waste // Magazine of Civil Engineering. 2019. 90(6). Pp. 3–14.
3. **Erofeev V.T., Rodin A.I., Kravchuk A. S., Kaznacheev S.V., Zaharova E.A.** Biostable silicic rock-based glass ceramic foams // Magazine of Civil Engineering. 2018. 84(8). Pp. 48–56.
4. **Erofeev V.T., Rodin A.I., Yakunin V.V., (...), Bochkin V. S., Chegodajkin A.M.** Alkali-activated slag binders from rockwool production wastes // Magazine of Civil Engineering. 2018. 82(6). Pp. 219–227.
5. **Yusupova A.A., Akhmetova R.T., Treshchev A.A., (...), Shafigullin L.N., Lakhno A.A.** Production and investigation of properties of sulfide composite materials based on technogenic sulfur waste with titanium chloride as an activator // Research Journal of Pharmaceutical, Biological and Chemical Sciences. 2016. 7(6). Pp. 1614–1619.
6. **Bulgakov A., Erofeev V., Bogatov A., Smirnov V., Schach, R.** Innovative production technology of binding and building composite materials on the basis of glass wastes // Insights and Innovations in Structural Engineering, Mechanics and Computation. – Proceedings of the 6th International Conference on Structural Engineering, Mechanics and Computation, SEMC. 2016. Pp. 1583–1586.
7. **Айменов А.Ж., Айменов Ж.Т., Сарсенбаев Б.К.** Композиционные вяжущие с использованием сырьевых ресурсов Казахстана // Вестник КазНАЕН. № 1. 2019. С. 8–9.
8. **Урханова Л.А., Балханова Е.Д.** Получение композиционных алюмосиликатных вяжущих на основе вулканических пород // Строительные материалы. 2006. С.51-53.
9. **Рахимов Р.З. Магдеев У.Х. Ярмаковский В.Н.** Экология, научные достижения и инновации в производстве строи-

тельных материалов на основе и с применением техногенного сырья / М-лы межд. конгресса «Наука и инновации в строительстве SIB-2008», Современные проблемы строительного материаловедения и технологии. 2008. С.441-448.

10. **Рахимова Н.Р.** Композиционные шлкощелочные вяжущие, растворы и бетоны на их основе // Научный вестник ВГАСУ. Строительство и архитектура. 2008. №4(12). С.110–118.
11. **Сарсенбаев Б.К., Естемесов З.А., Айменов Ж.Т., Сарсенбаев Н.Б., Айменов А.Ж.** Шлакощелочные вяжущие и бетоны // Шымкент: Изд-во ЮКГУ им. М. Ауэзова, 2016. 360 с.
12. **Bischembaew W., Sarsenbaew B., Altaewa S., Imanaliew K.** Strukturbildung von Alkalischlacken – Bindemitteln auf Basis von Djambulischer Schlacken // 16. internationale Baustofftagung. Ibausil. Weimar 2006. Tagungsbericht-Band 1. S.1 Pp.1153 – 1155.
13. **Aydin S., Baradan B.,** Engineering properties of reactive powder concrete without portland cement, ACI Mater. J. 110 (6) (2013) 619–627.
14. **Alharbi Y.R., Abadel A.A., Salah A.A., Mayhoub O.A., Kohail M.,** Engineering properties of alkali activated materials reactive powder concrete, Construct. Build. Mater. 271.
15. **Mayhoub O.A.,. Nasr E.S.A.R, Ali Y., Kohail M.** Properties of slag based geopolymer reactive powder concrete, Ain Shams Engineering Journal. 12 (1) Pp.99–105.
16. **Bouikni A, Swamy R. N, Bali A.** Durability properties of concrete containing 50 % and 65 % slag. Constr. Build. Mater. 2009.
17. **Caldarone M.A**. High-Strength Concrete. A practical guide. – 2009.
18. **Pacheco-Torgal F., Abdollahnejad Z., Camoes A.F., Jamshidi M., Ding Y**. Durability of alkali-activated binders: a clear advantage over Portland cement or an unproven issue // Construct. Build. Mater. 2012. 30. Pp. 400–405.
19. **Bajpai R., Choudhary K., Srivastava A., Sangwan K.S., Singh M.** Environmental impact assessment of fly ash and silica fume based geopolymer concrete. 2020. 254.
20. **So H.S., Yi J.B., Khulgadai J., So S.Y.** Properties of strength and pore structure of reactive powder concrete exposed to high temperature // ACI Mater J 2014.
21. **Ollivier J. P, Maso J. C., Bourdette B.** Interfacial transition zone in concrete // Adv. Cem. Based Mater. 1995.
22. **Scrivener KL, Crumbie AK, Laugesen P.** The interfacial transition zone (ITZ) between cement paste and aggregate in concrete. Interface Sci 2004.
23. **Айменов А.Ж., Айменов Ж.Т. Сарсенбаев Б.К.,** Разработка составов бетонов на основе композиционных цементов с добавкой отходов карбонатно-бариевых хвостов // Вестник КазНАЕН. № 1. С. 56–58.
24. **Айменов Ж.Т., Айменов А.Ж., Сарсенбаев Б.К. Сарсенбаев Н.Б.** Производства малоклинкерных тонкомолотых цементов на основе отходов горно-металлургических предприятий // Сб. тр. Межд. научно-практ, конф «Инновации в области естественных наук как основа экспортоориентированной индустриализаций Казахстана» 2019. С. 216–222.
25. **Айменов А.Ж., Зайнудинов А.К., Тасболатов К.М., Киизбай А.К.** Коррозия арматуры в бетонах на основе малоклинкерных тонкомолотых цементов из природных и техногенных наполнителей // Вестник Казахской головной архитектурно-строительной академии. Научный журнал. № 3. 2016. С. 77–83.
26. **Krishan A., Rimshin V., Erofeev V., Kurbatov V., Markov S.** The energy integrity resistance to the destruction of the long-term strength concrete // Procedia Engineering. 2015, 17(1). Pp. 211–217.

Zhambul T. Aimenov, Professor, Doctor of Technical Sciences, M. Auezov South Kazakhstan Research University, 160012, Kazakhstan, Shymkent, Tauke Khan Avenue, 5, Phone: +7(701)731-92-97, E-mail: zhambul_ukgu@mail.ru

Askar Z. Aimenov, Doctor PhD, M. Auezov South Kazakhstan Research University, 160012, Shymkent, 5 Tauke Khan Avenue, Phone: +7(701)731-92-97, E-mail: stroitelstvo_ukgu@mail.ru

Vladimir T. Erofeev, Professor, Doctor of Technical Sciences, Academician of the Russian Academy of Sciences, National Research Moscow State University of Civil Engineering, 26 Yaroslavskoye Shosse, 160012, Moscow, Russia, Phone: +7(927)276-04-76, E-mail: erofeevvt@bk.ru

Linar S. Sabitov, Associate Professor, Doctor of Technical Sciences, Advisor of the Russian Academy of Sciences, Kazan Federal University, 420008, Kazan, Kremlevskaya str., 18, Phone: +7(937)774-07-00, E-mail: l.sabitov@bk.ru

Sanyagina Yana Andreevna, applicant, Scientific Research Institute of Structural Physics RAASN, 127238, Russia, Moscow, Locomotive Passage, 21, Phone: +7(927)099-33-11, E-mail: sanyagi-na@mail.ru

Айменов Жамбул Талхаевич, профессор, доктор технических наук, Южно-Казахстанский исследовательский университет им. М. Ауэзова, 160012, Казахстан, Шымкент, проспект Тауке хана, д. 5, тел.: +7(701)731-92-97, E-mail: zhambul_ukgu@mail.ru

Айменов Аскар Жамбулович, доктор PhD, Южно-Казахстанский исследовательский университет им. М. Ауэзова, 160012, Казахстан, Шымкент, проспект Тауке хана, д. 5, тел.: +7(701)731-92-97, E-mail: stroitelstvo_ukgu@mail.ru

Ерофеев Владимир Трофимович, профессор, доктор технических наук, академик РААСН, Национальный исследовательский Московский государственный строительный университет, 160012, Россия, Москва, Ярославское шоссе, д. 26, тел.: +7(927)276-04-76, E-mail: erofeevvt@bk.ru

Сабитов Линар Салихзанович, доцент, доктор технических наук, советник РААСН, Казанский федеральный университет, 420008, Россия, Казань, ул.Кремлевская, д. 18, тел.: +7(937)774-07-00, E-mail: l.sabitov@bk.ru

Санягина Яна Андреевна, соискатель, Научно-исследовательский институт строительной физики РААСН, 127238, Россия, Москва, Локомотивный проезд, д. 21, тел.: +7(927)099-33-11, E-mail: sanyagi-na@mail.ru

International Journal for Computational Civil and Structural Engineering, 20(1) 171–181(2024)

DOI:10.22337/2587-9618-2024-20-1-171-181

MATHEMATICAL MODELING OF THE STRENGTH PROPERTIES OF LESSES BY THE METHOD OF CORRELATION-REGRESSION ANALYSIS

Elena O. Tarasenko

North Caucasus Federal University, Stavropol, RUSSIA

Abstract. The strength properties of subsiding loess soils are considered in the mathematical modeling of their compaction by deep explosions. Soil compaction is carried out in order to eliminate their subsidence properties. Correlation and regression analyzes of the dependences of strength on the physical characteristics of loess were carried out, using the soils of the North Caucasus as an example. The correlation dependence of the specific cohesion and the angle of internal friction on the physical characteristics of the subsidence soil is established. Correlation coefficients were obtained for various indices of moisture content and loess density. The studies were carried out before and after soil compaction in this way. Both positive and negative correlations between the studied characteristics of subsiding loess soil were recorded. With an increase in moisture, a high correlation was observed with the strength characteristics of the soil before and after its compaction by deep explosions. The equations of regression of specific cohesion and the angle of internal friction on soil moisture and density are constructed. The reliability coefficients of approximation of theoretical regression equations and experimental data demonstrate high values. The regression equations of specific adhesion and the angle of internal friction on soil moisture showed that the values of strength characteristics increase with decreasing values of soil moisture. The regression dependence of the specific cohesion and the angle of internal friction on the density of subsidence loess has been studied. It has been established that an increase in the values of strength characteristics was recorded with an increase in the density of loess soil before and after its compaction by deep explosions. The constructed regression equations make it possible to predict the strength characteristics of loess at the stage of designing the bases and foundations of construction objects.

Keywords: loess, subsidence, compaction, specific cohesion, angle of internal friction, correlation, regression

МАТЕМАТИЧЕСКОЕ МОДЕЛИРОВАНИЕ ПРОЧНОСТНЫХ СВОЙСТВ ЛЁССОВ МЕТОДОМ КОРРЕЛЯЦИОННО-РЕГРЕССИОННОГО АНАЛИЗА

Е.О. Тарасенко

Северо-Кавказский федеральный университет, г. Ставрополь, РОССИЯ

Аннотация. Рассмотрены прочностные свойства просадочных лёссовых грунтов при математическом моделировании их уплотнения глубинными взрывами. Уплотнение грунтов производится с целью устранения их просадочных свойств. Проведены корреляционный и регрессионный анализы зависимостей прочностных от физических характеристик лёссов, на примере грунтов Северного Кавказа. Установлена корреляционная зависимость удельного сцепления и угла внутреннего трения от физических характеристик просадочного грунта. Коэффициенты корреляции получены для различных показателей значений влажности и плотности лёсса. Исследования проводились до и после уплотнения грунта указанным способом. Зафиксирована как положительная, так и отрицательная корреляционная зависимость между исследуемыми характеристиками просадочного лёссового грунта. С ростом влажности наблюдалась высокая корреляционная зависимость с прочностными характеристиками грунта до и после его уплотнения глубинными взрывами.

Построены уравнения регрессии удельного сцепления и угла внутреннего трения от влажности и плотности грунта. Коэффициенты достоверности аппроксимации теоретических уравнений регрессий и экспериментальных данных демонстрируют высокие значения. Регрессионные уравнения удельного сцепления и угла внутреннего трения от влажности грунта показали, что значения прочностных характеристик увеличиваются при уменьшении значений влажности грунта. Исследована регрессионная

зависимость удельного сцепления и угла внутреннего трения от плотности просадочного лёсса. Установлено, что рост значений прочностных характеристик фиксировался при увеличении плотности лёссового грунта до и после его уплотнения глубинными взрывами. Построенные регрессионные уравнения позволяют прогнозировать прочностные характеристики лёссов на этапе проектирования оснований и фундаментов объектов строительства.

Ключевые слова: лёсс, просадочность, уплотнение, удельное сцепление, угол внутреннего трения, корреляция, регрессия

INTRODUCTION

Loess subsidence soils are widespread on the Earth's surface and have different origins. Loess covers more than 17% of Russia's territory. It is most common in the North Caucasian and Southern Federal Districts (about 80%). Loess is a dusty-clay soil containing at least 50% of dusty particles [1, 2]. Elimination of subsidence properties of such soils is an urgent task of contemporary engineering geology [3-6]. Correlation-regression analysis-based mathematical modeling of soil compaction with deep explosions allows estimating the relationship between strength and physical properties of soils.

Realization of engineering calculations during design of bases and foundations of construction objects, various earthworks, slopes, etc. requires information about strength and physical characteristics of soils [3, 4, 7, 8]. This determines the necessity of their application to solve a number of scientific and applied problems of engineering geology [9-13]. Therefore, the engineering practical task of assessing changes in the strength properties of subsidence soils and their influence on the stability of buildings and structures depending on natural and anthropogenic conditions is of special importance [14-16].

The main strength characteristics of dispersed subsidence soils are specific cohesion and angle of internal friction. As a rule, their values are determined in laboratory conditions according to standards, e.g. [17]. Triaxial compression devices, stabilimeters, shear gauges, etc. can be used in practice. It should be noted that the test results of the different evaluation methods may differ slightly from each other. This is explained by the difference in the stress state of soils [3, 18. 19].

RESEARCH METHODS

Let us describe the mathematical model of the problem of compaction of loess soils by deep explosions in the form [9]

$$\begin{gathered}\frac{\partial q}{\partial t}+U\frac{\partial q}{\partial x}=\frac{\partial}{\partial x}K_x\frac{\partial q}{\partial x}+\\+\frac{\partial}{\partial y}K_y\frac{\partial q}{\partial y}+\frac{\partial}{\partial z}K_z\frac{\partial q}{\partial z}+f,\\ t\in\left[t_0,T\right],\end{gathered}\tag{1}$$

with initial and boundary conditions

$$\begin{gathered}q\left(t_0,x,y,z\right)=\\=Q\delta\left(x-x^0\right)\delta\left(y-y^0\right)\delta\left(z-z^0\right),\end{gathered}\tag{2}$$

$$q\left(t,x,y,z\right)\big|_{z=z^0}=0,\ t>t_0.\tag{3}$$

$$K_z\frac{\partial q}{\partial z}\bigg|_{z=z^0}=0,\ t>t_0,\tag{4}$$

where $q\left(t,x,y,z\right)$ is the soil density at time unit t at the point with coordinates $\left(x,y,z\right)$; U is the vector of horizontal gas drift along the Ox axis; f is the source function; Q is the charge (source) capacity; δ is the unit impulse Dirac function; K_x, K_y, K_z is the diffusion coefficients.

Problems (1) … (3) correspond to the case of complete absorption of gas atoms by the surrounding soil in the borehole (consolidation

of the subsidence soil occurs). Problems (1), (2) and (4) describe the case of complete reflection of gas atoms from the surrounding ground (ground ejection to the surface occurs).
The solutions of problems (1) - (3) and (1), (2), (4) are [9]

$$q(t,x,y,z)=\frac{Q}{(2\pi)^{3/2}K_xK_yK_zt^3}\times$$
$$\times\exp\left\{-\frac{(x-Ut)^2}{2K_x^2t}-\frac{y^2}{2K_y^2t}\right\}\times$$
$$\times\left[\exp\left\{-\frac{(z-H)^2}{2K_z^2t}\right\}\pm\exp\left\{-\frac{(z+H)^2}{2K_z^2t}\right\}\right],$$

where H is the depth of charge embedment
Values of diffusion coefficients K_x, K_y, K_z depend on physical characteristics of soils.
Let us investigate the correlation between strength and physical properties of soils, which include density and moisture content. Let us construct regression equations of strength characteristics of loess in order to predict their condition [10, 16, 20].

RESULTS AND DISCUSSIONS

This section provides a correlation-regression analysis of strength and physical properties of soils based on experimental data [3]. We study the construction site "Severny microdistrict in Budennovsk". At the construction site the thickness of subsidence soils reaches 20 m. According to the data the density of the soil before compaction is equal to $q_0=1.51-1.54\,г/см^3$. The natural moisture content took values of $\omega=10\%-30\%$. 198 combined drainage-explosion wells with diameter of 180 mm and depth of 6 m were drilled. Through them soaking of the subsidence stratum was carried out in the excavation. As a result of compaction by the method of deep explosions of concentrated explosive charges, the density of the soil took the value of $q=1.56-1.73\,г/см^3$.
Table 1 shows correlation dependence of specific adhesion and angle of internal friction of loess soil before and after its compaction on soil moisture and density. Pearson correlation coefficient was adopted as a measure of interdependence between soil characteristics.

Table 1. Correlation between strength and physical indices of loess soil of Budyonnovsk city

Strength parameters	*Physical parameters*	*Before compaction*	*After compaction*
Specific adhesion C	Moisture ω, 10%±2%; Density q, g/cm^3	-0.055 0.189	-0.155 0.094
	Moisture ω, 20%±2%; Density q, g/cm^3	-0.363 0.272	-0.191 0.146
	Moisture ω, 30%±2%; Density q, g/cm^3	-0.809 0.837	-0.911 0.890
Angle of internal friction φ	Moisture ω, 10%±2%; Density q, g/cm^3	-0.040 0.086	-0.159 0.249
	Moisture ω, 20%±2%: Density q, g/cm^3	-0.363 0.220	-0.230 0.578
	Moisture ω, 30%±2%: Density q, g/cm^3	-0.848 0.848	-0.846 0.846

Correlation is recorded between strength (specific adhesion, angle of internal friction) and physical (moisture, density) characteristics of loess. Both positive and negative linear correlation is observed. In the first case, higher (low) values of specific adhesion and angle of internal friction correspond to higher (lower) values of soil moisture. In the second case, higher (low) values of strength characteristics correspond to lower (high) values of physical characteristics [20].

The values of Pearson correlation coefficient more than 0.8 module demonstrate high correlation of investigated strength and physical characteristics of loess soil. The proximity to unity of Pearson's coefficient is observed mainly at high moisture values, 30%±2%. Approximation to zero modulus of the values of correlation coefficients indicate not the absence of correlation relationship between the studied characteristics, but the presence of unknown factors affecting these relationships. The modulus value of Pearson correlation coefficient less than 0.5 shows weak correlation of loess soil characteristics.

Figures 1 and 2 show regression correlations of specific cohesion C with moisture ω before and after compaction of subsidence soils by I.M. Litvinov's deep explosions [4], respectively.

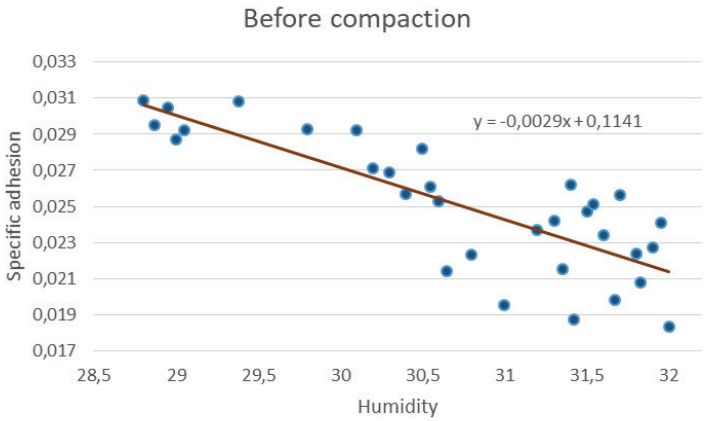

Figure 1. Regression correlation between specific cohesion and soil moisture before compaction

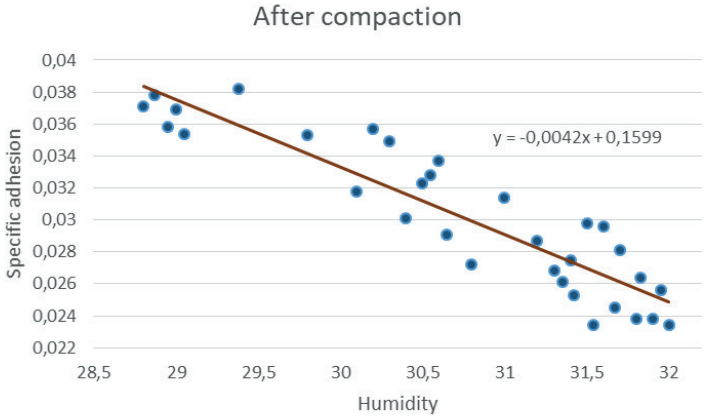

Figure 2. Regression correlation between specific cohesion and soil moisture after compaction

The equations of the regressions presented in Figures 1 and 2 have the following form

$$C = -0.0029 \cdot \omega + 0.1141, \quad (5)$$

$$C = -0.0042 \cdot \omega + 0.1599. \quad (6)$$

The approximation confidence factor for equation (5) is 0.6543. For equation (6), the approximation reliability coefficient is 0.8301. The closeness of the coefficients to unity indicates a significant degree of dependence of the regression model on the experimental data [3]. It is noted that with the increase in the moisture content of the subsidence soil, there is a decrease in the values of specific cohesion. This feature is characteristic of the corresponding regression dependences both before and after soil compaction.

Regression dependences of specific cohesion C on density q of loess soil are shown in Figures 3 and 4. The corresponding graphs both before and after realization of compaction of subsidence soils by the method of deep explosions are depicted. The regression lines are given by the following equations, respectively

$$C = 0.2684 \cdot q - 0.3835, \quad (7)$$

$$C = 0.0927 \cdot q - 0.1196. \quad (8)$$

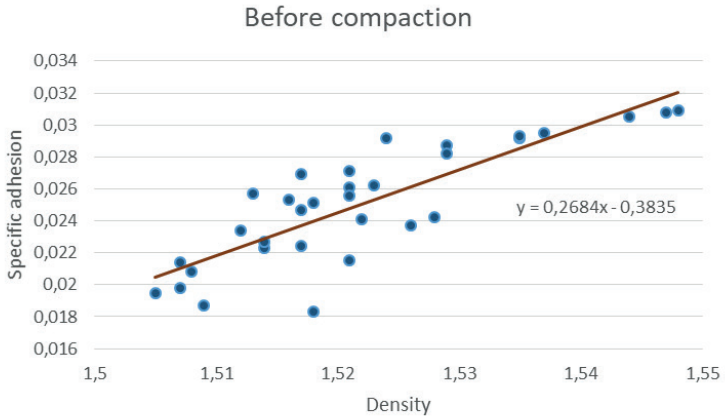

Figure 3. Regression correlation between specific cohesion and soil density before compaction

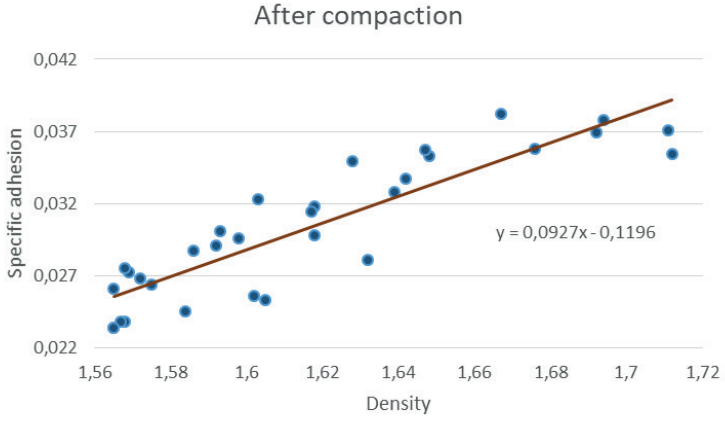

Figure 4. Regression correlation between specific cohesion and soil density after compaction

A positive regression correlation between specific cohesion and soil density was observed before and after compaction of loess soils by deep explosions. The increase in soil density leads to an increase in its strength characteristic, specific cohesion. Thus, for the regression equation before soil compaction (7) the approximation reliability coefficient is equal to 0.7003. After compaction of the subsidence soil for the regression equation (8) this indicator takes the value 0.7929.

According to Table 1, the angle of internal friction of the soil correlates with the indicators of physical characteristics of soils. Correlation between φ, moisture content ω and density ρ of loess soil is assessed by regression analysis.

Graphs of regression correlations of the angle of internal friction φ with soil moisture ω are presented in Figures 5 and 6. The regression equations show the dependences of the strength characteristic on the physical index for the state of the soil before and after its compaction by I.M. Litvinov's method of deep explosions [4].

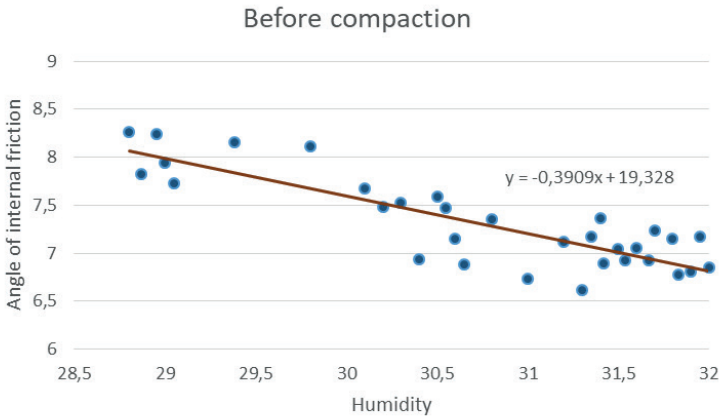

Figure 5. Regression correlation between the angle of internal friction and the moisture content of loess soil before compaction

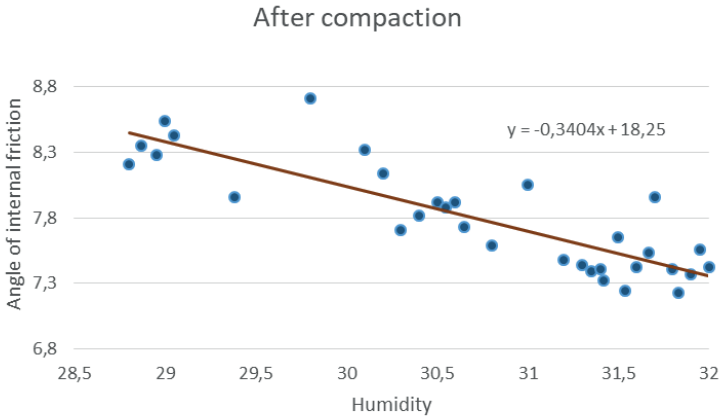

Figure 6. Regression correlation between the angle of internal friction and the moisture content of loess soil after compaction

The regression equations corresponding to Figures 5 and 6 have analytical representations of the following form

$$\varphi = -0.3909 \cdot \omega + 19.328, \quad (9)$$

$$\varphi = -0.3404 \cdot \omega + 18.25. \quad (10)$$

Analysis of the results showed the following. The regression equation (9) shows the degree of approximation to the experimental data with the approximation confidence coefficient 0.719. The approximation reliability coefficient of equation (10) is equal to 0.7157. The change of coefficient values is observed at realization of elimination of subsidence properties of soils by

depth explosions. Measurements of strength and physical characteristics of soil were carried out before and after engineering and production works.

The graphs of regression equations (Fig. 5, 6) show that the value of the angle of internal friction φ increases with decreasing values of loess soil moisture index ω. Table 1 also notes the negative linear correlation of the investigated soil characteristics.

The study of regression dependences of the angle of internal friction on the density of loess soil is presented in Figures 7 and 8. The graph of Figure 7 shows the dependence before soil compaction, and in Figure 8 after compaction.

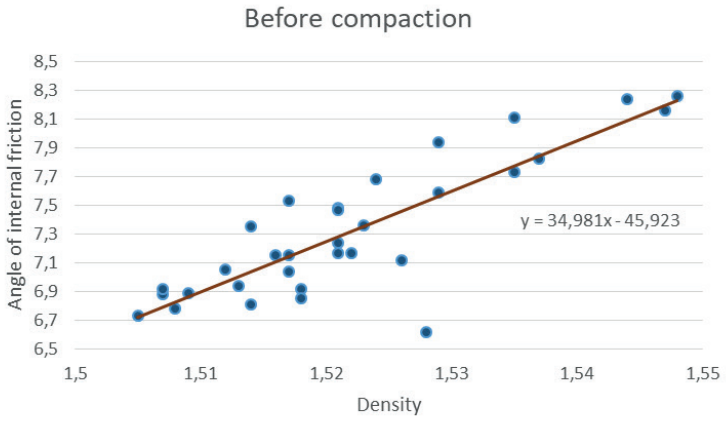

Figure 7. Regression correlation between the angle of internal friction and density of loess soil before compaction

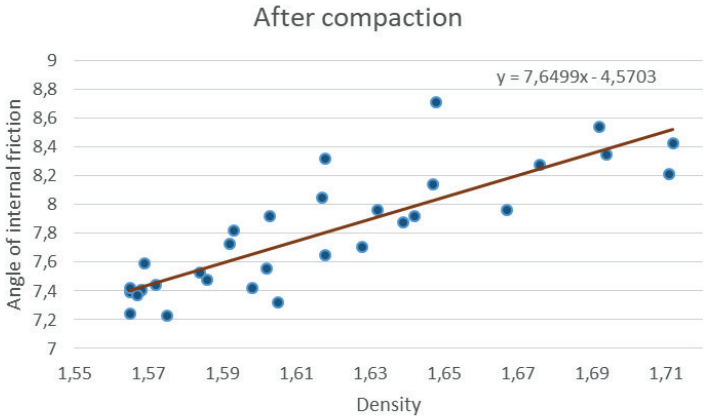

Figure 8. Regression correlation between the angle of internal friction and density of loess soil after compaction

The regression equations (Figs. 7, 8) are described by analytical relations, respectively

$$\varphi = 34.981 \cdot q - 45.923, \quad (11)$$

$$\varphi = 7.6499 \cdot q - 4.5703. \quad (12)$$

Regression equations (11) and (12) have a high degree of approximation to the experimental data. The approximation confidence coefficient for equation (11) is equal to 0.7192. For equation (12), the approximation confidence factor takes the value 0.7156. With increasing values of the angle of internal friction, there is

an increase in the density values of loess soil both before and after its compaction by deep explosions.

CONCLUSION

The article provides a mathematical modeling of the compaction of subsidence soils by explosion and studies the strength properties of loess by correlation and regression analysis. Specific cohesion and angle of internal friction correlate with moisture content and density of loess. Pearson correlation coefficients of strength and physical characteristics of soil showed that at soil moisture of 30%±2% their high intercorrelation is observed. This is characteristic of loess soils before and after elimination of their subsidence properties by depth explosions. Regression equations of specific adhesion, angle of internal friction and humidity, density, respectively, of subsidence soils before and after their compaction have been constructed. It is established that with the increase of soil moisture the values of indicators of soil strength characteristics decrease. With increasing density of loess the growth of values of specific cohesion and angle of internal friction is fixed. Regression equations can be used in calculation mathematical models of engineering-geological systems in the design of construction objects on subsidence loess soils. They allow predicting indicators of soil strength characteristics on the basis of their physical characteristics.

The author is grateful to the Doctor of Geological and Mineralogical Sciences, Professor, Professor of the Department of Construction of the North Caucasus Federal University, Boris Fedorovich Galai, for his assistance in writing the article.

REFERENCES

1. **Sergeyev Ye.M., Larionov A.K., Komissarova N.N.** (1986) *Lossovyye porody SSSR. Inzhenerno-geologicheskiye osobennosti i problemy ratsional'nogo ispol'zovaniya* [Loess rocks of the USSR. Engineering-geological features and problems of rational use]. Moscow: Nauka, vol.1 (in Russian)
2. **Sergeev E.M., Bykov V.S., Komissarov N.N.** (1986) *Lossovyye porody SSSR. Regional'nyye osobennosti* [Loess rocks of the USSR. Regional features]. Moscow: Nauka, vol.2 (in Russian)
3. **Galay B.F**. (2016) *Posobiye po uplotneniyu prosadochnykh lessovykh gruntov glubinnymi vzryvami v usloviyakh Severnogo Kavkaza (izyskaniya, proyektirovaniye, proizvodstvo rabot)* [Manual on compaction of subsident loess soils by deep explosions in the conditions of the North Caucasus (research, design, production of works)]. Stavropol: NCFU (in Russian)
4. **Litvinov I.M.** (1969) *Glubinnoye ukrepleniye i uplotneniye prosadochnykh gruntov* [Deep strengthening and compaction of subsiding soils]. Kyiv: Budivelnik (in Russian)
5. **Pantyushina E.V.** (2011) Lossovyye grunty i inzhenernyye metody ustraneniya ikh prosadochnykh svoystv [Loess soils and engineering methods for eliminating their subsidence properties]. *Polzunovsky vestnik*, vol. 1, pp. 127-130.
6. **Zhilenkov V.N.** (2010) Kharakternaya osobennost' konsolidirovannogo lineynogo uplotneniya vodonasyshchennykh glinistykh gruntov i torfa pod vozdeystviyem vneshnikh nagruzok [A characteristic feature of the consolidated linear compaction of water-saturated clay soils and peat under the influence of external loads]. *Izvestiya VNIIG im. B.E. Vedeneeva*, vol. 258, pp. 87-92.
7. **Nguyen P.D.** (2012) Issledovaniye zavisimosti prochnostnykh svoystv grunta ot yego fizicheskogo sostoyaniya [Investigation of the dependence of the strength properties of the soil on its

physical state]. *Inzhenerno-stroitel'nyi zhurnal*, vol. 9(35), pp. 23-28. DOI: 10.5862/MCE.35.3

8. **Braja M.D.** (2008) *Advanced Soil Mechanics*. New York: Taylor & Francis Group.
9. **Tarasenko E.O., Tarasenko V.S., Gladkov A.V.** (2019) Matematicheskoye modelirovaniye uplotneniya prosadochnykh lossovykh gruntov Severnogo Kavkaza glubinnymi vzryvami [Mathematical modeling of compaction of subsiding loess soils of the North Caucasus by deep explosions]. *Bulletin of the Tomsk polytechnic university. Geo assets engineering*. vol. 330, no 11, pp. 94-101. https://doi.org/10.18799/24131830/2019/11/2352
10. **Tarasenko E.O.** (2023) Numerical simulation of gas atom coordinate dispersion in a mathematical model of deep blast compaction for subsidence soils. *International Journal for Computational Civil and Structural Engineering*, vol. 19, Issue 1, pp. 147-154. https://doi.org/10.22337/2587-9618-2023-19-1-147-154.
11. **Tarasenko E.O.** (2023) Chislennaya otsenka plotnosti grunta metodom konechno-raznostnykh setok pri matematicheskom modelirovanii uplotneniya prosadochnykh gruntov glubinnymi vzryvami [Numerical estimation of soil density by the method of finite difference grids in mathematical modeling of compaction of subsible soils by deep explosions]. *Bulletin of the Tomsk polytechnic university. Geo assets engineering*. vol. 334, no 5, pp. 103-108. https://doi.org/10.18799/24131830/2023/5/4022.
12. **Tarasenko E.O., Gladkov A.V.** (2022) Chislennoye resheniye obratnykh zadach pri matematicheskom modelirovanii geologicheskikh sistem [Numerical solution of inverse problems in mathematical modeling of geological systems]. *Bulletin of the Tomsk polytechnic university. Geo assets engineering*. vol. 333, no 1, pp. 105-112. https://doi.org/10.18799/24131830/2022/1/3208.
13. **Tarasenko E.O., Gladkov A.V., Gladkova N.A.** (2022) Solution for Inverse Boundary Value Problems on the Power of a Concentrated Charge in a Mathematical Model of Subsidence Soils Compaction. *Mathematics and its Applications in New Computer* Systems. *MANCS 2021. Lecture Notes in Networks and Systems, Springer, Vol 424,* pp. 537–545. https://link.springer.com/book/10.1007/978-3-030-97020-8.
14. **Petrakov A.A., Prokopov A.Yu., Petrakova N.A., Panasyuk M.D**. (2021) Interpretatsiya prochnostnykh kharakteristik grunta dlya chislennykh issledovaniy [Interpretation of the strength characteristics of the soil for numerical research]. *Izvestiya TulGU. Earth sciences*, vol. 1, pp. 225-236.
15. **Prokopova M.V., Prokopov A.Yu., Zhur V.N.** (2017) Issledovaniye svoystv lèssovykh prosadochnykh gruntov Vostochnogo Donbassa [Study of the properties of loess subsidence soils of the Eastern Donbass]. Proceedings of the International scientific and practical conference "*Transport: science, education, production*", Rostov-on-Don, RSTU, pp. 354-358.
16. **Sukhoruchenko S.K.** (2012) Uravneniya regressii prochnostnykh kharakteristik lossovykh prosadochnykh gruntov ravninnogo Kryma [Regression equations for the strength characteristics of loess subsidence soils of the flat Crimea]. *Construction and technogenic safety*, vol. 44, pp. 58-63.
17. Russian State Standard GOST 12248.3–2020 (2020) *Opredeleniye kharakteristik prochnosti i deformiruyemosti metodom trekhosnogo szhatiya* [Determination of strength and deformability characteristics by the triaxial compression method]. Moscow, Standartinform (in Russian)

18. **Shvets V.B., Ginzburg L.K., Goldstein V.M.** and others (1987) *Spravochnik po mekhanike i dinamike gruntov* [Handbook of soil mechanics and dynamics]. Kyiv: Budivelnik (in Russian)
19. **Sergeyev E.M.** (1986) *Teoreticheskiye osnovy inzhenernoy geologii. Mekhaniko-matematicheskiye osnovy* [Theoretical foundations of engineering geology. Mechanical and mathematical foundations]. Moscow: Nedra (in Russian)
20. **Draper N.** (2019) *Prikladnoy regressionnyy analiz* [Applied regression analysis]. Moscow: Williams Publishing House (in Russian)

СПИСОК ЛИТЕРАТУРЫ

1. Лёссовые породы СССР. Т. 1. Инженерно-геологические особенности и проблемы рационального использования / Под ред. Сергеева Е.М., Ларионова А.К., Комиссаровой Н.Н. – Москва: Наука, 1986. – 273 с.
2. Лёссовые породы СССР. Т. 2. Региональные особенности / Под ред. Сергеева Е.М., Быковой В.С., Комиссаровой Н.Н. – Москва: Наука, 1986. – 276 с.
3. **Галай Б.Ф.** Пособие по уплотнению просадочных лессовых грунтов глубинными взрывами в условиях Северного Кавказа (изыскания, проектирование, производство работ). – Ставрополь: Изд-во СКФУ, 2016. – 142 с.
4. **Литвинов И.М.** Глубинное укрепление и уплотнение просадочных грунтов. – Киев: Будівельник, 1969. – 188 с.
5. **Пантюшина Е.В.** Лёссовые грунты и инженерные методы устранения их просадочных свойств // Ползуновский вестник, 2011, № 1. С. 127-130.
6. **Жиленков В.Н.** Характерная особенность консолидированного линейного уплотнения водонасыщенных глинистых грунтов и торфа под воздействием внешних нагрузок // Известия ВНИИГ им. Б.Е. Веденеева, 2010, №258. С. 87-92.
7. **Нгуен Ф. Зунг**. Исследование зависимости прочностных свойств грунта от его физического состояния // Инженерно-строительный журнал, 2012, №9(35). С. 23-28. https://doi.org/10.5862/MCE.35.3
8. **Braja M. Das**. Advanced Soil Mechanics. New York: Taylor & Francis Group, 2008, 567 pages.
9. **Тарасенко Е.О., Тарасенко В.С., Гладков А.В.** Математическое моделирование уплотнения просадочных лёссовых грунтов Северного Кавказа глубинными взрывами // Известия Томского политехнического университета. Инжиниринг георесурсов, 2019, Т. 330, № 11. С. 94-101. https://doi.org/10.18799/24131830/2019/11/2352
10. **Tarasenko E.O.** Numerical simulation of gas atom coordinate dispersion in a mathematical model of deep blast compaction for subsidence soils // International Journal for Computational Civil and Structural Engineering, 2023, Volume 19, Issue 1, pp. 147-154. https://doi.org/10.22337/2587-9618-2023-19-1-147-154.
11. **Тарасенко Е.О.** Численная оценка плотности грунта методом конечно-разностных сеток при математическом моделировании уплотнения просадочных грунтов глубинными взрывами // Известия Томского политехнического университета. Инжиниринг георесурсов, 2023, Т. 334, № 5. С. 103-108. https://doi.org/10.18799/24131830/2023/5/4022.
12. **Тарасенко Е.О., Гладков А.В.** Численное решение обратных задач при математическом моделировании геологических систем // Известия Томского политехнического

университета. Инжиниринг георесурсов, 2022, Т. 333, № 1. С. 105-112. https://doi.org/10.18799/24131830/2022/1/3208.
13. **Tarasenko E.O., Gladkov A.V., Gladkova N.A.** Solution for Inverse Boundary Value Problems on the Power of a Concentrated Charge in a Mathematical Model of Subsidence Soils Compaction // Mathematics and its Applications in New Computer Systems. MANCS 2021. Lecture Notes in Networks and Systems, Springer, 2022, Vol 424, pp. 537–545. https://link.springer.com/book/10.1007/978-3-030-97020-8.
14. **Петраков А.А., Прокопов А.Ю., Петракова Н.А., Панасюк М.Д.** Интерпретация прочностных характеристик грунта для численных исследований // Известия ТулГУ. Науки о Земле, 2021, Вып. 1. С. 225-236.
15. **Прокопова М.В., Прокопов А.Ю., Жур В.Н.** Исследование свойств лѐссовых просадочных грунтов Восточного Донбасса // Сборник научных трудов Международной научно-практической конференции «Транспорт: наука, образование, производство», Ростов-на-Дону: РГУПС, 2017. С. 354-358.
16. **Сухорученко С.К.** Уравнения регрессии прочностных характеристик лёссовых просадочных грунтов равнинного Крыма // Строительство и техногенная безопасность, 2012, №44. С. 58-63.
17. ГОСТ 12248.3–2020. Определение характеристик прочности и деформируемости методом трехосного сжатия. – Москва, Стандартинформ, 2020. – 33 с.
18. Справочник по механике и динамике грунтов / В.Б. Швец, Л.К. Гинзбург, В.М. Гольдштейн и др. / Под ред. В.Б. Швеца. – Киев: Будівельник, 1987. – 232 с.
19. Теоретические основы инженерной геологии. Механико-математические основы / Под ред. Е.М. Сергеева. – М.: Недра, 1986. – 254 с.
20. **Дрейпер Н.** Прикладной регрессионный анализ. – М.: Вильямс И.Д., 2019. – 912с.

Tarasenko Elena Olegovna, Associate Professor of the Department of Computational Mathematics and Cybernetics of the Faculty of Mathematics and Computer Sciences named after Professor N.I. Chervyakov, Candidate of Physical and Mathematical Sciences, Associate Professor, Russia, 355009, Stavropol, Pushkin str., 1, building 2, auditorium 308.
e-mail: galail@mail.ru

Тарасенко Елена Олеговна, доцент кафедры Вычислительной математики и кибернетики факультета Математики и компьютерных наук имени профессора Н.И. Червякова, кандидат физико-математических наук, доцент, SPIN-код 7730-0157, Россия, 355009, г. Ставрополь, ул. Пушкина, д. 1, корпус 2, аудитория 308.
e-mail: galail@mail.ru

К ЮБИЛЕЮ ВЛАДИМИРА ТРОФИМОВИЧА ЕРОФЕЕВА

10 марта 2024 года исполнилось 70 лет академику Российской академии архитектуры и строительных наук (РААСН), Почетному строителю России, Заслуженному деятелю науки Республики Мордовия, Лауреату Государственной и Огаревской премий Республики Мордовия, профессору, доктору технических наук, профессору кафедры строительного материаловедения Национального исследовательского Московского государственного строительного университета (НИУ МГСУ), члену Редакционного совета международного научного журнала "International Journal for Computational Civil and Structural Engineering".

Владимир Трофимович Ерофеев – признанный в России и за рубежом, крупный, авторитетный учёный в области строительного материаловедения и строительных технологий. Результаты его научных исследований изложены более чем в 900 печатных работах, в том числе в 20 монографиях. Он обладатель более 100 авторских свидетельств и патентов в области строительных материалов и строительных конструкций. Владимир Трофимович подготовил 26 кандидатов и одного доктора наук.

С 2002 года возглавляя факультет, в дальнейшем Институт архитектуры и строительства и кафедру строительных материалов технологий Национального исследовательского Мордовского государственного университета им. Н.П. Огарёва, Владимир Трофимович значительную часть результатов своей научной и образовательной деятельности посвятил созданию материалов, не изменяющих свои свойства в различных климатических условиях, исследованию, научному обоснованию применения и внедрению местных и новых композитных материалов, отходов предприятий, энергосберегающих технологий строительства в развитие производства эффективных строительных материалов и изделий, строительную практику Республики Мордовия, подготовку научных и научно-педагогических кадров, специалистов высшей квалификации в области строительства. В 2023 году В.Т. Ерофеев начал трудовую деятельность в НИУ МГСУ.

Желаем Вам, Владимир Трофимович, крепкого здоровья, дальнейших творческих успехов и благополучия!

Редакционный Совет международного научного журнала
"International Journal for Computational Civil and Structural Engineering"